The University of Adelaide

THE UNIVERSITY
of ADELAIDE

DOCTORAL THESIS

Investigation of Timepix Radiation Detector for Autoradiography and Microdosimetry in Targeted Alpha Therapy

Ruqaya O. Al Darwish

Supervisor: Prof. Eva Bezak
Co-Supervisors: Dr. Mohammad Mohammadi (until 2013)
& Dr. Alex Staudacher (2013-2016)

A thesis submitted in fulfilment of the requirements
for the degree of doctor of Philosophy
in
The School of Physical Sciences
University of Adelaide

August 2016

Declaration of Authorship

I, Ruqaya O. Al Darwish, certify that this thesis titled, 'Development of transmission alpha particle microdosimetry using Timepix radiation detector for targeted alpha therapy' and the work presented in it are my own.

I confirm that:

- This work contains no material which has been accepted for the award of any other degree or diploma in any university or other tertiary institution to Ruqaya O. Al Darwish, to the best of my knowledge and belief, contains no material previously published or written by another person, except where due reference has been made in the text.
- I give consent to this copy of my thesis, when deposited in the University Library, being made available for loan and photocopying, subject to the provisions of the Copyright Act 1968.
- The author acknowledges that copyright of published works contained within this thesis resides with the copyright holder(s) of those works.
- I also give permission for the digital version of my thesis to be made available on the internet, visa the University's digital research repository, the Library catalogue, the Australasian Digital Theses Program (ADTP) and also through web search engines, unless permission has been granted by the University to restrict access for a period of time.

Signed: _____

Date: 16 Oct 2017

Scholarship

- Ministry of Education of Saudi Arabia Scholarship

Publications Contained Within Thesis

Published

1. Al Darwish R., Staudacher A. H., Bezak E. and Brown M. P., "Autoradiography Imaging in Targeted Alpha Therapy with Timepix Detector," Computational and Mathematical Methods in Medicine (2015), Article ID 612580, 7 pages http://dx.doi.org/10.1155/2015/612580.

2. Al Darwish R., Staudacher A. H., Brown M. P. and Bezak E., "Development of a Transmission Alpha Particle Dosimetry Technique using A549 cells and a Ra-223 source for Targeted Alpha Therapy", Medical Physics 43, 6145 (2016); doi: 10.1118/1.4965805.

Submitted for Publication

1. Al Darwish R., Bezak E. Marcu L. and Rozenfeld A., "Timepix – technical aspects of a novel development in solid state radiation detectors", invited review article: submitted paper (invited paper). Submitted to: Radiation Measurements.

2. Al Darwish R., Bezak E. Marcu L. and Rozenfeld A., "Overview of current applications of the Timepix detector in radiation physics", invited review article: submitted paper (invited paper). Submitted to: Radiation Measurements.

4. Al Darwish R., Bezak E. and Mohammadi M., "Application of Timepix to Low Dose Radiation Dosimetry", research article: submitted paper. Submitted to: Radiation Protection Dosimetry.

Conference Presentations

National Presentations

1. AL Darwish R., Bezak E. and Mohammadi M., *Investigation of Timepix Detector Application for Radiation Imaging and Dosimetr*, Engineering & Physical Sciences in Medicine (EPSM), 2-6 December 2012, Gold Coast, Australia.

2. AL Darwish R., Bezak E. and Mohammadi M., *Investigation of Energy Deposition by Alpha Particles using Timepix Detector*, Engineering & Physical Sciences in Medicine (EPSM), 3-7 November 2013, Perth, Australia.

3. AL Darwish R., Staudacher A. H. and Bezak E., *Application of Timepix Detector in Targeted Alpha Therapy Autoradiography*, Fifth Australasian Cyclotron Users' Group Meeting, 25 April 2014, Adelaide, Australia.

4. AL Darwish R., Staudacher A. H. and Bezak E., *Application of Timepix detector to microdosimetry: Investigation of A549 lung carcinoma cells survival exposed to photons and alpha particles*, Combined Scientific Meeting, 4-7 September 2014, Melbourne, Australia.

5. AL Darwish R., Staudacher A. H. and Bezak E., *Development of transmitted alpha particle microdosimetry using A549 cells and Ra-223 source for targeted alpha therapy*, Engineering & Physical Sciences in Medicine (EPSM), 8-12 November 2015, Wellington, New Zealand.

International Presentations

1. AL Darwish R., Staudacher A. H. and Bezak E., *Application of Timepix for Autoradiography Imaging in Targeted Alpha Therapy*, European Society for Radiotherapy & Oncology (ESTRO 33), 4-8 April 2014, Vienna, Austria.

2. AL Darwish R., Staudacher A. H. and Bezak E., *Development of transmitted alpha particle microdosimetry using Timepix: Investigation of A549 lung carcinoma cells exposed to alpha particles irradiated from Ra-223,* The IUPESM World Congress, 7-12 June 2015, Toronto, Canada.

3. AL Darwish R., Staudacher A. H. and Bezak E., *Investigation of DNA double strand breaks correlation with absorbed dose from alpha particle irradiation using combination of radiation and biological dosimetry,* 14th International workshop on radiation damage, 20-24 March 2016, Melbourne, Australia.

Other Presentations and Publications

1. AL Darwish R., Staudacher A. H. and Bezak E., *Investigation of Timepix Detector Application for Radiation Imaging and Dosimetry,* the 2013 student paper night, Australian College of Physical Scientists and Engineers in Medicine (ACPSEM) / South Australian/Northern Territory Branch – Student Night, 20 March 2013, Adelaide, Australia.
2. Work included in chapter 9: *Targeted Alpha Therapy for Cancer,* by B.J. Allen, L.G. Marcu, and E. Bezak, in *Advances in Medical Physics*, editedly Godfrey, D.J., et al. Medical Physics Publishing. 2016.

Abstract

The Timepix detector developed by CERN is a novel and sophisticated particle detector. It consists of a semiconductor layer divided into an array of pixels. This array of pixels is bump-bonded to an electronics integrated layer (i.e. the readout chip). Timepix can be used for a wide range of measurements of electromagnetic radiation and particles and their applications in different fields such as space physics, nuclear physics, radiotherapy physics, imaging and radiation protection.

The Timepix detector used in this work was purchased from Amsterdam Scientific Instruments, the Netherlands, in order to investigate its use for microdosimetry purposes, in particular in targeted alpha therapy. The device has the following properties: 256 x 256 pixels of 55 x 55 μm^2 area each, the chip is effective for positive or negative charge and can be used to detect electrons, X-rays, neutrons and heavy charge particles. It can work as an energy spectrometer, has good spatial resolution and reasonable detection efficiency. The device can operate in three common modes: Timepix mode, Medipix mode, and Time-Over-Threshold (TOT) mode.

Targeted alpha therapy (TAT) is a novel type of radionuclide therapy in which an alpha emitting radioisotope is attached to a cancer cell seeking vector (so called radioimmunoconjugate (RIC)). Once attached to a cancer cell, it causes localized damage due to traversal and energy deposition high LET α-particles.

There is, however, a lack of data related to α-particle distribution in TAT. These data are required to more accurately estimate the absorbed dose on a cellular level. As a result, this work aims to develop a microdosimetry technique, using Timepix detector that will estimate, or better yet determine the absorbed dose deposited by α-particles in cells as well as will measure the biodistribution of the radioisotope in a tumour.

Initially, extensive Timepix characterization and testing has been done to evaluate the detector's response, including linearity, reproducibility, and sensitivity to low doses of radiations (μGy-mGy dose region) and energy dependence. I-125 seeds and superficial X-rays (below 70 kVp), produced by the Gulmay superficial X-ray unit, were used. The measured Timepix pixel value was correlated with the known dose (based on the irradiation time used and TLD-100 measurements) and a pixel-value-to- dose calibration curve was obtained. It was confirmed that Timepix value increased linearly with the dose delivered. The dose calibration curves using the superficial X-ray beams showed that the pixel value, however, depended on the energy of the X-ray beam.

The application of Timepix to measure radioisotope biodistribution (i.e. autoradiography) was investigated. Mice with Lewis lung (LL2) tumours were treated with about 18 kBq of ^{227}Th-labelled DAB4 murine monoclonal antibody that bounds to necrotic tumour cells. The rationale is to develop α-particle-mediated bystander kill of nearby viable tumour cells. To generate more necrotic tumour cells for ^{227}Th-DAB4 binding, some mice also received chemotherapy before being injected with Th-227-DAB4. Finally, 5 mm tumour sections were cut from treated mice for autoradiography with Timepix. Each tumour section was mounted onto a slide with front face uncovered to allow emission of α-particles from the tumour section. Simple steel collimator (1 cm radius, 2 cm length) was manufactured in-house and positioned around the tumour section. The slide was placed 2 cm away from the Timepix detector. Bias voltage of 7 V was applied, and α-particle filter was selected for acquisition. Detector cover was removed, exposing the Si layer, to allow the emitted α-particles (~ 6 MeV) to reach the detector. Image acquisition took ~14 h. Good resolution autoradiographs of radiolabelled tumour sections were acquired, showing α-particle, electron and X-ray tracks. Timepix measurements also showed an increased Th-227–DAB4 uptake following chemotherapy due to increase in necrotic tissue volume.

Timepix was also used to measure the uptake of Cr-51 by A549 cells (lung carcinoma cell line) for different pH levels and the dependence of uptake on pH was investigated. Timepix was observed to be sensitive to detect small changes in the activity/uptake of radioactive sources depending on the environmental condition and the number of cells.

The last part of this thesis deals with the development of a transmitted α-particle microdosimetry technique. First, A549 cells were grown in vitro using standard protocols and were irradiated using a 6 MV photon beam with different doses varying between 2-8 Gy and Ra-226 source was used for α-particle irradiation to evaluate A549 radiation sensitivity using clonogenic assay and MTT assay. The cell line was found radiosensitive, with D50 of ~ 2 Gy for X-ray irradiation.

For transmitted dosimetry, A549 cells were either unirradiated (control) or irradiated for ½, 1, 2 or 3 hours with α-particles emitted from a Ra-223 source positioned below a monolayer of A549 cells. The HTS Transwell® 96 well system (Corning, USA), consisting of 2 compartments, was used to develop a method for tracking α-particles through a cell monolayer. This system comprises of two compartments, with liquid Ra-223 evaporated in the lower compartment to avoid α-particle self-absorption inside the liquid. The measured activity of 5 kBq was uniformly distributed, as confirmed by Timepix detector. The second compartment consists of a flat bottom polycarbonate membrane (10 μm thick) where cells are plated. It is sufficiently thin to allow α-particles to penetrate through and hit the cells. Fifteen thousand A549 cells were seeded in the upper compartment that was then inserted into the lower compartment containing the evaporated Ra-223. The transwell system was positioned under the Timepix detector. Transmitted α-particles were detected for ½, 1, 2 or 3 hour irradiation times. Additionally, DNA double strand breaks (DSBs) in the form of γ-H2AX foci, were examined by fluorescence microscopy. The number of transmitted α-particles was correlated

with the observed DNA DSBs and the delivered radiation dose was estimated. Additionally, the dose deposited was calculated using Monte Carlo code SRIM.

Approximately 20% of α-particles were transmitted and detected by Timepix. The frequency and number of γ-H2AX foci increased significantly following α-particle irradiation as compared to unirradiated controls. The RBE equivalent dose delivered to A549 cells was estimated to be approximately 0.66 Gy, 1.32 Gy, 2.53 Gy and 3.96 Gy after ½, 1, 2 and 3 h irradiation, respectively, considering a relative biological effectiveness of α-particles of 5.5.

In summary, the Timepix detector can be used effectively for autoradiography in TAT, providing high resolution images and excellent spatial resolution of detected α-particles, as well as a transmitted α-particle microdosimetry detector. If cross-calibrated using biological dosimetry, this method will give a good indication of the biological effects of α-particles without the need for repeated biological dosimetry which is costly, time consuming and not readily available.

Acknowledgements

I want to thank my supervisor Eva Bezak. It has been an honour to be her PhD student. I appreciate all her time and ideas to develop my experience and for motivating me even during tough times in the PhD. And mainly I am thankful for the example that she set to me as a teacher, supervisor, leader and a human being.

A special thanks to my co-supervisor Alex Staudacher for his continuous support, effort and for being a good reference for the biological part of my work.

Thanks also to Mohammad Mohammadi for his three years of co-supervision and his advice since the start of my PhD.

A special thanks to John Schneider for his contributions to creating a design from just an idea on paper to an actual product.

Thanks to Artem Borysenko and Benjamin Crouch for their assistance with radiation sources.

Also, thanks to Michael Paul Brown for allowing us to access the Translational Oncology Laboratory, Centre for Cancer Biology, SA Pathology for biological experiments.

Thanks to Prof Eric Yeoh for giving us his support of my applications for use funding from special purposes fund, Royal Adelaide Hospital, to attend several conferences.

Thanks to my colleagues at The Adelaide University and The Royal Adelaide Hospital and special thanks with best wishes to my friend Jiahua Zhu, who walked with me on this rough and isolated road.

Thanks to Claudia, Thuraya, Nizar, Mona, Noor, Alkadijatan, Ghadeer, Zhara, Hashmiah, Alwehayb and Alhejab family, Eman, Nowal, Alfawatom, Saliha, Huda, Howra, Narjess, Zaman and my family and friends.

Contents

List of Figures

List of Papers' Figures

List of Tables

Abbreviations

A	Activity
α-particle	Alpha particle
CMOS	Complementary metal–oxide–semiconductor
CERN	European Organization for Nuclear Research
D	Dose
DNA DSBs	DNA double strand breaks
E	Energy
HHL	Higher energy threshold
ICRU	International Commission on Radiation Units and Measurer
LET	Linear energy transfer
PBS	Phosphate-buffered saline
RBE	Relative biological effectiveness
RIC	Radioimmunoconjugate
SoPhy	Software for Physics
TAT	Targeted alpha therapy
THL	Lower energy threshold
TOT mode	Time Over Threshold mode
y	lineal energy
WHO	World Health Organisation

Chapter 1

Introduction

1.1 Introduction

Cancer is defined as a group of complex diseases where normal cells transition to cancer cells through abnormal gene expression resulting from gene mutations, translocations, transcription or translations (Ruddon 1995, Kopans 2002), and cells enter into a random, continuous division phase (Ruddon 1995). According to the World Cancer Reports from 2008 to 2014 (WHO 2008, WHO 2014) there are three major factors contributing to developing cancer: biomedical factors, lifestyle factors and environmental factors (Welfare 2010).

Different cancer types differ in growth rate, cellular differentiation state, diagnostic detectability, invasiveness, metastatic potential, treatment response and prognosis (Ruddon 1995). There are many modalities to control and cure cancer such as surgery, chemotherapy and radiation therapy which can be used alone or in combination. Radiation therapy has been found beneficial and used for almost half of cancer patients (Wambersie, Pihet et al. 1990).

Radiation therapy includes many types of treatments, which use either direct or indirect ionizing radiation and includes X-ray therapy, electron therapy, light and heavy ion therapy and neutron therapy. As the treatment beams differ in particle type and energy, it is understandable that the biological effects differ between radiation modalities. As a result, the treatment outcome depends on the interplay between the interaction of radiation with tissue and the resulting biological response. Determination of the absorbed dose and the effective dose is therefore critical to improve disease eradication and to protect healthy tissue. Several dosimetry techniques have been used over the years (ICRU 2007) to measure radiation dose and to determine the absorbed dose in patients. This is usually done on a macroscopic level in terms of a radiation dose to a tumour volume. However, a novel radiotherapy modality, that differs from the localized external beam radiation therapy (which uses a beam to directly irradiate a specific target volume inside the body), and that is known as targeted therapy, can target individual cells in the tumour and hence can be applied to treatment of disseminated/systemic disease. This is a relatively new area of dosimetry known as microdosimetry. Microdosimetry enables the monitoring of a single ionization event within an irradiated volume on a micrometre (cellular) level. Microdosimetry can use measuring devices similar to those used in dosimetry, such as proportional counters and tissue equivalent proportional counters (Waker 1995).

1.2 Dose Measurement Techniques in Radiation Therapy

1.2.1 Dose and Quantities

According to the International Commission on Radiation Units and Measurements (ICRU), dose is defined as the amount of energy absorbed, dE, per unit mass, dm, of the irradiated material (Mayles, Nahum et al. 2007):

$$Dose = \frac{dE}{dm}\left(\frac{J}{kg}\right) \quad (1.1)$$

The SI unit of absorbed dose is Gray (Gy) and is equal to one joule of energy per kilogram of mass. Another older unit also used is rad and it is equal to 100 erg/gram (Hall and Giaccia 2006). The relationship between Gray and rad is given in equation (1.2):

$$1\,Gy = 1\frac{J}{kg} = 100\ \text{rad} \quad (1.2)$$

To estimate the biological effect of a given dose, the absorbed dose is multiplied by a relative biological effectiveness (RBE) factor. RBE compares the doses required to produce the same biological effect which results from a standard radiation dose delivered by 250 kVp X-rays or ^{60}Co γ-rays and a test radiation dose, as given in equation (1.3) (Mayles, Nahum et al. 2007). RBE varies according to radiation type, dose, dose rate, LET, cell type and the biological end-point (Podgorsak 2005).

$$RBE = \frac{\text{Dose of reference radiation}}{\text{Dose of radiation under investigation}} \quad (1.3)$$

The ability of radiation to produce more biological damage increases with an increase in linear energy transfer (LET). LET is defined as the average energy, dE, locally imparted by a charged particle with specific energy travelling a specific distance, dx, in the absorber (Podgorsak 2005) as shown in equation (1.4).

This means that the RBE is higher for radiation with higher LET than it is for radiation with lower LET, as shown in Figure 1.1.

$$LET = \frac{dE}{dx}\left(\frac{keV}{\mu m}\right) \tag{1.4}$$

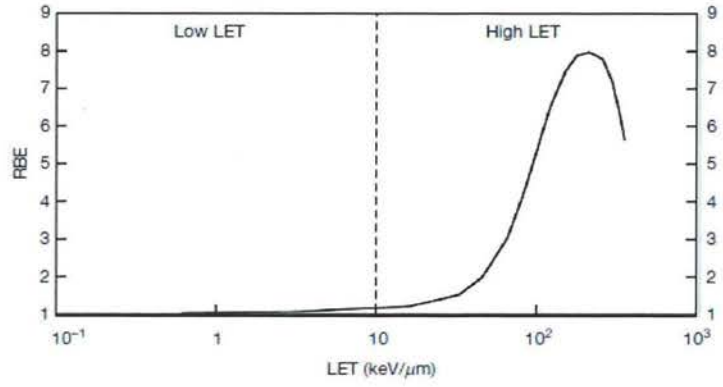

Figure 1.1. The relationship between RBE and LET, courtesy of (Podgorsak 2005).

1.2.2 Cancer Cells and Radiation Therapy

The relationship between the cancer cell responses, which is the observed biological effect on the tumour population, resulting from different absorbed radiation doses is called the dose response curve, while the relationship between the fraction of surviving cells and different absorbed radiation doses is called the cell survival curve. These responses have been studied extensively for different radiation types (Podgorsak 2005, Hall and Giaccia 2006). An example of a typical cell survival curve is shown in Figure 1.2.

The aim of radiation therapy is to maximize damage to cancer cells to control tumour growth, while minimizing the dose to the surrounding healthy tissues. Typical probabilities for tumour control and normal tissue complications are shown in Figure 1.3. The difference between the two curves (the red line) identifies the most suitable treatment dose, which will maximise tumour control while keep the damage to normal tissue at an acceptable level (Thwaites and Williams 2000, Podgorsak 2005).

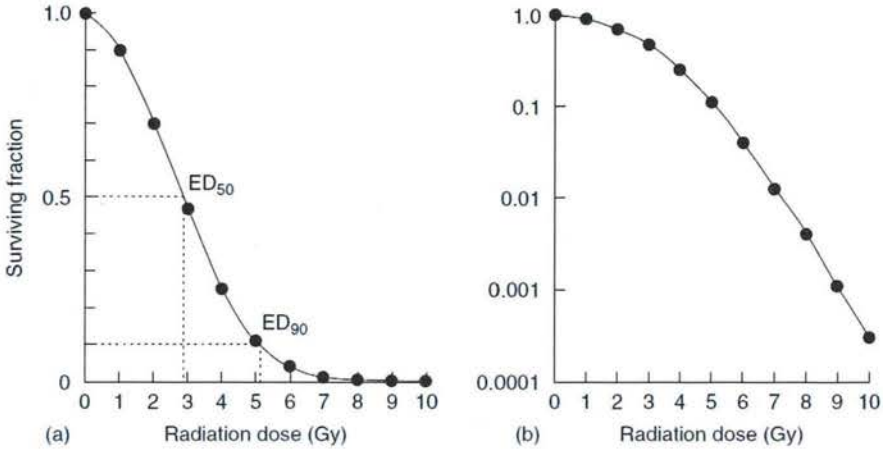

Figure 1.2. An example of a cell survival curve using linear (a) and semi logarithmic (b) scale, courtesy of (Mayles, Nahum et al. 2007).

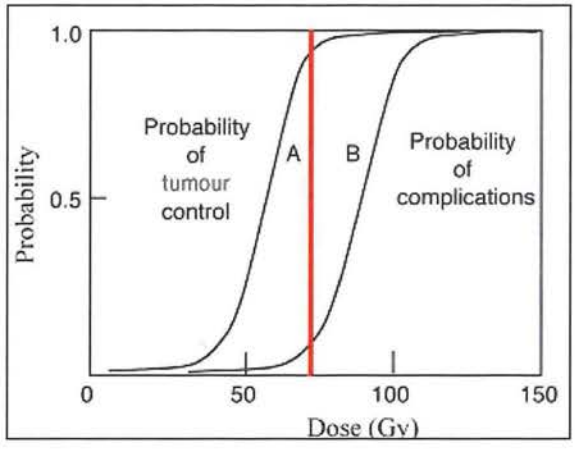

Figure 1.3. An example of the therapeutic ratio plot where curve A shows the probability of tumour response, while curve B shows the probability of complications of the normal tissues, courtesy of (Podgorsak 2005). The red line illustrates the suitable treatment dose.

This aim is achieved by controlling the shape of dose distribution (ICRU 2007, Mayles, Nahum et al. 2007) within the irradiated volume. Selection of an optimum type of radiation therapy and treatment planning depend on many factors (Podgorsak 2005) such as: cancer type and stage, tumour size, tumour depth, and location (Chao, Perez et al. 2011).

Further improvements in radiotherapy require research in different areas, such as studies of the biological effects, for example, the radiation damage to DNA and the other sites in a cell which can be targeted and may cause cell death, as well as the interaction between the radiation and matter (e.g. better knowledge of low energy cross-sections) (Podgorsak 2005). Furthermore, the development of novel tools for quality assurance (QA) is essential to accurately deliver and monitor the radiation dose to a patient (Rosenfeld, Cutajar et al. 2006).

There are many forms of radiation therapy used in cancer treatment. This thesis will concentrate on dosimetry applications for the special form of radiotherapy, known as targeted alpha particle radiotherapy

1.3 Radiation Dosimeters

In order to determine the accuracy of dose delivery, various dosimetry techniques can be used before and during treatment.

A dosimeter is defined as a device or instrument which provides a measurement of the average absorbed dose that is deposited in the dosimeters volume by ionizing radiation. The dosimeter and the reader are called the dosimetry system (Podgorsak 2005). Specific dosimetry design depends on one of the four requirements: the accuracy of the absorbed dose determination, the measuring system's sensitivity, the energy and dose-rate dependence and the spatial resolution (ICRU 2007).

An ideal dosimeter should have the following properties:

1. The imparted energy distribution is measured for the material of interest (e.g. tissue equivalent materials).
2. It measures all ranges of the imparted energies.
3. It can be used for a wide range of irradiation volumes.
4. The resulting signal is proportional to the imparted energy.

5. It has only a small background noise (ICRU 1983).

For any dosimeter, there are many properties used to judge the performance of the dosimeter, for example:

1. Predictability of the measurements under the similar conditions.
2. Accuracy of the measured values relative to the true values.
3. Linearity of readings as they need to be proportional to doses.
4. Dose rate dependence.
5. Energy dependence.
6. Directional dependence.
7. Temperature dependence.
8. Spatial resolution (Podgorsak 2005).

There are many types of dosimeter systems including an ionisation chamber, thermoluminescense dosimeters (TLD), gel dosimeters, semiconductor dosimeters, films and others. The WHO recommends, that *in vivo* dosimetry is carried out on patients (Thwaites and Williams 2000). There are two major *in vivo* dosimetry groups: thermoluminescense dosimetry and semiconductor dosimetry. Each of these groups contains several different types of dosimeters. This proposal will focus on semiconductor dosimetry and, where applicable, its application to microdosimetry.

1.3.1 Semiconductor Dosimeter

Semiconductors represent a group of elements from column IV of the Periodic Table (David 1990). Semiconductor materials are elements with highly desirable characteristics such as high density, low energy requirement to produce an electron-hole pair, have the ability to work in

unbiased or biased mode and are efficient even under low voltage (Rosenfeld, Cutajar et al. 2006). Furthermore, they are attractive to use for dosimetry because they offer instant and high readout speed, and the possibility of having a detector and a reader assembled in a single unit (Lutz 2007). The readings are performed in real-time and no post processing is required unlike TLD and gels dosimeters.

Furthermore, compound semiconductors which mainly use a combination of the elements located in column III and V of the Periodic Table such as GaAs or InP can also be manufactured (David 1990) and used in dosimetric applications.

1.3.1.1 PN Junctions Diodes

Semiconductor diodes are used for radiation dosimetry because of the small volume, high sensitivity (almost 18,000 times the sensitivity of an ionisation chamber), high spatial resolution, real-time readout and air pressure independence (Thwaites and Williams 2000, ICRU 2007, Mayles, Nahum et al. 2007). Measured readings are accurate (Mayles, Nahum et al. 2007). Usually, diodes use silicon as a substrate, which is described as being n-type and of light density. It is then implanted with a high density of p-type material (Podgorsak 2005, Mayles, Nahum et al. 2007).

The PN junction is made from a combination of materials from column III and column V of the Periodic Table of Elements as shown in Figure 1.4. Materials from column III are rich in electrons and are called n types or donors. These include materials such as phosphorus and arsenic. The elements from column V are rich in holes and are called p types or acceptors. These include materials such as boron and gallium.

After this combination, an area between the two types is generated, called the depletion layer (i.e. the PN junction) resulting from recombination of electrons and holes in this area, as illustrated in Figure 1.4.

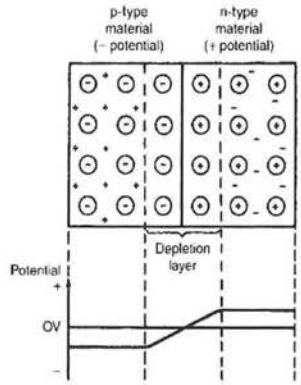

Figure 1.4. PN junction's depletion layer, courtesy of (Bird 2007).

1.3.1.2 Principle of PN Junction Diode Detectors

If the radiation passes through a diode, an electron-hole pair is generated in a depletion layer. The minority charge carriers are formed on the detector surface where there are likely to diffuse to the depletion layer due to the intrinsic potential which generates an adverse current to the diode (Figure 1.5). A short-circuit mode (current) is used because it provides the detector with a linear relationship between the charge carriers produced and the dose (Thwaites and Williams 2000). It is also used to minimize the leakage (Podgorsak 2005, Mayles, Nahum et al. 2007).

1.3.1.3 General characteristic of PN Junction Diode Detectors

a) Background Signal

Diodes have dark current because of the charge particles generated by thermal effects. This can cause problems when measuring low doses and low dose rates. The background signal is

dependent on temperature. Some diodes give high currents with rising temperature even when the accumulated dose is low. Therefore, high temperature will not only cause background noise, but it will also increase the accumulated dose. Background signals can change by up to 4 mGy per minute between room and patient's body temperatures (Thwaites and Williams 2000, Mayles, Nahum et al. 2007).

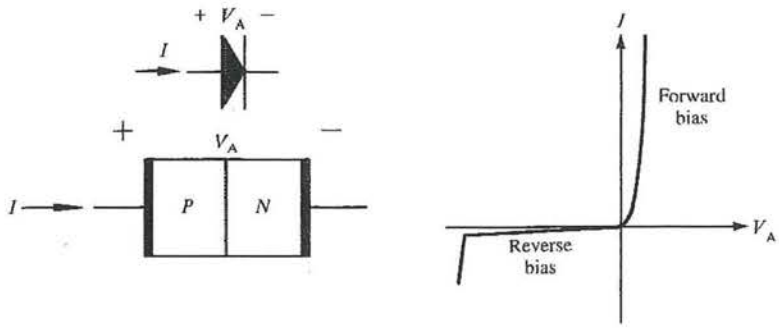

Figure 1.5. The P-N junction diode polarity, courtesy of (Neudeck 1989).

b) Temperature Effects

The temperature affects the charge carrier mobility as well as the number of traps in the detector and decreases the resistance. Moreover, unlike the usual behaviour where the sensitivity is increased with increasing temperature, the diode detectors sensitivity decreases when temperature increases (Thwaites and Williams 2000, Mayles, Nahum et al. 2007).

c) Detection Threshold

The detection threshold is the minimum dose detectable by a detector. For diodes, it depends on the doping level of the semiconductor detector and the pre-irradiation dose. The detection threshold for a commercial diode is between 0.1 cGy and tenths of cGy (Mayles, Nahum et al. 2007).

1.3.1.4 Advantages and Disadvantages of the PN Junction Diode Dosimetry

The advantages of PN Junction diode dosimetry are their small size, sensitivity, the ability to assemble the detector and the reader into a single piece, instant readout and no need for external bias voltage.

The diode disadvantages include calibration and sensitivity changes as a function of the temperature and with the accumulated dose (Podgorsak 2005). Diodes are also energy, dose rate and orientation dependent. Furthermore, diode detectors have high threshold in comparison to TLD threshold which is between 1 to 40 μGy depending on the TLD material (Mayles, Nahum et al. 2007).

1.4 Microdosimetry

Microdosimetry is a technique of measuring absorbed dose at a micrometre level (i.e. the cellular level). In microdosimetry, a quantity called lineal energy, y, is used rather than the linear energy transfer. This quantity is the energy imparted into the matter of volume, ε, by a single energy deposition event to the mean chord length, $\bar{l}$, in a volume and its unit is keV/μm or J/m (ICRU 1983, Attix 1986), as is given in equation (1.5):

$$y = \frac{\epsilon}{\bar{l}} \left(\frac{keV}{\mu m}\right) \qquad (1.5)$$

Where the mean chord length is the mean length of randomly oriented chords in a volume.

The lineal energy transfer depends on the radiation type (ICRU 1983) and the energy imparted ε in a volume, and is the sum of all energies, ε_i, in that volume in eV (Bardies and Pihet 2000).

In addition, the distribution function, F(y), is used to describe the probability that the lineal energy is equal or less than y. Therefore, the density of probability, f(y), is given by the equation (1.6):

$$f(y) = \frac{dF(y)}{dy} \tag{1.6}$$

f(y) is called the lineal energy distribution and is independent of the absorbed dose and dose rate (ICRU 1983).

The dose probability density d(y) is then given by equation (1.7):

$$d(y) = \frac{dD(y)}{dy} \tag{1.7}$$

Where d(y) is the fraction of the absorbed dose that is delivered with lineal energy equal or less than y (ICRU 1983).

1.4.1 Microdosimetric Spectra

A microdosimetric spectrum illustrates the relationship between the lineal energy, (y), and yd(y), as is shown in Figure 1.6. A number of parameters affect the resultant microdosimetric spectra such as the particle type (e.g. its track length distribution, LET distribution and straggling) and the volume size (ICRU 1983). From microdosimetric spectra, the contributions of different radiation types has been identified (Sabol and Weng 1995).

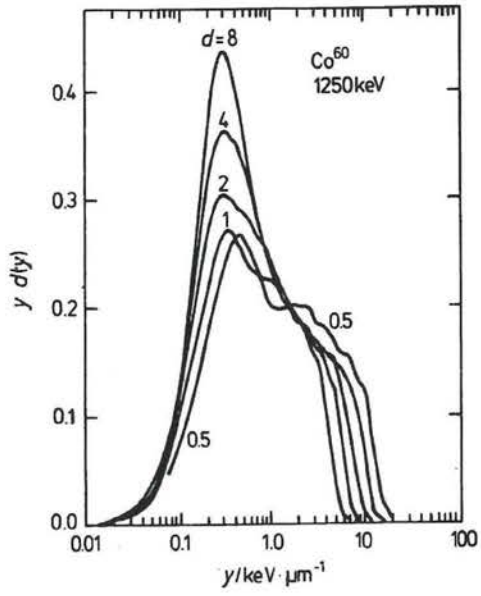

Figure 1.6. Microdosimetric spectra for ^{60}Co gamma radiation on a logarithmic scale, courtesy of (ICRU 1983).

Microdosimetric spectra can be obtained by experimental or calculation methods. Both methods can be applied to γ-rays with energies between 50 keV and 5 MeV and for thermal and fast neutrons with energies lower than 10 MeV (ICRU 1983). For these radiation types, the methods are applied without any corrections, but other radiations types or other energy ranges require correction factors to be applied. The calculation methods for a known interaction cross-section for a given particle of certain energy are more accurate than experimental measurements and take less time (ICRU 1983). On the other hand, even though the calculation is more accurate than the experiment, it usually contains a simplification, which leads to uncertainties of the results.

The calculation methods can be divided as follows:

Analytical calculations: these are mostly applied to neutrons (ICRU 1983) and the main assumption is that of radiation equilibrium, meaning that the secondary charged particles are produced with equal probability through the whole irradiated volume.

Monte Carlo calculations: these are applied to fast neutrons, electrons and ions. The main assumption of radiation equilibrium is assumed as well. In Monte Carlo calculations, many physical effects, such as energy loss straggling and delta ray production, can be taken into the account (ICRU 1983).

The shapes of microdosimetric spectra depend on a number of factors for each single event, namely distribution of track lengths, distribution of linear energy transfers, and the energy loss straggling per collision and the number of primary collisions. These factors are common for both experimental and calculation methods, but in case of experimental methods using a proportional counter, there are additional factors such as the number of ions produced per unit energy, deposition factors known as Fano-fluctuations (ICRU 1983) and others.

The next section discusses some studies in the field of semiconductor dosimetry and microdosimetry devices. Number of these devices can be used for both imaging (i.e. autoradiography) and dosimetry.

1.5 Current Semiconductor Dosimeters and Microdosimeters

1.5.1 Medipix

The Medipix detector was developed at CERN in the 1990s, and was developed for tracking of high energy particles by using a hybrid silicon pixel detector (CERN 2011). At present, there are multiple generations of Medipix, which are in chronological order are Medipix1, Medipix2, Timepix and Medipix3.

I) Medipix1

The Medipix1, also called Photon Counting Chip (PCC) provides noise-free single photon counting. In order to minimize blurring in the image, a sensor layer consisting of chip of Si or

GaAs is bump-bonded to an electronic layer of complementary metal–oxide–semiconductor (CMOS) which provides direct photon conversion to charge (CERN 2011). The radiation generates a positively charged hole in the sensor layer, which is then collected in the electronics layer. If the charge produced by incoming particles is higher than the threshold, the event is counted. For each pixel, there is a comparator with three bits to ensure that the threshold distribution is homogenous through the whole chip (CERN 2011). The Medipix1 properties are: each chip contains 64 × 64 pixels, each pixel has an area of 170 × 170 μm^2, the active area of the chip is approximately 1.2 cm^2, the maximum count rate is almost 2 MHz and the minimum threshold that can be collected is ~ 1500 e^- (that equals to ~5.5 keV energy deposition in a Si sensor). For each pixel, there is a fifteen bit counter capable of storing up to 32767 single events and the acquisition time is variable.

A study with a narrow beam and "edge" image contrast was done by Sinor et al. (2003) (Sinor, Jakubek et al. 2003) to investigate the charge sharing (charge sharing is an event in a single pixel where charge generated is shared with surrounding pixels) between pixels and to examine the spatial resolution of Medipix1 Si and GaAs pixel devices. Two types of radiation were investigated: X-rays (from an X-ray tube with voltage < 35 kV, Mo anode) where the narrow beam was applied using a small hole in a thin lead foil, and using a Cd filter and alpha particles (from decay of ^{241}Am isotopes). A special point α-source was produced by electrostatic collection technique of Rn-220 daughter on a tip of tungsten needle (needle diameter was 50 or 100 mm) and a collimated point alpha source was obtained by using a plastic chromatography capillary (capillaries of 300 and 500 mm diameter to collimate the special point α-source)).

The results indicate the pixel-sharing behaviour differs for photons of different energies and for alpha particles collimated with collimators of different capillary diameter. For photon

beams with energy of 35 kV, the charge sharing can be neglected unlike for alpha particles which are detected in a cluster of pixels (cluster diameter ≈ 2.5 pixels). The measurements have been found in this study to have position precision of 150 μm for both X-rays and heavy charged particles (same as pixel size) and it affected by the parallax effect (Sinor, Jakubek et al. 2003).

II) Medipix2

Medipix2 was developed in late 1990s also at CERN (CERN 2011). The use of the sub-micron CMOS, enabled the pixel size to be decreased and therefore resulted in the increased number of pixels per chip. The advantage of the Medipix2 was the enhancement of the pixel cell function and the reduction of pixel size (CERN 2011). A development extension of Medipix2 is Timepix (2004) that not only counts hits on the detector but can measure arrival time of the first particle to the chip and also record time over threshold (meaning it can measure the energy of the particle).

The Medipix2 has the following properties: each pixel has size equal to 55 μm^2, the chip is effective for positive or negative charge and the energy to be detected can be selected to ensure uniform performance.

1.5.2 Microdosemeter based on Silicon on Insulator (SOI) PN Junction

The early tests of silicon detectors were based on bulk silicon. This type of microdosimeter was tested at the Harper Hospital in Detroit (USA). The experiment was done using a water phantom with fast neutron therapy and microdosimetric spectra of the secondary recoil protons were measured. The disadvantage of using the bulk silicon lies in the fact that it may lead to charge diffusion between the p-n junction between the silicon and the bulk silicon, affecting the sensitive volume (Rosenfeld and Bradley 1999).

SOI is a microdosemeter based on silicon on insulator (SOI) p-n junction array (i.e. using electrical isolation between silicon cells) as shown in Figure 1.7. It has the advantages of small size with no requirement for gas or high voltage power supply compared to proportional counter, ease of conversion from measured amplitude spectra to tissue-equivalent microdosimetric spectra, the possibility of merging the sensor with the readout electronics together in the same chip and the diffusion effects are minimised as the sensitive volume is in the silicon layer (Rosenfeld and Bradley 1999). Furthermore, it measures a full beam without any pile up effect and it has high spatial resolution (Rosenfeld and Bradley 1999). It is suitable for dosimetry applications in fast neutron therapy (FNT) and boron neutron capture therapy (BNCT), proton therapy (PT) and for personal radioprotection (Rosenfeld and Bradley 1999). The SOI microdosimeter has been tested in Northeastern Proton Therapy Center, Boston and in Proton Medical Research Center, Tsukuba with 230 MeV and with 250 MeV proton beams, respectively. The microdosimeter has a good spatial resolution, especially around the proton Bragg peak when compared to a proportional gas counter (Rosenfeld, Bradley et al. 2000).

Fujitsu Research Laboratories Ltd (Japan) manufacture microdosemeters from SOI wafers bound with 2, 5 and 10 μm sensitive layers. Each chip consists of two types of p-n junction arrays with dimensions $100 \times 100\ \mu m^2$ (with 150 diodes) and $10 \times 10\ \mu m^2$ (with 4800 diodes) which are connected in parallel (Rosenfeld and Bradley 1999).

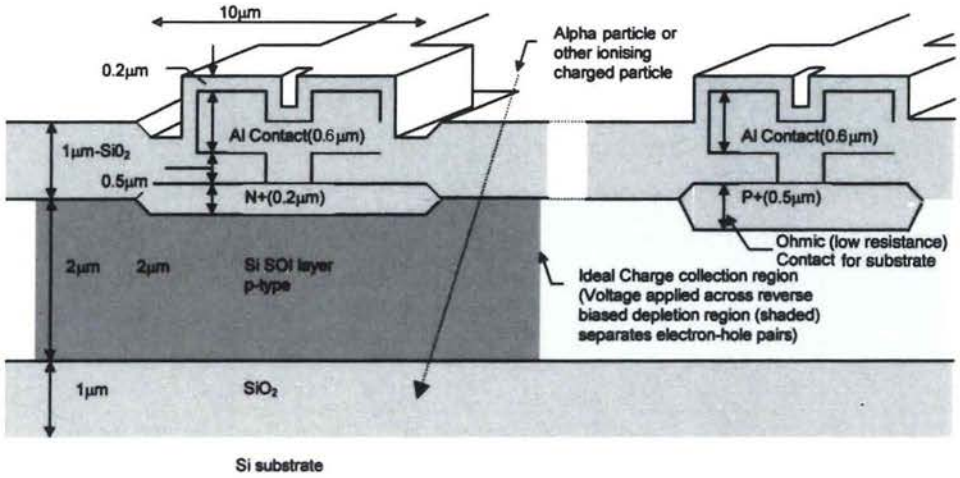

Figure 1.7. Schematics of a SOI microdosemeter, courtesy of (Rosenfeld and Bradley 1999).

The proton beam energy in Proton Medical Research Center was adjusted to be suitable for medical applications from 500 MeV to 200 MeV by using carbon based degraders and a filter. Also in Northeastern Proton Therapy Center, the proton beam was adjusted to a dose rate of 200 cGy/min. Microdosimetric spectra for both experiments are shown in Figure 1.8 and Figure 1.9 respectively.

Rosenfeld and Bradley (1999) (Rosenfeld and Bradley 1999) also tested the SOI microdosemeters for FNT, BNCT and PT as well as mixed radiation fields of high and low LET were examined as well. The SOI microdosimeter's physical characteristics included: sensitive volume thickness of 2 μm, the chip was in a ceramic dual in line (DIL) package, and this package was lodged in a $1 \times 1 \times 7.5$ cm^3 Perspex probe. A low voltage (0-10 V) was used for the readout electronics and a PC based multichannel analyser (MCA) was used to measure the amplitude spectra of deposited energy from the secondary charged particles, produced in a $15 \times 15 \times 15$ cm^3 Perspex phantom. The results confirmed that this microdosemeter could measure a lower lineal energy limit of 0.1 $keV.\mu m^{-1}$ (Rosenfeld and Bradley 1999).

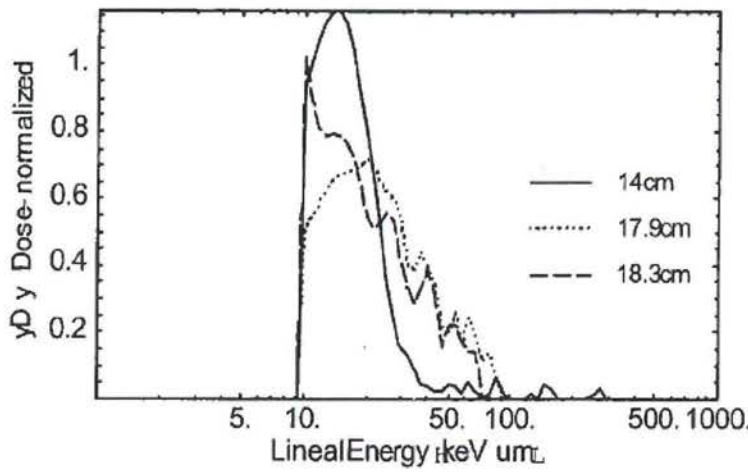

Figure 1.8. Microdosimetric spectra of a 200 MeV proton beam at different depths in a Lucite phantom (proton range ≈ 18 cm) obtained in the Proton Medical Research Center in Japan, courtesy of (Rosenfeld, Bradley et al. 2000).

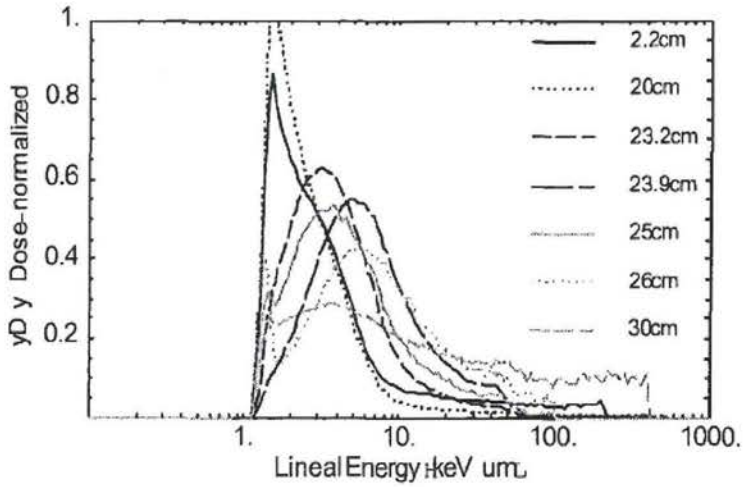

Figure 1.9. Microdosimetric spectra of a 191.5 MeV proton beam at different depths in a water phantom (proton range ≈ 23.7 cm) obtained in the Northeastern Proton Therapy Center in Boston, courtesy of (Rosenfeld, Bradley et al. 2000).

1.5.3 Printed Circuit Silicon-Board Semiconductor Detector for Personal Dosimeter

Ishikura et al., (2008) (Ishikura, Aoyama et al. 2008) developed a small semiconductor detector composed of a radiation sensor made of silicon, an electronic circuit for analogue amplifier and

a circuit for sensor bias filter, all on a single silicon circuit board. This detector has a size of 14 × 6 × 3 mm^3. The silicon circuit board is a silicon substrate with dimensions of 14 × 6 × 0.5 mm^3. Sixteen built-in resistors, two built-in capacitors and thin resistive, insulative and conductive films are set on the silicon substrate as illustrated in Figure 1.10 and Figure 1.11.

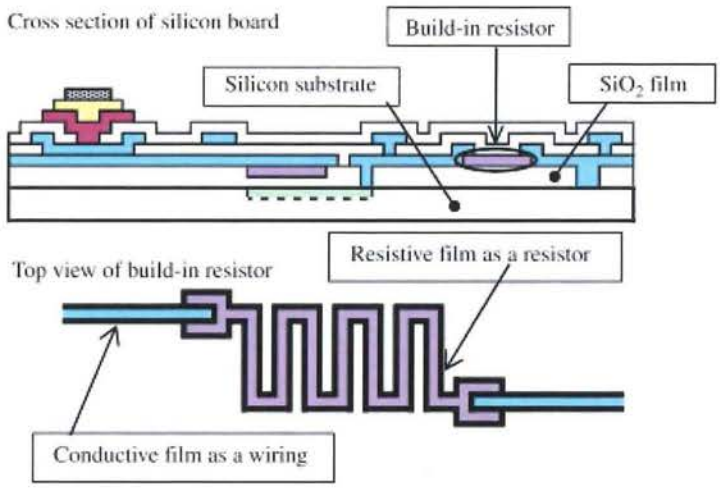

Figure 1.10. Cross section of a silicon board with the built-in resistor, courtesy of (Ishikura, Aoyama et al. 2008).

This detector is 85% smaller than the commercial detector, which is composed of the same sensor and the same circuit with a plastic circuit board and covered with a ceramic case produced by Fuji Electric System Co. Ltd. The physical characteristics of the commercial detector are 103 × 55 × 15 mm^3 and 100 g for a gamma ray dosimeter and 120 g for a multifunctional dosimeter (measures gamma rays, beta rays, and fast and thermal neutrons).

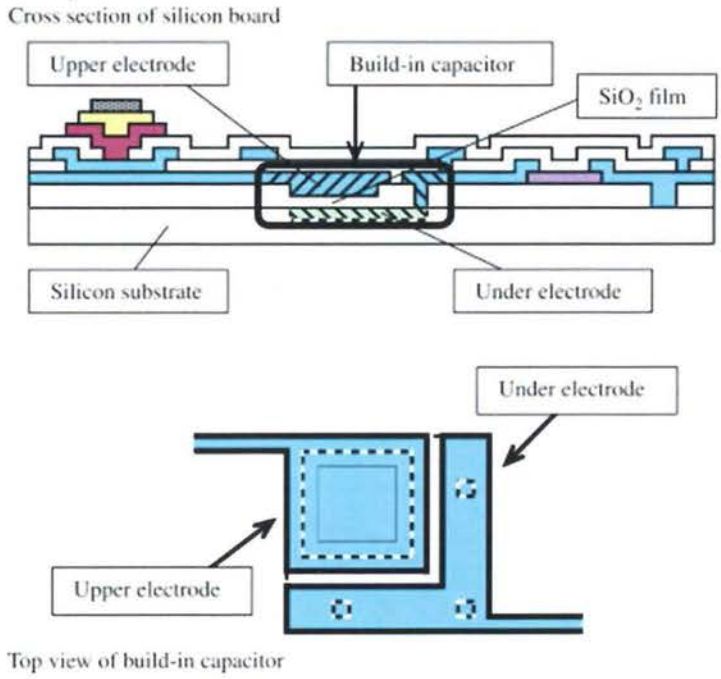

Figure 1.11. Cross section of a silicon board with the built-in capacitor, courtesy of (Ishikura, Aoyama et al. 2008).

The built-in resistors and built-in capacitors in the silicon circuit board are smaller than they are in the plastic board. In addition, the silicon circuit board is used for the analogue amplifier, where it was originally used as a digital circuit. Furthermore, the silicon sensor is set on the silicon board directly with a conductive silver paste and without using the ceramic case.

The new detector was investigated using ^{241}Am, ^{57}Co, ^{137}Cs, ^{60}Co gamma rays and X-rays in the range of 49-157 keV to study the energy response that corresponds to a personal dose equivalent (Hp (10)), in mSv and its linearity to dose equivalent rate (the personal dose equivalent, Hp (d), is defined as the dose equivalent in soft tissue at the depth, d, below a specific point, p, (Podgorsak 2005)). In order to estimate the energy response, the new detector was attached to an acrylic phantom and energy spectra were measured for 60 keV ^{241}Am, 122

keV ^{57}Co, 662 keV ^{137}Cs and 1250 keV ^{60}Co gamma rays (Figure 1.12). In addition, the energy spectra for X-rays ranging from 49 to 157 keV were also measured.

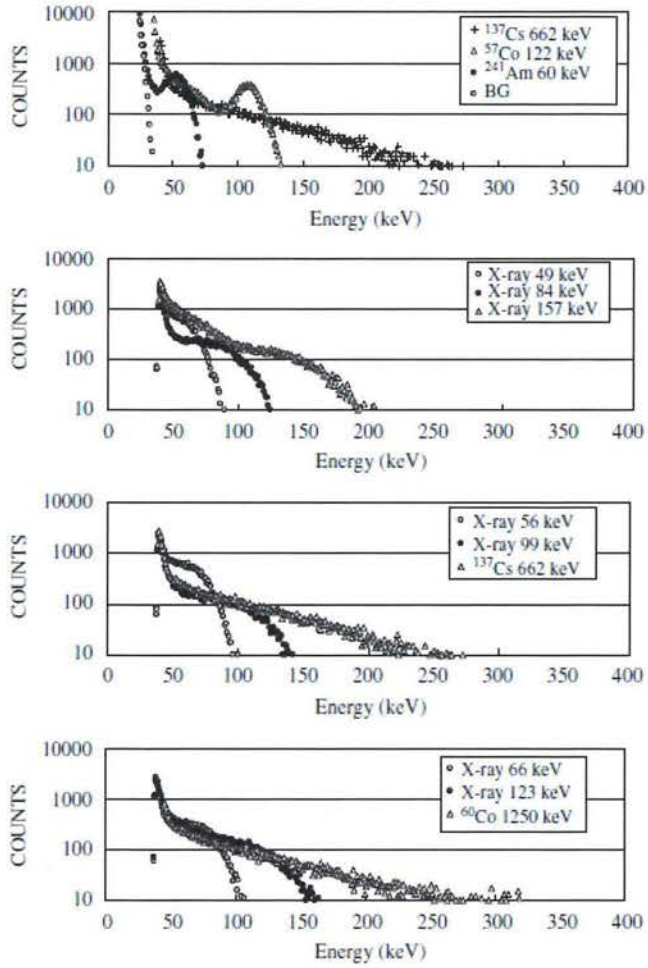

Figure 1.12. Pulse height spectra for different γ-ray and X-ray sources measured with the newly developed silicon circuit board detector, courtesy of (Ishikura, Aoyama et al. 2008).

The results showed peaks for ^{241}Am 60 keV γ-rays and the spectra were linearly proportional for ^{57}Co 122 keV γ-rays. The X-ray spectra of various energies had continuous distribution.

The linearity of detection efficiency to dose equivalent rate for different distances between the detector and the gamma source (to provide different source intensity) was measured. A good linearity between 1 and 500 mSv/h was seen (Figure 1.13).

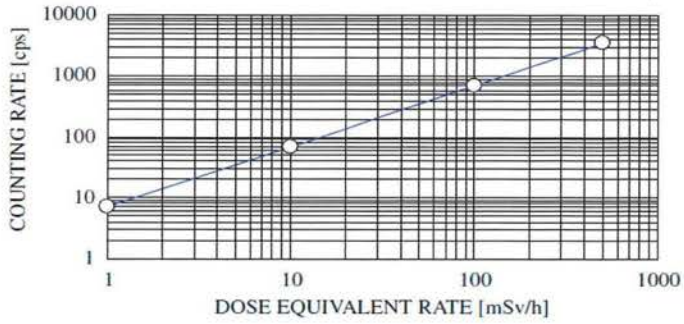

Figure 1.13. Linearity of detection efficiency to dose equivalent rate of newly developed silicon circuit board detector, courtesy of (Ishikura, Aoyama et al. 2008).

The comparison between the commercial silicon circuit board detector and the new developed detector is shown in Table 1.1. The new device is smaller, also the relative detection efficiency is slightly higher than that of the commercial detector and has lower electrical noise.

Table 1.1.Comparison between newly developed silicon circuit board detector and commercial detector (NRY), courtesy of (Ishikura, Aoyama et al. 2008).

	Developed detector	Commercial detector
Relative size	0.15	1
Relative detection efficiency	1.02	1
Noise level (keV)	40	41
Circuit current (mA)	0.3	0.3

1.5.4 Metal Oxide Semiconductor Field Effect Transistors (MOSFETs)

MOSFETs are dosimeters based on metal oxide semiconductor field effect transistors. MOSFETs work by producing an electron-hole pair in SiO_2 after radiation exposure. These dosimeters are used in *in vivo* dosimetry because of instantaneous readout, energy and dose rate independence. The dose can be also stored for later use. The detector is dose rate independent up to 10^8 Gys^{-1} and the sensitivity can be changed by changing the bias (Rosenfeld, Cutajar et al. 2006). In addition, it has an excellent spatial resolution. It requires a bias voltage during irradiation. When the radiation penetrates the oxide, electron-hole pairs are generated. These positive charges are trapped, changing the threshold voltage. The relationship between the threshold voltage and the absorbed dose is a linear function (Podgorsak 2005). MOSFETs have disadvantages of temperature dependence and non-linearity of response (Podgorsak 2005).

Two systems used for MOSFET dosimetry in radiation therapy are: the commercial system (Thomson Nielson MOSFETs) and the MOSFETs online system (MOSPLOT DAQ hardware and Software) developed at the University of Wollongong. This clinical dosimetry system is considered to be the first real-time application of MOSFETs (Rosenfeld, Cutajar et al. 2006).

1.5.5 Miniature Semiconductor Detector

Rosenfeld et al. (2006) (Rosenfeld, Cutajar et al. 2006) created a miniature semiconductor detector for personal dosimetry and *in vivo* dosimetry in radiation therapy. This miniature semiconductor detector is a combination of metal oxide semiconductor transistor in a spectroscopy mode and silicon p-n junction detector. It is sensitive to only neutron radiation. Unlike other semiconductor detectors, which operate in "ionising energy loses (IEL)" mode (Rosenfeld, Cutajar et al. 2006), such as diodes (in current and spectroscopy modes) and MOSFETs, this miniature semiconductor detector (p-i-n diodes) operates in "non-ionising

energy loses (NIEL)" (Rosenfeld, Cutajar et al. 2006) mode which is for neutron dosimetry. The miniature semiconductor detector measures the energy deposition by the secondary charged particles produced by neutrons.

For personal and *in vivo* dosimetry, a silicon p-n junction with a different converter is used along with a processor to convert the data to the equivalent dose. To detect neutrons, a combination of convertors is used namely, polyethylene converter for fast neutrons, ^{235}U convertor or ^{6}Li and ^{10}B converter for thermal neutrons (Rosenfeld, Cutajar et al. 2006).

For *in vivo* dosimetry, a new dosimetry technique called spectroscopical dosimetry (developed from high energy-resolution nuclear spectroscopy) was developed as modern silicon detectors can measure the absorbed dose for a very low dose rate, as well as the relative biological efficiency (Rosenfeld, Cutajar et al. 2006).

Rosenfeld et al. (2006) (Rosenfeld, Cutajar et al. 2006) applied spectroscopic dosimetry for low energy photons (15 -35 keV) in prostate brachytherapy using developed urethral alarm probe consists of a Si-mini-detector connected to an amplifier and discriminator. The probe is small enough to be inserted within the urethral catheter. For clinical purposes, this application has multiple alarms, which can inform the medical staff to avoid overdosing.

1.6 Motivation and Thesis Structure

1.6.1 Motivation

The relationship between the characteristic of the radiation hitting the tissue and affected targets plays an important role in estimating the effect of targeted therapy.

Radionuclide dosimetry is difficult and complex to accurately determine due to a number of factors including the physical properties of the radionuclide including radiation type and half-life, and biological transit time (uptake and clearance). Additionally on a cellular level, the dose can be quite heterogeneous depending on the spatial distribution of the radioisotope in the

tumour. As a result, there is need for real-time microdosimetry of alpha particles to determine the radiation dose delivered to the tumour is this stage for TAT 2.

The literature shows that there is lack of information related to the use of semiconductor detectors for measurements of subcellular damage, such as that occurring in targeted alpha therapy. The knowledge and measurement of energy deposited by α-particles is required to accurately estimate the absorbed dose on a cellular level and to determine radiobiological endpoints. This knowledge will then assist with development of dosimetry protocols and dose prescription for TAT. The ability to accurately measure cellular damage resulting from localised alpha particle irradiation will allow to determine what radioisotope doses should be injected to patients to achieve tumour control while minimising the damage to normal tissues.

1.6.2 Project Objectives

Objective 1.

To study the performance of the Timepix radiation detector and its physical characteristics such as reproducibility, accuracy, dose linearity and its performance for different radiation types and energies.

Objective 2.

To investigate the use of Timepix for autoradiography to measure biodistribution of the Th-227 isotope in tumour sections.

Objective 3.

To investigate Timepix suitability for use in clinical microdosimetry for targeted alpha therapy as well as the conditions affecting the calibration and use.

1.6.3 Thesis Outline

This thesis includes combination of the five papers listed on page iv. These papers present investigations that have been performed in order to achieve the objections of this thesis.

Chapter 2 contains a brief overview of targeted alpha therapy. Research was conducted to investigate alpha emitters along with chelates and suitable specific proteins to target different types of cancers. The review focuses on Th-227 and Ra-223 alpha emitters and their application in targeted alpha therapy. Some important pre-clinical and clinical trials are also presented.

Chapter 3 contains a literature review of Timepix radiation detector. This chapter is based on two submitted literature review papers; one about the technical aspects of Timepix, including general characteristics, acquisition modes and calibration. The second papers briefly reviews possible applications of Timepix relevant to medical physics, e.g. Timepix as a photomultiplier, use for stopping power measurements, neutron detection, hadron therapy and brachytherapy and targeted alpha therapy.

Chapter 4 investigates the use of Timepix in dosimetry, characterising its physical properties such as reproducibility, accuracy, dose linearity and energy dependence, in addition to Timepix requirements for dose calibration. Radioactive sources from the Medical Physics Department at the Royal Adelaide Hospital such as Iodine-125 and Strontium-90 were used. In addition, superficial Gulmay D3150 X-ray unit at the Royal Adelaide Hospital with beam HVLs between 0.5 to 3 mm Al and peak voltages between 40 to 100 kV was used for the measurements.

Chapter 5 discibes the applications of Timepix as a spectrometer using Am-241, Ra-223, Pu-223 and Fe-55 sources.

Furthermore, a brief investigation of Timepix for imaging applications is also presented using different radiation sources and different objects.

Chapter 6 discusses the details of using Timepix for autoradiography in Targeted alpha therapy using Lewis lung tumour sections from mice treated with or without chemotherapy and then

administered ^{227}Th-labelled antibody (DAB4). Furthermore, this chapter has the results of uptake measurements of Cr-51 by A549 cells (lung carcinoma cell line) for different pH levels of the medium.

Chapter 7 discusses the design of transmitted α-particle microdosimetry technique. A549 cells and Ra-223 source were used to evaluate the cell damage (DNA double strand breaks) induced by α-particles and to determine absorbed dose at a culler level. The results were examined and correlated with biological dosimetry (γ-H2AX assay) and Monte Carlo simulations using SRIM program.

Chapter 8 contains conclusions and future work to further enhance the transmitted α particle microdosimetry design.

Chapter 2

Targeted Alpha Therapy

2.1 Introduction

According to the World Cancer Report, it is expected that by 2030 the number of new cases of cancer will reach more than 20 million, and there will be 17 million deaths from cancer per annum (WHO 2008, WHO 2014). In developed countries, 25 to 30 per cent of the population will develop cancer at some stage in their life (Wambersie, Pihet et al. 1990). A cancer patient can be treated using different modalities: surgery, chemotherapy and radiotherapy, or a combination of more than one modality. Radiation therapy is used for almost half of all cancer patients (Wambersie, Pihet et al. 1990) and includes many types of treatments, (using either direct or indirect ionizing radiation) such as X-ray therapy, electron therapy, light and heavy ion therapy and neutron therapy (Podgorsak 2005).

Most of the external radiotherapy beam techniques are beneficial in treatment of localized disease. However, the primary cause of cancer death is the disseminated (or systemic) disease requiring different treatment and targeting approaches.

Targeted radionuclide therapy is a radiation therapy technique that takes advantage of the development in radionuclide production and pharmaceuticals that can specifically target tumours (Mayles, Nahum et al. 2007). Targeted radionuclide therapy directs doses of radiation (which can be high linear energy transfer (LET) radiation) to individual tumour cells, while reducing the dose to off-target normal tissues (Allen 2006, 2007, Mayles, Nahum et al. 2007). This is achieved by having a cancer-targeting protein (commonly peptides, monoclonal antibodies (mAbs) or derivatives of mAbs) labelled with a radionuclide, knowing as radioimmunoconugate. This radioimmunoconugate (RIC) then attaches itself to a specific antigen on a cancer cell. The decaying radioisotope emits radiation directly into the tumour cells, causing localized radiation damage, as shown in Figure 2.1 (Wheldon and O'Donoghue 1990). Many studies have been undertaken on targeted radionuclide therapy, investigating the process from different points of view such as pharmacology, biology, dosimetry/microdosimetry, radiation production and others (Wheldon and O'Donoghue 1990, Roeske and Stinhcomb 1997, McDevitt, Sgouros et al. 1998, Sgouros, Ballangrud et al. 1999, Allen, Raja et al. 2004, Mather and Britton 2004, Sgouros 2008, Sgouros, Roeske et al. 2010, Kim and Brechbiel 2012, IAEA 2013, Seidl 2014, AL Darwish, Staudacher et al. 2015, Fichou, Gouard et al. 2015). This chapter will highlight briefly some of the important studies in targeted radionuclide therapy and the results of some of the trials that have been conducted. Further, this chapter will focus on targeted alpha therapy (TAT); and specifically on the application of Th-227 and Ra-223 radionuclides in TAT.

2.2 Targeted Radionuclide Therapy

Selection of a specific radionuclide for targeted therapy requires many physical and biological studies (Mayles, Nahum et al. 2007). An ideal radionuclide must have well-characterised

properties, including a good knowledge of the physical and biological half-lives of the emitted particles types and their energies and ranges and how these compare with the size of the tumour (Wheldon and O'Donoghue 1990, Reilly 2010). Other factors that must be taken into account are radionuclide's chemical properties (i.e., stability), the possible administration route and uptake (according to Mather and Britton, 1-2% of the injected dose will be taken up by the tumour and the rest be distributed in normal tissue (Mather and Britton 2004)) and distribution of the radionuclide between the tumour and the other organs (Mather and Britton 2004). Pharmaceutical studies have an important role in identifying a carrier (e.g. protein/monoclonal antibody) that has high uptake by the tumour and low uptake in the healthy organs and in developing an agent (i.e. chelator) to combine the carrier and the radionuclide which known as the radioimmunoconjugate (RIC) (Wheldon and O'Donoghue 1990).

In targeted radionuclide therapy, the instantaneous tumour dose-rate can vary significantly depending on the injected activities, radioimmunoconjugate uptake, tumour size and others. For tumours with low alpha/beta ratios (alpha/beta ratio gives the dose where cell killing, due to both linear and quadratic components of the linear quadratic model, is equal (Podgorsak 2005)), the dose-rate effects on cell survival could be significant. According to (Wheldon and O'Donoghue 1990), depending on the dose-rate, the following occurs:

a) High dose-rate: Cell cycle progression is inhibited and the cells are killed proportionally to the dose delivered.

b) Medium dose-rate: Limited cell cycle progression can occur with a potential block in G_2 (G_2 is the postsynthetic phase where the cell prepares for division) (Marcu, Bezak et al. 2012).

c) Low dose-rate: Cell cycle progresses and repair/repopulation are possible.

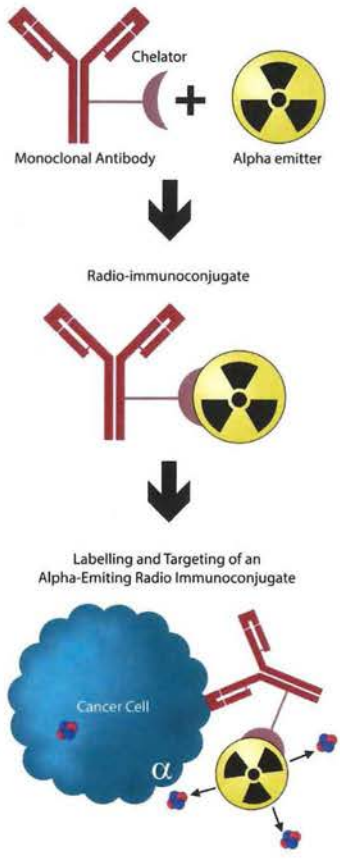

Figure 2.1: Targeted alpha therapy as an example of targeted radionuclide therapy (2007).

Radionuclides that emit β-particles and α-particles are attractive for use in targeted therapy due to their physical properties. For instance, the limited range of these particles in tissue is unlike that of the penetrating X-ray and γ-ray radiation (Reilly 2010). Some of the radioactive sources that are used for radionuclide targeted therapy have been summarised by Reilly in Table 2.1 (Reilly 2010).

Another group of potential radionuclides suitable for use in targeted therapy are those that emit Auger electrons. An Auger electron is emitted from an atom when the inner-shell vacancy is filled with another electron. These emitters can be used for targeted therapy when they are

close to the nucleus due to the short range of most Auger electrons (≈1 μm) and their high cytotoxicity (LET ≈ 100 keV/μm) (O'Donoghue and Wheldon 1996, Mayles, Nahum et al. 2007, Reilly 2010). Auger electron energies can vary between several of eV and tens of eV (O'Donoghue and Wheldon 1996) (< 30 keV in (Reilly 2010)). The radionuclides that only emit Auger electrons have the advantage of only irradiating the targeted cells that the emitter is bound to (Reilly 2010). This makes them an excellent choice for pre-angiogenic tumours, cell clusters or micro-metastasis. Some Auger electron emitters also emit γ-rays and X-rays, which can be used for imaging at the same time as for targeted therapy, e.g. ^{125}I (Wheldon and O'Donoghue 1990).

To date, many sources conjugated with different agents have been used in targeted Auger electron therapy for different types of cancer. One example is ^{117m}Sn (IV)-DTPA (DTPA: diethylenetriamine pentaacetic acid) which is used for palliative therapy in bone cancer therapy (Krishnamurthy, Swailem et al. 1997).

β emissions occur when the nucleus has an excess of either neutrons or protons, which leads to the release of an electron or a positron as shown in the following equations:

$$ {}^{A}_{Z}X \rightarrow {}^{A}_{Z+1}Y + \beta^{-} + \bar{\nu}_{e} \qquad (2.1) $$

$$ {}^{A}_{Z}X \rightarrow {}^{A}_{Z-1}Y + \beta^{+} + \nu_{e} \qquad (2.2) $$

Table 2.1: Examples of some radionuclides which can be used for targeted radiation therapy, sourced from (Reilly 2010).

Radionuclide	Production Method	Particulate Emissions (Energy)	Maximum Range in Tissues	$T_{1/2}$ phys	Labelling Methods
^{125}I	$^{124}Xe(n,g)^{125}Xe \rightarrow ^{125}I$	Auger electrons (<30 keV)	<10 μm	59.4 days	Direct radioiodination with Chloramine-T or Iodogen; indirect conjugation using ATE, SIPC, SGMIB
^{123}I	$^{124}Xe(p,2n)^{123}Cs \rightarrow ^{123}Xe \rightarrow ^{123}I$	Auger electrons	<10 μm	13.2 h	Same as for ^{125}I
^{131}I	Neutron irradiation of ^{130}Te	β-Particles (0.6 MeV)	2 μm	8.0 days	Same as for ^{125}I
^{211}At	$^{209}Bi(a,2n)^{211}At$	α-Particles (5.9–7.4 MeV)	50–100 μm	7.2 h	Indirect conjugation with ATE, SAB, SAPC
^{186}Re	$^{185}Re(n,g)^{186}Re$	β-Particles (1.1 MeV)	3 μm	3.7 days	Binding to thiols; chelation by tetradentate complexes; HYNIC; interaction of carbonyl complex with histidine residues; trisuccin
^{188}Re	$^{188}W/^{188}Re$ generator	β-Particles (1.1 MeV)	8 μm	3.7 days	Same as for ^{186}Re
^{90}Y	$^{90}Sr/^{90}Y$ generator	β-Particles (2.3 MeV)	12 μm	2.7 days	Chelation by DOTA
^{67}Ga	$^{68}Zn(p,2n)^{67}Ga$	Auger electrons (<30 keV)	<10 μm	3.3 days	Chelation by DFO and DOTA
^{64}Cu	$^{68}Zn(p,an)^{64}Cu$	β-Particles (0.6 MeV)	2 μm	12.7 h	Chelation by DOTA, BAT, or TETA
^{67}Cu	$^{nat}Zn(p,2p)^{67}Cu$ or $^{68}Zn(p,2p)^{67}Cu$	β-Particles (0.4–0.6 MeV)	2 μm	2.6 days	Same as for ^{64}Cu
^{177}Lu	$^{76}Yb(n,g) \rightarrow ^{177}Yb \rightarrow ^{177}Lu$	β-Particles (0.5 MeV)	2 μm	6.6 days	Chelation by DOTA or CHX-DTPA
^{212}Pb	$^{224}Ra/^{212}Pb$ generator	α-Particles (7.8 MeV)	100 μm	10.5 h	TCMC-trastuzumab
^{213}Bi	$^{225}Ac/^{213}Bi$ generator	α-Particles (8 MeV)	50–100 μm	46 min	Chelation by DOTA or CHX-DTPA
^{225}Ac	$^{233}U \rightarrow ^{225}Ac$	α-Particles (several daughter radionuclides with different energies)	50–100 μm	10 days	Chelation by DOTA

β-particles that are suitable for targeted radionuclide therapy have ranges in tissue between 0.5–12 mm and deposit most of their energy (0.3–2.3 MeV) at the end of their track (Hassfjell and Brechbiel 2001, Reilly 2010). Low-, medium- and high-energy β emitters are widely used for targeted therapy delivering high local dose to the tumour and a relatively smaller dose to normal neighbouring tissues if a pure β emitter is used. Another advantage of using pure β emitters is the small risk of irradiating others around the treated patient. Many β emitters, however, also emit γ-rays; for example, I-131 which is used for thyroid cancer and to treat non-Hodgkin's lymphoma (2007, Stigbrand, Carlsson et al. 2008, Reilly 2010). In this case, the treatment gives a greater dose to the whole body, but it offers a potential advantage of using the emitted γ-rays for counting and imaging the area outside the body using a gamma camera, which allows monitoring of the isotope uptake and its distribution (Reilly 2010).

Mayles et al. (Mayles, Nahum et al. 2007) listed a number of attractive low-, medium- and high-energy β emitters and their properties, such as their half-life, which ranges from 0.10 to 163 days, (see Table 2.2). As β-particles have a maximum range in the order of millimeters in water (Mayles, Nahum et al. 2007). For small tumours, there is a risk of irradiating not only the tumour, but also other adjacent cells. However, this can be an advantage for the treatment of large tumours (Reilly 2010).

Table 2.2: Examples of β emitters for targeted therapy, sourced from (Mayles, Nahum et al. 2007).

Radionuclide	$T_{1/2}$ (days)	E (MeV)
Low-energy β emitters		
^{191}Os	15.4	0.038
^{35}S	87.4	0.049
^{33}P	25.4	0.077
^{45}Ca	163.0	0.077
^{199}Au	3.2	0.082
^{169}Er	9.3	0.101
^{67}Cu	2.6	0.121
^{47}Sc	3.4	0.143
^{177}Lu	6.7	0.149
^{161}Tb	6.9	0.154
^{105}Rh	1.4	0.179
Medium-energy β emitters		
^{131}I	8.0	0.192
^{153}Sm	2.0	0.229
^{77}As	1.6	0.232
^{143}Pr	13.6	0.314
^{198}Au	2.7	0.315
^{159}Gd	0.77	0.319
^{109}Pd	0.56	0.361
^{186}Re	3.8	0.362
^{111}Ag	7.5	0.363
^{149}Pm	2.2	0.370
High-energy β emitters		
^{165}Dy	0.10	0.455
^{89}Sr	50.5	0.583
^{32}P	14.3	0.695
^{166}Ho	1.1	0.695
^{188}Re	0.71	0.764
^{114m}In	49.5	0.777
^{142}Pr	0.80	0.833
^{90}Y	2.7	0.935
^{76}As	1.1	1.267

2.3 Introduction to Targeted alpha therapy

Targeted alpha therapy is a promising treatment modality where an alpha particle, emitted from a single radionuclide decay, has the potential to eradicate individual cancer cells. This is considered an advantage compared to β-particles which may require ~ 100 - 1000 times of β-particles to cross the cell to cause enough radiation damage to kill it (Jurcic, Larson et al. 2002,

Mulford, Scheinberg et al. 2005, Allen, Huang et al. 2014, Elgqvist, Frost et al. 2014). Moreover, the short range of alpha particles (micrometres) is another important advantage compared to the longer ranged β-particles (millimetres), which will also irradiate the normal cells surrounding the tumour (Wheldon and O'Donoghue 1990, Kim and Brechbiel 2012). Unlike the low LET of β-particles, alpha particles have a high LET and can deliver a greater dose to the targeted tumour cells (lethal dose) (Wheldon and O'Donoghue 1990, McDevitt, Sgouros et al. 1998, Marcu, Bezak et al. 2012, Allen, Huang et al. 2014). However, presently there is still not enough dosimetric information about the delivered dose, its distribution and the effects of alpha particles on both the tumour cells and potentially the surrounding healthy cells (Wheldon and O'Donoghue 1990, Roeske and Stinhcomb 1997, Kim and Brechbiel 2012).

Alpha particles are emitted from nuclides with high atomic numbers (mostly higher than 82) leading to decay and emission of two protons and two neutrons as shown in equation (2-3) (Khan 1994, Reilly 2010):

$$ {}^{A}_{Z}X \rightarrow {}^{A-4}_{Z-2}Y + \alpha + Q \qquad (2.3) $$

Where Q is the total amount of energy released.

Therefore, the alpha particle (-particle) can be defined as a nucleus of the helium atom (). The two protons mean that the α-particle holds a positive charge that allows it to be accelerated (Hall and Giaccia 2006). There are many nuclides that decay via alpha emission, such as and, shown in equations (2.4) and (2.5):

$$ {}^{223}_{88}Ra \rightarrow {}^{219}_{86}Rn + \alpha + Q \qquad (2.4) $$

$$ {}^{227}_{90}Th \rightarrow {}^{223}_{88}Ra + \alpha + Q \qquad (2.5) $$

Alpha particles have a short path length (less than 100 μm) in tissue (equivalent to a few cell diameters), high LET (mean energy deposition ~100 keV/μm) (Larsen, Borrebaek et al. 2007, Mayles, Nahum et al. 2007, Reilly 2010, Kim and Brechbiel 2012) and the cell damage, caused by α-particles, is independent of cell proliferation and oxygenation (Roeske and Stinhcomb 1997, McDevitt, Ma et al. 2001, Mulford, Scheinberg et al. 2005, Elgqvist, Frost et al. 2014). According to Sgouros (Sgouros 2008), α-particles deposit energy along their track at densities between 100 and 1,000 times higher compared to those of photons and electrons. Similarly, the biological effects are 3-7 times higher than those for beta targeted therapy. The high density of ionisation events caused by α-particles results in unrepaired DNA double strand breaks in the tumour cells, even within an environment lacking oxygen (Sgouros 2008, Kim and Brechbiel 2012, Allen 2013). All of these advantages, along with evidence provided in various *in vitro* and *in vivo* studies (Allen, Raja et al. 2004), have lead to the first clinical TAT trial conducted in 1995. Since then, more studies have been carried out to produce agents that can be conjugated with alpha emitting sources, distributed inside the body and attached to the tumour (Kim and Brechbiel 2012). TAT has now been used in clinical trials to treat prostate, ovarian cancer, melanoma, leukaemia and neuroendocrine tumours (Jurcic, Larson et al. 2002, IAEA 2013).

One α-particle source, that is used for targeted alpha therapy, is ^{225}Ac (half-life 10 days with six daughter isotopes produced until the stable daughter of ^{209}Bi is reached) (Kim and Brechbiel 2012). It is produced naturally from the decay of ^{223}U and/or ^{229}Th or artificially, by neutron irradiation of ^{226}Ra target (McDevitt, Sgouros et al. 1998, IAEA 2013). It can be chelated by DOTA and attached to HuM195 antibody to treat myeloid leukaemia (Kim and Brechbiel 2012). A phase I clinical trial has already been conducted involving 23 patients with advanced

myeloid leukaemia to determine the maximum dose tolerance for ^{225}Ac-HuM195 (^{225}Ac labelled with anti-CD33 antibody lintuzumab) (IAEA 2013, ClinicalTrials.gov 2015). In another study, 20 patients were injected with Ac-225 with an activity between 851 and 14,430 kBq. At the 5-month follow up, there was limited toxicity observed and the dose tolerance was found to be less than 148 kBq/kg (IAEA 2013).

Another alpha-emitting radionuclide used for TAT is ^{213}Bi (alpha (8.4 MeV) and beta emitter) (Dahle, Abbas et al. 2011, IAEA 2013, Fichou, Gouard et al. 2015). Even though the ^{213}Bi half-life is 46 minutes, meaning that is has restricted usage due to delivery and uptake limitations, it has been used in several targeted alpha therapy clinical trials (Jurcic, Larson et al. 2002, Allen, Raja et al. 2004, Elgqvist, Frost et al. 2014). It is produced as a generator product of the parent ^{225}Ac (Allen, Raja et al. 2004, Kim and Brechbiel 2012). Bi-213 emits γ-rays, which can be beneficial for adjunct imaging, assessment of biodistribution or dosimetry (Kim and Brechbiel 2012). It has been used in several clinical trials when chelated with monoclonal antibodies (mAbs), such as with the C-functionalised trans cyclohexyldiethylenetriamine penta-acetic acid moiety (CHX-A-DTPA), or chelated with proteins such as plasminogen activator inhibitor-2 (PAI2), or C595 or used with HuM195 to cure leukaemia and melanoma (McDevitt, Sgouros et al. 1998, Sgouros, Ballangrud et al. 1999, Jurcic, Larson et al. 2002, Allen, Raja et al. 2004, Raja, Graham et al. 2007, Marcu, Bezak et al. 2012, IAEA 2013). Preclinical studies from the Centre for Experimental Radiation Oncology (CERO), Australia, have shown that there is an enhancement in the TAT cytotoxicity compared to targeted beta radiotherapy (Allen, Raja et al. 2004). Furthermore, a clinical trial of TAT for melanoma in humans has proven the safety and the efficacy of TAT in melanoma regression (Allen, Raja et al. 2004, Raja, Graham et al. 2007).

2.3.1 Targeted Alpha Therapy using Th-227

Thorium-227 has a half-life of 18.72 days (Lederer, Hollander et al. 1967, Dahle, Abbas et al. 2011). It decays by emitting both and β particles. Figure 2.2 shows a diagram of the Th-227 decay scheme. The main decay energies of -particles are 6.04 MeV (23% occurrence), 5.98 MeV (24%), 5.76 MeV (21%) and 5.72 MeV (14%).

A number of preclinical studies have investigated Th-227-immunoconjugates for treatment of lymphoma, breast, and ovarian cancer using animal models (Seidl 2014), with Th-227 commonly bound to antibodies with p-SCN-benzyl-DOTA chelator (Dahle, Abbas et al. 2011, IAEA 2013). For example, Th-227 labelled anti-CD20 antibody rituximab has been used for treating lymphoma in animal models (Allen, Huang et al. 2014). In both *in vitro* and *in vivo* studies, the results showed that a single treatment of ^{227}Th-DOTA-p-benzyl-rituximab (200 kBq/kg) resulted in a 60% regression of lymphoma cells and an increase in survival from 21 days in the untreated mice to 119 days for treated mice (Dahle, Borrebaek et al. 2007, Seidl 2014). Moreover, even a low dose rate alpha-radioimmunotherapy with ^{227}Th-rituximab; i.e. using low injected activities (between 50 to 200 kBq/kg), was effective to regress tumours (Dahle, Borrebaek et al. 2007). Another study assessed the long-term toxicity of low dose rate ^{227}Th-rituximab (Dahle, Jonasdottir et al. 2010), where mice were injected with 50, 200 or 1,000 kBq/kg ^{227}Th-rituximab and then followed up for a period of one year. The results suggest that achievement of a therapeutic effect is possible with safe dose levels of ^{227}Th-rituximab (Dahle, Jonasdottir et al. 2010).

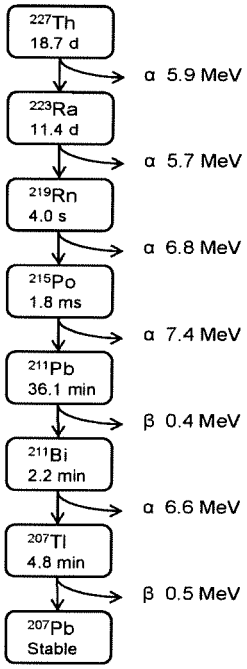

Figure 2.2: Thorium-227 decay scheme, courtesy of (Heyerdahl, Abbas et al. 2012).

Another monoclonal antibody studied for TAT is trastuzumab. Trastuzumab has been radiolabeled with Th-227 using p-SCN-benzyl-DOTA chelator and its effects were investigated in mouse models of breast and ovarian cancer (Larsen, Borrebaek et al. 2007, Seidl 2014). The cytotoxic effect of using the low dose rate radioimmunoconjugate ^{227}Th-DOTA-p-benzyl-trastuzumab was tested using SKOV-3 ovarian cancer cell lines and as a potential therapeutic agent for metastatic cancers (Heyerdahl, Abbas et al. 2012). Different specific activities of ^{227}Th-trastuzumab were used to treat SKOV-3 cells; 11 kBq/μg was the highest specific activity. It caused higher cell suppression than the lowest specific activity of 2.8 kBq/μg. However, similar amounts of apoptosis were seen for both of the specific activities using this agent (Heyerdahl, Abbas et al. 2012). Furthermore, the effects of ^{227}Th-trastuzumab on HER2-positive breast cancer cells was studied in term of their survival, growth and apoptosis. Survival was decreased, cell growth was inhibited and apoptosis was induced in this

cells line, and each of these effects was found to be dependent on the amount of specific activity of ^{227}Th-trastuzumab (Heyerdahl, Abbas et al. 2012).

Another study investigated 200, 400 and 600 kBq/kg of ^{227}Th-trastuzumab in mice using HER2-expressing breast cancer xenografts. The results suggest a dose-dependent anti-tumour effect with limited toxicity (Abbas, Heyerdahl et al. 2011, Seidl 2014).

In addition, responses of HER-2-positive ovarian cancer xenografts in mice to ^{227}Th (α-particles) versus ^{177}Lu (β-particles) labelled trastuzumab were compared (Abbas, Bruland et al. 2012). The mean survival of mice treated with 400 and 600 kBq/kg ^{227}Th-trastuzumab was 107 ± 9 and 129 ± 12 days, respectively, which was significantly improved compared to a control or 72 MBq/kg ^{177}Lu-trastuzumab treatment (88±11 days and 85±8 days, respectively) (Abbas, Bruland et al. 2012).

Moreover, fractionation of the same concentration of ^{227}Th-trastuzumab could reduce the toxicity while maintaining the same therapeutic effect. However, this is not applicable for targeted alpha therapy in rapidly growing tumours, as the dose rate will be lower than necessary for tumour control (Heyerdahl, Abbas et al. 2012).

The Th-227-labelled murine monoclonal antibody DAB4 (APOMAB) has been used in preliminary *in vivo* investigation of Lewis lung tumour in mice (Staudacher, Bezak et al. 2014). This group studied the effect of ^{227}Th-DAB4 (18 kBq) with and without prior chemotherapy administration to tumour bearing mice. To assess the tumour uptake, tissue biodistribution of the RIC after 1, 2, 3 and 5 days of ^{227}Th-DAB4 administration were examined. The tumour uptake was significantly higher for mice treated with chemotherapy prior to ^{227}Th-DAB4 administration compared to mice treated with ^{227}Th-DAB4 alone. Combining ^{227}Th-DAB4 with chemotherapy increased tumour regression significantly compared to treatment with

^{227}Th-DAB4 alone, which gave a modest anti-tumour response, compared to untreated mice (Staudacher, Bezak et al. 2014).

Nevertheless, a major issue associated with Th-227 implementation in TAT is production of the daughter nuclide (^{223}Ra) which accumulates in bones as it targets calcium hydroxyapatite in the stroma of the bone (Seidl 2014). Ra-223 realises alpha particles too that causes many unwanted toxic side-effects. Ra-223 also releases alpha particles that may cause additional toxicities.

2.3.2 Targeted Alpha Therapy using Ra-223

Ra-223, with a half-life of 11.4 days, is produced either from an Ac-227 generator or from Th-227 decay (Lederer, Hollander et al. 1967, Kim and Brechbiel 2012). It emits four α-particles (energy range between 5 to 7.05 MeV (Lien, Tvedt et al. 2015)) and two β^--particles and γ-rays before reaching the stable state of ^{207}Pb.

Different preclinical studies have investigated Ra-223 (Ra-223 is bone-seeking radionuclides and there is no need to associate with antibody) for bone cancer, and especially metastatic disease associated with prostate and breast cancer. This led to the introduction of Alpharadin@ (^{223}Ra chloride, or Xofigo@) by the Norwegian company Algeta ASA and Bayer Schering Pharma AG. As Alpharadin naturally targets to bone metastases, it gives the advantage of effectively localising the radiation damage to cancer cells in the bone. Alpharadin has been examined in phase II and III clinical trials for prostate cancer patients with bone metastases (Nilsson, Franzen et al. 2007, Kim and Brechbiel 2012, IAEA 2013, Joung, Ha et al. 2013, Allen, Huang et al. 2014). Furthermore, Ra-223 dichloride (formerly Alpharadin) is the first alpha emitter approved for the treatment of castration-resistant prostate cancer patients with bone metastases.

The results of a clinical trial (Shirley and McCormack 2014, Lien, Tvedt et al. 2015, Shore 2015) that used a regimen of six injections of Ra-223 (50 kBq/kg body weight) over a period of four weeks revealed a general improvement in patient survival (including a 30% reduction in the risk of death) and reduction in noticeable pain and symptomatic skeletal events, where the Ra-223 skeletal uptake was between 40 to 60% of the administered dose, and was well tolerated by patients (Croke, Leung et al. 2012).

For breast cancer patients with bone metastases, *in vitro* preclinical studies have shown the ability of Ra-223 to combine with bone matrix and control the breast cancer cell proliferation. *In vivo* study resulted in 56% and 43% decrease in osteolysis and tumour growth, respectively, while DNA double strand breaks were produced in the breast cancer cells culture (Suominen, Rissanen et al. 2013, Nilsson 2014). This led to a metastatic breast cancer clinical trial using Ra-223 dichloride. In a phase IIa clinical trial, 23 patient received a weekly dose of Ra-223 (50 kBq/kg of body weight) over four weeks (Coleman, Aksnes et al. 2014). After 17 weeks, the patients showed a decrease in the hypermetabolic osteoblastic bone lesion metabolic response rate of 41.5%. Furthermore, the investigation emphasised the safe use and a good tolerability of Ra-223 dichloride for breast cancer patients with bone metastases. Compared to beta therapy (such as Sm-153 and Sr-89) Ra-223 has less myelotoxicity (Coleman, Aksnes et al. 2014).

2.4 Conclusion

Targeted alpha therapy is a modality belonging to targeted radionuclides therapies that provides localised tumour treatment to cancer patients due to the unique properties of α-particles, such as their short range and high LET, meaning that α-particles are highly cytotoxic to tumour cells.

The selection of an alpha emitter should involve consideration of the physical range of α-particles relative to the cell and tumour size, along with commercial availability and bioavailability of suitable antibodies. Moreover, intensive dosimetric studies need to be conducted to evaluate the dose rate and dose distribution in TAT.

Chapter 3

Timepix Radiation Detector

3.1 Introduction

With the development of hadron and targeted therapies, there is a renewed interest in novel microdosimetry detectors. The Timepix detector, developed at CERN as an extension of the Medipix2 detector, represents such a microdosimeter. It can be used for experiments with photons, electrons and heavy particles and in a wide range of applications in space physics, nuclear physics, radiotherapy physics, imaging and radiation protection. This chapter reviews some of the published works utilizing Timepix as a radiation detector, a spectroscope or as a camera for photons, and charged particles. Specific applications of Timepix are described, showing that more investigation is still required to gain the full benefit of Timepix applications, especially in the fields of radiation therapy and imaging. More specifically, the application of Timepix to targeted radiotherapies remains absent despite the main advantage of Timepix: tracking energy deposition at the micrometer level.

3.2 Statement of Contribution

3.2.1 Conception

The first concept of reviewing the latest papers on Timepix was suggested by Eva Bezak.

3.2.2 Realisation

These two review papers were primarily written by Ruqaya Al Darwish. Eva Bezak assisted by editing the manuscript.

3.2.3 Documentation

This paper was primarily written by Ruqaya Al Darwish. Editing was conducted by Eva Bezak. Loredana Marcu and Anatoly Rozenfeld both provided assistance with editing the final versions of these papers.

Statement of Authorship

Title of Papers	Timepix – technical aspects of a novel development in solid state radiation detectors
Publication Status	☐ Published ☐ Accepted for Publication ☑ Submitted for Publication ☐ Unpublished and Unsubmitted work written in manuscript style
Publication Details	Ruqaya AL Darwish, Eva Bezak, Loredana Marcu, and Anatoly Rozenfeld. Timepix – technical aspects of a novel development in solid state radiation detectors

Principal Author

Name of Principal Author (Candidate)	Ruqaya AL Darwish		
Contribution to the Paper	Reviewed Timepix commission and calibration. This paper was primarily written by Ruqaya Al Darwish, who also acts as the corresponding author.		
Overall percentage (%)	80%		
Certification:	This paper reports on review I conducted during the period of my Higher Degree by Research candidature and is not subject to any obligations or contractual agreements with a third party that would constrain its inclusion in this thesis. I am the primary author of this paper.		
Signature		Date	30/8/2016

Co-Author Contributions

By signing the Statement of Authorship, each author certifies that:

i. the candidate's stated contribution to the publication is accurate (as detailed above);

ii. permission is granted for the candidate in include the publication in the thesis; and

iii. the sum of all co-author contributions is equal to 100% less the candidate's stated contribution.

Name of Co-Author	Eva Bezak		
Contribution to the Paper	The initial concept of the review as well as transcript editing was done by Eva Bezak.		
Signature		Date	30/8/16

Name of Co-Author	Loredana Marcu		
Contribution to the Paper	Loredana Marcu provided assistance with paper editing.		
Signature		Date	29/8/2016

Name of Co-Author	Anatoly Rozenfeld		
Contribution to the Paper	Assistance with paper editing.		
Signature		Date	30/08/2016

Timepix – technical aspects of a novel development in solid state radiation detectors

Ruqaya AL Darwish[1,2,3], Eva Bezak[2,4,5], Loredana Marcu[2,6], Anatoly Rozenfeld[7]

[1] Department of Medical Physics, Royal Adelaide Hospital, Adelaide, Australia
[2] School of Physical Sciences, University of Adelaide, Adelaide, Australia
[3] Ministry of Higher Education, Saudi Arabia
[4] International Centre for Allied Health Evidence, Sansom Institute, University of South Australia, Adelaide, Australia
[5] Sansom Insitute for Health Research, University of South Australia, Adelaide, Australia
[6]Faculty of Science, University of Oradea, Oradea 410087, Romania
[7]Centre of Medical Radiation Physics, University of Wollongong, Wollongong, NSW, Australia.

Structure:

Abstract

The Timepix detector, developed at CERN as an extension of the Medipix2 detector, represents a versatile microdosimeter. It can be used for experiments with photons, electrons and heavy particles and in a wide range of applications in space physics, nuclear physics, radiotherapy physics, medical imaging and radiation protection. This paper reviews the general characteristics of Timepix, including calibration, Timepix modes, spatial resolution and other features revealed by current research.

Key words: Timepix, detector, microdosimeter, spectroscopy, TOT mode.

1. Introduction

With the rapid development of hadron therapy as well as of various particle based targeted therapies, further development in detection and dosimetry technology is required in a form of an accurate tool which can track ionization events on a micrometer or even nanometer level. In other words, a detector able to monitor individual particle tracks that can also measure the peak energy deposited is needed.

Semiconductor materials have many highly desirable characteristics for dosimetry including high density, low energy requirements to produce an electron-hole pair (i.e. high sensitivity and resolution), ability to work in unbiased or biased modes, and high efficiency even at low voltage bias (Rosenfeld et al., 2006). Furthermore, they offer high readout speed and have compact design with both detector and reader generally assembled in a single unit. Particle energy and position can be measured simultaneously and precisely (Lutz, 2007). Developments in semiconductor technologies have led to a new generation of highly efficient radiation detectors with very small pixel size and low noise such as Medipix detectors, with several generations (Medipix1, Medipix2, Timepix and Medipix3) having evolved over the past two decades at CERN within two frameworks of international collaborations (Llopart et al., 2007; Vallerga et al., 2008).

This review discusses a prototype of a semiconductor microdosimeter, namely Timepix. It provides detailed discussion of some of the major studies that examine the use of Timepix as a detector, a spectrometer and a camera. Another review paper published in 2010 studied development and applications of Medipix2 over a ten year period including its modifications ultimately leading to Timepix development (Campbell, 2011). However, the review did not focus on Timepix and its applications. According to the INSPEC database, there have been 274 articles related to Medipix2 published since 2001 until 2015, while the number of articles published on Timepix has reached over 240 since 2007. This timely review is the first one focussing specifically on Timepix since its introduction in 2004.

As an additional impetus, development of Timepix applications is no longer restricted to CERN framework collaboration (requiring a cost-prohibitive licence) as the technology (the naked chip and the detector assembly) has now been released for commercial production and purchase through several companies, including: Amsterdam Scientific Instruments (The Netherlands), X-ray Imaging Europe GmbH (Germany) and X-Ray Imatek (Spain). The cost, on average, for a single Timepix chip is approximately € 10.000, making the detector affordable and more departments may be looking into including this novel semiconductor detector into their radiation detection and dosimetry equipment arsenal.

2. General characteristics

Timepix is a semiconductor detector evolved from the original Medipix1 system, also called Photon Counting Chip (PCC), developed in the 1990s, using a hybrid semiconductor pixel detector to detect particles in high energy physics experiments (Abate et al., 2000; Amendolia et al., 1999; Amendolia et al., 2000; Bardelloni et al., 2000; Bertolucci et al., 1999; Bisogni et al., 1998; Campbell et al., 1998; CERN, 2011; Mikulec, 2000; Mikulec et al., 2001; Schwarz et al., 1999). Medipix1 consisted of a sensor layer of 64 x 64 pixels with a single pixel area of 170 x 170 μm^2 (Campbell et al., 1998; Davidson et al., 2003; Faruqi and Cattermole, 2002; Mitschke et al., 2004; Niederlöhner et al., 2003; Pfeiffer et al., 2003; Sinor et al., 2003). Each pixel was made of Si or GaAs and was bump-bonded to a second readout layer made of a complementary metal-oxide-semiconductor (CMOS) (Bert et al., 2003; CERN, 2011).

In the late 1990s, CERN developed Medipix2 using sub-micron CMOS technology (Bello et al., 2001; Chmeissani and Mikulec, 2001; Rossi et al., 2006). This technology resulted in the improvement of the pixel function and also enabled the decrease of the pixel size, increasing the number of pixels per chip (CERN, 2011; Pfeiffer et al., 2004). Medipix2 has the following properties: pixel size of 55 x 55 μm^2 (Dammer et al., 2009; Faruqi and Cattermole, 2002; Manach and Gal, 2002; Mettivier et al., 2003), the chip can collect positive or negative charge, the upper and lower charge thresholds can be selected to ensure uniform performance and, to avoid dead time, the read-out is performed after exposure (Bisogni et al., 2003; CERN, 2011; Llopart et al., 2002).

Medipix3 was developed using an 8-metal 0.13 μm CMOS readout chip connected to a pixelated semiconductor sensor layer (Ballabriga et al., 2007; CERN, 2011). The sensor layer is a matrix of an 8 x 8 pixel square with 55 x 55 μm^2 individual pixel area (Ballabriga et al., 2011; Ballabriga et al., 2007; Gimenez et al., 2011). It is still under development and aims to eliminate the spectral distortion due to so-called charge sharing effect (Ballabriga et al., 2007), to operate free of dead time (CERN, 2011).

A development extension of Medipix2 is Timepix. While Timepix can count particle hits same as Medipix2, it can also record time over a certain energy threshold allowing direct energy measurement in each pixel and it can measure arrival time of the first particle to the chip. This represents the main advantage of Timepix as it can measure the amount of energy deposited in the Time Over Threshold mode (Campbell et al., 2007). Although Timepix and Medipix2 share some physical properties such as pixel size (Bamberger et al., 2007; CERN, 2011) and the ability to detect both positive and negative charges (CERN, 2011), they differ in three aspects. In Timepix (Llopart et al., 2007):

1. Each pixel has a single energy threshold with 4-bit threshold adjustment;
2. Each pixel can operate in three main modes (Medipix mode, Timepix mode and Time Over Threshold);
3. Each pixel's counting clock is synchronized with an external clock reference.

As mentioned above, Timepix consists of a semiconductor layer divided into an array of pixels. This array is bump-bonded to readout ASIC (Application Specific Integrated Circuit) as an integrated electronic layer (Fig. 1). Each pixel has an individual charge-sensitive preamplifier, a discriminator and a counter (CERN, 2011; Rügheimer et al., 2008) and a 4-bit digital-to-analogue convertor (DAC) to adjust the charge threshold (4-bit DAC for threshold adjustment) (Llopart et al., 2007) as shown in Fig. 2 and Table 1.

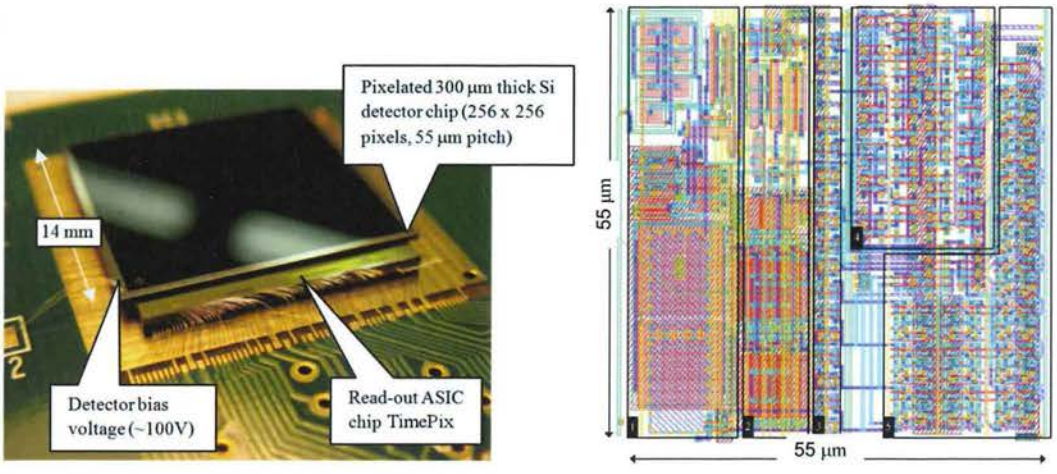

Fig. 1: Timepix structure, courtesy of (Kraus et al., 2011) and the structure of one pixel: 1) preamplifier, 2) discriminator with 4-bit threshold equalization, 3) 8-bit Pixel Configuration Register, 4) reference clock buffer and Timepix Synchronization Logic and 5) 14-bit shift register and overflow control, courtesy of (Llopart et al., 2007).

Timepix performs its functions using a synchronization logic and a 14-bit counter per pixel. The detector can cope with count rates of up to 100 kHz for each pixel (in single particle counting mode) (Llopart et al., 2007) and has an overflow limit of up to 11810 counts (CERN, 2011). It also has the advantage of low electric noise of almost 100 e⁻rms (root mean square) (Pugatch et al., 2011).

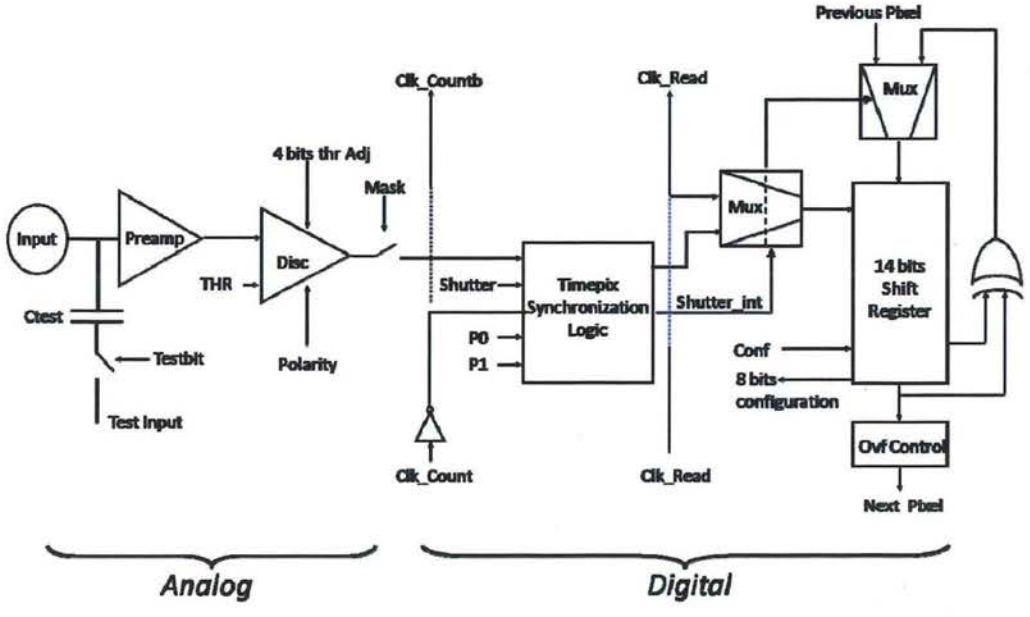

Fig. 2: Timepix pixel schematic. Each pixel consists of two main parts: analog part and digital part, courtesy of (Campbell, 2011).

Table 1: Physical properties of Timepix adopted from different references (for more information refer to the text).

Number of pixels	256 x256 or 512x512
Pixel size	55 x 55 μm^2
Chip size	1.408 x 1.408 cm^2 or 2.8160 x 2.8160 cm^2
Active area	About 2 cm^2 (for 512x512 chip)
Type of accepted charge	Positive or negative charge
Modes	1. Medipix mode to count single particle 2. Timepix mode to measure the arrival time of particle interaction 3. Time Over Threshold (TOT) to measure the energy deposited in each pixel for events between the thresholds
Type of Timepix chip	Single, quad and octo

Timepix can be linked to an integrated USB-based readout interface that can connect to a PC/notebook. Windows compatible software package Pixelman determines the control and data acquisition of Timepix detector (Granja et al., 2010).

3. Calibration

Calibration of any radiation detector, including Timepix, is an important procedure before employing that system for radiation measurement purposes. Timepix calibration establishes the relationship between the collected charge and the deposited energy where the total charge recorded in each pixel depends on the incoming particle's energy, the place and the depth of the interaction (i.e. charge sharing effect), the detector bias voltage, preamplifier and the energy threshold (Jakubek, 2009; Jakubek et al., 2008). Additionally, pixel equalization needs to be performed as there is a need for uniform performance of all pixels. Calibration and equalization can be performed using low energy X-rays (Jakubek, 2009; Jakubek et al., 2008). This is potentially not a trivial task, as there are 65536 (256 x 256) or 262144 (512 x 512) individual pixels.

According to Jakubek et al. (Jakubek et al., 2008), radioactive sources can be used to calibrate Timepix in TOT mode: ^{55}Fe (5.9 keV), ^{241}Am (59.5 keV) as well as fluorescent materials emitting characteristic X-rays produced using tungsten X-ray tube (^{26}Fe (6.4 keV), ^{29}Cu (8.0 keV), ^{40}Zr (15.8 keV), ^{42}Mo (17.5 keV), ^{48}Cd (23.2) keV and ^{49}In (24.2 keV) (Jakubek et al., 2008). By selecting one pixel cluster and by fitting the corresponding peaks in the energy spectrum with a Gaussian distribution curve, the resulting calibration is a nonlinear surrogate function as shown in Fig. 3.

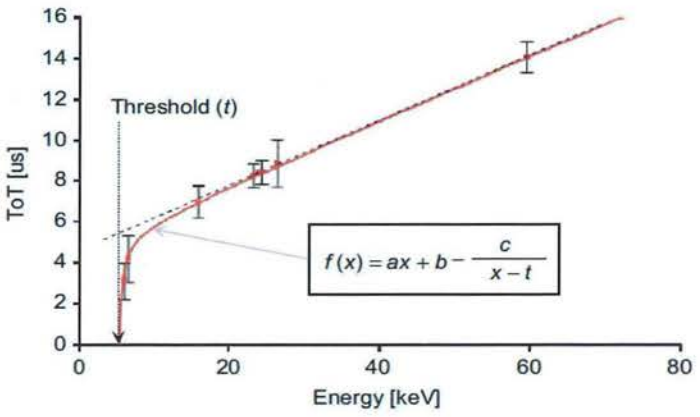

Fig. 3: Calibration curve (surrogate function), courtesy of (Jakubek et al., 2008).

The surrogate function (i.e. the calibration curve) is given by:

$$f(x) = ax + b - \frac{c}{x-t} \quad (1)$$

The parameters *a, b, c* and *t* should be determined for each pixel "using the least-squares fit". To determine these parameters, the measurement for each pixel is repeated at least four times (Jakubek, 2011).

Jakubek and his group (Jakubek et al., 2008) also studied Timepix performance with alpha particles passing through a sample material. Initially, Timepix calibration was conducted using gamma radiation from different radioactive sources and fluorescent materials that emit characteristic X-rays and those produced by a tungsten X-ray tube. First, γ-rays of 59.5 and 26.3 keV from ^{241}Am source (750 MBq) were used with exposure time of 50 ms and the threshold of about 4.5 keV (taking 2000 frames) to study the measured energy spectrum of photons without energy calibration of Timepix. The results show that the cluster-volume spectrum will be distorted if it is measured without energy calibration, while pixels calibrated with the same source give a well-aligned peak. Fig. 4 shows the results for a non-calibrated and a calibrated Timepix and subsequent measurement of ^{241}Am γ-rays.

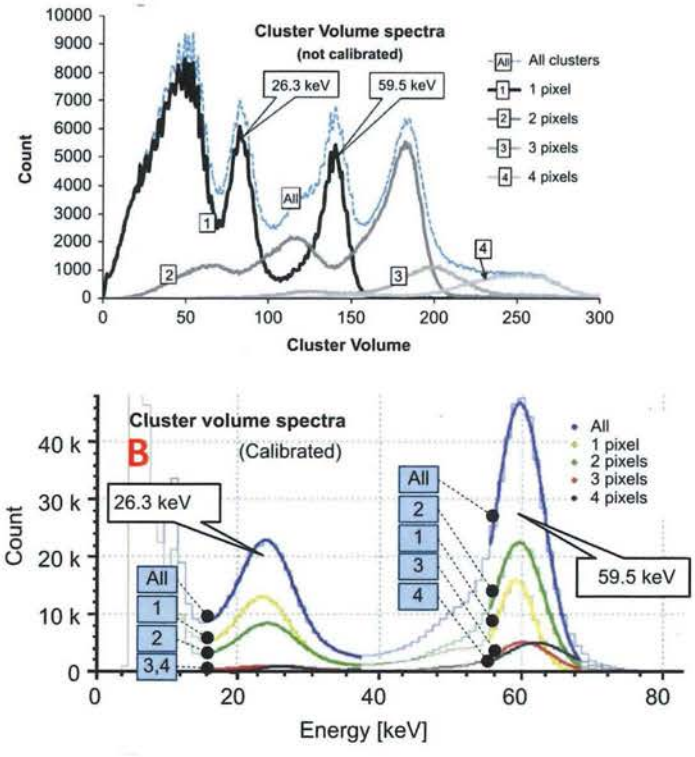

Fig. 4: A) Cluster volume spectrum of ^{241}Am obtained from a non-calibrated Timepix for all clusters (dashed line) and for different cluster sizes (number of pixels) (solid lines), B) Cluster volume spectrum of ^{241}Am obtained from a calibrated Timepix in TOT mode for all clusters and for different cluster sizes, courtesy of (Jakubek et al., 2008).

Secondly, the alpha particle cluster-volume (energy) spectrum was measured in air for two sources (^{241}Am and ^{239}Pu) with results shown in Fig. 5.

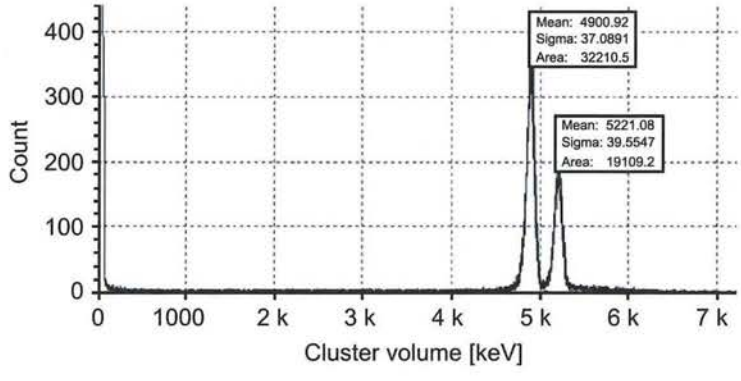

Fig. 5: Cluster volume spectrum of alpha particles from combined ^{241}Am and ^{239}Pu sources measured in air, courtesy of (Jakubek et al., 2008).

The calibration in TOT is a demanding process as it requires analysing at least 250 thousand spectra. In 2011, Jakubek presented a new calibration method based on precise analysis of the spectral peaks shapes and requiring just two to three calibration points in order to have "the number of least-squares fits needed" (Jakubek, 2011). Instead of using a plain Gaussian for the low energy part of the calibration curve, a combination between Gaussian and surrogate function is recommended. The resulting fit depends on 7 parameters:

$$M_{a,b,c,t,\mu,\sigma,A}(S) = G_{\mu,\sigma,A}\left(f^{-1}_{a,b,c,t}(S)\right) \tag{2}$$

where $M_{a,b,c,t,\mu,\sigma,A}(S)$ is the new spectral peak model obtained from the combination of Gaussian ($G_{\mu,\sigma,A}(e)$) and the inverse surrogate function ($f_{a,b,c,t}(e)$). The surrogate function shows the energy transformation to TOT signal(s) which works as a pixel calibration function; e is the particle's energy; μ is a Gaussian parameter that gives mean energy in the calibration peak; σ is a Gaussian parameter that gives energy noise; A is also a Gaussian parameter that gives spectral peak intensity or area (Jakubek, 2011).

The calibration was tested by using multi-energy source: a combination of an ^{241}Am that emits 59.5 keV γ-ray penetrating indium and iron plates and XRF materials, where the characteristic fluorescence X-ray generated for In is 24.1 keV and for Fe is 6.4 keV, as shown in Fig. 6. The threshold was higher than the noise level of about 3.2 keV with 100 V bias voltage and 10 MHz clock frequency. This method of calibration improved the quality of energy calibration and simplified the procedures (Jakubek, 2011).

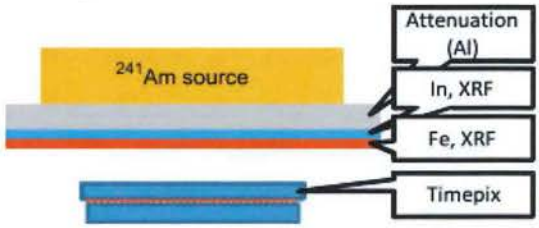

Fig. 6: Timepix calibration testing setup, courtesy of (Jakubek, 2011).

The quality of calibration was further tested for higher energy alpha particles of 5.5 MeV energy from ^{241}Am concluding that the surrogate function was not valid for very high ionization particles as the pixel electronics presented unexpected distortion for energies higher than 0.9 MeV. However, this behaviour can be corrected extending the calibration range up to 1.2 MeV per pixel.

4. Timepix modes

The architecture and functionality of Timepix characterisation were evaluated in 2007 by LIopart et al. (Llopart et al., 2007). This group also presented the first electrical measurement to test the three modes (as shown in Table 1).

In the counting mode (Medipix mode), an s-curve method was used to measure the electronic noise and effective threshold. First, a fixed threshold was chosen and the input charge was taken under the threshold (no counter counts) to higher than the threshold (all pulses are

counted). The results can be built as an s-shaped curve where the effective threshold can be obtained at 50% of the curve. The results show linearity for both polarities up to 20 ke$^-$ in one pixel at the matrix centre (see Table 2).

Table 2: Electrical characterization of Timepix in Medipix mode adopted from (Llopart et al., 2007).

Polarity / Measurement	For hole collection	For electron collection
Measured electronic noise	99.4 ± 3.8 e$^-$ rms	104.8 ± 6 e$^-$ rms
Measured DAC step gain	24.7 ± 0.7 e$^-$/step	25.4 ± 1.2 e$^-$/step

In TOT mode, the linearity was tested up to 40 ke$^-$. The results show a relationship between the input charge and the measured time at three different thresholds. This relationship is linear when the input charge is higher than the threshold by 3-4 ke$^-$.

The measurement in arrival time mode (Timepix mode) measures the time-walk, which is the difference between the time measured for an input charge higher than the threshold by 1 ke$^-$ and for the infinite input charge. Fig. 7 shows the relationship between the time-walk measured for five threshold values and two preamp current DAC settings (to control the preamplifier peaking time) for a pixel at the matrix centre. Having a faster preamplifier peaking time gives better value of time-walk. For the higher preamp current DAC setting, the measured time-walk was less than 50 ns.

The study concludes that each pixel in a Timepix device can be programmed individually to one of the three modes: counting mode, particle arrival time mode or energy mode [4]. The initial measurement of the electronic pixel noise is almost 100 e$^-$rms, but after equalization of the whole matrix, threshold variation between pixels is about 35 e$^-$rms. Furthermore, as the charge deposition for a single event spreads between a number of neighbouring pixels, Timepix chip can be operated in more than one mode at the same time: TOT mode and arrival time mode to compensate off-line time-walk considering the neighbouring pixels' input to deposited charge.

5. Spatial resolution

Spatial resolution of Timepix was also studied with alpha particles produced by ^{241}Am decay (alpha particles of 5.5 MeV) penetrating a sample of eight overlapping Mylar foils, each with thickness of 4 μm (Jakubek et al., 2008). The measured spectra are shown in Fig. 8. The results show that if the energy loss of a single alpha particle is measured, there is a possibility to measure the thickness of a thin organic sample with a resolution between 300 to 600 nm. This resolution can be augmented by increasing the energy of the particles, while the precision of thickness can be improved by increasing the number of particles.

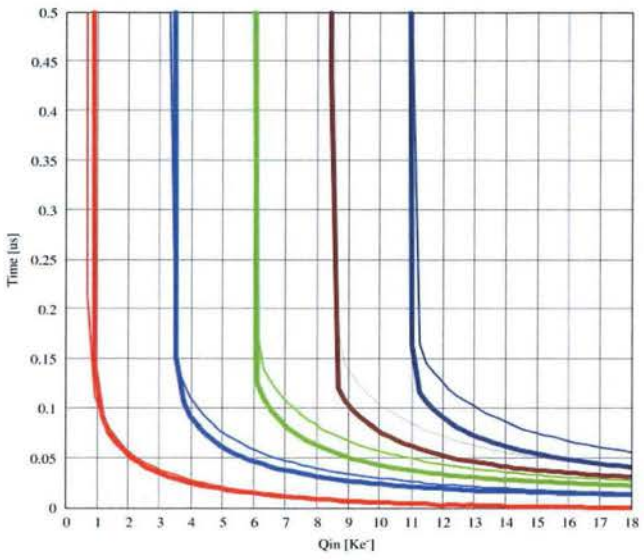

Fig. 7: Time-walk of a single pixel at the centre where the thick and thin line curves correspond Preamp = 1.8 μA and 900 nA, respectively, courtesy of (Llopart et al., 2007).

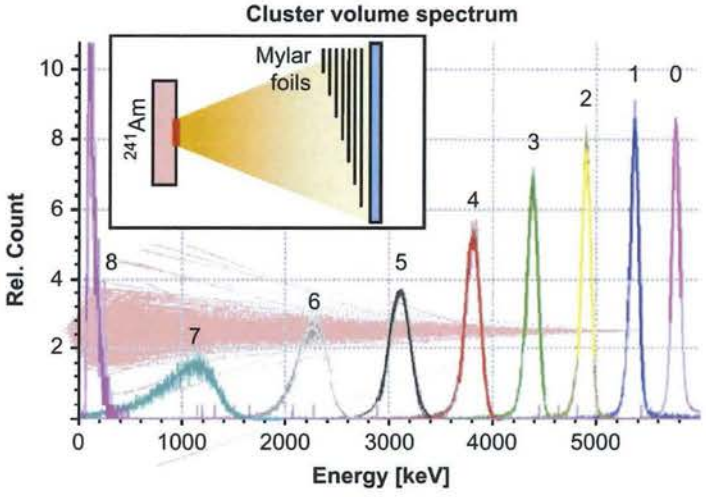

Fig. 8: Energy spectra of alpha particles passing through a stack of Mylar foils, courtesy of (Jakubek et al., 2008).

Another test done by this group was to take radiographic images with ^{241}Am alpha particles in vacuum of a spider slough placed on the detector surface and fixed by Mylar foil as shown in Fig. 9. About 60,000 frames were taken during 16 hours.

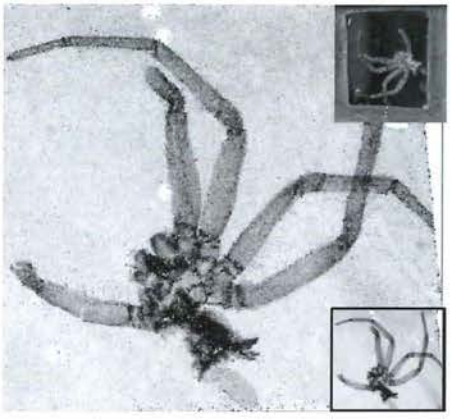

Fig. 9: Spider slough radiographic images taken with ^{241}Am alpha particles (720,000 alpha particles per 1 megapixel) in vacuum, courtesy of (Jakubek et al., 2008).

The results confirm the appropriateness of using Timepix for radiography with heavy particles by measuring their energy loss while transiting the sample of interest.

As any individual interaction event causes spreading of charge deposition between neighbouring pixels, Jakubek published a study dealing with the charge sharing effect in Timepix (Jakubek, 2009). The charge sharing effect occurs when the incoming particle produces sharing between adjacent pixels during the charge collection from a primary ionization event. This results in a cluster (i.e. signal from several neighbouring pixels) and leads to a reduction of the total amount of measured energy compared to the original energy because the amount recorded in each pixel depends on its threshold. If it is higher than the threshold, the contributed energy is recorded. If it is lower than the threshold, it is neglected. This is shown in Fig. 10. The charge sharing effect depends on three elements: (a) the deposited energy, (b) the speed of charge collection and (c) the thickness of the detector.

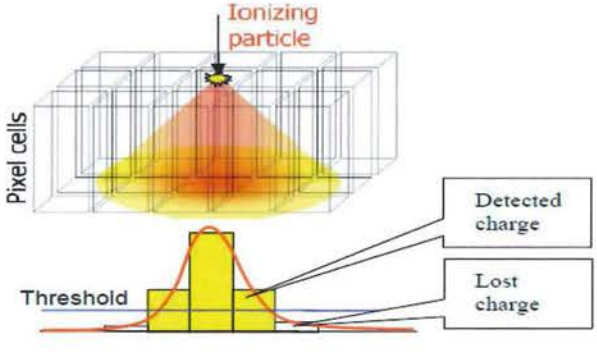

Fig. 10: Charge sharing effect process, courtesy of (Jakubek, 2009).

This effect can be studied in more detail with Timepix as it can work in TOT mode, which allows the study of each individual pixel. Jakubek compared the results of a simplified model of the charge sharing effect with experimental data. Just one pixel cluster was considered and neighbouring pixels were neglected. To study the effect of interaction depth on the charge

sharing effect of the detector, the detector was tilted in front of a narrow X-ray beam as shown in Fig. 11; the resulting cluster analysis showed a linear dependence of the cluster size on the interaction depth. This means that diffusion is responsible for the charge spread. Results were compared with simulations of 3 x 3 pixels irradiated with monoenergetic X-ray beam perpendicularly. The depth of interaction was chosen by applying the exponential absorption law to the incoming X-ray beam of a given energy and the attenuator (silicon). The simulations agreed with the experimental data.

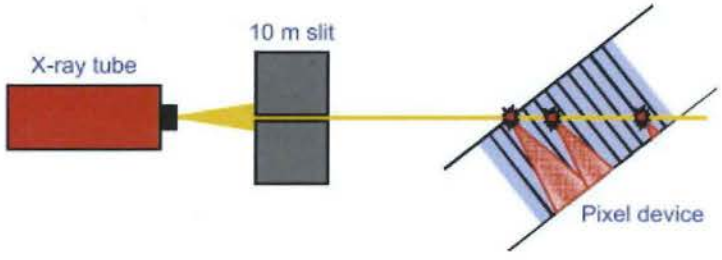

Fig. 11: The experimental setup to study the relationship between the cluster size and the depth of interaction, courtesy of (Jakubek, 2009).

Jakubek also used the energy calibrated Timepix for material-sensitive X-ray radiography. A tungsten anode X-ray tube (40 kV), very low current (1 μA) and exposure time equal to 1 ms were used to irradiate a PMMA-water sample (taking ~ 40,000 frames). From the spectra, Jakubek concluded that the energy resolution of Timepix using energy-sensitive X-ray radiography has the ability to recognize the soft biological tissue leading to potential application in medical physics. In Fig. 12, a tungsten anode X-ray tube (40 kV and 1 mA) was used to irradiate a PMMA-water sample that simulates fat and muscle tissue.

Fig. 12: a PMMA-water sample used with low X-ray tube current where about 40,000 frames (1 ms per frame) were taken with Timepix, courtesy of (Jakubek, 2009).

In order to extend the imaging applications of Timepix, a method based on Monte Carlo simulations was presented by Žemlička et al. (Žemlička et al., 2009) for X-ray fluorescence (XRF) imaging. Measurements of characteristic fluorescence spectra of pure elements were

first conducted, in order to measure complex spectra from an unknown sample composition. The geometric setup using a pin-hole collimator for this experiment is shown in Fig. 13 (Žemlička et al., 2009). As a result of this setup, the Timepix's spatial resolution is equal to the diameter of the collimator pin-hole. Simulation method using pixel decomposition was employed to decompose the complex spectra to distinguish the element distribution area in a sample.

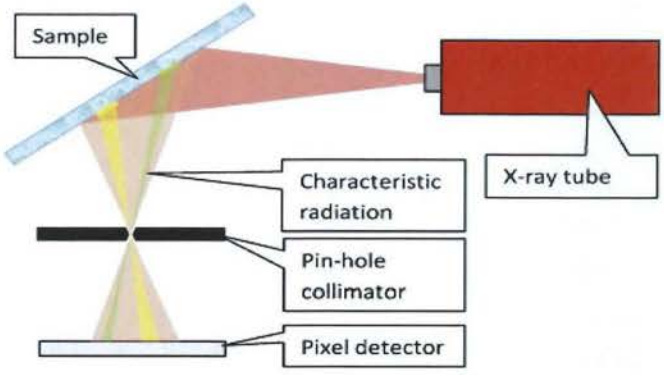

Fig. 13: Pin-hole camera setup with XRF imaging, courtesy of (Žemlička et al., 2009).

The method was later applied to two samples: a modified printed circuit board and a Euro coin. The results proved the validity of this method and showed the ability to distinguish elements with atomic numbers heavier than potassium. This method is valid even for samples made of composed elements as presented in Fig. 14.

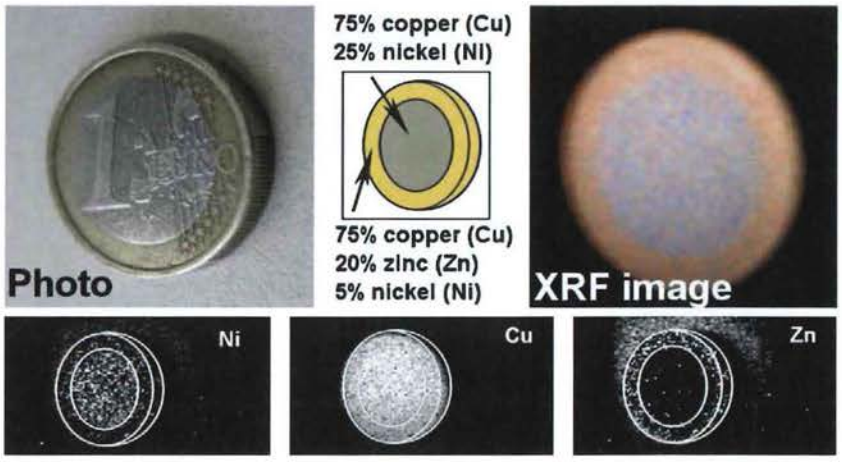

Fig. 14: Euro coin image top (Photograph, scheme and X-ray fluorescence: grayscale RGB coded reconstruction). Bottom images are the results of the per pixel decomposition method, courtesy of (Žemlička et al., 2009).

First measurements of low and high energy electrons using Timepix were reported by Esposito et al. (Esposito et al., 2011). Timepix was used in a TOT mode, and was calibrated for energies down to 3.1 keV using γ-rays and X-rays emitted from ^{241}Am, ^{55}Fe and In $_{K\alpha 1}$ and also by using alpha particles from ^{241}Am (Esposito et al., 2011). This study also took into account the charge sharing effects affecting the detector performance in energy distribution and spatial resolution. Electrons from ^{90}Sr/ ^{90}Y sources (10 cm distance from the Timepix) were measured and the resulted energy spectrum was compared with β^- decay spectrum and simulated spectrum obtained from Monte Carlo calculation. The measured and simulated results are shown in Fig. 15. There is a good agreement between the measured and the simulated results except for energies lower than 50 keV. In this area the measured results were higher than the simulation results. This is due to electronic noise and energy losses from laterally diffused charge which are in fact under the threshold. The peak at 100 keV is due to particles that lose some of their energy but leave the detector.

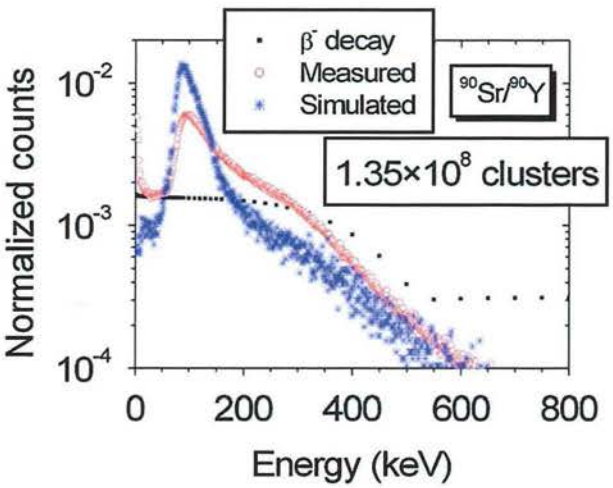

Fig. 15: Measured and simulated spectra for ^{90}Sr/^{90}Y electrons and β^- decay spectrum, courtesy of (Esposito et al., 2011).

Using low frame rate to reduce the chance of individual electron tracks overlapping, the group identified all charge clusters generated by a single electron and identified the (x, y) position of electron centroids. This indicates the location the first pixel was hit by an electron, thus limiting the resulting image blur. Esposito et al. (Esposito et al., 2011) refer to a similar procedure that can be applied for UV, alpha and neutron imaging with Timepix.

An absorbing edge method applied in their work used a slightly tilted steel edge to take an image (100 μm thick) with ^{90}Sr/ ^{90}Y (10 cm distance) as shown in Fig. 16. The measured oversampled Edge Response Function (ERF) and the corresponding oversampled Line Spread Function (LSF) (with and without centroid approximation) are shown in Fig. 17. The spatial resolution in terms of LSF width with and without the calculation of the cluster centroid were reported to be about 27.5 ± 1.1 μm and 45.6 ± 1.6 μm, respectively.

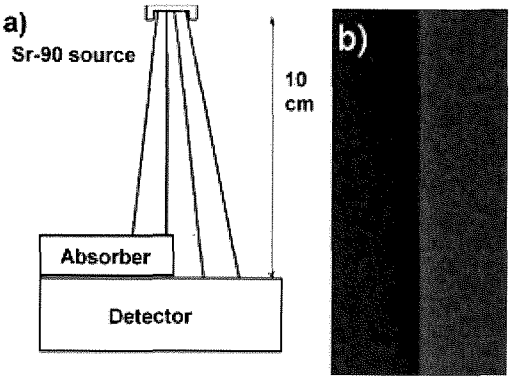

Fig. 16: a) Spatial resolution measurements setup, b) Image (52 x 109 pixel) of a steel edge obtained using $^{90}Sr/^{90}Y$ source away ~ 10 cm from the detector, courtesy of (Esposito et al., 2011).

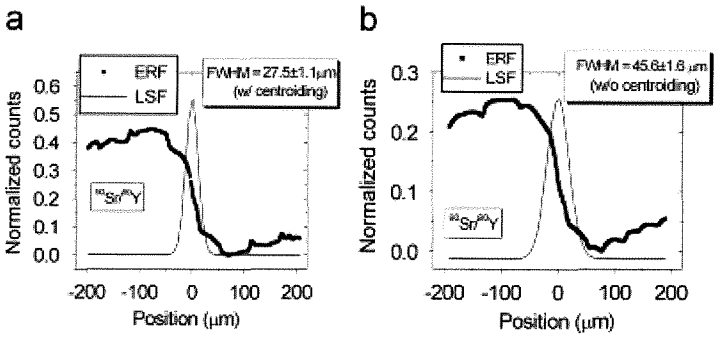

Fig. 17: Edge response function (ERF) and the corresponding oversampled Line Spread Function (LSF) with centroid approximation, b) ERF and LSF without centroid approximation, courtesy of (Esposito et al., 2011).

In addition, a ^{14}C β^- source was placed in front of the detector surface for autoradiography and spectrometry data. Fig. 18 (b) shows an image of ^{14}C taken with Timepix, where ^{14}C labelled solution was deposited on a low density paper foil with a thickness equal to 200 μm, evaporated, pressed and packed in Mylar foil of 10 μm thickness and then placed on the detector surface. The measured energy spectrum for ^{14}C electrons was compared with Monte Carlo simulation spectrum for ^{14}C electrons as shown in Fig. 18(a). The figure shows a good agreement between both data.

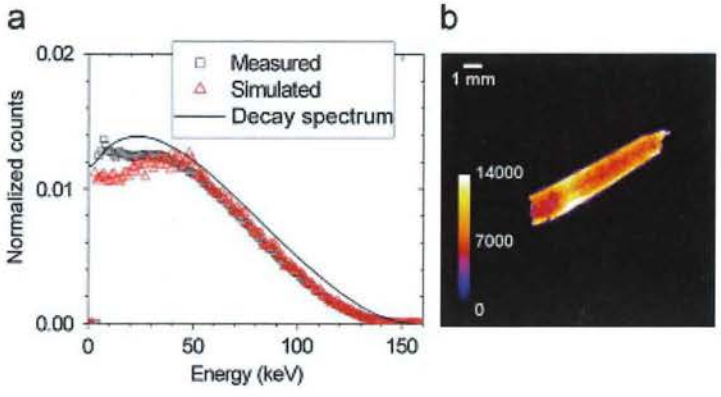

Fig. 18: a) ^{14}C measured and simulated spectrum, b) Autoradiography image of ^{14}C source placed on the surface of the Timepix, courtesy of (Esposito et al., 2011).

The results from Monte Carlo simulation agreed with the cluster analysis method used to limit the image blur in the measured tracks. In addition, the results suggest the ability to use Timepix for autoradiography with β^- tracers and for electron microscopy.

4. Conclusion

Timepix is a state of the art microdosimetry system. Its unique properties offer possibilities for use in a range of fields such as space research (Granja and Pospisil, 2014; Pinsky et al., 2008; Pinsky et al., 2011a; Pinsky et al., 2011b; Pinsky et al., 2010; Stoffle et al., 2015; Turecek et al., 2011), imaging (Dudak et al., 2015; Lemaire et al., 2013; Moats et al., 2011), medicine (Baek and Uher, 2013; Martisikova et al., 2012a) and radiation protection (Martisikova et al., 2012b). At present, most research related to Timepix is laboratory-focussed and its properties have been studied purely for research/characterisation purposes. Even though it has highly advantageous properties, the applications have not been fully exploited to date.

References:

Abate, L., Bertolucci, E., Conti, M., Di Cosmo, A., Di Cristo, C., Mettivier, G., Montesi, M.C., Russo, P., 2000. Quantitative dynamic imaging of biological processes with solid state radiation detector. Nuclear Science, IEEE Transactions on 47, 1907-1910.

Amendolia, S.R., Bertolucci, E., Bisogni, M.G., Bottigli, U., Ceccopieri, A., Ciocci, M.A., Conti, M., Delogu, P., Fantacci, M.E., Maestro, P., Marzulli, V., Pernigotti, E., Romeo, N., Rosso, V., Rosso, P., Stefanini, A., Stumbo, S., 1999. MEDIPIX: a VLSI chip for a GaAs pixel detector for digital radiology. Nuclear Instruments and Methods in Physics Research Section A: Accelerators, Spectrometers, Detectors and Associated Equipment 422, 201-205.

Amendolia, S.R., Bisogni, M.G., Bottigli, U., Ciocci, M.A., Delogu, P., Dipasquale, G., Fantacci, M.E., Giannelli, M., Maestro, P., Marzulli, V.M., Pernigotti, E., Rosso, V., Stefanini, A., Stumbo, S., 2000. Low contrast imaging with a GaAs pixel digital detector. Nuclear Science, IEEE Transactions on 47, 1478-1482.

Baek, S.H., Uher, J., 2013. Simulated dental cone beam computed tomography using Timepix, Nuclear Science Symposium and Medical Imaging Conference (NSS/MIC), 2013 IEEE, pp. 1-3.

Ballabriga, R., Campbell, M., Heijne, E., Llopart, X., Tlustos, L., Wong, W., 2011. Medipix3: A 64 k pixel detector readout chip working in single photon counting mode with improved spectrometric performance. Nuclear Instruments and Methods in Physics Research Section A: Accelerators, Spectrometers, Detectors and Associated Equipment 633, Supplement 1, S15-S18.

Ballabriga, R., Campbell, M., Heijne, E.H.M., Llopart, X., Tlustos, L., 2007. The Medipix3 Prototype, a Pixel Readout Chip Working in Single Photon Counting Mode With Improved Spectrometric Performance. Nuclear Science, IEEE Transactions on 54, 1824-1829.

Bamberger, A., Desch, K., Renz, U., Titov, M., Vlasov, N., Wienemann, P., Zwerger, A., 2007. Resolution studies on 5 GeV electron tracks observed with triple-GEM and MediPix2/TimePix-readout. Nuclear Instruments and Methods in Physics Research Section A: Accelerators, Spectrometers, Detectors and Associated Equipment 581, 274-278.

Bardelloni, G., Bertolucci, E., Boerkamp, A.L.J., Calvet, D., Conti, M., Maiorino, M., Russo, P., Visschers, J.L., 2000. A new read-out system for an imaging pixel detector, Nuclear Science Symposium Conference Record, 2000 IEEE, pp. 12/57-12/60 vol.12.

Bello, D.S.S., Nauta, B., Visschers, J., 2001. Design of analog-to-digital converters for energy-sensitive hybrid pixel detectors. Nuclear Instruments and Methods in Physics Research Section A: Accelerators, Spectrometers, Detectors and Associated Equipment 466, 218-225.

Bert, C., Niederlöhner, D., Giersch, J., Pfeiffer, K.F., Anton, G., 2003. Computed tomography using the Medipix1 chip. Nuclear Instruments and Methods in Physics Research Section A: Accelerators, Spectrometers, Detectors and Associated Equipment 509, 240-250.

Bertolucci, E., Conti, M., Mettivier, G., Russo, P., Amendolia, S.R., Bisogni, M.G., Bottigli, U., Ceccopieri, A., Ciocci, M.A., Delogu, P., Fantacci, M.E., Maestro, P., Marzulli, V.M., Pernigotti, E., Romeo, N., Rosso, V., Stefanini, A., Stumbo, S., 1999. GaAs pixel radiation detector as an autoradiography tool for genetic studies. Nuclear Instruments and Methods in Physics Research Section A: Accelerators, Spectrometers, Detectors and Associated Equipment 422, 242-246.

Bisogni, M.G., Campbell, M., Conti, M.D., P ; Fantacci, M.E., Heijne, E.H.M., Maestro, P., Magistrati, G., Marzulli, V.M., Meddeler, G., Mikulec, B., Pernigotti, E., Rosso, V., Schwarz, C., Snoeys, W., Stumbo, S., Watt, J., 1998. Performance of 4096 pixel photon counting chip, 43rd SPIE International Symposium on Optical Science, Engineering and Instrumentation : Hard X-ray and Gamma-Ray Detector Physics and Applications, San Diego, CA, USA.

Bisogni, M.G., Delogu, P., Fantacci, M.E., Mettivier, G., Montesi, M.C., Novelli, M., Quattrocchi, M., Rosso, V., Russo, P., Stefanini, A., 2003. A Medipix2-based imaging system for digital mammography with silicon pixel detectors, Nuclear Science Symposium Conference Record, 2003 IEEE, pp. 1509-1512 Vol.1503.

Campbell, M., 2011. 10 years of the Medipix2 Collaboration. Nuclear Instruments and Methods in Physics Research Section A: Accelerators, Spectrometers, Detectors and Associated Equipment 633, Supplement 1, S1-S10.

Campbell, M., Havranek, V., Heijne, E., Holy, T., Idarraga, J., Jakubek, J., Lebel, C., Leroy, C., Llopart, X., Novotny, J., Pospisil, S., Tlustos, L., Vykydal, Z., 2007. Charge collection from proton and alpha particle tracks in silicon pixel detector devices, Nuclear Science Symposium Conference Record, 2007. NSS '07. IEEE, pp. 1047-1050.

Campbell, M., Heijne, E.H.M., Meddeler, G., Pernigotti, E., Snoeys, W., 1998. Readout for a 64 x 64 pixel matrix with 15-bit single photon counting. Nuclear Science, IEEE Transactions on 45, 751-753.

CERN, 2011. Medipix.

Chmeissani, M., Mikulec, B., 2001. Performance limits of a single photon counting pixel system. Nuclear Instruments and Methods in Physics Research Section A: Accelerators, Spectrometers, Detectors and Associated Equipment 460, 81-90.

Dammer, J., Frallicciardi, P.M., Jakubek, J., Jakubek, M., Pospisil, S., Prenerova, E., Vavrik, D., Volter, L., Weyda, F., Zemek, R., 2009. Real-time in-vivo μ-imaging with Medipix2. Nuclear Instruments and Methods in Physics Research Section A: Accelerators, Spectrometers, Detectors and Associated Equipment 607, 205-207.

Davidson, D.W., Watt, J., Tlustos, L., Mikulec, B., Campbell, M., Mathieson, K., O'Shea, V., Smith, K.M., Rahman, M., 2003. Detective quantum efficiency of the Medipix pixel detector. Nuclear Science, IEEE Transactions on 50, 1659-1663.

Dudak, J., Zemlicka, J., Krejci, F., Polansky, S., Jakubek, J., Mrzilkova, J., Patzelt, M., Trnka, J., 2015. X-ray micro-CT scanner for small animal imaging based on Timepix detector technology. Nuclear Instruments and Methods in Physics Research Section A: Accelerators, Spectrometers, Detectors and Associated Equipment 773, 81-86.

Esposito, M., Jakubek, J., Mettivier, G., Pospisil, S., Russo, P., Solc, J., 2011. Energy sensitive Timepix silicon detector for electron imaging. Nuclear Instruments and Methods in Physics Research Section A: Accelerators, Spectrometers, Detectors and Associated Equipment 652, 458-461.

Faruqi, A.R., Cattermole, D.M., 2002. Digital detectors for electron microscopy. Nuclear Instruments and Methods in Physics Research Section A: Accelerators, Spectrometers, Detectors and Associated Equipment 478, 88-94.

Gimenez, E.N., Ballabriga, R., Campbell, M., Horswell, I., Llopart, X., Marchal, J., Sawhney, K.J.S., Tartoni, N., Turecek, D., 2011. Characterization of Medipix3 With Synchrotron Radiation. Nuclear Science, IEEE Transactions on 58, 323-332.

Granja, C., Jakubek, J., Platkevic, M., Pospisil, S., Vykydal, Z., 2010. Detection and Real Time Spectroscopy of Charged Particles with the TimePix Pixel Detector. AIP Conference Proceedings 1204, 75-79.

Granja, C., Pospisil, S., 2014. Quantum dosimetry and online visualization of X-ray and charged particle radiation in commercial aircraft at operational flight altitudes with the pixel detector Timepix. Advances in Space Research 54, 241-251.

Jakubek, J., 2009. Energy-sensitive X-ray radiography and charge sharing effect in pixelated detector. Nuclear Instruments and Methods in Physics Research Section A: Accelerators, Spectrometers, Detectors and Associated Equipment 607, 192-195.

Jakubek, J., 2011. Precise energy calibration of pixel detector working in time-over-threshold mode. Nuclear Instruments and Methods in Physics Research Section A: Accelerators, Spectrometers, Detectors and Associated Equipment 633, Supplement 1, S262-S266.

Jakubek, J., Cejnarova, A., Holy, T., Pospisil, S., Uher, J., Vykydal, Z., 2008. Pixel detectors for imaging with heavy charged particles. Nuclear Instruments and Methods in Physics Research Section A: Accelerators, Spectrometers, Detectors and Associated Equipment 591, 155-158.

Kraus, V., Holik, M., Jakubek, J., Kroupa, M., Soukup, P., Vykydal, Z., 2011. FITPix — fast interface for Timepix pixel detectors. JINST 6, C01079.

Lemaire, H., Amgarou, K., Khalil, R.A., Angelique, J.C., Bonnet, F., De Toro, D., Carrel, F., Giarmana, O., Gmar, M., Menaa, N., Menesguen, Y., Normand, S., Patoz, A., Schoepff, V., Talent, P., Timi, T., 2013. Implementation of an imaging spectrometer for localization and identification of radioactive sources. 2013 3rd International Conference on Advancements in Nuclear Instrumentation, Measurement Methods and their Applications (ANIMMA), 5 pp.-5 pp.

Llopart, X., Ballabriga, R., Campbell, M., Tlustos, L., Wong, W., 2007. Timepix, a 65k programmable pixel readout chip for arrival time, energy and/or photon counting measurements. Nuclear Instruments and Methods in Physics Research Section A: Accelerators, Spectrometers, Detectors and Associated Equipment 581, 485-494.

Llopart, X., Campbell, M., Dinapoli, R., San Segundo, D., Pernigotti, E., 2002. Medipix2: A 64-k pixel readout chip with 55-μm square elements working in single photon counting mode. Nuclear Science, IEEE Transactions on 49, 2279-2283.

Lutz, G., 2007. Semiconductor Radiation Detectors Device Physics, 2nd ed. Springer-Verlag Berlin Heidelberg, New York.

Manach, E., Gal, O., 2002. Simulation of single-event energy-deposition spreading in a hybrid pixellated detector for γ imaging. Nuclear Instruments and Methods in Physics Research Section A: Accelerators, Spectrometers, Detectors and Associated Equipment 487, 142-150.

Martisikova, M., Hartmann, B., Gwosch, K., Jakubek, J., Granja, C., Jakel, O., 2012a. Study of the Capabilities of the Timepix Detector for Ion Beam Radiotherapy Applications. 2012 IEEE Nuclear Science Symposium and Medical Imaging Conference Record (NSS/MIC 2012) & Workshop on Room-Temperature Semiconductor X-Ray and Gamma-Ray Detectors, 4324-4328.

Martisikova, M., Jakubek, J., Gwosch, K., Hartmann, B., Telsemeyer, J., Pospisil, S., Jakel, O., 2012b. Monitoring of ion beam energy by tracking of secondary ions: First measurements in a patient-like phantom. 2012 IEEE Nuclear Science Symposium and Medical Imaging Conference Record (NSS/MIC 2012) & Workshop on Room-Temperature Semiconductor X-Ray and Gamma-Ray Detectors, 1914-1917.

Mettivier, G., Montesi, M.C., Russo, P., 2003. First images of a digital autoradiography system based on a Medipix2 hybrid silicon pixel detector. Physics in medicine and biology 48, N173-181.

Mikulec, B., 2000. Single Photon Detection with Semiconductor Pixel Arrays for Medical Imaging Applications, in: University of Vienna, A. (Ed.), CERN-Thesis 2000-021. Geneva : CERN, 2000., Vienna U., p. 185 p.

Mikulec, B., Campbell, M., Dipasquale, G., Schwarz, C., Watt, J., 2001. Characterisation of a single photon counting pixel system for imaging of low-contrast objects. Nuclear Instruments and Methods in Physics Research Section A: Accelerators, Spectrometers, Detectors and Associated Equipment 458, 352-359.

Mitschke, M., Giersch, J., Anton, G., 2004. Simulation of signal generation processes in semiconductor sensor layers for Medipix1 and 2. Nuclear Instruments and Methods in Physics Research Section A: Accelerators, Spectrometers, Detectors and Associated Equipment 531, 62-67.

Moats, R.A., Yang, T., Hugg, J.W., Meier, D., Koos, D., Hartsough, N.E., Patt, B.E., Wagenaar, D.J., 2011. Basic design and simulation of a SPECT microscope for in vivo stem cell imaging. Proceedings of the SPIE - The International Society for Optical Engineering 7961, 79614B (79618 pp.)-79614B (79618 pp.).

Niederlöhner, D., Bert, C., Giersch, J., Pfeiffer, K.F., Anton, G., 2003. Threshold characterisation of the Medipix1 chip. Nuclear Instruments and Methods in Physics Research Section A: Accelerators, Spectrometers, Detectors and Associated Equipment 509, 138-145.

Pfeiffer, K.F.G., Giersch, J., Anton, G., 2004. How good is better? A comparison between the Medipix1 and the Medipix2 chip using mammographic phantoms. Nuclear Instruments and Methods in Physics Research Section A: Accelerators, Spectrometers, Detectors and Associated Equipment 531, 246-250.

Pfeiffer, K.F.G., Giersch, J., Anton, G., Bätz, L., Hoheisel, M., 2003. Large-scale images taken with the Medipix1 chip. Nuclear Instruments and Methods in Physics Research Section A: Accelerators, Spectrometers, Detectors and Associated Equipment 509, 340-345.

Pinsky, L., Chancellor, J., Minthaka, D., 2008. Evolving the Medipix2 Technology For Use As An Active Space Radiation Dosimeter, Aerospace Conference, 2008 IEEE, pp. 1-8.

Pinsky, L., Stoffle, N., Empl, A., Jakubek, J., Pospisil, S., Leroy, C., Kitamura, H., Yasuda, N., Uchihori, Y., 2011a. Application of the Medipix2 technology to space radiation dosimetry and hadron therapy beam monitoring. Radiation Measurements 46, 1610-1614.

Pinsky, L.S., Empl, A., Gutierrez, A., Jakubek, J., Kitamura, H., Miller, J., Leroy, C., Stoffle, N., Pospisil, S., Uchihori, Y., Yasuda, N., Zeitlin, C., 2011b. Penetrating heavy ion charge and velocity discrimination with a TimePix-based Si detector (for space radiation applications). Nuclear Instruments and Methods in Physics Research Section A: Accelerators, Spectrometers, Detectors and Associated Equipment 633, Supplement 1, S190-S193.

Pinsky, L.S., Empl, A., Stoffle, N., Leroy, C., Gutierrez, A., Jakubek, J., Pospisil, S., Kitamura, H., Uchihori, Y., Nakahiro, Y., Miller, J., Zeitlin, C., 2010. Heavy ion charge and velocity resolution with a Medipix-based active Space Radiation Dosimeter, Aerospace Conference, 2010 IEEE, pp. 1-6.

Pugatch, V., Campbell, M., Chaus, A., Eremenko, V., Homenko, S., Kovalchuk, O., Llopart, X., Okhrimenko, O., Pospisil, S., Shelekhov, A., Storizhko, V., Tlustos, L., 2011. Metal and hybrid TimePix detectors imaging beams of particles. Nuclear Instruments and Methods in Physics Research Section A: Accelerators, Spectrometers, Detectors and Associated Equipment 650, 194-197.

Rosenfeld, A.B., Cutajar, D., Lerch, M.L.F., Takacs, G., Cornelius, I.M., Yudelev, M., Zaider, M., 2006. Miniature semiconductor detectors for in vivo dosimetry. Radiation protection dosimetry 120, 48-55.
Rossi, L., Fischer, P., Rohe, T., Wermes, N., 2006. Pixel Detectors: From Fundamentals to Applications. Springer Berlin Heidelberg, The Netherlands.
Rügheimer, T.K., Gebert, U., Michel, T., Anton, G., Séguinot, J., Joram, C., 2008. Experimental demonstration of a hybrid photon detector concept based on the Timepix detector. Nuclear Instruments and Methods in Physics Research Section A: Accelerators, Spectrometers, Detectors and Associated Equipment 595, 353-358.
Schwarz, C., Campbell, M., Goeppert, R., Heijne, E.H.M., Ludwig, J., Meddeler, G., Mikulec, B., Pernigotti, E., Rogalla, M., Runge, K., Söldner-Rembold, A., Smith, K.M., Snoeys, W., Watt, J., 1999. X-ray imaging using a hybrid photon counting GaAs pixel detector. Nuclear Physics B - Proceedings Supplements 78, 491-496.
Sinor, M., Jakubek, J., Linhart, V., Mikulec, B., Pospisil, S., Sopko, B., 2003. Charge sharing studies with a Medipix1 pixel device. Nuclear Instruments and Methods in Physics Research Section A: Accelerators, Spectrometers, Detectors and Associated Equipment 509, 346-354.
Stoffle, N., Pinsky, L., Kroupa, M., Hoang, S., Idarraga, J., Amberboy, C., Rios, R., Hauss, J., Keller, J., Bahadori, A., Semones, E., Turecek, D., Jakubek, J., Vykydal, Z., Pospisil, S., 2015. Timepix-based radiation environment monitor measurements aboard the International Space Station. Nuclear Instruments and Methods in Physics Research Section A: Accelerators, Spectrometers, Detectors and Associated Equipment 782, 143-148.
Turecek, D., Pinsky, L., Jakubek, J., Vykydal, Z., Stoffle, N., Pospisil, S., 2011. Small Dosimeter based on Timepix device for International Space Station. Journal of Instrumentation 6, C12037.
Vallerga, J., McPhate, J., Tremsin, A., Siegmund, O., 2008. High-resolution UV, alpha and neutron imaging with the Timepix CMOS readout. Nuclear Instruments and Methods in Physics Research Section A: Accelerators, Spectrometers, Detectors and Associated Equipment 591, 151-154.
Žemlička, J., Jakůbek, J., Kroupa, M., Tichý, V., 2009. Energy- and position-sensitive pixel detector Timepix for X-ray fluorescence imaging. Nuclear Instruments and Methods in Physics Research Section A: Accelerators, Spectrometers, Detectors and Associated Equipment 607, 202-204.

Statement of Authorship

Title of Papers	Overview of current applications of the Timepix detector in radiation physics
Publication Status	☐ Published ☐ Accepted for Publication ☑ Submitted for Publication ☐ Unpublished and Unsubmitted work written in manuscript style
Publication Details	Ruqaya AL Darwish, Eva Bezak, Loredana Marcu, and Anatoly Rozenfeld, Overview of current applications of the Timepix detector in radiation physics

Principal Author

Name of Principal Author (Candidate)	Ruqaya AL Darwish
Contribution to the Paper	Reviewed Timepix publication This paper was primarily written by Ruqaya Al Darwish and acted as corresponding author
Overall percentage (%)	80%
Certification:	This paper reports on review I conducted during the period of my Higher Degree by Research candidature and is not subject to any obligations or contractual agreements with a third party that would constrain its inclusion in this thesis. I am the primary author of this paper.
Signature	Date: 30/8/2016

Co-Author Contributions

By signing the Statement of Authorship, each author certifies that:

i. the candidate's stated contribution to the publication is accurate (as detailed above);

ii. permission is granted for the candidate in include the publication in the thesis; and

iii. the sum of all co-author contributions is equal to 100% less the candidate's stated contribution.

Name of Co-Author	Eva Bezak
Contribution to the Paper	Introduced the initial concept of the review as well as transcript editing.
Signature	Date: 30/8/16

Name of Co-Author	Loredana Marcu		
Contribution to the Paper	Loredana Marcu provided assistance with paper editing.		
Signature		Date	29/8/2016

Name of Co-Author	Anatoly Rozenfeld		
Contribution to the Paper	Assistance with paper editing.		
Signature		Date	30/08/2016

Overview of current applications of the Timepix detector in radiation physics

Ruqaya AL Darwish[1,2,3], Eva Bezak[2,4,5], Loredana Marcu[2,6], Anatoly Rozenfeld[7]

[1] Department of Medical Physics, Royal Adelaide Hospital, Adelaide, Australia
[2] School of Physical Sciences, University of Adelaide, Adelaide, Australia
[3] Ministry of Higher Education, Saudi Arabia
[4] International Centre for Allied Health Evidence, Sansom Institute, University of South Australia, Adelaide, Australia
[5] Sansom Insitute for Health Research, University of South Australia, Adelaide, Australia
[6] Faculty of Science, University of Oradea, Oradea 410087, Romania
[7] Centre of Medical Radiation Physics, University of Wollongong, Wollongong, NSW, Australia.

Abstract

With the development of hadron and targeted therapies, there is a renewed interest in novel microdosimetry detectors. One detector that fulfils the criteria to be used in this sense is Timepix.

The current overview describes specific applications of Timepix that may be of interest to medical physicists showing that more investigation is still required to gain the full benefit of Timepix applications in the fields of radiation therapy and imaging. More specifically, the application of Timepix to targeted radiotherapies remains absent despite the main advantage of Timepix, which is tracking energy deposition at a micrometer level.

1. Introduction

The aim of this article is to review the major applications of Timepix for X-ray, gamma ray, electron and heavy particle detection, which opens a window to some promising applications in the field of medical radiation. The paper is a compilation of Timepix applications in radiation detection and they are discussed in the sections below.

2. Timepix in Photomultiplier Applications

The standard photomultiplier tubes (PMTs) (Fig. 1) are essential devices in particle, atomic, solid state, or medical physics. A PMT consists of a sealed vacuum tube with an electric field between a photo-cathode and a silicon anode. To improve the spatial resolution of a PMT, its dynode system can be modified using Timepix detector. Consequently, in 2008 a hybrid photon detector (HPD) based on Timepix was presented by Rügheimer and his group as illustrated in Fig. 20 (Rügheimer et al., 2008). Silicon anode was replaced by pixelated silicon Timepix detector in a new modified design of HPD this time. As shown by the results, this HPD with the Timepix anode has the advantage of higher spatial and time resolution for detection of photo-electron compared to conventional anode. In this experiment, energies between 6 and 20 keV of photo-electrons were detected and the data was fitted with a linear fit to extract the time-walk effect (i.e. the time when the charge pulse exceeds the discriminator threshold). The slope of that linear fit gives the peaking time of the preamplifier output pulse of 130 ns. Time-resolution of 10.5 ns was measured if the time-walk due to charge-sharing among neighbouring pixels was neglected and only single clusters were considered.

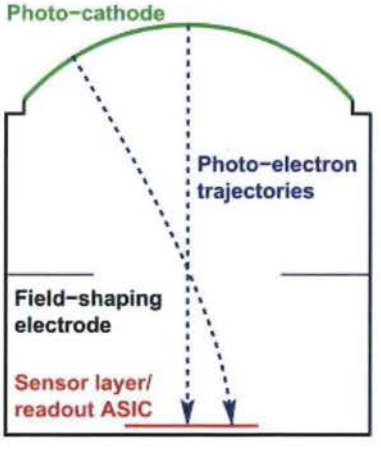

Fig. 1: The general concept of HPD where Timepix replacing the sensor layer. ASIC: application specific integrated circuit, courtesy of (Rügheimer et al., 2008).

Comparing these results with the simulation data performed by Geant4 Monte Carlo tool kit as shown in Fig. 2, the group determined the limiting factors of time resolution to be: electron backscattering from the sensor layer, charge sharing effect and the finite rise time of the preamplifier output pulse. However, future work should be focused on improving time resolution by using larger pixels and reducing the sensor thickness.

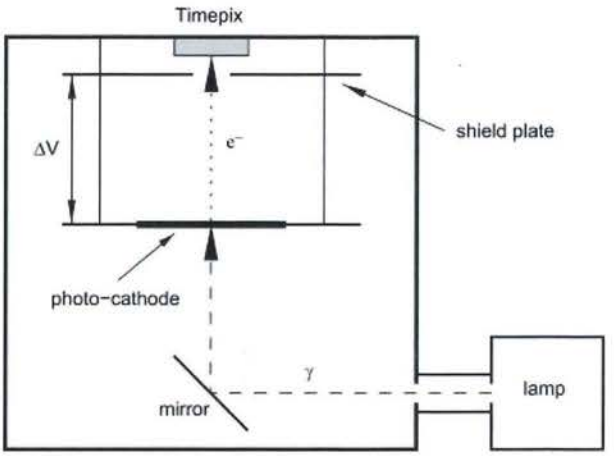

Fig. 2: HPD/Timepix setup with Timepix detector on the top 41 mm away from the photo-cathode to investigate Timepix detector response to photo-electrons, courtesy of (Rügheimer et al., 2008).

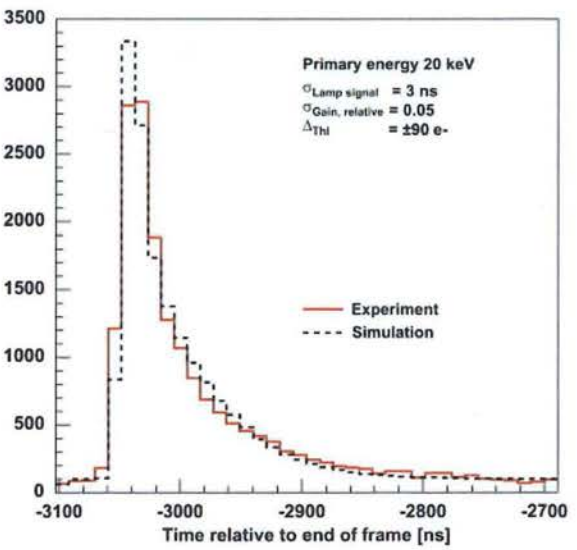

Fig. 3: Experimental and simulation data, courtesy of (Rügheimer et al., 2008).

Anton et al. (Anton et al., 2009) considered the same HPD assembly from Rügheimer et al. (Rügheimer et al., 2008) and developed a computational model to calculate the photo-electron energy deposited in each pixel, the charge signal arriving to each pixel electrode, and the time response of the energy distribution (Anton et al., 2009). In their experiments, photo-electrons in the range 6 to 20 keV were detected. It was found that the electron-hole pairs were created within a distance of 10 μm of the pixel's surface and then diffused to neighbouring pixels. This presented the need to have a further development to optimise ASIC design. The development is called Photopix and comes with a thinner silicon sensor and a larger pixel pitch. In addition, Anton et al. (Anton et al., 2009) emphasised the advantages of the proposed HPD compared to other HPDs with silicon sensors. Even though, the HPD used in their work has high total

acquisition rate, each individual pixel deals with low rate signal. That means the pixel's electronics can process the signals effortlessly.

Detection of optical photons and imaging properties were also studied for this HPD /Timepix setup (Gebert et al., 2010). Gebert and his group specifically investigated the time resolution, imaging properties and dark-count rate. In this experiment, the detector was placed into a pumped vacuum tube as shown in Fig. 3. CsI photocathode released photo-electrons by pulses of self-triggering UV discharge lamp and electrons were then accelerated towards the detector. Timepix was operated in Timepix mode to determine the time of events. Fifty thousand frames were recorded.

It was concluded that unlike PMTs, the new assembly was able to detect optical photons and to distinguish between noise, one, two or more photo-electrons. The experiments proved the ability of Timepix to control electronic noise using an appropriate threshold setting and to deal with high dark-count rates as a consequence of both the high number of pixels and the location of the electronics in Timepix (Gebert et al., 2010).

3. Timepix and Stopping Power Measurements

The spatial, spectral and temporal resolutions of Timepix for detection and visualization of charged particles was investigated by Granja et al. (Granja et al., 2010).

Since the stopping of charged particles depends on the particle momentum, they can be stopped in a sensor, depositing all their energy, or pass through a sensor volume while depositing some of their kinetic energy along their trajectory. As a result, Timepix can be used as a stopping or $\Delta E/\Delta x$ detector (Granja et al., 2010). This may have an application in photon therapy and ion therapy. Fig. 4 shows detection of ^{136}I ion (36 MeV) in portion (19 x 19 pixels) of Timepix in TOT mode. The particle's full energy is calculated approximately by summing the charge collected in every pixel (Granja et al., 2008; Granja et al., 2010).

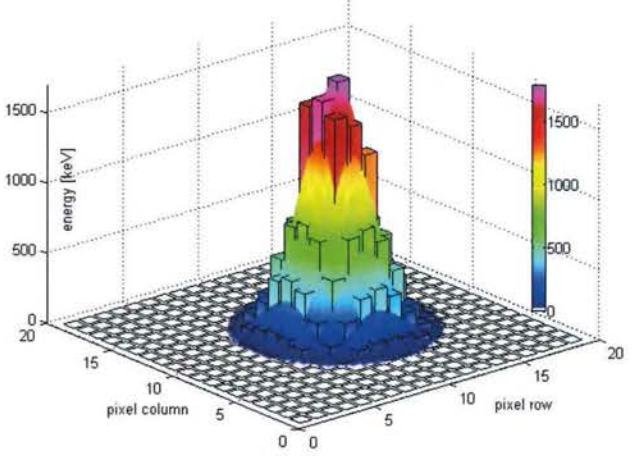

Fig. 4: ^{136}I ion detection in 19 x 19 pixels of Timepix detector operated in TOT mode, courtesy of (Granja et al., 2010).

The response of Timepix in TOT mode to heavy ions with kinetic energies between 4 to 110 MeV and mass range between 3 and 136 emitted from a fission-fragment separator Lohengrin (at the Institute Laue Langevin in Grenoble, France) was investigated (Granja et al., 2011).

Timepix was placed on Lohengrin focal plane and the fission fragments were focused towards the Timepix. ^{239}Pu and ^{235}U were placed in a neutron flux of 5 x 10^4 n/cm^2/s to cause fission. Fission products were then detected by Timepix. Spatial distribution of detection of predominantly ^{90}Sr with energy 110 MeV and the exposure time of 19 s is shown in Fig. 5 (Timepix bias of 11 V and pixel energy threshold of 8 keV). The collected energy per pixel is shown as a colour bar in keV in picture on the right, while the left picture shows the full detector (256 x 256 pixels).

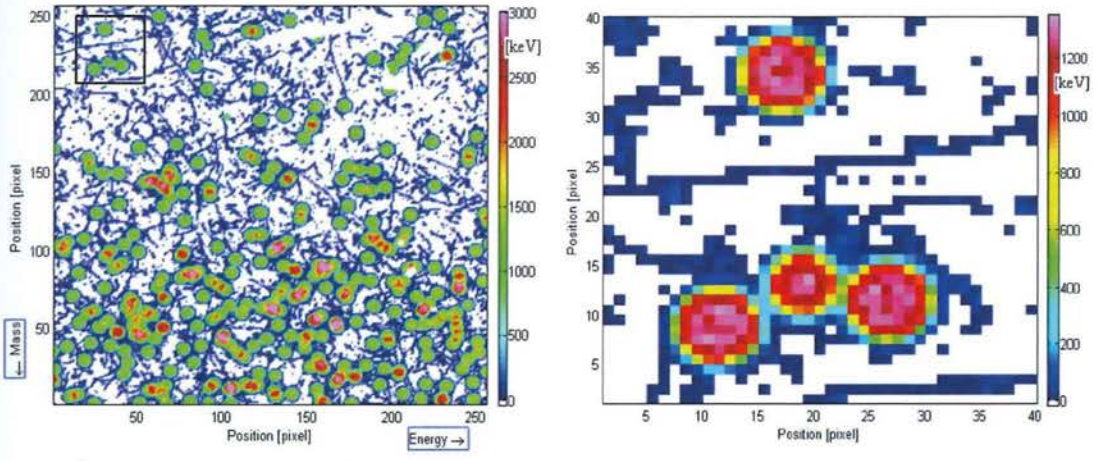

Fig. 5: Timepix detection of ^{90}Sr (110 MeV) in TOT mode. The figure shows an example of the spatial distribution of ions along the mass- and energy- dispersive directions, courtesy of (Granja et al., 2011).

The pixel signal response is linear for charged particles with energy range of low MeV such as alpha particles. In this case, the charge spread cluster has a Gaussian shape while for charged particles with higher energy range ($\geq$ 10 MeV), the charge spread cluster will be distorted from the normal Gaussian shape. This distortion depends on the pixel bias voltage, pixel baseline and the threshold as shown in Fig. 6.

It was found that for conventional detector settings, the electronic pixel signal responses were distorted when the energy collected per pixel reached around 1 MeV which can happen for heavy ions with energies above several tens of MeV, as the detector will saturate gradually with increasing energy. This effect can be managed using suitable pixel signal baseline, threshold levels, sensor chip bias voltage (Granja et al., 2011).

The group concluded that the optimal settings for Timepix are 5 to 10 V bias voltage with baseline parameter FBK 128 (parameter used in software specification). These setting were tested for different ions and the results are shown in Fig. 7.

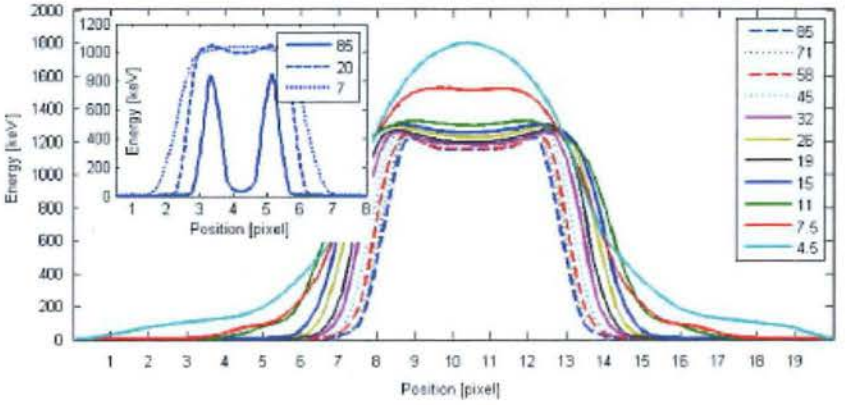

Fig. 6: Sectional view profile of cluster shape of ^{98}Zr ions (100 MeV) at different bias voltage in TOT mode, courtesy of (Granja et al., 2011).

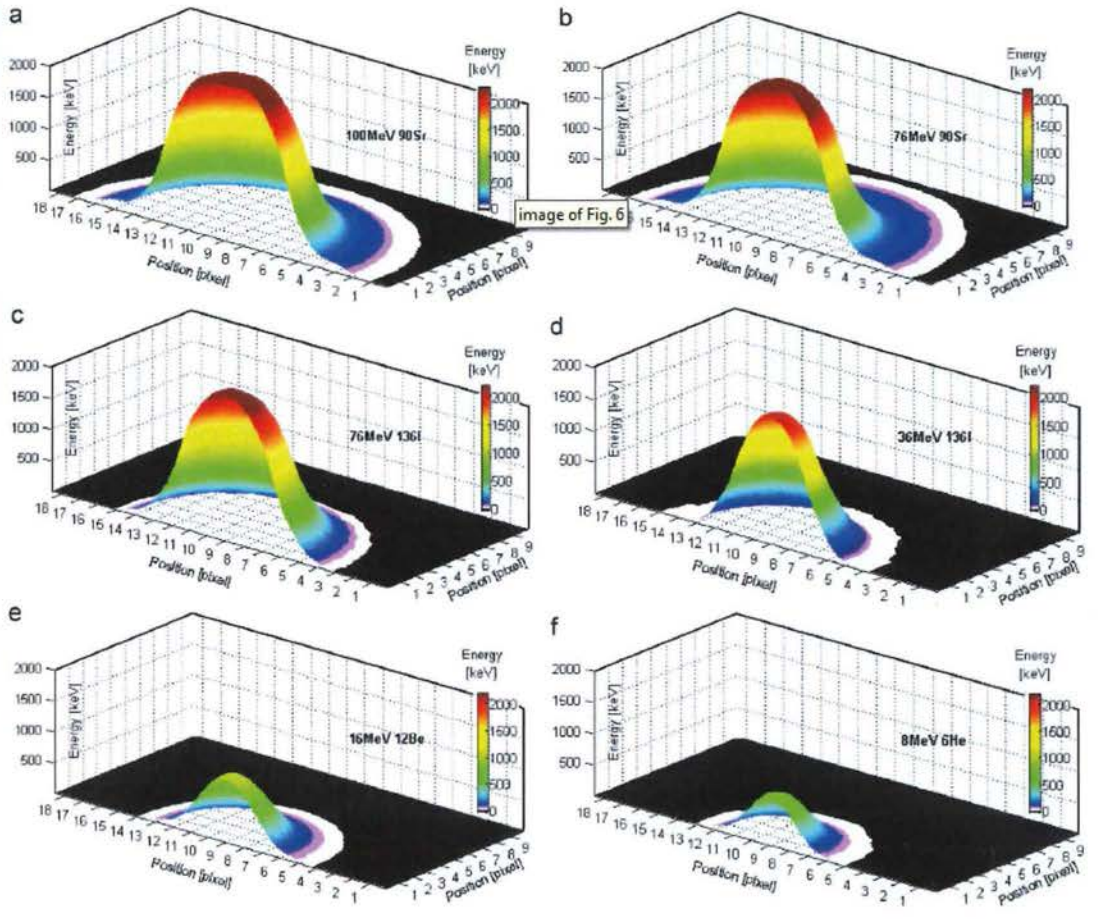

Fig. 7: Timepix detection of ions in TOT mode with bias voltage 7.5 V and Baseline FBK = 128 for a) 100 MeV ^{90}Sr, b) 76 MeV ^{90}Sr, c) 76 MeV ^{136}I, bias voltage 11 V and Baseline FBK = 128 for d) 36 MeV and bias voltage 11 V and Baseline FBK = 160 for e) 16 MeV ^{12}Be, f) 8 MeV ^{6}He, courtesy of (Granja et al., 2011).

4. Timepix and Neutron Detection

A combination of Timepix and a thin plastic scintillator (placed on the surface of the Timepix) were used as a spectrometer and camera of fast neutrons (Uher and Jakubek, 2011) as shown in Fig. 8. The fast neutrons recoil protons in the scintillator, which are then detected by the Timepix detector. The response was analysed to retrieve the energy and the direction of protons. At the same time, the light from the scintillator was detected by a Silicon Photo-Multiplier (SiPM). The energy and direction from Timepix and the SiPM were reconstructed to predict the energy and direction of the neutrons. The results were compared with a simulation using Monte Carlo methods (Uher and Jakubek, 2011).

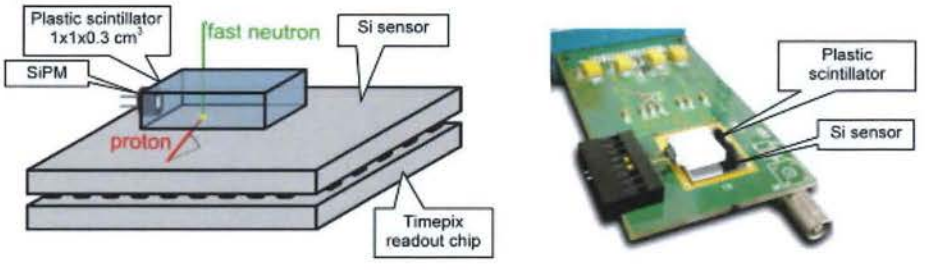

Fig. 8: Fast neutron detection with Timepix and scintillator setup, courtesy of (Uher and Jakubek, 2011).

A Monte Carlo simulation was done for a monoenergetic neutron beam of 14 MeV. Results showed a good agreement between the simulated and measured data. The differences observed between the simulated and measured data were due to the converted protons, from the neutron, that can pass through the 300 μm of the Timepix chip, which requires a reconstruction of the neutron energy spectrum. The data is presented in Fig. 9.

The paper concluded that when combined with plastic scintillators, Timepix works as a spectrometer and a camera for fast neutrons, so both energies and direction of fast neutrons can be measured. Furthermore, the neutron energy reconstruction produced by protons during their passage through the sensor layer of Timepix was also discussed.

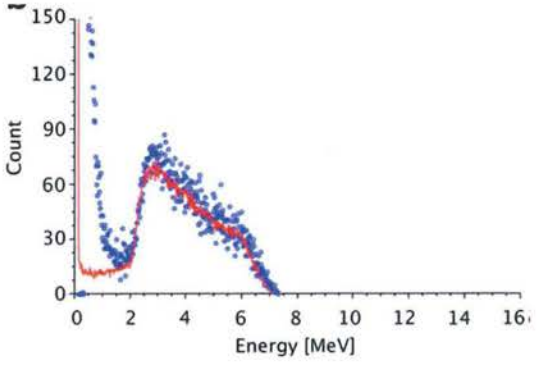

Fig. 9: A comparison between a measured (circles) and simulated (full line) energy deposited spectra by proton inside Timepix for monoenergetic beam (14 MeV neutrons), courtesy of (Uher and Jakubek, 2011).

5. Timepix and Hadron Therapy

Timepix was applied in hadron therapy by Opalka and his group (Opalka et al., 2012) in Heidelberg Ion-Beam Therapy Center (HIT), Germany (Opalka et al., 2012). The objective of this work was to use Timepix in a TOT mode to detect and characterise secondary radiation generated from monoenergetic carbon ion beams (250 MeV/u) of 10.1 mm FWHM in a water phantom of dimensions 355 × 355 × 420 mm^3. The positioning of Timepix in the water phantom is shown in Fig. 10 (15 mm and 40 mm away from the beam axis) where it was placed inside a waterproof rubber sleeve. The number of frames was 1500 with 1 ms exposure time. Each track observed on the PC monitor corresponds to one particle, and from the shape of the cluster generated the particle can be differentiated. Small clusters correspond to photons, curvy tracks to electrons, large clusters to alpha particles and linear clusters to protons. Beam particle energy can be measured, as well as the total energy deposited by secondary particles. More than five million events were processed. As the beam intensity varied for each detector position, the number of events in each particle group was normalized to the total number of events in each position (not to the initial beam intensity) which reflected the changes in the relative composition of the beam in water depending on the depth in a phantom, as shown in Fig. 11.

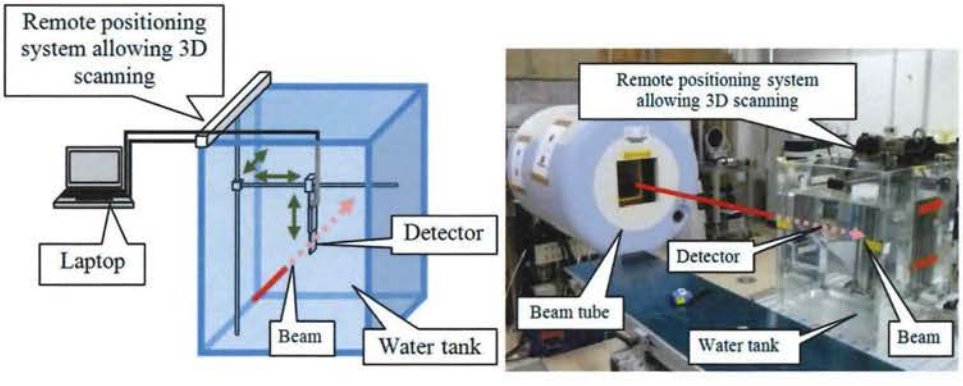

Fig. 10: Setup of measurement of radiation distribution in water tank phantom using Timepix detector for hadron therapy, courtesy of (Opalka et al., 2012).

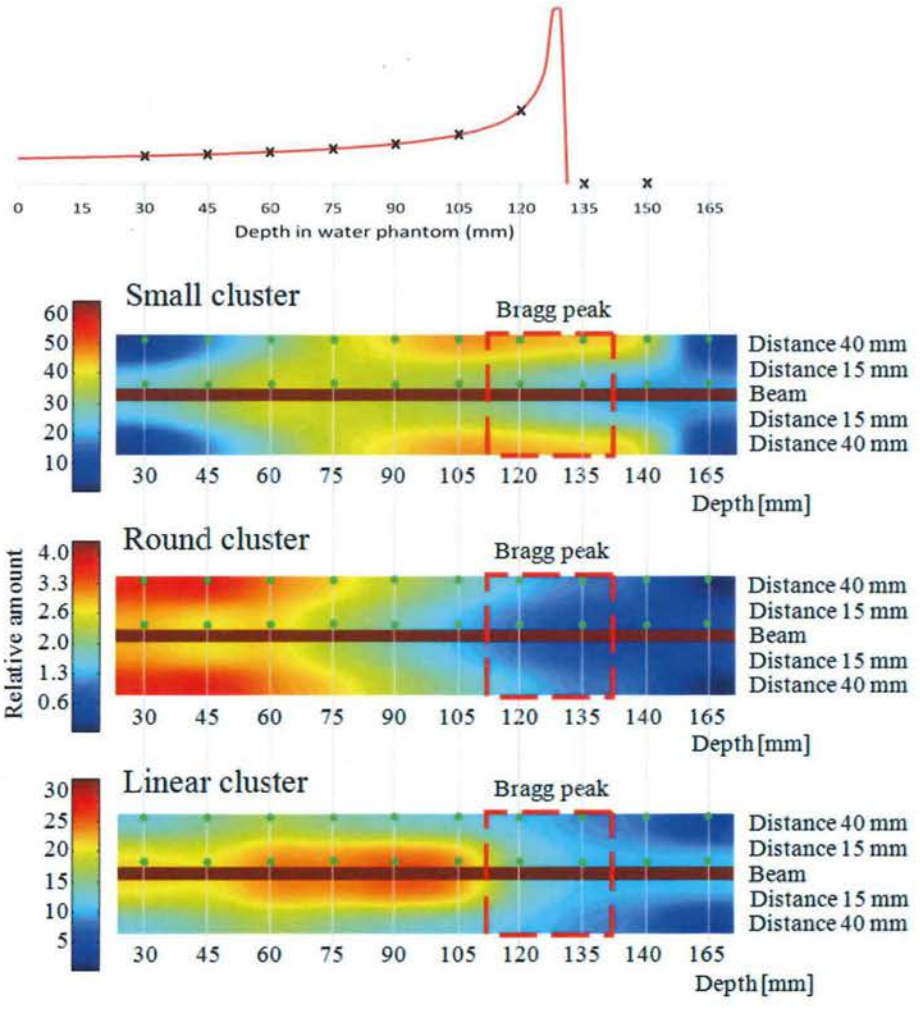

Fig. 11: Spatial distribution of radiation in the water tank phantom for small, round and linear clusters events where the Bragg curve is on top, courtesy of (Opalka et al., 2012).

The study (Opalka et al., 2012) concluded that Timepix allows identification of secondary ions traces as well as their angular distribution. Additionally, depending on the phantom depth, the relative amount of particles of each type will be different. For instance, the number of small clusters decreased with increasing the depth.

In another study Opalka et al. (Opalka et al., 2013) conducted the same experiment using a PMMA target instead of a water tank (Fig. 12) with the aim to determinate secondary particles and their angular direction and to evaluate the difference in stopping powers for different particles which can be used to correct the total therapeutic dose.

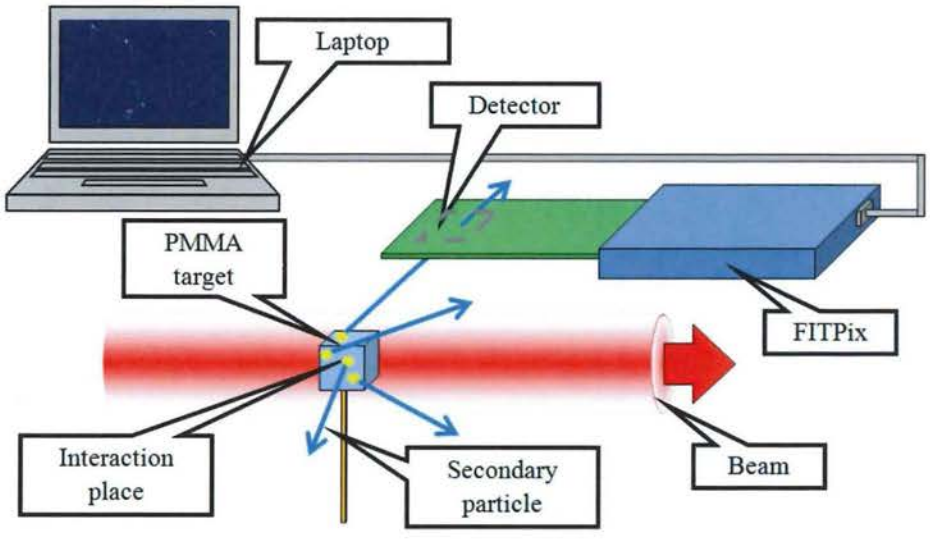

Fig. 12: Experimental setup to measure the secondary radiation produced as a result of irradiating a PMMA target with monoenergetic carbon ion beams setup, courtesy of (Opalka et al., 2013).

A monoenergetic carbon ion beam with 4.3 mm FWHM and energy of 430 MeV/u was used to irradiate a 1 mm^3 PMMA target. Timepix was placed in parallel position with the beam at 30 mm distance and secondary particles were detected. 33000 frames were acquired in a 1 ms exposure time.

The LET for each particle was calculated and compared with Monte Carlo simulations (Fig. 13). The difference between the two data sets is in the low energy region where a peak is recorded in the experimental spectrum. This peak corresponds to electrons that were not considered in the simulation (Opalka et al., 2013). After subtracting it from the spectrum the results fit the experimental function.

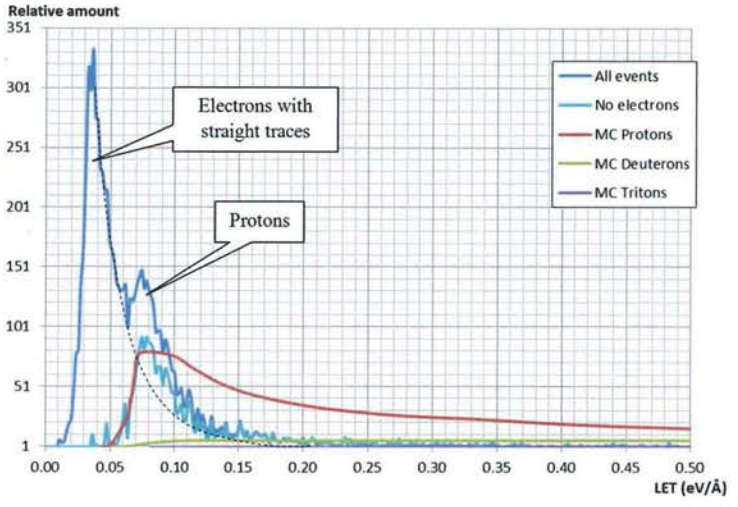

Fig. 13: Experimental (blue lines) and Monte Carlo simulation of LET spectra of different particles, courtesy of (Opalka et al., 2013).

Timepix was also used to investigate the ion beam fragmentation by Martisikova et al. (Martišíková et al., 2012). Many ion species are produced as a result of nuclear reactions during ion beam therapy. Each of these secondary ions has its own biological effectiveness and therefore it is very important to identify them inside a patient/phantom to account for additional dose and/or associated radiobiological effects. The group tested the Timepix response to proton and carbon ions. The results showed that Timepix can identify the primary, scattered and secondary ions associated with the therapy. The group studied Timepix signals, sizes and distribution of charge clusters as well as cluster energy. They found them to be different for protons and carbon ions for the same range in a phantom which makes Timepix useful for spectroscopic use and as a tool for biological effectiveness estimations (Martišíková et al., 2012).

6. Timepix and Brachytherapy

In the work of Loo at al. (Loo et al., 2014; Loo et al., 2013) Timepix was incorporated into a so called BrachyView system and used for real time in-body imaging during prostate brachytherapy to monitor the position of low dose seeds. Loo et al. (Loo et al., 2014) also presented quantitative analysis of Timepix imaging performance for different thicknesses of tissue-equivalent plastic inserted into a prostate phantom. The study demonstrated the ability of Timepix to identify different soft tissue thicknesses when used with both standard (300 μm) and thick (1 mm) sensor layers. The 1 mm thick sensor resulted in higher detection efficiency and required lower acquisition times compared with the standard 300 μm sensor (Loo et al., 2014).

7. Timepix in Targeted Alpha Therapy

An autoradiography imaging study of Targeted Alpha Therapy with Timepix detector was performed in 2015 (AL Darwish et al., 2015). This work aimed to record individual alpha particles emitted from Lewis Lung carcinoma tumour sections grown in mice that were treated

with Th-227 labelled radioimmunoconjugate (RIC). Mice (and the tumour sections imaged) were divided into two groups; a group treated with chemotherapy prior to treatment with Th-227 labelled RIC and a group that was not treated with chemotherapy at all. The Timepix sensitivity was investigated in monitoring variations in tumour uptake of Th-227 labelled RIC based on the necrotic tissue volume (AL Darwish et al., 2015). The alpha particle, photon, electron and muon tracks were recognised by Timepix detector in tumour section images. The results (Fig. 14) show that the uptake was four times greater when using chemotherapy prior to treatment with Th-227 labelled RIC. The difference when compared to the uptake of tumours without chemotherapy pre-treatment had a significant p-value of 0.026 as shown in Fig. 15.

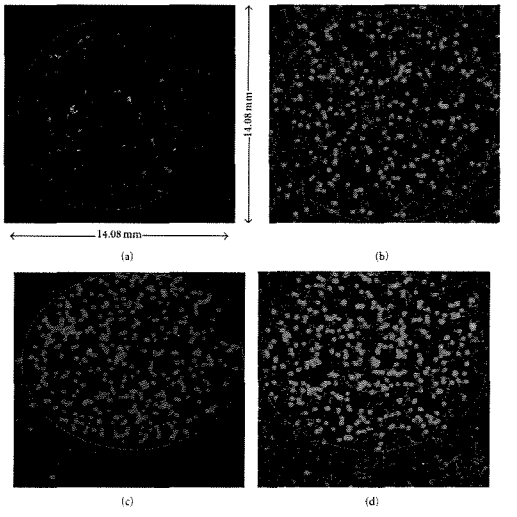

Fig. 14: Images of tumour sections from mice treated (a) and (b): with ^{227}Th-DAB4 alone, (c) and (d): with chemotherapy followed by 227Th-DAB4. The red circles represent the approximate tumour section boundaries, courtesy of (AL Darwish et al., 2015).

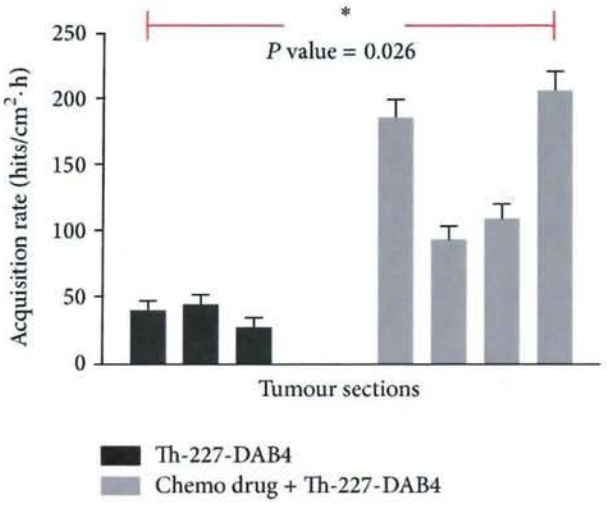

Fig. 15: Measured alpha particle hits per unit tumour area per 1 hour for: 3 tumour sections without application of chemotherapy prior to administration of Th-227 radioimmunoconjugate and 4 tumour sections with application of chemotherapy prior to administration of Th-227 radioimmunoconjugate, courtesy of (AL Darwish et al., 2015).

Conclusions

The ability of Timepix to detect photons, neutrons and heavy charge particles as well as to measure their arrival time, energy and number and the ability to produce images of their distributions makes it a highly versatile detector. This review has demonstrated that Timepix has the possibility to be used in a range of practical applications. For medical physics purposes it can be used to detect and track photons, electrons and charge particles down to the microdosimetry level as well as for imaging. We have shown that this aspect of Timepix should be investigated further. Timepix provides an excellent opportunity for researchers in both pure and applied science.

References:

AL Darwish, R., Staudacher, A.H., Bezak, E., Brown, M.P., 2015. Autoradiography Imaging in Targeted Alpha Therapy with Timepix Detector. Computational and Mathematical Methods in Medicine 2015, 7.

Anton, G., Gebert, U., Michel, T., Rügheimer, T.K., 2009. A hybrid photodetector using the Timepix semiconductor assembly for photoelectron detection. Nuclear Instruments and Methods in Physics Research Section A: Accelerators, Spectrometers, Detectors and Associated Equipment 602, 205-208.

Gebert, U., Rügheimer, T.K., Michel, T., Anton, G., Séguinot, J., Joram, C., 2010. Detection of optical photons with the Timepix in an HPD set-up. Nuclear Instruments and Methods in Physics Research Section A: Accelerators, Spectrometers, Detectors and Associated Equipment 623, 288-290.

Granja, C., Jakubek, J., Kopatch, Y., Pospisil, S., Telezhnikov, S., Vykydal, Z., 2008. Position-, spectral- and time-sensitive spectroscopy of fission fragments with TimePix pixel detectors, Nuclear Science Symposium Conference Record, 2008. NSS '08. IEEE, pp. 1659-1660.

Granja, C., Jakubek, J., Köster, U., Platkevic, M., Pospisil, S., 2011. Response of the pixel detector Timepix to heavy ions. Nuclear Instruments and Methods in Physics Research Section A: Accelerators, Spectrometers, Detectors and Associated Equipment 633, Supplement 1, S198-S202.

Granja, C., Jakubek, J., Platkevic, M., Pospisil, S., Vykydal, Z., 2010. Detection and Real Time Spectroscopy of Charged Particles with the TimePix Pixel Detector. AIP Conference Proceedings 1204, 75-79.

Loo, K.J., Jakubek, J., Zemlicka, J., Petasecca, M., Safavi-Naeini, M., Bucci, J., Zaider, M., Rosenfeld, A.B., 2014. BrachyView: Feasibility study into the application of Timepix detectors for soft tissue thickness imaging in prostate brachytherapy treatment. Radiation Measurements 71, 329-332.

Loo, K.J., Petasecca, M., Safavi-Naeni, M., Han, Z., Lerch, M., Bucci, J., Jakubek, J., Zemlicka, J., Meikle, S., Zaider, M., Rosenfeld, A., 2013. BrachyView: Tomographic reconstruction using Timepix detectors in post-implant dosimetry checks for permanent prostate brachytherapy implants, Nuclear Science Symposium and Medical Imaging Conference (NSS/MIC), 2013 IEEE, pp. 1-3.

Martišíková, M., Granja, C., Jakůbek, J., Hartmann, B., Telsemeyer, J., Huber, L., Brons, S., Pospíšil, S., Jäkel, O., 2012. Two-dimensional silicon-based detectors for ion beam therapy. AIP Conference Proceedings 1423, 327-334.

Opalka, L., Granja, C., Hartmann, B., Jakubek, J., Jaekel, O., Martisikova, M., Pospisil, S., Solc, J., 2012. 3D measurement of the radiation distribution in a water phantom in a hadron therapy beam. Journal of Instrumentation 7, C01085.

Opalka, L., Granja, C., Hartmann, B., Jakubek, J., Jaekel, O., Martisikova, M., Pospisil, S., Solc, J., 2013. Linear energy transfer and track pattern recognition of secondary radiation generated in hadron therapy beam in a PMMA target. Journal of Instrumentation 8, C02047.

Rügheimer, T.K., Gebert, U., Michel, T., Anton, G., Séguinot, J., Joram, C., 2008. Experimental demonstration of a hybrid photon detector concept based on the Timepix detector. Nuclear Instruments and Methods in Physics Research Section A: Accelerators, Spectrometers, Detectors and Associated Equipment 595, 353-358.

Uher, J., Jakubek, J., 2011. Detection of fast neutrons with particle tracking detector Timepix combined with plastic scintillator. Radiation Measurements 46, 1624-1627.

3.3 Conclusion

Timepix is a state of the art microdosimetry system. Its unique properties offer possibilities for use in a range of fields such as space research (Pinsky, Chancellor et al. 2008; Pinsky, Empl et al. 2010; Pinsky, Stoffle et al. 2011; Pinsky, Empl et al. 2011; Turecek, Pinsky et al. 2011; Granja and Pospisil 2014; Stoffle, Pinsky et al. 2015), imaging (Moats, Yang et al. 2011; Lemaire, Amgarou et al. 2013; Dudak, Zemlicka et al. 2015), medicine (Martisikova, Hartmann et al. 2012; Baek and Uher 2013) and radiation protection (Martisikova, Jakubek et al. 2012). Its ability to detect photons, neutrons and heavy charge particles as well as to measure their arrival time, energy and number and the ability to produce images of their distributions makes it a highly versatile detector. At present, most research related to Timepix is laboratory-focussed and its properties have been studied purely for research/characterisation purposes. Even though it has highly advantageous properties, the applications have not been fully exploited to date. This review has demonstrated that Timepix has a range of practical applications. For example, for medical physics purposes it can be used to detect and track the photons, electrons and charge particles down to the microdosimetry level as well as for imaging. We have shown that this aspect of Timepix should be investigated further. Timepix provides an excellent opportunity for researchers in both pure and applied science.

Chapter 4

Timepix as a Dosimeter

4.1 Introduction

Semiconductor detectors such as the Timepix radiation detector play an important role in radiation dosimetry and particle tracking. As the radiation hits the Timepix sensor, charges are liberated in one or more pixels depending on the radiation type and its energy, as shown in Figure 4.1. These charges are collected in the readout chip by an external electric field if the amount of free charge produced is higher than the set threshold level. These particular properties are useful in dosimetry applications, in particular if the amount of charge produced is proportional to the absorbed energy. However, in order to use this system for radiation protection and clinical dosimetry, Timepix must meet the specific requirements such as: high accuracy and precision, linear response to absorbed dose, dose rate independence, flat energy response, high sensitivity, low noise and high spatial resolution. As such, the aim of this chapter was to use Timepix as a dosimeter using photon and electron sources.

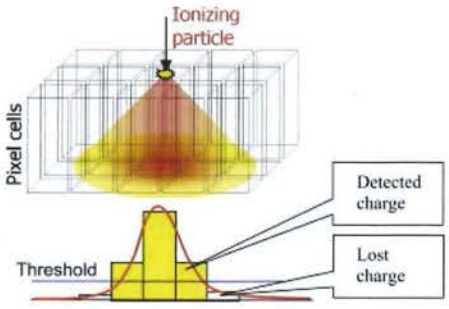

Figure 4.1: Timepix response to ionizing particles and the resulting charge measured compare to the threshold, courtesy of (Jakubek 2009).

4.2 Statement of Contribution

4.2.1 Conception

The aim is to investigate the use of Timepix detector for dosimetry purposes in the low dose region (μGy- mGy), using different radiation sources. The first concept was suggested by Eva Bezak and Mohammad Mohammadi. The methods by which to achieve this concept were conceptualised by Ruqaya Al Darwish, Mohammad Mohammadi and Eva Bezak.

4.2.2 Realisation

The practical work was done by Ruqaya Al Darwish under supervision of Mohammad Mohammadi and Eva Bezak. All work using radiation was performed according to the conditions of Operating an ionising radiation apparatus licence and Using and handling radioactive substances licence (Radiation Protection and control Act 1982) by South Australian Environment Protection Authority. Data collection and analysis was done by Ruqaya AL Darwish.

4.2.3 Documentation

This paper was primarily written by Ruqaya Al Darwish. Editing was done by all authors.

Note:

Dosemeter spelling was used in the following manuscript instead of dosimeter, as the former is mandated by the Radiation Protection Dosimetry journal, where the manuscript has been submitted to.

Statement of Authorship

Title of Paper	Application of Timepix to Low Dose Radiation Dosimetry.
Publication Status	☐ Published ☐ Accepted for Publication ☑ Submitted for Publication ☐ Unpublished and Unsubmitted w ork w ritten in manuscript style
Publication Details	Ruqaya AL Darwish, Mohammad Mohammadi and Eva Bezak, An Investigation of Timepix Detector Detection of Low Dose Radiation.

Principal Author

Name of Principal Author (Candidate)	Ruqaya AL Darwish
Contribution to the Paper	Timepix preparation and setup, data acquisition and analysis. This paper was primarily written by Ruqaya Al Darwish and acted as corresponding author.
Overall percentage (%)	85%
Certification:	This paper reports on original research I conducted during the period of my Higher Degree by Research candidature and is not subject to any obligations or contractual agreements with a third party that would constrain its inclusion in this thesis. I am the primary author of this paper.
Signature	Date 30/8/16

Co-Author Contributions

By signing the Statement of Authorship, each author certifies that:

i. the candidate's stated contribution to the publication is accurate (as detailed above);

ii. permission is granted for the candidate in include the publication in the thesis; and

iii. the sum of all co-author contributions is equal to 100% less the candidate's stated contribution.

Name of Co-Author	Mohammad Mohammadi
Contribution to the Paper	The practical works were done under supervision of Mohammad Mohammadi, who also helped with manuscript evaluation.
Signature	Date 30.08.16

Name of Co-Author	Eva Bezak
Contribution to the Paper	Eva Bezak supervised development of this work and helped with data interpretation. Also, she helped with manuscript evaluation.
Signature	Date 30/8/16

Application of Timepix to Low Dose Radiation Dosimetry

R. Al Darwish[1,2,3]*, M. Mohammadi[1,2] and E. Bezak[2,4,5]

[1] Department of Medical Physics, Royal Adelaide Hospital, Adelaide, Australia
[2] School of Physical Sciences, University of Adelaide, Adelaide, Australia
[3] Ministry of Higher Education, Saudi Arabia
[4] International Centre for Allied Health Evidence, Sansom Institute, University of South Australia, Adelaide, Australia
[5] Sansom Institute for Health Research, University of South Australia, Adelaide, Australia

*Corresponding author: Ruqaya.aldarwsih@adelaide.edu.au

Keywords: Timepix, radiation dose. Iodine-125, superficial X-rays.

Abstract

Timepix is a pixelated semiconductor detector. It has the ability to measure and discriminate the energy of detected particles. This paper investigates the performance of a commercial Timepix using low doses radiations in the μGy to mGy range. Timepix sensitivity, reproducibility and linearity were investigated to determine its suitability for low dose dosimetry. The measured doses were compared with doses using TLD100. The results show that Timepix has a linear response with increasing absorbed dose (R-square of the regression line ~1). Timepix also has good short and medium term reproducibility ($p < 0.0001$). Furthermore, its response to X-ray beams of different HVLs (0.5 – 3 mm Al) showed energy dependence. Good agreement of ~ 3% was observed between the doses measured by Timepix and the extrapolated doses measured by TLD100 using ^{125}I source.

In conclusion, the Timepix detector is a stable and sensitive dosemeter that can be used for low dose dosimetry subject to energy calibration.

INTRODUCTION

The Timepix detector, developed at CERN by the Medipix Collaboration [1,2], is a sophisticated microdosemeter that can be used for a wide range of experiments with photons, electrons and heavy charged particles [3] and has applications in research fields such as space physics, nuclear physics, radiotherapy physics, imaging and radiation protection [1, 4-14]. Timepix is essentially a development extension of Medipix2 [15]. Its main advantage over Medipix2 is that it can also measure the amount of energy deposited using the ''Time Over Threshold'' (TOT) mode [16]. Medipix2 and Timepix share some of the same physical properties. For example, they have the same pixel size of 55 × 55 μm^2 [15, 17], and in both cases the readout chip can collect both positive and negative charges [15].

Timepix consists of a semiconductor layer divided into an array of pixels. This array of pixels is bump-bonded to a readout Application Specific Integrated Circuit (ASIC), which is basically an electronic integrated layer (Figure 1). Each pixel has its own charge-sensitive preamplifier, discriminator, counter [15, 18] and 4-bit digital-to-analogue convertor (DAC) used to adjust the charge threshold [1] (see Figure 2).

Additionally, Timepix has the following properties [1]:

1. Each pixel contains a single energy threshold with 4-bit threshold adjustment;
2. Each pixel can operate in three main operating modes (Medipix mode, Time Over Threshold mode and Timepix mode);
3. Each pixel has its own counting clock that synchronizes with an external clock reference.

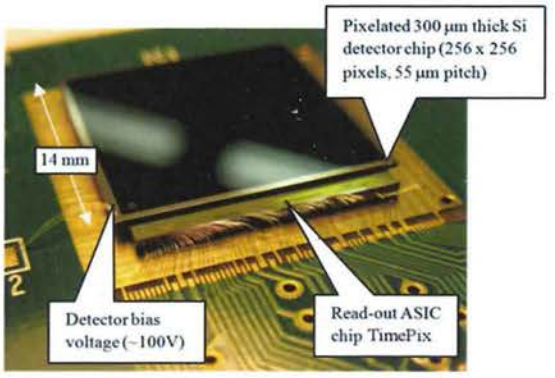

Figure 1: Timepix structure, courtesy of [19].

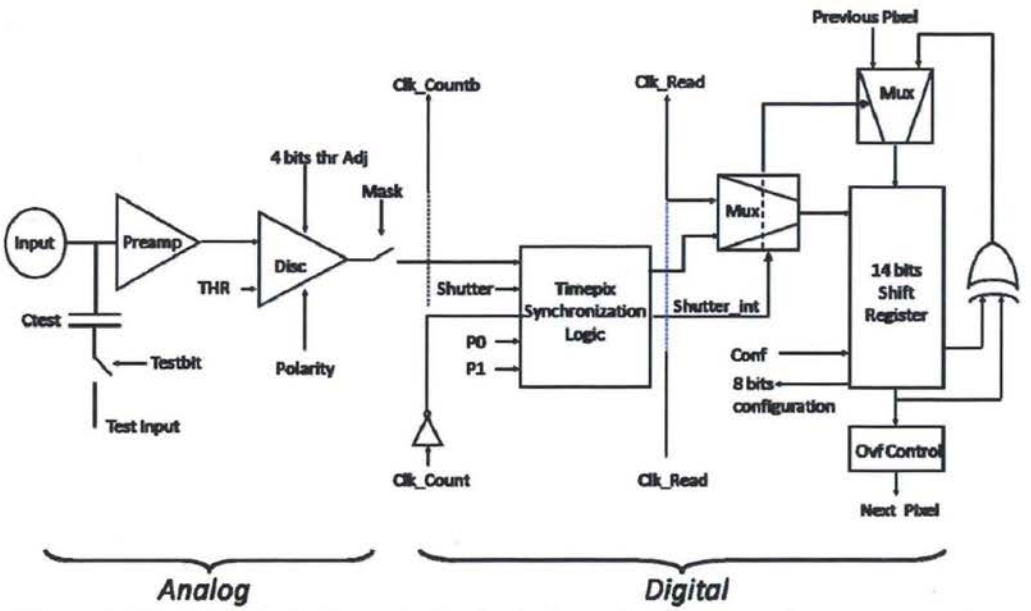

Figure 2: Timepix pixel schematic. Each pixel consists of two main parts: an analog part and digital part, courtesy of [4].

Timepix performs its functions using synchronization logic and a 14-bit counter per pixel. It can cope with count rates of up to 100 kHz for each pixel (in the single particle counting mode) [1] and has an overflow control of up to 11810 counts [15]. It also has the advantage of low electric noise of ~ 100 e^- rms (root mean square) [20].

Timepix uses an integrated USB-based readout interface which is connected to a computer. Windows compatible software package, Pixelman, is used to control Timepix detector and data

acquisition [21]. This assembly can be used as an imaging device as well, with the image displayed on the computer screen [9].

Early laboratory investigations of Timepix and Medipix detectors studied their architecture, functionality and characteristics, along with applications in spectrometry, imaging and tomography [1, 2, 6, 8, 16, 17, 22-24]. Eventually, the technology of Medipix generations (i.e. the naked chip and detector assembly (ASIC bump-bonded to the sensor material)) has been released for trading. Timepix can be purchased as a commercial product through several companies, for example: Amsterdam Scientific Instruments (The Netherlands), X-ray Imaging Europe GmbH (Germany) and X-Ray Imatek (Spain). The cost on average for a single Timepix chip (256 × 256 pixels) is ~ € 10,000. Commercially available Timepix chips can be purchased in single (256 × 256 pixels), quad (512 × 256 pixels) and octo (1024 × 1024 pixels) configurations, with the cost increasing more than linearly.

As mentioned previously, the Timepix radiation detector has broad applications in particle detection, imaging, and clinical and radiation protection dosimetry [5, 8, 10, 12, 14, 25]. In general, the Timepix dosimetry system consists of a dosemeter and a reader that is able, directly or indirectly, to measure the number of particles and the absorbed dose deposited by incident radiation. However, in order to use this system for radiation protection and clinical dosimetry, Timepix must meet the specific requirements such as: high accuracy and precision, linear response to absorbed dose, dose rate independence, flat energy response, high sensitivity, low noise and high spatial resolution [26-28]. As a result, this paper aims to characterise Timepix as a dosemeter for low doses using low energy clinical photon beams (i.e. ^{125}I gamma rays and superficial X-rays). We have specifically investigated the low dose sensitivity (in the μGy to mGy region), linearity, reproducibility and energy dependence.

MATERIALS

Timepix

The Timepix detector used in this work was purchased from Amsterdam Scientific Instruments, the Netherlands. The detector chip consists of 256 × 256 pixels with an individual pixel size of 55 × 55 μm^2 and 300 μm depth. The total size of the chip is 1.408 × 1.408 cm^2. Each pixel

contains a charge-sensitive preamplifier, a discriminator and a counter and has its own power supply, meaning that Timepix is a device that consists of over 65,000 individual detectors.

As mentioned earlier, Timepix can be operated in one of three main acquisition modes [7]. These are:

a) Medipix mode: the particle number is counted where the shift register counts digital signals if higher than a threshold;

b) Timepix mode: the arrival time of a particle to the chip is recorded. Here, the counter works as a timer and measures the time of the particle detection;

c) Time Over Threshold (TOT) mode: the counter allows each pixel to measure the detected particle's energy.

The acquisition modes are run through the multi-platform software package, Pixelman v3, developed at the Institute of Experimental and Applied Physics (Czech Technology University, Prague). The software controls Timepix data acquisition and is also used to process the acquired data [29].

Iodine-125

Iodine-125 radioactive seeds (Oncura calibration strand; Oncura Inc., Arlington Heights, IL) were used in the current work to investigate Timepix use in dosimetry. The average length of the single seed was 4.5 mm and the diameter was 0.8 mm [30]. ^{125}I has a half-life of 59.4 days and it decays by electron capture to Tellurium-125 as shown in equation 1 [26]. It emits a maximum energy gamma ray of 35.5 keV, while the average energy of all photons emitted is between 28 and 30 keV [26, 31] (Figure 3).

$$^{125}_{53}I + e^{-} \rightarrow ^{125}_{52}Te + \gamma \qquad (1)$$

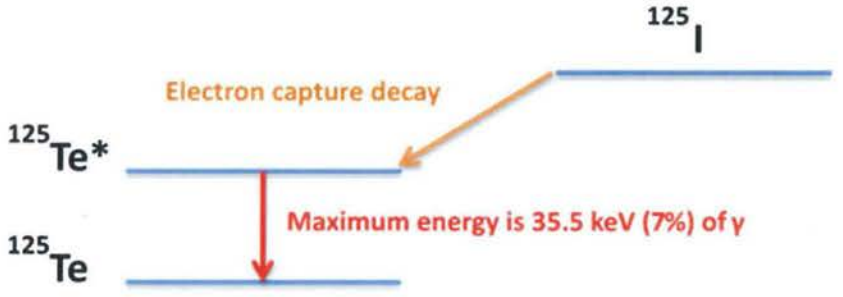

Figure 3: Iodine-125 decay. Based on information from [26, 32].

Gulmay D3150 superficial X-ray Unit

In addition to ^{125}I, measurements of X-rays were also performed using a Gulmay D3150 superficial X-ray Unit (Gulmay Limited, Surrey, United Kingdom) at the Radiation Oncology Department, Royal Adelaide Hospital. X-ray beams with Half Value Layers (HVLs) between 0.5 to 3 mm Al and peak voltage between 40 to 100 kV were used for dosimetric measurements. The output dose rates (Gy/min) in water of these beams were determined using the Institution of Physics and Engineering in Medicine and Biology (IPEMB) code of practice for the determination of absorbed dose for X-rays below 300 kV [33].

Thermoluminescent dosemeter (TLD100)

Verification of doses delivered to Timepix, calculated using equation 4 below, was done with thermoluminescent dosimetry using TLD100 (Krakow, Poland) chips. TLD100 consists of LiF:Mg,Ti and it is considered to be almost soft tissue equivalent with Z_{eff} of 8.2 [26, 31]. Its main glow curve is between 180°C to 260°C. In the current work, the Harshaw TLD Reader 3500 (Thermo Fisher Scientific, Waltham, MA) was used to heat the TLD100 chips and to detect the thermoluminescent light emission by a photomultiplier tube (PMT) within the reader [26].

METHODS

Before Timepix can be used for dosimetry purposes, it needs to be characterised; this includes pixel calibration, dose linearity, reproducibility, energy dependence, dose rate dependence and even particle response. The following sections describe measurements conducted in this work.

Pixel Response Calibration – Threshold Equalization

Pixel equalization/calibration is one of the most important tasks to be conducted prior to Timepix use for any purpose. Pixel calibration ensures the uniform response of all pixels for the same irradiation signal. In order to calibrate all 65536 pixels, the manufacturer's calibration procedure, included in Pixelman, known as threshold equalization was followed. Threshold equalization is used to compensate the pixel to pixel threshold variations due to local transistor threshold voltages and current mismatches [34]. During the equalization process, each pixel is adjusted to make its threshold as near as possible to the average of the mean values of the threshold distribution. This is done using a 4-bit current DAC placed in the discriminator chain of each pixel to conduct low threshold (THL) and high threshold (THH) adjustments as shown in Figure 4 [1].

The THL and THH are separately scanned above the noise edge and to the direction of noise [35, 36]. The THL value is set to a DAC value which would give as low a threshold level as possible before sensor noise would start to appear. The DAC value corresponding to THL is calculated as follows:

$$\text{THL DAC} = (\text{mean distribution of thresholds})_{\text{after equalization}} - 10\,(\text{standard deviation of distribution})_{\text{after equalization}} \quad (2)$$

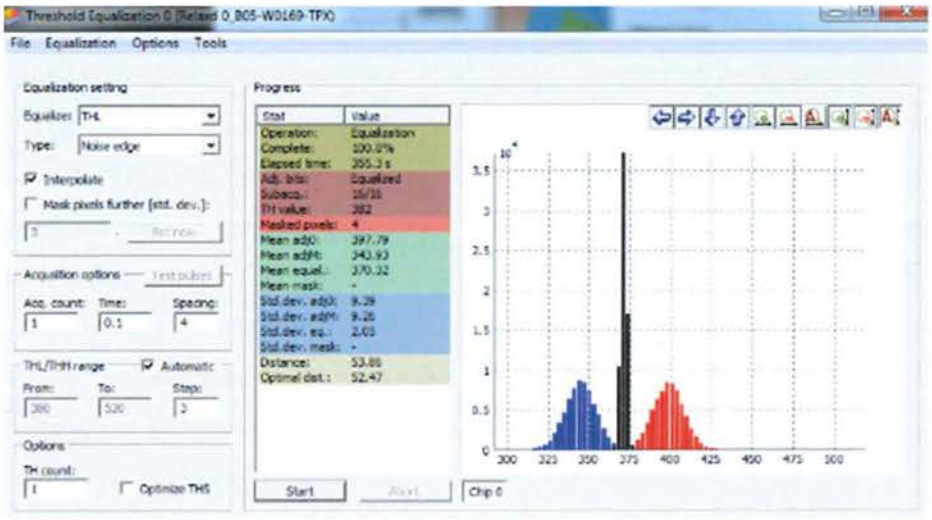

Figure 4: Threshold equalization procedures.

Upon completion, the equalization parameters of all pixels are saved and uploaded every time Timepix is used. THL DAC value must also be set in Pixelman prior to any measurements.

The literature also shows that equalization reduces the threshold variation as well as the minimum detectable charge (from 1600 e^- before, to 650 e^- after equalization) [1].

The equalization procedure in this work was done under dark current conditions and a 100 V bias was applied to the sensor. The saved equalization file was uploaded prior to each measurement. After equalization, Timepix was irradiated with ^{125}I gamma rays to check the response to the flood field and to check the image uniformity. The acquisition time was set to 1 second per frame and 700 frames were acquired. To further check Timepix's basic functionality, a lead block was used to cover one corner of the detector. An image was acquired using 1 second per frame acquisition time, collecting 500 frames.

Timepix dosimetry with low energy gamma rays and X-rays

I-125 measurements

The measurements performed with ^{125}I seeds aimed to investigate Timepix linearity, reproducibility and low dose sensitivity. A schematic diagram of the experimental setup is shown in Figure 5. The ^{125}I seed with the initial activity of 14.6 MBq was placed in front of the Timepix detector surface at a distance of 15 cm. In order to assess the dose sensitivity and the dose response linearity, the acquisition rate was set to 1 second per frame. Timepix was operated in Medipix mode (i.e. particle counting), and all acquired frames were integrated to give the final reading. Timepix was irradiated to different doses by varying the exposure time between 1 and 100 seconds on the same day. The mean Pixel Value (PV) was obtained from each measurement and plotted against the dose delivered. Linearity of the dose response was investigated using the line of best fit.

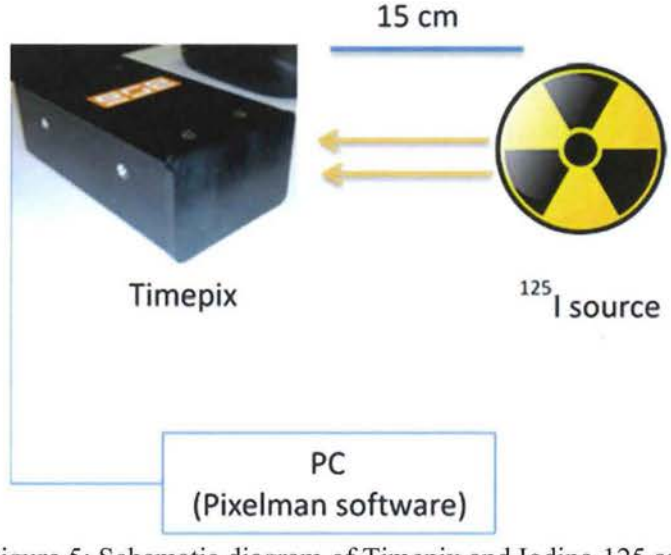

Figure 5: Schematic diagram of Timepix and Iodine-125 setup.

To calculate the dose delivered by ^{125}I, the standard mathematical calculation was followed [37], using the known initial apparent activity (A_{pp0}) of the ^{125}I seed (i.e. corrected for the source self-absorption in the seed), the half-life time ($T_{1/2}$) and the time (t) since the initial activity had been measured to calculate the activity (A) at time t:

$$A(t) = A_{pp0}\, e^{-t/T_{1/2}} \qquad (3)$$

Using the activity in GBq, the air kerma rate was calculated by multiplying the air kerma rate constant (35.8 $\mu Gym^2/hGBq$) by the actual activity and divided by the square of distance from

the source (i.e. $(15)^2$ cm^2). The absorbed dose rate (μGy/h) to Timepix sensitive layer can be calculated when the air kerma rate is multiplied by the ratio of the mean mass energy absorption coefficients for silicon and air [37]:

$$\dot{D}(r) = \dot{K}(r)\frac{(\mu_{en}/\rho)^{silicon}}{(\mu_{en}/\rho)^{air}} \quad (4)$$

Finally, the dose delivered to Timepix was calculated by multiplying the absorbed dose rate to Timepix and the exposure time.

The measurements described above were repeated after one week and the mean PVs were compared.

Gulmay D3150 superficial X-ray unit measurements

The Gulmay D3150 superficial X-ray (SXR) unit was also used to investigate the linearity, reproducibility and energy dependence of Timepix. Because of the high dose output from this unit, Timepix was positioned at 165 cm from the focal spot of the SXR unit, using a 1.5 cm diameter cone. The SXR exposure times ranged between 0.01 and 0.35 minutes. The Timepix measurement was initiated prior to the SXR unit being energized and the acquisition stopped after the irradiation. This was achieved by using a data acquisition time of 1 min (1 frame per second) for Timepix. The measurements were repeated at least four times for each point using X-ray beams of different qualities as shown in Table 1.

To calculate the dose delivered to Timepix, in terms of dose to water, standard equations from the departmental protocol (equations 5 and 6) were used in conjunction with the calibration values, current at the time of the measurement, shown in Table 1:

$$\dot{D}_{water} = \dot{D}_{waterref} \times FCF \times ISCF \quad (5)$$

$$Dose = \dot{D}_{water} \times Time \quad (6)$$

Where the dose to water is calculated when the reference (i.e. calibrated) dose rate was corrected by the Field Correction Factor, FCF, and the Inverse Square Correction Factor (ISCF). Finally, the dose was obtained by multiplying the dose rate and the exposure time.

Table 1: Dose rate and energy of different HVL of superficial X-ray unit (10 cm diameter collimator).

HVL	kV	Dose rate (15 cm FSD) (Gray/min)
0.5 mm Al	40	5.454 ± 0.11
1 mm Al	50	3.832 ± 0.08
2 mm Al	80	13.968 ± 0.28
3 mm Al	100	18.332 ± 0.37

Mean PVs were obtained from the Pixelman software and plotted against the calculated dose values for each X-ray beam. Dose response linearity and reproducibility over a 2-week period as well as energy dependence were evaluated.

Dose verification using TLD 100

Annealing and reading of TLD100 chips was performed using a standard TLD protocol implemented at the clinic [38]. In the current work, the readout of each chip was corrected for its individual Sensitivity Correction Factor (SCL) to account for slight mass differences between the chips. The TLD readings, R, were corrected for the background and the TLD dose was calculated using the following equation:

$$TLDs\ dose = (R_{Reading}\ (nC) - R_{Backgrond}\ (nC)) \times SCF \times CF\ (\mu Gy/nC) \qquad (7)$$

Where CF is the calibration factor to convert the TLD readings from nanoCoulombs (nC) to dose in μGy. In this experiment, the correction factor of 0.108 Gy/nC was used as determined from irradiation of TLDs to a known dose.

In order to compare the TLD doses with those calculated to be delivered to Timepix, 21 TLD100 chips were irradiated for 1 hour using iodine-125 and six chips were used to measure

the background. The distance between the TLD100 chips and the source was 15 cm. The TLD100 chips were read by the Harshaw 3500 Reader and the dose was calculated using equation 7. This dose corresponds to a dose in water, however, in order to compare it with the dose delivered to Timepix, it needed to be converted to the dose to silicon. This was done by multiplying the TLD100 dose by 7.29 which is the ratio of silicon to water mass energy absorption coefficients [39].

The TLD100 doses were then compared with the doses calculated using equations 3 and 4.

RESULTS

Threshold Equalization

As shown in Figure 4, the mean and the standard deviation of the threshold distribution following equalization were found to be 370.32 and 2.05, respectively. Therefore, based on these equalization results, and using equation 3, the THL DAC was determined to be 350. This number was set in Pixelman manually for all Timepix measurements in the current report.

Figure 6 shows the Timepix response to a radiation flood field, using ^{125}I seed, for two set-ups: open field and blocked at one corner by a lead block. As shown in Figure 6A and B, a good uniform image was acquired where the mean and the standard deviation of PV distribution were 135 and 20 respectively (Figure 6C). No dead/damaged pixels were detected. Individual photons can be distinguished in single frames and they appear as small square dots occupying 1-4 pixels.

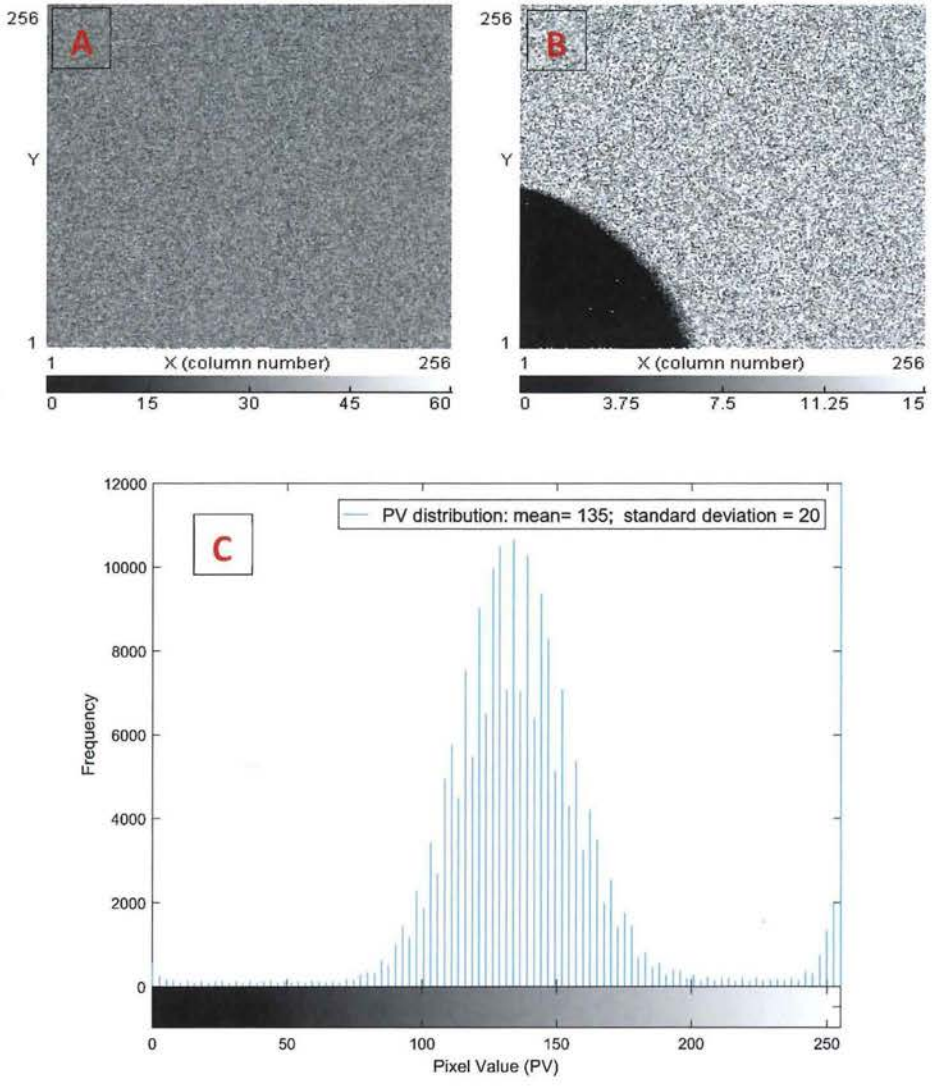

Figure 6: (A) a flood field image of ^{125}I, (B) a flood field image with one corner blocked with a lead block, (C) the PV distribution for flood image shown in A.

Timepix Measurements using ^{125}I

Dose linearity

The Timepix response to irradiation by a ^{125}I seed as a function of the absorbed dose, calculated using equation 4 for the exposure times used, is shown in Figure 7. There is a good linearity observed between the mean PV measured and the absorbed dose in the range from 0 to 8 μGy. The R-square of the regression line, i.e. the measure of the goodness-of-fit, on the graph is

0.9993 supporting our claim that a linear fit adequately describes the measured data. The standard errors of the mean PVs shown in Figure 7 varied between 0.002 and 0.27.

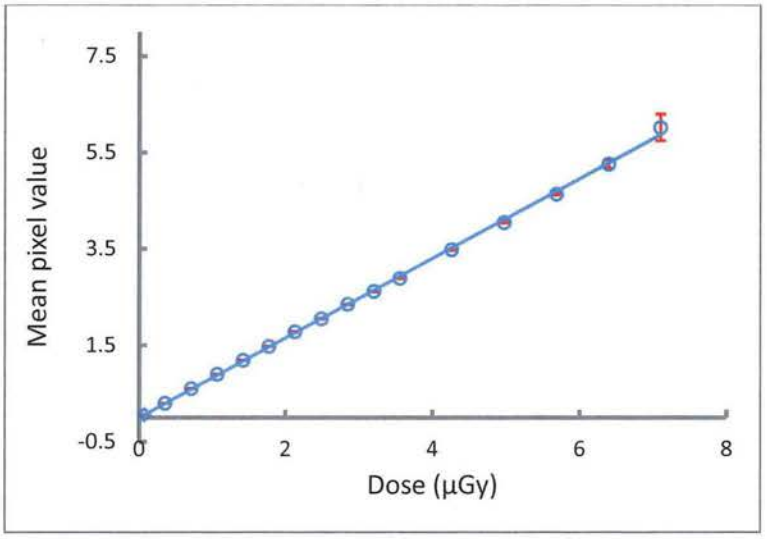

Figure 7: Dependence of Timepix mean pixel value as a function of the absorbed dose (single day data) for dose linearity assessment, using an ^{125}I seed.

Additionally, Timepix showed a high sensitivity when measuring very low gamma radiation doses and was able to detect doses as low as 0.5 μGy.

Timepix response to two irradiations, using the ^{125}I seed, conducted one week apart is shown in Figure 8, where the mean pixel values are not corrected for the ^{125}I decay. As a result, the doses delivered for the same irradiation time are ~8% higher for the first irradiation. This difference has been detected by Timepix. The standard errors of mean PVs ranged between 0.002 and 0.27 for the first measurement and 0.01 and 0.14 for the second. The ratio of activities of the ^{125}I seed during the first and the second measurement was ~ 1.09, while the average ratio of the mean PVs for the two measurements was 1.12 (see Figure 8). The results once again demonstrate the ability of Timepix to resolve doses in the μGy region.

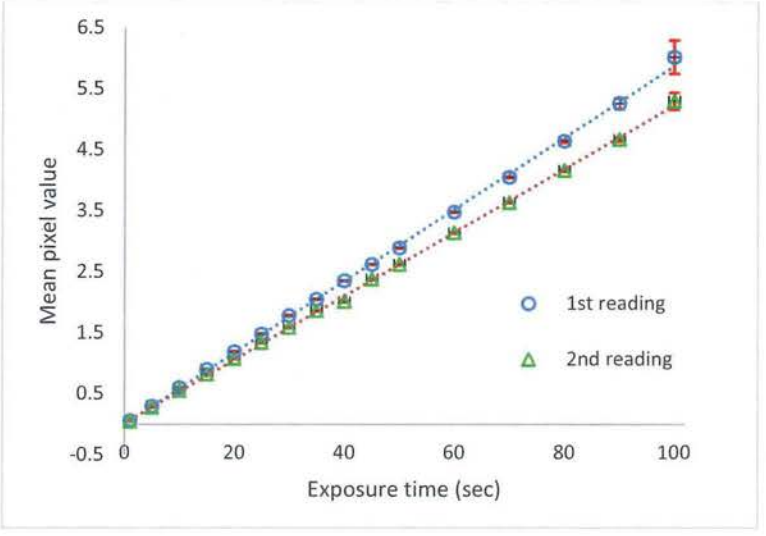

Figure 8: Timepix response to ^{125}I as a function of the exposure time. The data presented relate to two sets of data acquisitions one week apart. Note that the data for the second reading is not corrected for ^{125}I decay.

After the mean PVs from the second measurement were corrected for the ^{125}I decay, the agreement percentage between the mean PVs from the two measurements was on average 98.49%. Using a paired t-test, a significant p-value of 0.0043 (correlation coefficient ≈ 1) was obtained, showing that the two sets of PVs were identical when applying the decay correction.

Dose verification using TLD 100

A comparison between absorbed doses measured by TLD 100 chips and calculated doses delivered to Timepix, for the same apparent activity and the same irradiation time, are presented in Figure 11. The standard errors for calculated Timepix doses were ~5% and were determined from multiple readings. The standard error for the measured and extrapolated TLD doses were estimated ~10%. A good agreement of 96.62% between the calculated doses and measured doses was obtained using a correlation factor of 1.

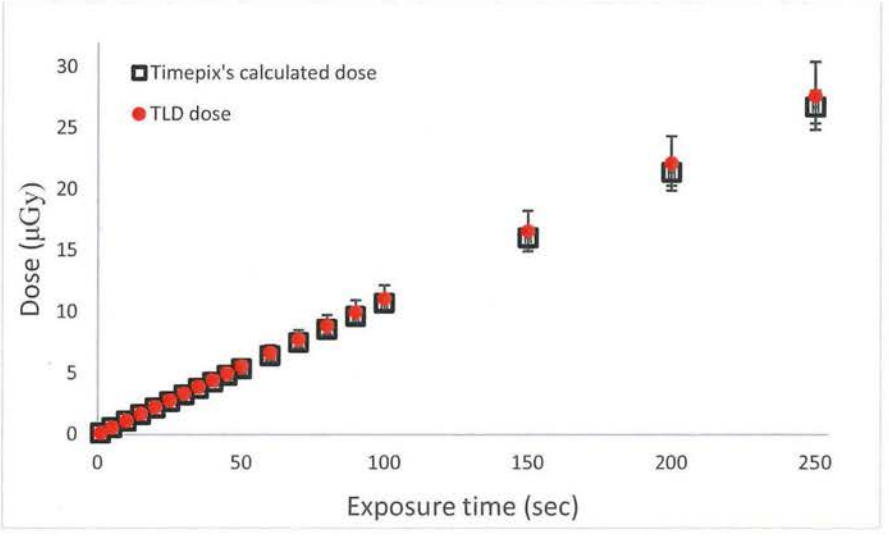

Figure 9: A comparison of the absorbed dose versus exposure time as measured by TLD LiF 100 chips and calculated (equation 4) for Timepix.

Timepix Measurements using Gulmay D3150 superficial X-ray unit

The dependence of mean pixel values, measured for Timepix irradiation with 40 kV, 0.5 mm Al HVL X-ray beam, as a function of the absorbed dose (mGy), is shown in Figure 10. It can be seen that Timepix exhibits very good linearity as a function of the absorbed dose in the mGy region. An R-square value of 0.9997 was obtained, indicating that a linear regression fit closely approximates the measured data.

Figure 11 shows the relationship between the mean pixel reading and the exposure time for 50 kV, 1 mm Al HVL X-ray beam repeated 5 times over a period of 2 weeks. A good reproducibility of measured mean PVs during a period of two weeks was obtained. The data from the 5 measurements were analysed using Paired t-test (GraphPad Prism 6 software, (GraphPad Software, Inc., CA, USA)). Statistical significance, i.e. the p value for the agreement between the 5 measurements, between the data was found to be less than 0.0001 and an R-square value of 0.9996 was obtained.

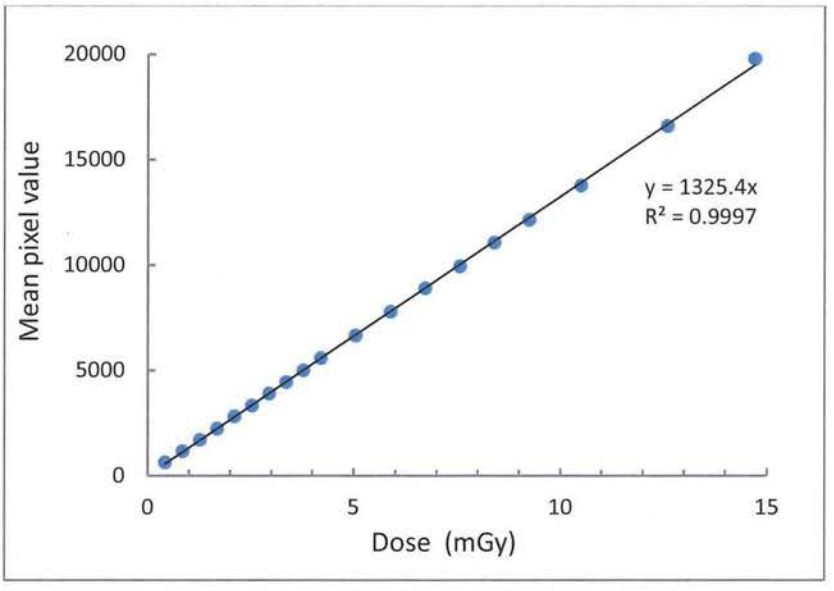

Figure 10: The dependence of mean pixel values, measured for Timepix irradiation with 40 kV, 0.5 mm Al HVL X-ray beam, as a function of the absorbed dose (mGy); PV standard errors were between 2 and 32.

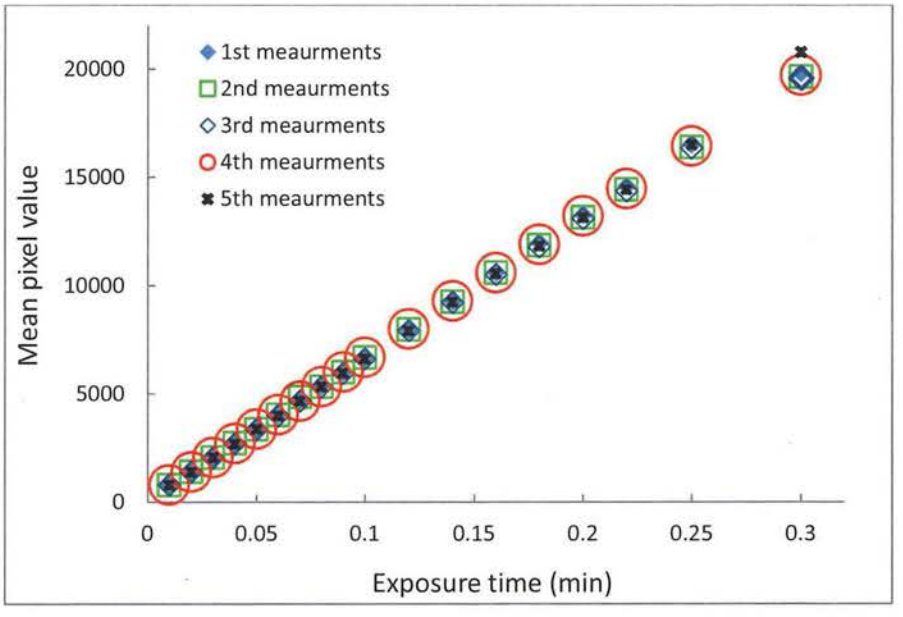

Figure 11: Timepix Mean Pixel values measured as a result of irradiation by 50 kV, 1 mm Al HVL X-ray beam, collected over two weeks, as a function of exposure time. The obtained PV standard error was range from 2 to 37. The R-square value is ~0.999.

The energy dependence of the Timepix response is presented in Figures 12 and 13 for 40 kV/0.5 mm Al, 50 kV/1 mm Al, 80 kV/2 mm Al and 100 kV/3 mm Al HVL X-ray beams. The results are presented in terms of the mean pixel reading as a function of the dose delivered by different kV/HVL X-ray beams. As can be seen, Timepix is energy dependent and therefore must be calibrated separately for each X-ray beam (i.e. for a given energy spectrum) if it is to be used for dosimetric purposes. The energy dependence, however, appears to be reducing as a function of increasing kV and HVL, as the mean PVs measure for 80 kV/2 mm Al and 100 kV/3 mm Al HVL X-ray beams appear to lie on the same line (Figure 13).

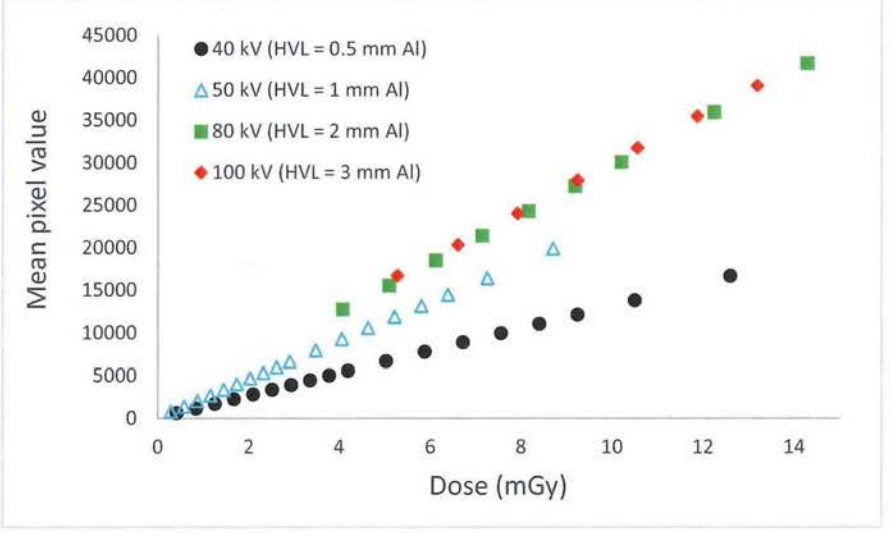

Figure 12: Measured mean Timepix PVs as a result of exposure to 40, 50, 80 and 100 kV X-ray beams, as a function of the absorbed dose.

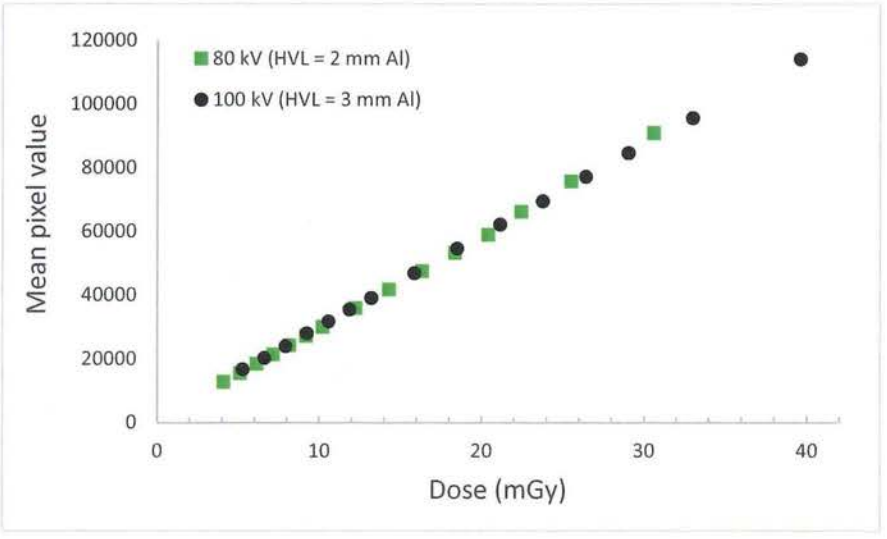

Figure 13: Measured mean Timepix PVs as a result of exposure to 80 and 100 kV X-ray beams, as a function of the absorbed dose.

DISCUSSION AND CONCLUSION

The results show that the Timepix response to low energy photons was linear to the absorbed dose in the μGy-mGy region. Timepix was found to be very sensitive to low absorbed doses as well as sensitive to day-to-day variation in doses, for example in case of radioactive materials due to changes in the activity as a result of radioactive decay. A good medium term reproducibility of Timepix was also shown. The results identified that Timepix is energy dependent, and thus requires energy calibration for a given photon spectrum before it can be used for dosimetry purposes.

Several dosemeters are routinely used for clinical and radiation protection dosimetry applications, for example ionization chambers, TLDs, scintillation dosemeters, optically stimulated luminescence dosemeters and others. However, the absorbed dose range they cover is generally in the mGy to Gy ranges. Optically stimulated luminescence dosemeters have been found to be sensitive in μGy region, however they do not provide immediate on-line readout and require a special stimulating/reading apparatus to obtain dose [40]. An additional advantage of Timepix is that it is considered a noise-free dosemeter. It gives a zero reading when a pixel has not been hit by radiation. This is one of the reasons for its superb sensitivity. For example, the PMMA plastic optical fibre dosemeter is affected by noise at low radiation doses.

Therefore, it is suggested a further signal processing is required to improve the radiation-induced attenuation and the resolution of that sensor [41]. That is not required for Timepix.

While this work investigated Timepix performance under low energy photon irradiation, further dosimetry investigations of Timepix will be performed using electron and alpha particle sources in the future.

Disclosure of Conflicts of Interest

The authors have no relevant conflicts of interest to disclose.

REFERENCS:

1.Llopart, X., Ballabriga, R., Campbell, M., Tlustos, L. and Wong, W. Timepix, a 65k programmable pixel readout chip for arrival time, energy and/or photon counting measurements. Nuclear Instruments and Methods in Physics Research Section A: Accelerators, Spectrometers, Detectors and Associated Equipment. 581, 485-494 (2007).

2. Vallerga, J., McPhate, J., Tremsin, A. and Siegmund, O. High-resolution UV, alpha and neutron imaging with the Timepix CMOS readout. Nuclear Instruments and Methods in Physics Research Section A: Accelerators, Spectrometers, Detectors and Associated Equipment. 591, 151-154 (2008).

3. Pinsky, L. S., Empl, A., Gutierrez, A., Jakubek, J., Kitamura, H., Miller, J., Leroy, C., Stoffle, N., Pospisil, S., Uchihori, Y. et al. Penetrating heavy ion charge and velocity discrimination with a TimePix-based Si detector (for space radiation applications). Nuclear Instruments and Methods in Physics Research Section A: Accelerators, Spectrometers, Detectors and Associated Equipment. 633, Supplement 1, S190-S193 (2011).

4. Campbell, M. 10 years of the Medipix2 Collaboration. Nuclear Instruments and Methods in Physics Research Section A: Accelerators, Spectrometers, Detectors and Associated Equipment. 633, Supplement 1, S1-S10 (2011).

5. Esposito, M., Jakubek, J., Mettivier, G., Pospisil, S., Russo, P. and Solc, J. Energy sensitive Timepix silicon detector for electron imaging. Nuclear Instruments and Methods in Physics Research Section A: Accelerators, Spectrometers, Detectors and Associated Equipment. 652, 458-461 (2011).

6. Granja, C., Jakubek, J., Kopatch, Y., Pospisil, S., Telezhnikov, S. and Vykydal, Z. Position-, spectral- and time-sensitive spectroscopy of fission fragments with TimePix pixel detectors. (2008) ISBN 1095-7863.

7. Jakubek, J., Cejnarova, A., Platkevic, M., Solc, J. and Vykydal, Z. Event by event energy sensitive imaging with TimePix pixel detector and its application for gamma photon tracking. (2008) ISBN 1095-7863.

8. Žemlička, J., Jakůbek, J., Kroupa, M. and Tichý, V. Energy- and position-sensitive pixel detector Timepix for X-ray fluorescence imaging. Nuclear Instruments and Methods in Physics Research Section A: Accelerators, Spectrometers, Detectors and Associated Equipment. 607, 202-204 (2009).

9. Granja, C., Jakubek, J., Platkevic, M., Pospisil, S. and Vykydal, Z. Detection and Real Time Spectroscopy of Charged Particles with the TimePix Pixel Detector. AIP Conference Proceedings. 1204, 75-79 (2010).
10. Dammer, J., Weyda, F., Benes, J., Sopko, V., Jakubek, J. and Vondracek, V. Microradiography of biological samples with Timepix. Journal of Instrumentation. 6, C11005 (2011).
11. Jose, J. M., Čermák, P., Štekl, I., Čermák, J., Fiederle, M., Fauler, A., Shitov, Y. A., Rukhadze, E. N., Rukhadze, N. I., Brudanin, V. B. et al. Timepix background studies for double beta decay experiments. Journal of Instrumentation. 6, C11030 (2011).
12. Martisıkova, M., Jakubek, J., Granja, C., Hartmann, B., Opalka, L., Pospısilb, S. and Jakela, O. Measurement of secondary radiation during ion beam therapy with the pixel detector Timepix. Journal of Instrumentation. 6, C11014 (2011).
13. Bulanek, B., Ekendahl, D. and Prouza, Z. Fast Neutron Dosemeter using Pixelated Deetctor Timepix. Radiation protection dosimetry(2013).
14. Stoffle, N., Pinsky, L., Kroupa, M., Hoang, S., Idarraga, J., Amberboy, C., Rios, R., Hauss, J., Keller, J., Bahadori, A. et al. Timepix-based radiation environment monitor measurements aboard the International Space Station. Nuclear Instruments and Methods in Physics Research Section A: Accelerators, Spectrometers, Detectors and Associated Equipment. 782, 143-148 (2015).
15. CERN. Medipix. (2011).
16. Campbell, M., Havranek, V., Heijne, E., Holy, T., Idarraga, J., Jakubek, J., Lebel, C., Leroy, C., Llopart, X., Novotny, J. et al. Charge collection from proton and alpha particle tracks in silicon pixel detector devices. (2007) ISBN 1095-7863.
17. Bamberger, A., Desch, K., Renz, U., Titov, M., Vlasov, N., Wienemann, P. and Zwerger, A. Resolution studies on 5 GeV electron tracks observed with triple-GEM and MediPix2/TimePix-readout. Nuclear Instruments and Methods in Physics Research Section A: Accelerators, Spectrometers, Detectors and Associated Equipment. 581, 274-278 (2007).
18. Rügheimer, T. K., Gebert, U., Michel, T., Anton, G., Séguinot, J. and Joram, C. Experimental demonstration of a hybrid photon detector concept based on the Timepix detector. Nuclear Instruments and Methods in Physics Research Section A: Accelerators, Spectrometers, Detectors and Associated Equipment. 595, 353-358 (2008).
19. Kraus, V., Holik, M., Jakubek, J., Kroupa, M., Soukup, P. and Vykydal, Z. FITPix — fast interface for Timepix pixel detectors. JINST. 6, C01079 (2011).
20. Pugatch, V., Campbell, M., Chaus, A., Eremenko, V., Homenko, S., Kovalchuk, O., Llopart, X., Okhrimenko, O., Pospisil, S., Shelekhov, A. et al. Metal and hybrid TimePix detectors imaging beams of particles. Nuclear Instruments and Methods in Physics Research Section A: Accelerators, Spectrometers, Detectors and Associated Equipment. 650, 194-197 (2011).
21. Michel, T., Durst, J. and Jakubek, J. X-ray polarimetry by means of Compton scattering in the sensor of a hybrid photon counting pixel detector. Nuclear Instruments and Methods in Physics Research Section A: Accelerators, Spectrometers, Detectors and Associated Equipment. 603, 384-392 (2009).
22. Jakubek, J. Energy-sensitive X-ray radiography and charge sharing effect in pixelated detector. Nuclear Instruments and Methods in Physics Research Section A: Accelerators, Spectrometers, Detectors and Associated Equipment. 607, 192-195 (2009).
23. Jakubek, J., Cejnarova, A., Holy, T., Pospisil, S., Uher, J. and Vykydal, Z. Pixel detectors for imaging with heavy charged particles. Nuclear Instruments and Methods in Physics Research Section A: Accelerators, Spectrometers, Detectors and Associated Equipment. 591, 155-158 (2008).
24. Jakubek, J., Platkevic, M., Schmidt-Wellenburg, P., Geltenbort, P., Plonka-Spehr, C. and Daum, M. Position-sensitive spectroscopy of ultra-cold neutrons with Timepix pixel detector. Nuclear Instruments and Methods in Physics Research Section A: Accelerators, Spectrometers, Detectors and Associated Equipment. 607, 45-47 (2009).
25. Martisikova, M., Jakubek, J., Gwosch, K., Hartmann, B., Telsemeyer, J., Pospisil, S. and Jakel, O. Monitoring of ion beam energy by tracking of secondary ions: First measurements in a patient-like phantom. 2012 IEEE Nuclear Science Symposium and Medical Imaging Conference Record (NSS/MIC

2012) & Workshop on Room-Temperature Semiconductor X-Ray and Gamma-Ray Detectors, 1914-1917 (2012).
26. Podgorsak, E. B. Radiation Oncology Physics : a Handbook for Teachers and Students. (Vienna: IAEA) (2005).
27. ICRU 4DOSIMETRY. Journal of the ICRU. 7, 49-81 (2007).
28. ICRU Report 36. Microdosimetry. (1983).
29. Turecek, D., Holy, T., Jakubek, J., Pospisil, S. and Vykydal, Z. Pixelman: a multi-platform data acquisition and processing software package for Medipix2, Timepix and Medipix3 detectors. Journal of Instrumentation. 6, C01046 (2011).
30. Marcu, L., Bezak, E. and Allen, B. J. Biomedical physics in radiotherapy for cancer (Australia: Collingwood, Vic. : CSIRO Publishing) (2012) ISBN 9780643094048 (pbk.)
31. Mayles, P., Nahum, A. and Rosenwald, J. C. Handbook of Radiotherapy Physics: Theory and Practice. (New York: ayler & Francis Group) (2007).
32. Bushberg, J. T., Seibert, J. A., Leidholdt, E. M. and Boone, J. M. The Essential Physics of Medical Imaging. (Philadelphia: Philadelphia : Lippincott Williams & Wilkins) (2002) ISBN 9780683301182 (hbk.); 0683301187 (hbk.)
33. The IPEMB code of practice for the determination of absorbed dose for x-rays below 300 kV generating potential (0.035 mm Al-4 mm Cu HVL; 10-300 kV generating potential). Institution of Physics and Engineering in Medicine and Biology. Physics in medicine and biology. 41, 2605-25 (1996).
34. Pelgrom, M. J. M. Matching properties of MOS transistors. Nuclear Instruments and Methods in Physics Research Section A: Accelerators, Spectrometers, Detectors and Associated Equipment. 305, 624-626 (1991).
35. Tureček, D., Holý, T. and Vykydal, Z. Pixelman - Manual.
36. Severino, C. T. Real-time measurement of radon activity and mixed radiation fields characterization with silicon pixel detector. (CERN-THESIS-2014-236: the University of Bern) (2014).
37. Khan, F. M. and Potish, R. A. Treatment planning in radiation oncology. Williams & Wilkins) (1998) ISBN 0683046071.
38. Bensaleh, S. and Bezak, E. The impact of uncertainties associated with MammoSite brachytherapy on the dose distribution in the breast. (2011) ISBN 15269914|escape}.
39. (NIST), T. N. I. o. S. a. T. X-Ray Mass Attenuation Coefficients.
40. O'Keeffe, S., Fitzpatrick, C., Lewis, E. and Al-Shamma'a, A. I. A review of optical fibre radiation dosimeters. Sensor Review. 28, 136-142 (2008).
41. Keeffe, S. O., Lewis, E., Santhanam, A., Winningham, A. and Rolland, J. P. Low dose plastic optical fibre radiation dosimeter for clinical dosimetry applications. (2009) ISBN 1930-0395.

4.3 Investigation of Timepix Application for Electron Dosimetry

4.3.1 Strontium/Yttrium-90

Strontium-90 is a pure electron emitter (β^- decay) and has a half-life of 28.8 years with maximum electron energy of 546 keV. This source was used as an electron source in this work (Massillon-JL, Minniti et al. 2009; Marcu, Bezak et al. 2012). Sr-90 decays to its daughter product Yttrium-90, which is also a pure beta emitter with half-life of 64 hours and emits 2.28 (~99.9%) and 0.523 (~0.1%) MeV electrons (Massillon-JL, Minniti et al. 2009; Marcu, Bezak et al. 2012). Because Sr-90 is encapsulated in stainless steel, the emitted low energy betas will mostly be absorbed by the capsule, meaning that most of the detected beta particles are emitted from Y-90 (2.28 MeV) (LNHB ; Massillon-JL, Minniti et al. 2009).

In this work, the used Sr-90 source (IBA dosimetry, Germany) had an initial activity of 16 MBq. The distance between the electron source and the Timepix detector was 2 cm.

4.3.2 Investigation of Timepix Pixel Value Linearity using Sr/Y-90 Source

Timepix Medipix mode was chosen to investigate linearity of measured pixel values as a function of exposure time, when irradiated with Sr/Y-90. Pixel values from the total/ integrated acquisition frame were used for the analysis. Acquisition time of 1 second per frame was used and the number of frames varied between 1 and 400 frames.

4.3.3 Results of Investigation Timepix Pixel Value linearity using Sr/Y-90 Source

Figure 4.2 shows the relationship between Timepix mean pixel value and the exposure time in seconds, as a result of irradiation with Sr/Y-90 β-particle source.

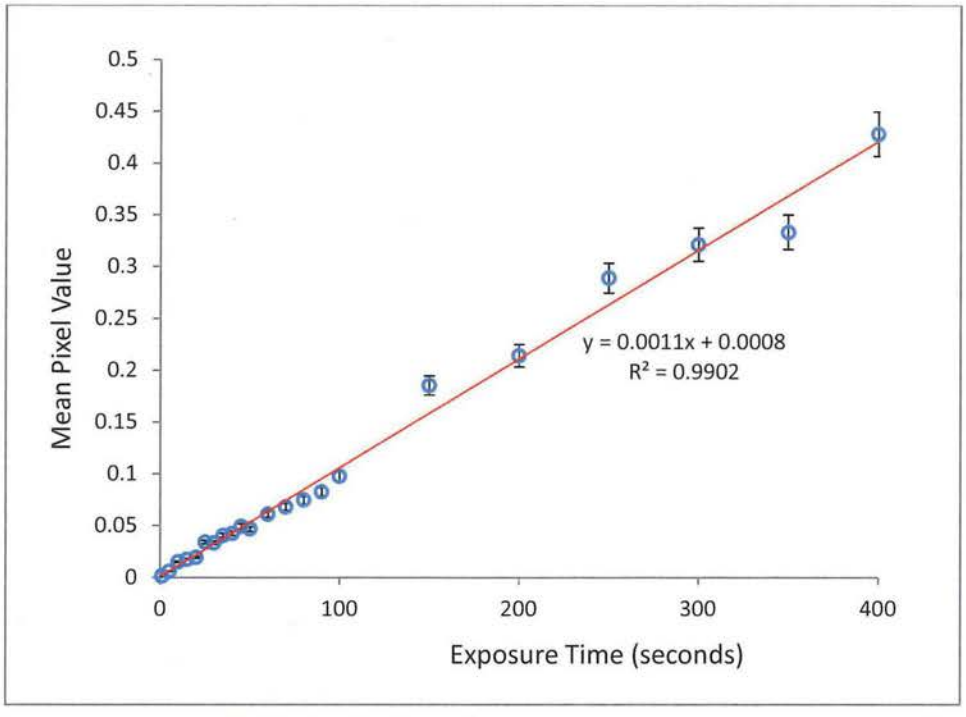

Figure 4.2: Timepix response to electrons (the relationship between the mean pixel value and exposure time). The PV statistical variation (i.e. the error bars) was estimated as 5% of the mean pixel reading.

It can be seen that the mean pixel value increases linearly as a function of exposure time in seconds. An R-square value of 0.9902 was obtained. The divergence of some readings from the linear fit is a result of electron energy distribution present at the sensitive layer of Timepix. As electrons deposit their energy in curly tracks, as shown in figure 4.3, they hit more than one pixel and the energy deposited is shared between the pixels.

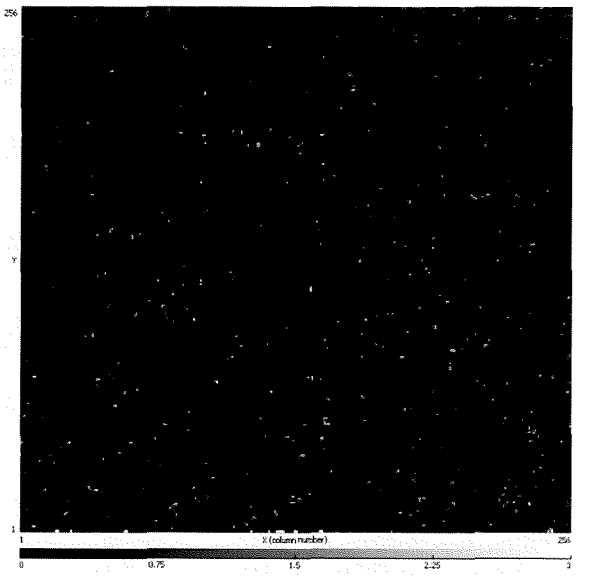

Figure 4.3: Curly electron tracks recorded by Timepix (100 second exposure time).

4.4 Conclusion

The results in this chapter show that the Timepix pixel values increased linearly with the absorbed dose in the μGy to mGy region as a result of irradiation by low energy photons and electrons. The detector response was found to be very sensitive to low absorbed doses and to day-to-day variations in doses as a result of radioactive decay. It also has a good medium term reproducibility, but is energy dependent, requiring energy calibration for different radiation types and energy spectra before it can be used for a dosimetry purposes.

Chapter 5

Timepix as a Spectrometer and an Imager

5.1 Introduction

The Timepix detector can be also used as a spectrometer if used in Time Over Threshold mode (TOT mode). The calibration of Timepix pixels, performed to achieve a uniform response to radiation using Pixelman software, was reviewed in detail in the review articles studying Timepix characteristics: "Timepix – technical aspects of a novel development in solid state radiation detectors" and "Overview of current applications of the Timepix detector in radiation physics", by Ruqaya AL Darwish, Eva Bezak, Loredana Marcu and Anatoly Rozenfeld (chapter 3).

The following paper describes the use of Timepix in TOT mode in order to evaluate its spectroscopic and imaging capabilities. This is required to fully characterize the detector, should be used for medical physics, imaging and dosimetry purposes (in addition to characterization conducted in chapter 4. The Sophy software used was developed by

Amsterdam Scientific Instruments (ASI), the Netherlands, and is provided with the detector purchase.

The investigation in this chapter was performed using several radioactive sources: Am-241, Ra-223, Pu-238 and Fe-55. The effect of bias voltage, applied to the Timepix sensitive layer, on the measured energy spectra was also investigated.

5.2 Statement of Contribution

5.2.1 Conception

The objective is to investigate the Timepix radiation detector performance for spectrometry applications using different radiation types. The first concept was suggested by Ruqaya Al Darwish. The methods by which to achieve this concept were conceptualised by Ruqaya Al Darwish and Eva Bezak.

5.2.2 Realisation

The practical works were done by Ruqaya Al Darwish under supervision of Eva Bezak for all experiments. Radiation measurements were conducted according to the conditions of Operating an ionising radiation apparatus licence and Using and handling radioactive substances licence (Radiation Protection and control Act 1982) by the South Australian Environment Protection Authority. Part of this work was conducted at Amsterdam Scientific Instruments, the Netherlands. Data collection and analysis were performed by Ruqaya Al Darwish.

5.2.3 Documentation

This paper was primarily written by Ruqaya Al Darwish. Editing was performed by all authors.

Statement of Authorship

Title of Paper	Autoradiography Imaging in Targeted Alpha Therapy with Timepix Detector
Publication Status	☑ Published ☐ Accepted for Publication ☐ Submitted for Publication ☐ Unpublished and Unsubmitted w ork w ritten in manuscript style
Publication Details	Ruqaya AL Darwish, Alex Hugo Staudacher, Eva Bezak and Michael Paul Brown, Autoradiography Imaging in Targeted Alpha Therapy with Timepix Detector, Computational and Mathematical Methods in Medicine, Volume 2015, 2015

Principal Author

Name of Principal Author (Candidate)	Ruqaya AL Darwish
Contribution to the Paper	Timepix measurements. Data analysis and theoretical calculations. This paper was primarily written by Ruqaya Al Darwish, who also acted as the corresponding author.
Overall percentage (%)	75%
Certification:	This paper reports on original research I conducted during the period of my Higher Degree by Research candidature and is not subject to any obligations or contractual agreements with a third party that would constrain its inclusion in this thesis. I am the primary author of this paper.
Signature	Date: 30/8/2016

Co-Author Contributions

By signing the Statement of Authorship, each author certifies that:

i. the candidate's stated contribution to the publication is accurate (as detailed above);

ii. permission is granted for the candidate in include the publication in the thesis; and

iii. the sum of all co-author contributions is equal to 100% less the candidate's stated contribution.

Name of Co-Author	Alex Hugo Staudacher
Contribution to the Paper	Input into experimental design and sample preparation. He also helped with paper editing.
Signature	Date: 30/8/16

Name of Co-Author	Eva Bezak		
Contribution to the Paper	Input into experimental design and calculation, paper editing.		
Signature		Date	30/3/16

Name of Co-Author	Michael Paul Brown		
Contribution to the Paper	Michael Paul Brown gave advice on the biological aspects of the sample preparation and the paper.		
Signature		Date	

Name of Co-Author	Eva Bezak		
Contribution to the Paper	Input into experimental design and calculation, paper editing.		
Signature		Date	

Name of Co-Author	Michael Paul Brown		
Contribution to the Paper	Michael Paul Brown gave advice on the biological aspects of the sample preparation and the paper.		
Signature		Date	30-AUG-2016

Technical Investigation of Timepix Use for Spectrometry Applications

Ruqaya Al Darwish [1,2,3] and Eva Bezak [2,4,5]

[1] Department of Medical Physics, Royal Adelaide Hospital, Adelaide, Australia
[2] School of Physical Sciences, University of Adelaide, Adelaide, Australia
[3] Ministry of Higher Education, Saudi Arabia
[4] International Centre for Allied Health Evidence, Sansom Institute, University of South Australia, Adelaide, Australia
[5] Sansom Insitute for Health Research, University of South Australia, Adelaide, Australia

Abstract

Timepix is a detector that can be used for dosimetry, imaging and spectrometry purposes. This technical report evaluates the use of Timepix for spectrometry using the Time Over Threshold (TOT) mode and the energy calibration file provided with the device. The report also evaluates the parameters that can affect the spectrometry measurements. Two radiation types (photons and alpha particles) from different radiation sources were used in this work: Am-241, Ra-223, Pu-238 and Fe-55. The effect of bias voltage, applied to the Timepix sensitive layer, on the measured energy spectra was also investigated. Finally, Mylar foils were used to deconvolve the measured spectra.

It was concluded that, while Timepix, if energy calibrated for a given bias voltage and a given radiation type, can be used for spectrometry of low energy γ-rays, X-rays and alpha particles in the MeV range, its energy resolution is not excellent and is inferior to, for example, germanium detectors.

1. Introduction

The Timepix TOT mode allows direct measurement of particle energy in each pixel, when calibrated using a surrogate function between the TOT response and the particle energy in keV. This surrogate function must be derived for at least two radioactive sources (Jakubek 2011; Platkevic, Jakubek et al. 2013) .

The calibration is usually done using 5.9 keV ^{55}Fe and 59.9 keV ^{241}Am and certain fluorescent materials emitting characteristic X-rays that are generated in a tungsten tube (Jakubek, Cejnarova et al. 2008; Jakubek 2011; Platkevic, Jakubek et al. 2013). Studies have shown that in the TOT mode the Timepix detector is able to measure energy spectra of photons, heavy charged particles and neutrons (if a converter, such as ^{6}LiF has been used) (Jakubek, Cejnarova et al. 2008; Jakubek, Schmidt-Wellenburg et al. 2009; Granja, Jakubek et al. 2011; Jakubek 2011; Platkevic, Jakubek et al. 2013). Furthermore, the calibrated device shows good agreement between the Timepix energy spectra and simulated or measured (by other methods) spectra (Jakubek, Schmidt-Wellenburg et al. 2009). However, in the TOT mode, the pixel count, used to determine the energy, depends on the cluster size (1, 2, 3 and 4 pixels) as well as the incidence beam angle with respect to the detector (Jakubek, Cejnarova et al. 2008; Granja, Jakubek et al. 2011). Figure 1 shows an example of the energy spectrum of ^{241}Am generated by a calibrated Timepix detector. The figure shows variations in energy spectra as a function of the number of pixels in which the radiation has deposited its energy (cluster size).

The energy resolution achieved was about 2.8 keV at 15.8 keV, 3.2 keV at 24.2 keV (Ka lines of Zr and Indium), and about 35 keV at 5.5 MeV (alpha particles from ^{241}Am) expressed in terms of full width at half maximum (FWHM) (Tureček, Holý et al.). In another study, the energy resolution of 30 keV was achieved for 5.5 MeV alpha particles from ^{241}Am (Tureček, Holý et al.).

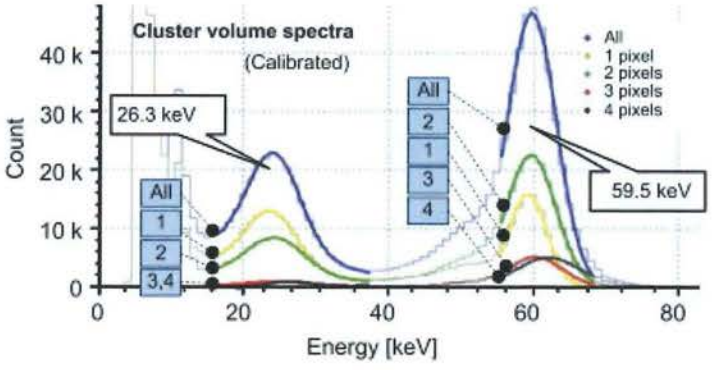

Figure 1: Energy spectra of ^{241}Am for different cluster size measured by Timepix in the TOT mode, courtesy of (Jakubek, Cejnarova et al. 2008).

2. Materials and Methods

2.1 Sophy software

The Timepix software used in this work was developed by the Timepix manufacturer, Amsterdam Scientific Instruments, the Netherlands, and is called software for physics (Sophy software). It is displayed in two windows: one to control the detector functions, such as the acquisition time, the number of frames, the mode of operation and the energy threshold (Figure 2). The second window shows quick-access icons to select procedures. From the main menu, the 'Preview' button opens several windows to display Timepix data acquisition, such as individual frames so that the events (i.e. individual particle hits) can be observed frame by frame. 'Spectral image (cluster analysis)' is another display window where a total/integrated image of all the events recorded in all frames is shown. In addition, the 'Spectra (cluster analysis)' window can be selected to display the energy spectra as well as the total pixel count from all recorded events.

The TOT mode can be selected using the measurement type button. In general, the Sophy software has more functionality compared to that offered by the Pixelman software (Pixelman

has been discussed in chapter 4). The 'Gear' icon, near the measurement type selection, opens up another set of possible measurement options, where a filter can be applied to choose the radiation type to be counted as well as the cluster size. The whole data acquisition can be recorded and replayed or saved as an image or an ASCII file for subsequent export to other software, such as Matlab and Excel, for further analysis. The device can be energy calibrated. The energy calibration file is provided with the device and can be uploaded to give the energy of detected particles in keV.

For advanced detector settings, tool driver can be opened for more specific detector settings, such as the bias voltage, which should be between 5 and 100 V depending on the particle type and the source activity. The bias voltage determines the charge collection speed and the size of the collected charge cluster (Tureček, Holý et al. ; Jakubek 2011; Janik, Ploc et al. 2016). Furthermore, a lower bias voltage gives a larger cluster response compared to a larger bias voltage (Granja, Jakubek et al. 2011; Janik, Ploc et al. 2016). However, a higher bias voltage increases the probability that Timepix will reach repletion due to charge depletion before the generated charges diffuse into the neighbouring pixels (Granja, Jakubek et al. 2011).

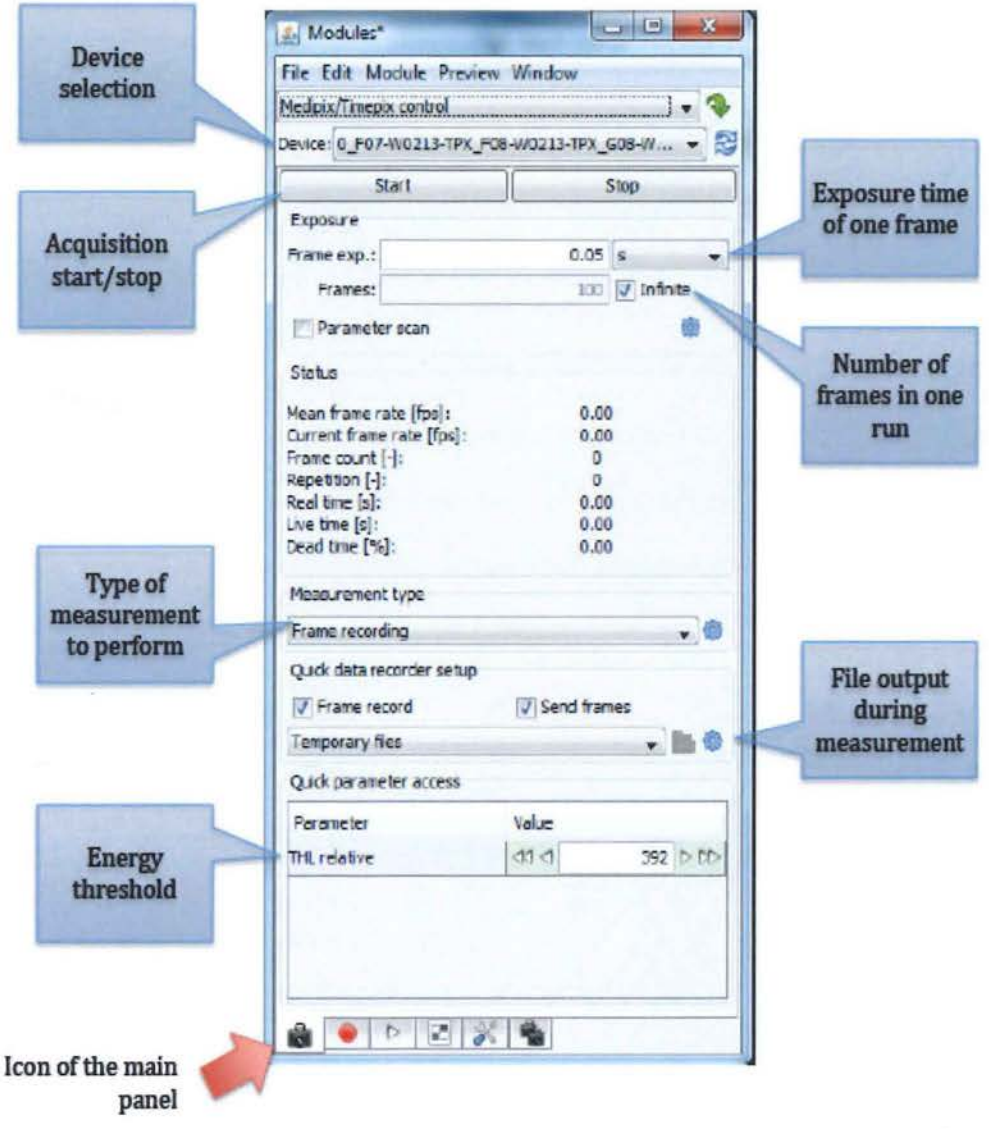

Figure 2: Timepix operating window in Sophy Software, courtesy of (Instruments 2013).

2.2 Radioactive sources

To investigate the energy spectra measured by the Timepix detector, different radioisotopes with different particle and photon energies were tested. The radioisotopes tested were: Am-241, Ra-223, Pu-238 and Fe-55.

Am-241 decays by emitting α-particles and γ-rays (Figure 3) with a half-life of 432.2 years (Lederer, Hollander et al. 1967). It has an α-particle energy range of between 5.389 and 5.545 MeV and γ-rays energy range between 0.033 and 0.097 MeV (Vajda, Martin et al. 2012). The Am-241 used in this study was a sealed radioactive source with an activity of 1.3 MBq. It was purchased from Eckert & Ziegler Nuclitec GmbH, Germany.

Ra-223, purchased from Algeta ASA, Norway, has a half-life of 11.43 days (Lederer, Hollander et al. 1967) and the activity used was 1.67 MBq. It emits α-particles (mean energy range ~ 6 MeV) and γ-rays and X-rays (80 and 270 keV) (McDevitt, Sgouros et al. 1998; Bruland, Nilsson et al. 2006; Lien, Tvedt et al. 2015).

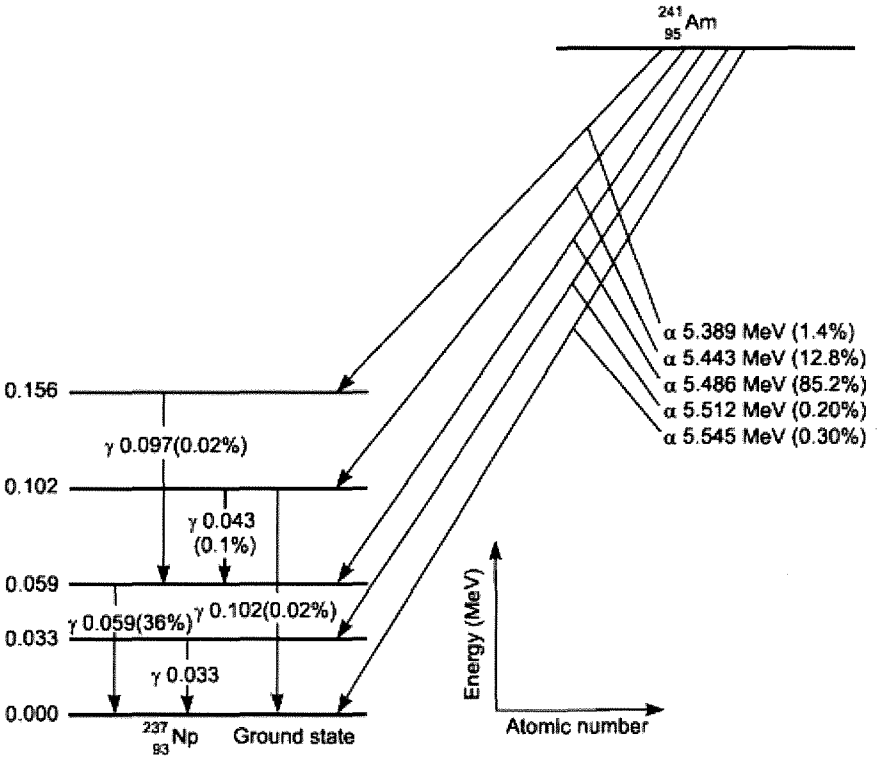

Figure 3: Am-241 decay scheme (all energies are in MeV), courtesy of (Vajda, Martin et al. 2012).

Pu-238 (a sealed source from the Radiochemical Centre, Amersham, England) has a half-life of 87.7 y and the activity used was 4.13 nCi. Pu-238 decays by emitting α-particles (100%) to U-234 with energies of 5.4 MeV (0.1%), 5.55 (28,85%) and 5.6 MeV (71%) (LNHB).

Fe-55 (half-life of 2.737 years) decays to Mn-55 by electron capture as shown in Figure 4. This decay is followed by the emission of Auger electrons that produce bremsstrahlung X-rays resulting in a continuous spectrum of up to 231 keV (LNHB). The electron capture can also be accompanied by the emission of Mn-55 characteristic X-rays with energies of 5.89875 keV (16.2%), 5.88765 keV (8.2%) and 6.49045 keV (2.85%) (LNHB). This source was provided by the ASI facility, Amsterdam.

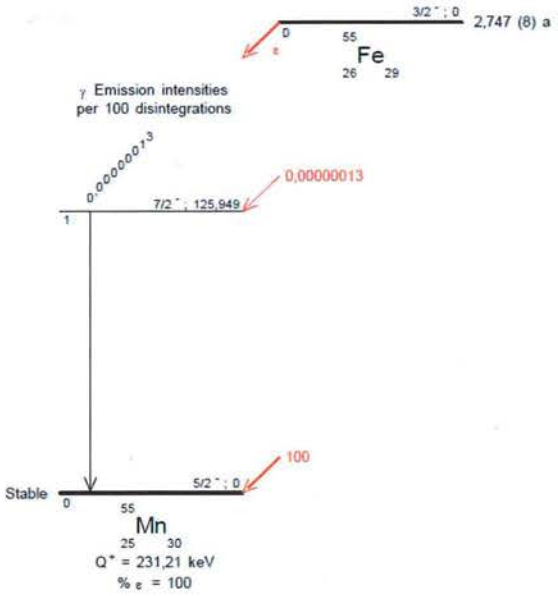

Figure 4: Fe-55 decay scheme, courtesy of (LNHB).

2.3 Experimental set up

The sources were placed at a distance of 0.5 cm from the sensitive layer of the detector. The cover of Timepix was removed only for α-particle emitters and was kept on for other sources. The TOT mode was selected as the Timepix operation mode along with spectral imaging (i.e. cluster analysis) as the measurement type. 100 V was applied as the bias voltage during a 15 minute to 2 hour irradiation times with 0.1 seconds per frame to investigate the spectra of radioactive sources. The THL threshold used was 330 (resulting from calibration of the whole detector matrix). Different filters were selected in the software, depending on the radiation type, with the inclusion of corner pixels. These filters apply specific requirements for cluster shapes for each radiation type. For example, the X-ray filter has a cluster area of 1 and the α-particle filter accepts cluster areas from 9 to 65,536 pixels and a peak height of >7 (i.e. clusters with areas below 9 pixels will be rejected when detecting alpha particles).

Another test was performed using Am-241 to investigate the effects of two bias voltages on the resulting spectra. 5 and 100 V were used to perform this investigation.

Additionally, the Am-241 γ-ray spectra were measured and compared when using 0, 1, 3 and 6 Mylar foils (0.5 μm thick each)) positioned in front of the Am-241 source. The face of the Timepix was covered with the lid in order to prevent α-particles from reaching the sensitive layer of the detector, and an X-ray filter was applied during the 12 hour acquisition time.

Mylar foils (0-2) were also used measure the reduction/changes in energy spectra of α-particles emitted from Pu-238 during a 24 hour acquisition time. The face of Timepix detector was uncovered and the α-particle filter was applied.

To measure the energy resolution of Timepix for Am-241, using 5 and 100 V bias voltages, and for Ra-223, using 100 V bias voltage, the full width at half maximum (FWHM) was determined from each measured spectrum as well as the energy at the center of the peak.

Timepix energy resolution was then calculated using the following equation (Bushberg, Seibert et al. 2002):

$$Energy\_resolution = \frac{FWHM}{Pulse\_height\_at\_center\_of\_peak} \times 100\%$$

Finally, Timepix performance as an energy spectrometer was evaluated based on the energy resolution observed.

3. Results and Discussion

3.1 Am-241 spectrum

Am-241 was used to calibrate the Timepix detector in the TOT mode. Two peaks are expected in the Am-241 energy spectrum: a peak for γ-rays and a peak for α-particles. As the energies of α-particles emitted from Am-241 are close to each other (Figure3), it is not expected that Timepix can be capable of distinguishing between these energies. The same applies to γ-rays. Due to the limited energy resolution of Timepix, it will produce continuous peaks for all α-particle energies in the total/combined spectrum (i.e. non-filtered spectrum in blue) as well as in the α-particle only (i.e. filtered spectrum in red), as shown in Figure 5.

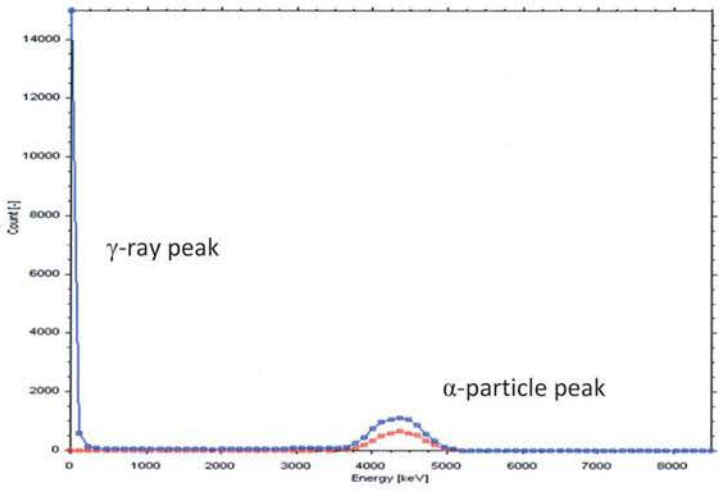

Figure 5: The combined Am-241 γ-ray and α-particle spectrum in blue taken with a bias voltage of 5 V. The red line corresponds to an α-particle spectrum only.

The acquired images of α-particle hits are shown in Figure 6 when using the two bias voltages. As can be seen, the α-particle cluster area is larger when 5 V was applied compared to 100 V. The spatial resolution for a single α-particle cluster is 385 and 575 μm, corresponding to bias voltages of 5 and 100 V, respectively.

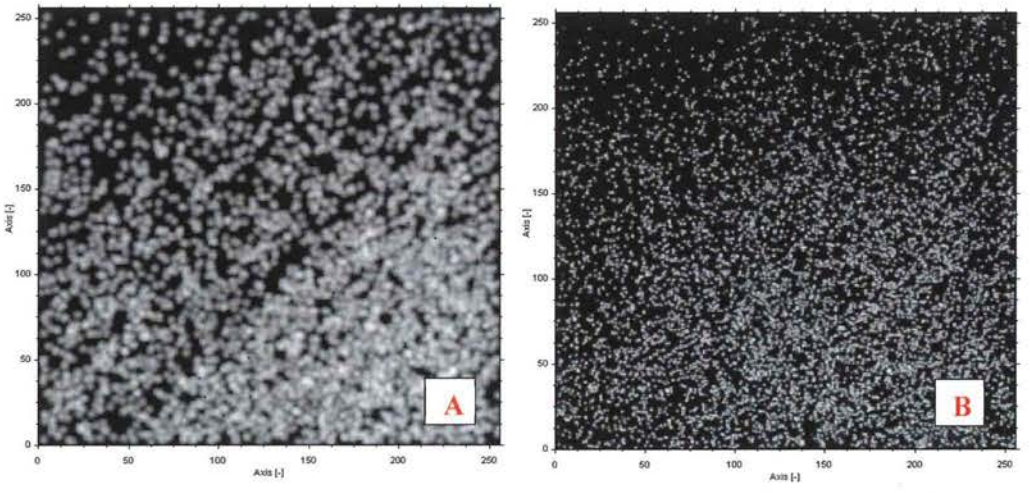

Figure 6: Timepix images of Am-241 α-particle hits acquired with a bias voltage of A) 5 V and B) 100 V.

The corresponding energy spectra for these two bias voltages are shown in Figure 7. Using a bias voltage of 100 V resulted in the spectrum being shifted towards a higher energy as compared to the real α-particle energy.

The measured energy resolution for bias voltage of 5 and 100 V was approximately 17% and 26%, respectively.

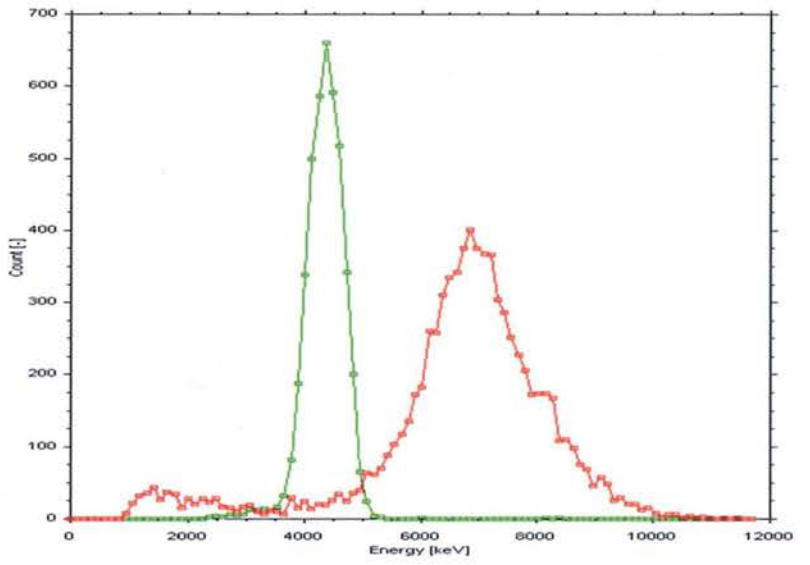

Figure 7: Am-241 α-particle spectra collected using a bias voltage of 5 V (green spectrum) and 100 V (red spectrum).

The Am-241 γ-ray spectra measured without and with 1, 3 and 6 Mylar foils positioned in front of the Am-241 source are shown in Figure 8. As expected for photons, the energy has not changed, but the number of these low energy photons detected is reduced slightly due to scatting and absorption in the foil.

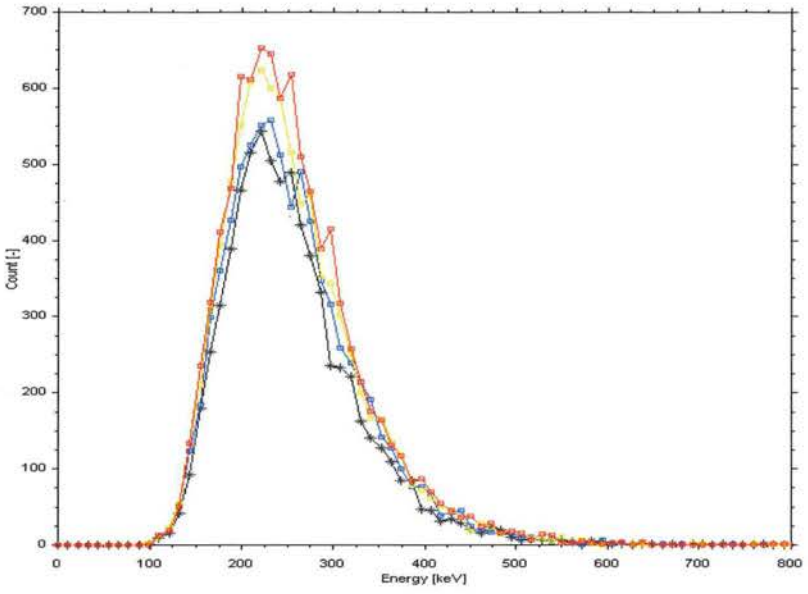

Figure 8: Am-241 γ-rays spectra after 12 h acquisition time, where red, yellow, blue and black lines correspond to spectra with 0, 1, 3 and 6 Mylar foils covering the source.

3.4 Ra-223 spectrum

The image acquired after 15 minute irradiation using Ra-223, is shown in Figure 9, where the right-hand image shows all particles that hit the Timepix during that time, while the left-hand image displays only α-particle events. The spectrum resulting from the 15 minute irradiation is shown in Figure 10. It also contains two separate groups of peaks, representing the α-particle spectrum and the γ-ray spectrum. The mean energy reading for α-particles, shown in Figure 10, is shifted towards higher energies (as the bias voltage of 100 V was used) compared to the real mean α-particle energy.

Timepix energy resolution for Ra-223 was determined to be 32%.

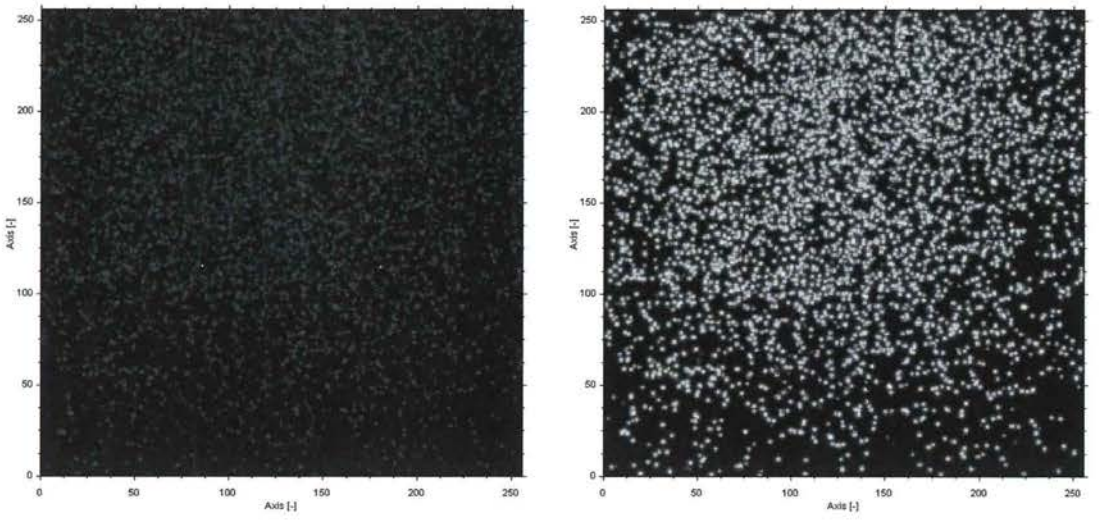

Figure 9: Ra-223 emissions: the image on the right shows α-particle and γ-ray hits and the image on the left shows α-particle hits only.

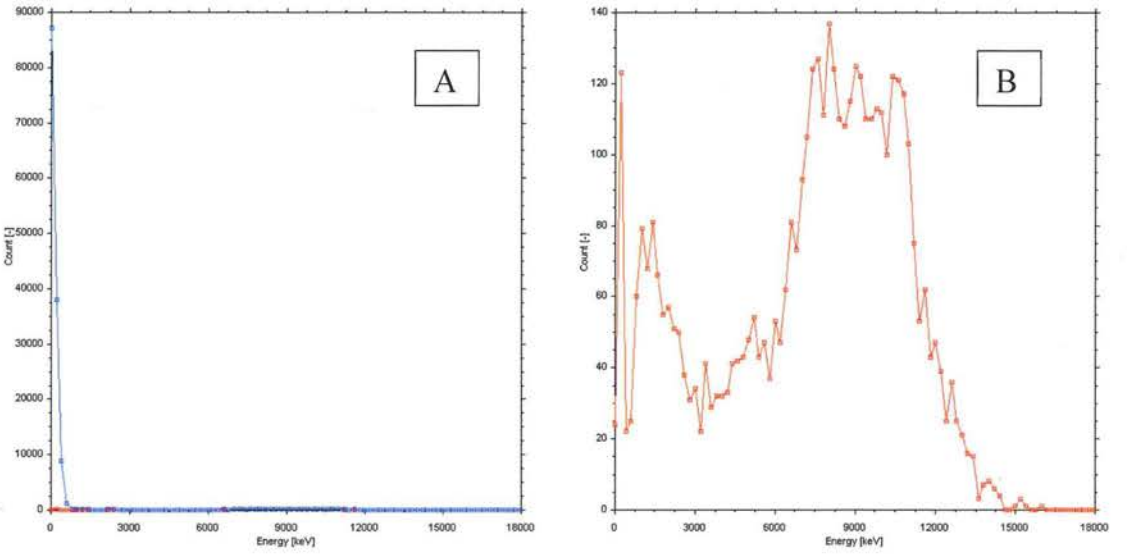

Figure 10: Ra-223 spectra: (A) A combined spectrum with α-particles (red) and γ-rays (blue) and (B) an α-particle spectrum only. The measurement was done using the bias voltage of 100 V.

3.2 Pu-238 spectrum

The acquired Pu-238 spectra for γ-rays and α-particles are shown in Figure 11.

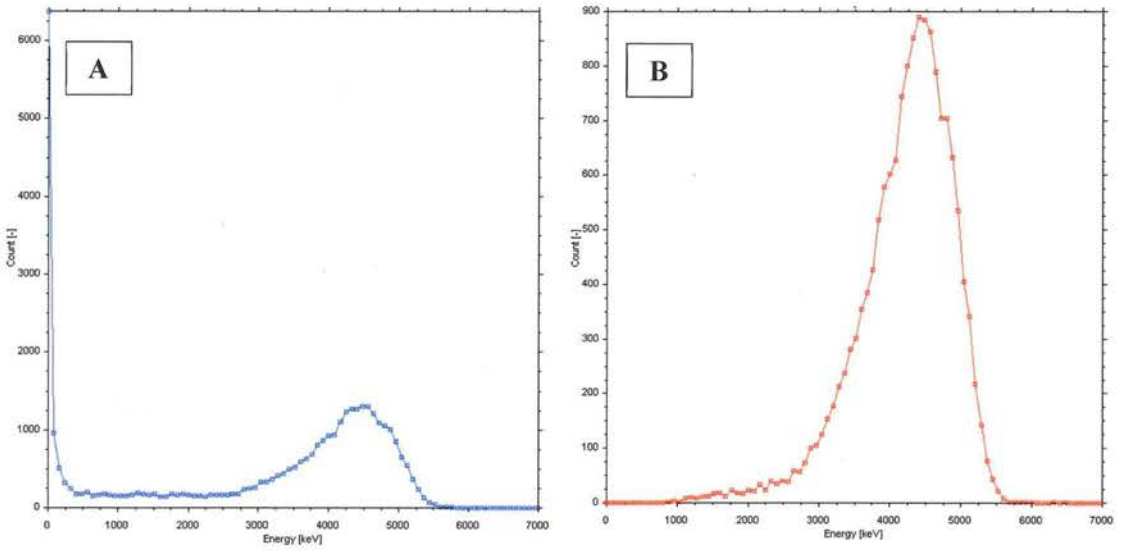

Figure 11: Pu-238 A) A combined γ-ray and α-particle spectrum and B) the α-particle spectrum. 100 V bias voltage was used.

When the source was covered with 1 or 2 Mylar foils, the α-particle spectra shown in Figure 12 were measured. As expected, the energy of α-particles decreased with the increasing number of Mylar foils.

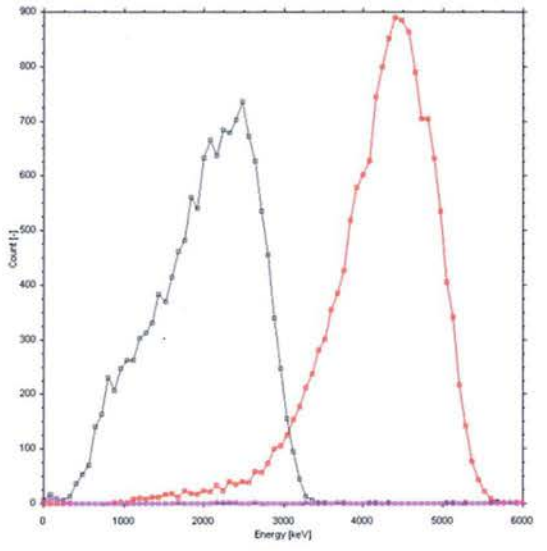

Figure 12: Pu-238 α-particle spectra measured using Mylar foils: 0 (red spectrum), 1 (grey spectrum) and 2 Mylar foils (pink spectrum).

3.3 Fe-55 spectrum

An X-ray filter was used to obtain the Fe-55 spectrum. The measured spectrum is shown in Figure 13. A single broad continuous bremsstrahlung X-ray spectrum is observed.

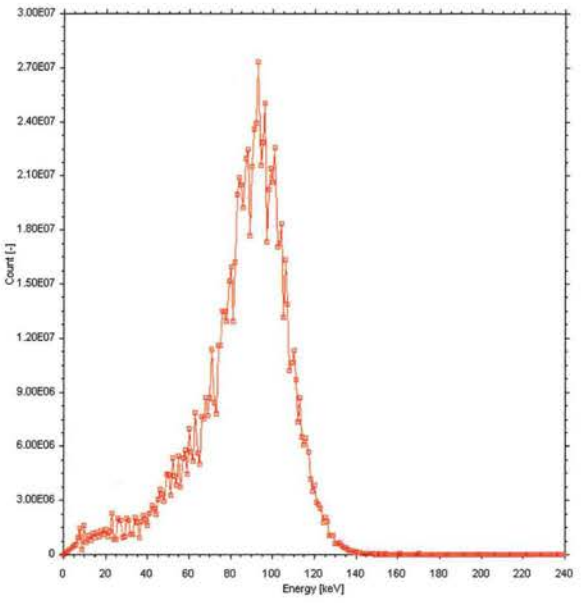

Figure 13: The measured Fe-55 continuous Bremsstrahlung X-ray spectrum. The Mo-55 characteristic X-rays cannot be distinguished.

4. Conclusion

Timepix performance shows that it has capacity to function as a spectrometer, albeit with limited ability to distinguish between close particle energies (within 1 MeV), although with poor resolution. Photons and α-particles emitted from several radioactive sources were identified and their spectra were studied. Investigation of Timepix energy calibration, provided by the manufacturer, was also performed. The results demonstrate that the energy calibration cannot be applied to all bias voltages but only for the one it has been generated for. More accurate calibration for a range of radiation sources is still required.

It is also concluded that while Timepix, if energy calibrated for a given bias voltage and a given radiation type, can be used for spectrometry of low energy γ-rays, X-rays and alpha particles in the MeV range, its energy resolution is not excellent and is inferior to, for example, germanium detectors. This is possibly a consequence of the pixel sharing effect as well as of the very thin detector layer (300 μm).

References

Bruland, Ø. S., S. Nilsson, et al. (2006). "High-Linear Energy Transfer Irradiation Targeted to Skeletal Metastases by the α-Emitter 223Ra: Adjuvant or Alternative to Conventional Modalities?" Clinical Cancer Research **12**(20): 6250s-6257s.

Bushberg, J. T., J. A. Seibert, et al. (2002). The Essential Physics of Medical Imaging. Philadelphia, Philadelphia : Lippincott Williams & Wilkins.

Granja, C., J. Jakubek, et al. (2011). "Response of the pixel detector Timepix to heavy ions." Nuclear Instruments and Methods in Physics Research Section A: Accelerators, Spectrometers, Detectors and Associated Equipment **633, Supplement 1**(0): S198-S202.

Instruments, A. S. (2013). Timepix QTPX-262k and STPX-65k Quick start manual The Netherlands. .

Jakubek, J. (2011). "Precise energy calibration of pixel detector working in time-over-threshold mode." Nuclear Instruments and Methods in Physics Research Section A: Accelerators, Spectrometers, Detectors and Associated Equipment **633, Supplement 1**(0): S262-S266.

Jakubek, J., A. Cejnarova, et al. (2008). "Pixel detectors for imaging with heavy charged particles." Nuclear Instruments and Methods in Physics Research Section A: Accelerators, Spectrometers, Detectors and Associated Equipment **591**(1): 155-158.

Jakubek, J., P. Schmidt-Wellenburg, et al. (2009). "A coated pixel device TimePix with micron spatial resolution for UCN detection." Nuclear Instruments and Methods in Physics Research Section A: Accelerators, Spectrometers, Detectors and Associated Equipment **600**(3): 651-656.

Janik, M., O. Ploc, et al. (2016). "Optimization of the Timepix chip to measurement of radon, thoron and their progenies." Appl Radiat Isot **107**: 220-224.

Lederer, C. M., J. M. Hollander, et al. (1967). Table of isotopes. New York John Wiley & Sons.

Lien, L. M., B. Tvedt, et al. (2015). "Treatment of castration-resistant prostate cancer and bone metastases with radium-223 dichloride." Int J Urol Nurs **9**(1): 3-13.

LNHB. (24th June 2016). "Table of Radionuclides ".

McDevitt, M. R., G. Sgouros, et al. (1998). "Radioimmunotherapy with alpha-emitting nuclides." European Journal of Nuclear Medicine **25**(9): 1341-1351.

Platkevic, M., J. Jakubek, et al. (2013). "Evaluation of local radiation damage in silicon sensor via charge collection mapping with the Timepix read-out chip." Journal of Instrumentation **8**(04): C04001.

Tureček, D., T. Holý, et al. "Pixelman - Manual." Retrieved 26 April, 2016, from http://aladdin.utef.cvut.cz/ofat/others/Pixelman/Pixelman_manual.html.

Vajda, N., P. Martin, et al. (2012). Chapter 6 - Alpha Spectrometry A2 - L'Annunziata, Michael F. Handbook of Radioactivity Analysis (Third Edition). Amsterdam, Academic Press: 363-422.

5.3 Timepix as an Imager

Imaging applications of detectors from the Medipix family are possible as a result of the combination of the small pixels (μm), and high density electronic components and the pulse processing electronics (Cudie 2007).

A simple evaluation of the Timepix radiation detector was performed in this chapter in order to examine its imaging ability. The evaluation was conducted using different objects such as ball bearings, optical fibre and a rectangular block of lead.

Furthermore, evaluation of Timepix's spatial resolution was also performed using a sharp edge. The spatial resolution is determined by the ability of an imaging system to accurately illustrate the details of an object in two dimensions (Bushberg, Seibert et al. 2002). The spatial resolution of any imaging system can be obtained by either the point spread functions (PSF) which is considered a difficult task as it requires an infinitesimal point source or by the line spread function (LSF) which should be performed with infinitesimal line source. LSF however, can be acquired using a sharp edge object via the edge response function (ERF) (Smith 1997-1998, Lee 2001, Bushberg, Seibert et al. 2002). PSF, LSF and ERF are shown in Figure 4.4.

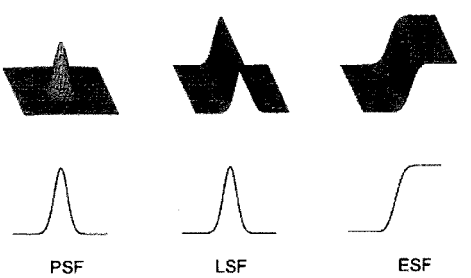

Figure 5.1. Point spread functions (PSF), line spread functions (LSF) and edge response function (ERF) and their profile in bottom, courtesy of (Bushberg, Seibert et al. 2002).

ERF is defined as the distance between 10 and 90% of the edge response and LSF is the first derivative of the ERF.

In this experiment, a sharp edge image was used to measure the edge response function using a rectangular block of lead to cover part of the detector. These tests were performed with X-rays emitted from an I-125 seed and also using α-particles emitted from Pu-238.

5.3.1 Materials

5.3.1.1 Radiation Sources

Two sources were used in these experiments: I-125 (two seeds of Iodine-125 were used where the average length of the single seed was 4.5 mm and the diameter was 0.8 mm) and a Pu-238 source with a circular area of 2 cm diameter. More information about these two sources was presented in chapters 4 and chapter 5, respectively.

5.3.1.2 Imaging Objects

In order to determine Timepix's ability to image fine objects, four metal ball bearings (2 mm diameter each), F2 fractal optical fibre with an air core (0.22 mm diameter) and a complex optical fibre with multi size air holes (~ 8 mm diameter) were used. The optical fibres were provided by the OptoFab node of the Australian National Fabrication Facility. A rectangle block of lead was also used.

5.3.2 Methods

5.3.2.1 Imaging

The objects were placed one by one directly on the top of the Timepix cover and radiation source was positioned 15 cm away from Timepix. Medipix mode (chapter 2) was used and integrated frames were applied to produce an image of our objects. Between 300 and 43,200 frames were acquired using an acquisition time of 1 second/frame. Ability to identify/resolve fine details of the structure of the imaged objects was evaluated qualitatively only.

5.3.2.2 Measurements of Spatial Resolution using Sharp Edge Images

A rectangular block of lead was used to cover part of the Timepix detector and the sharp edge images were acquired using X-rays emitted from I-125 seeds and α-particles emitted from Pu-238. Medipix mode was used. The total acquisition time was 2 hours with 0.1 second/frame.

Each sharp edge image in Timepix preview window was exported as an ASCII matrix, and processed using Matlab software. The mean pixel value of each row (i.e. 256 rows) in the image matrix was calculated and plotted on the y-axis with the corresponding pixel number on the x-axis. In order to determine the ERF, the distance between 10 and 90% of the edge response width was calculated (Figure 5.2).

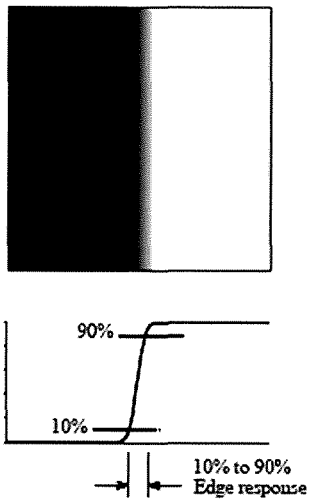

Figure 5.2. Determination of the edge response function, courtesy of (Smith 1997-1998).

5.3.3 Results and Discussion

5.3.3.1 Images

Figure 5.3 shows the four ball bearings imaged using I-125 seeds after 12 hours acquisition/irradiation time. The ball bearings are clearly visible. Some image artefacts are present as well, represented as shadowing between the individual ball-bearings.

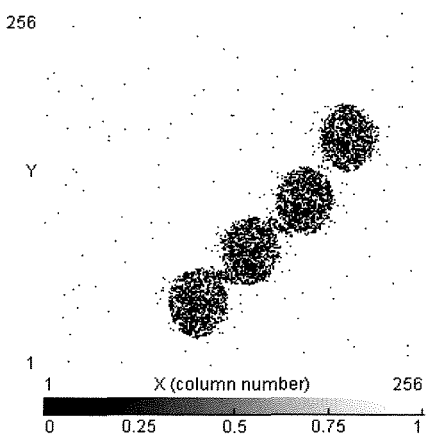

Figure 5.3. An image of four ball bearings acquired with an I-125 seed source.

The image of the F2 fractal optical fibre acquired using the I-125 source is shown in Figure 5.4. 300 frames with 1 s per frame were taken. The mean reading per pixel was 45.9 counts. The F2 fractal optical fibre has a diameter of 0.62 mm. The air core in the fibre is clearly visible, confirming that Timepix is capable of imaging objects with submillimetre structures.

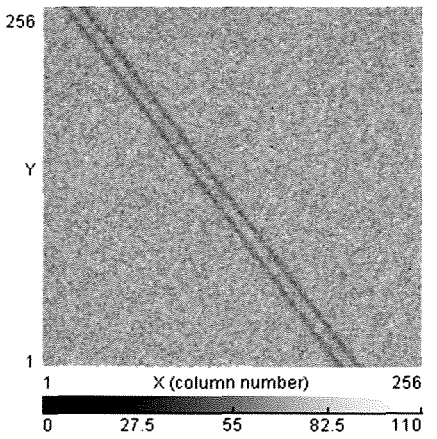

Figure 5.4. F2 fractal optical fibre image acquired with an I-125 seed source.

The image of the optical fibre with multi holes (I-125 source, 1 second peer frame) is shown in Figure 5.5. The smallest and the largest measured inner oval holes had widths of 0.6 and 1.26 mm, respectively and are clearly distinguishable in the image.

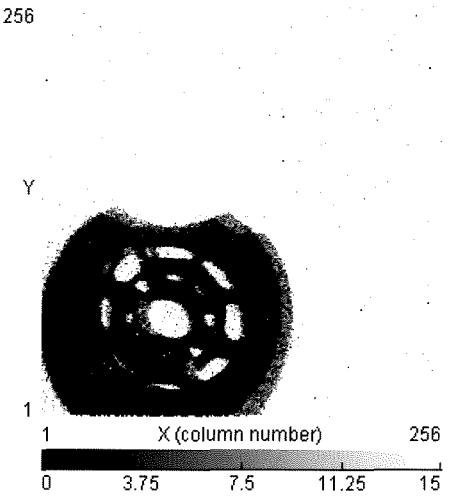

Figure 5.5. Optical fibre with air holes imaged by Timepix using I-125 seed source.

5.3.3.2 Sharp Edge Images

The sharp edge image acquired with I-125 seeds and the lead block is shown Figure 5.6. The measured edge response function is 0.79 mm is shown in Figure 5.7.

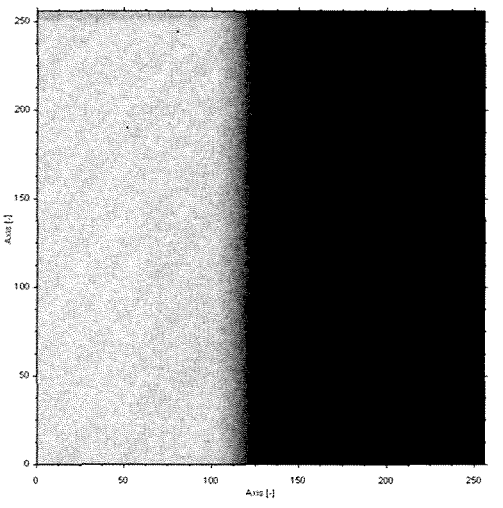

Figure 5.6. Sharp edge image acquired with Timepix and X-rays emitted from two I-125 seeds.

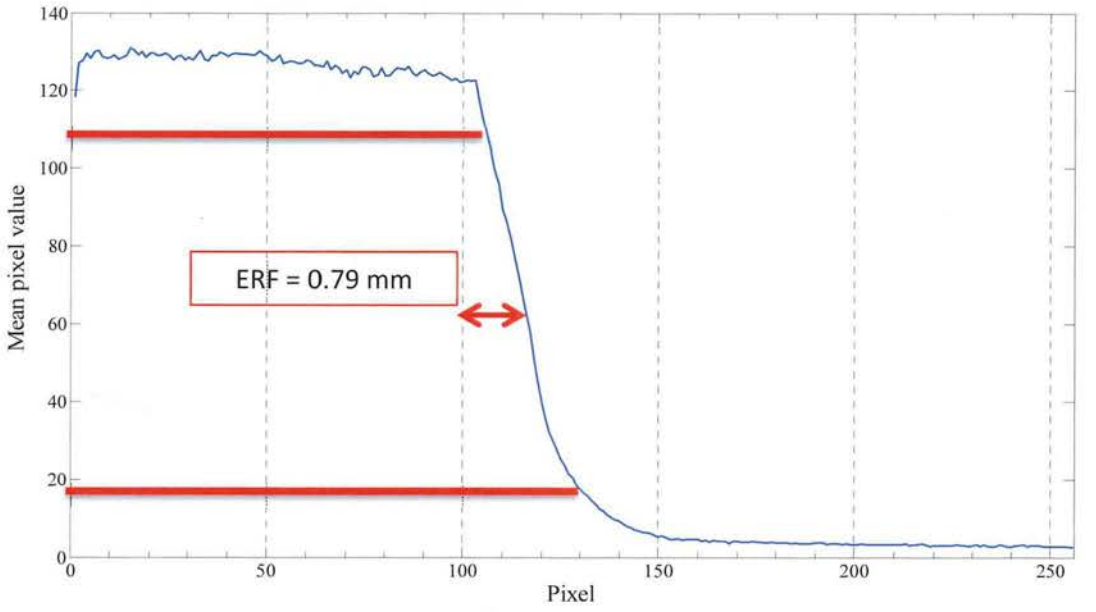

Figure 5.7. The edge response function of the sharp edge imaged using Timepix and I-125 X-rays. Each pixel, on the x-axis, has the width of 55 μm.

The sharp edge image acquired using Pu-238 and Timepix is shown in Figure 5.8; where (A) is an actual response of Timepix to α-particles, showing α-particles as clusters and (B) is a processed image where each α-particle hit is represented by the centroid pixel only (i.e. the central pixel in a cluster). The ERF, determined by using mean pixel values in each row, is 1.28 mm (Figure 5.9).

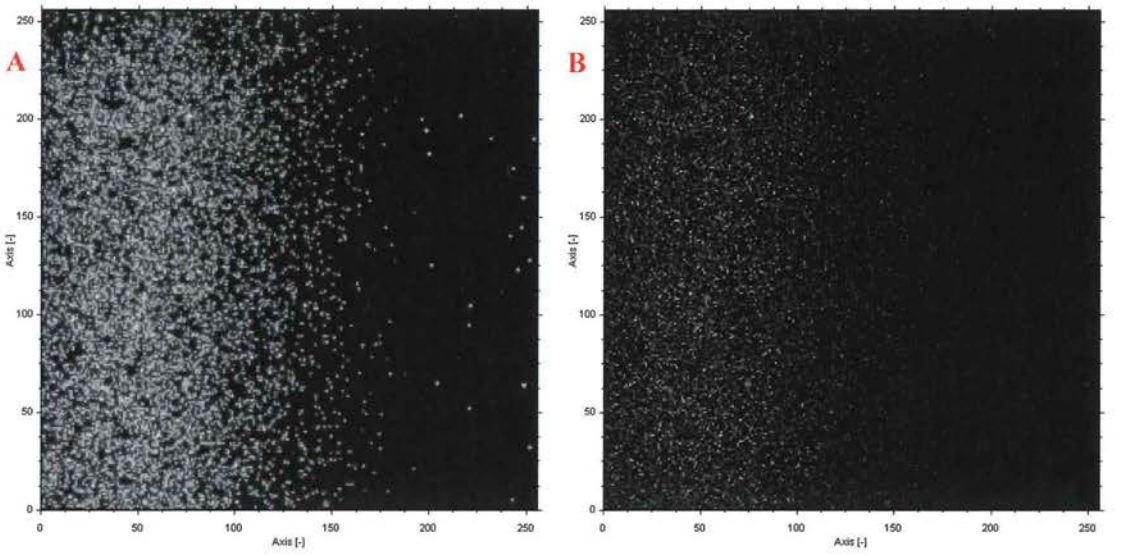

Figure 5.8. The sharp edge image acquired with Timepix and Pu-238 α-particles: (A) α-particles clusters and (B) centroid pixels only of each α-particle cluster.

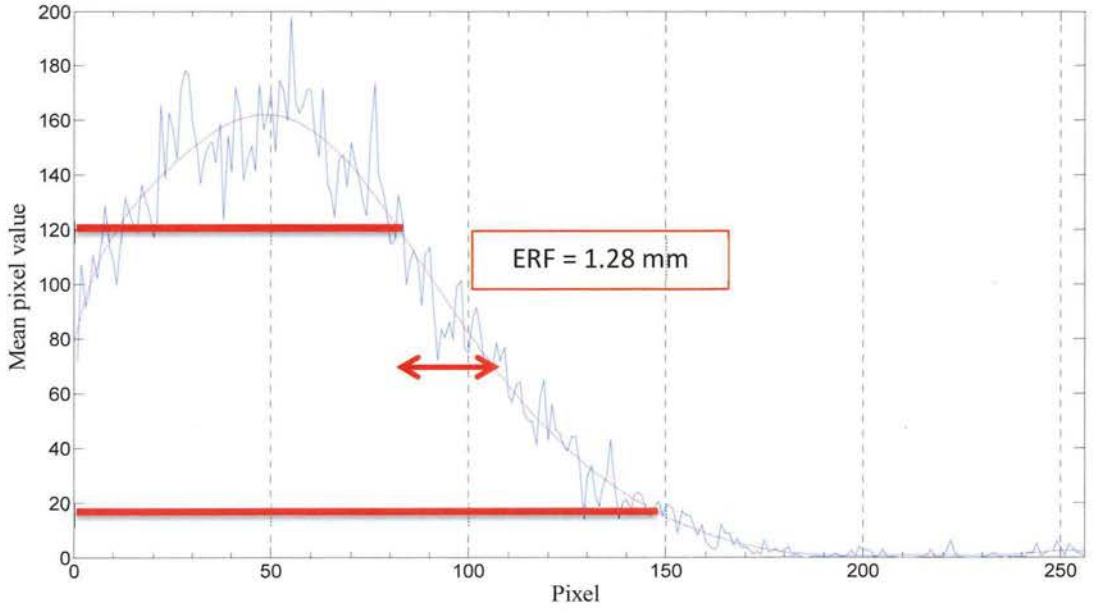

Figure 5.9. The edge response function of the sharp edge imaged using Timepix and Pu-238 α-particles. Each pixel, on the x-axis, has the width of 55 μm.

5.4 Conclusions

The studies in this chapter show that Timepix can be used as a spectrometer and an imager. Timepix can detect and identify photons, α-particles and electrons emitted from various radioactive sources and can also measure their energies, although not with very good resolution. The TOT mode can be used to measure the energy of the impinging radiation directly, provided that Timepix is calibrated for the given energy range and the same acquisition parameters are used for the calibration and the measurement (e.g. the bias voltage).

The energy resolution was found to be 17% and 26% for Am-241α-particles with a bias voltage of 5 and 100 V, respectively and 32% for Ra-223 α-particles. Selection of the optimal bias voltage depends on the activity of the radioactive source and the radiation type.

As an imager, Timepix can image fine details of an object (from 0.2 mm diameter). The measured edge response functions measured with I-125 X-rays and Pu-238 α-particles were 0.79 mm and 1.28 mm, respectively. These values result from the fact that the sources used were not point sources. Far superior resolution can be achieved with Timepix if a point source is used, for example, a nano-focus X-ray tube with a focal spot size of less than 1 μm (Dammer, Frallicciardi et al. 2009).

Chapter 6

Application of Timepix in Autoradiography for TAT

6.1 Introduction

Autoradiography monitoring tools are essential to detect radiation in *ex vivo* experiments of targeted therapy and to provide precise quantitative measurements of radiation uptake. Different devices with different abilities can be used for such measurements and include a gamma counter such as Geiger–Muller (GM) counter, well-type scintillation counter, α-camera and QID camera (Pearson, Hodes et al. 1969; Bäck and Jacobsson 2010; Chouin, Lindegren et al. 2013; Karimi, Lee et al. 2014; Miller, Gregory et al. 2014; Frost, Miller et al. 2015).

Now that the Timepix performance has been comprehensively characterised, using radiation sources only, additional degree of complexity was added to the experiments, introducing measurements of radiation emitted from biological samples, namely: radiolabeled cells and radiolabeled tumour sections. Capacity of Timepix for autoradiography and radiolabeling counting (i.e. efficiency of radioisotope uptake by cells) has been investigated.

In this chapter, the use of Timepix for autoradiography in TAT is described. Additionally, Timepix use as a radiolabelling detector is also discussed.

6.2 Statement of Contribution

6.2.1 Conception

The first concept of investigation of Timepix use for autoradiography was suggested by Eva Bezak and Alex Staudacher. The methods by which to achieve this concept were conceptualised by Ruqaya Al Darwish, Alex Staudacher, Eva Bezak and Michael Paul Brown.

6.2.2 Realisation

The experimental work was done by Ruqaya Al Darwish under supervision of Alex Hugo Staudacher and Eva Bezak. All experiments using radiation were conducted according to the conditions of Operating an ionising radiation apparatus licence and Using and handling radioactive substances licence (Radiation Protection and control Act 1982) by South Australian Environment Protection Authority. Data collection and analysis was done by Ruqaya AL Darwish.

6.2.3 Documentation

This paper was primarily written by Ruqaya Al Darwish. Editing was performed by all authors.

Statement of Authorship

Title of Paper	Autoradiography Imaging in Targeted Alpha Therapy with Timepix Detector
Publication Status	☑ Published ☐ Accepted for Publication ☐ Submitted for Publication ☐ Unpublished and Unsubmitted work written in manuscript style
Publication Details	Ruqaya AL Darwish, Alex Hugo Staudacher, Eva Bezak and Michael Paul Brown, Autoradiography Imaging in Targeted Alpha Therapy with Timepix Detector, Computational and Mathematical Methods in Medicine, Volume 2015, 2015

Principal Author

Name of Principal Author (Candidate)	Ruqaya AL Darwish
Contribution to the Paper	Timepix measurements. Data analysis and theoretical calculations. This paper was primarily written by Ruqaya Al Darwish, who also acted as the corresponding author.
Overall percentage (%)	75%
Certification:	This paper reports on original research I conducted during the period of my Higher Degree by Research candidature and is not subject to any obligations or contractual agreements with a third party that would constrain its inclusion in this thesis. I am the primary author of this paper.
Signature	Date 30/8/2016

Co-Author Contributions

By signing the Statement of Authorship, each author certifies that:

i. the candidate's stated contribution to the publication is accurate (as detailed above);

ii. permission is granted for the candidate in include the publication in the thesis; and

iii. the sum of all co-author contributions is equal to 100% less the candidate's stated contribution.

Name of Co-Author	Alex Hugo Staudacher
Contribution to the Paper	Input into experimental design and sample preparation. He also helped with paper editing.
Signature	Date 30/8/16

Name of Co-Author	Eva Bezak		
Contribution to the Paper	Input into experimental design and calculation, paper editing.		
Signature		Date	30/3/16

Name of Co-Author	Michael Paul Brown		
Contribution to the Paper	Michael Paul Brown gave advice on the biological aspects of the sample preparation and the paper.		
Signature		Date	

Name of Co-Author	Eva Bezak		
Contribution to the Paper	Input into experimental design and calculation, paper editing.		
Signature		Date	

Name of Co-Author	Michael Paul Brown		
Contribution to the Paper	Michael Paul Brown gave advice on the biological aspects of the sample preparation and the paper.		
Signature		Date	30-AUG-2016

Hindawi Publishing Corporation
Computational and Mathematical Methods in Medicine
Volume 2015, Article ID 612580, 7 pages
http://dx.doi.org/10.1155/2015/612580

Hindawi

Research Article

Autoradiography Imaging in Targeted Alpha Therapy with Timepix Detector

Ruqaya AL Darwish,[1,2] Alexander Hugo Staudacher,[3,4] Eva Bezak,[1,2] and Michael Paul Brown[3,4,5]

[1] *Department of Medical Physics, Royal Adelaide Hospital, Adelaide, Australia*
[2] *School of Chemistry and Physics, University of Adelaide, Adelaide, Australia*
[3] *Translational Oncology Laboratory, Centre for Cancer Biology, SA Pathology and University of South Australia, Adelaide, Australia*
[4] *School of Medicine, University of Adelaide, Australia*
[5] *Cancer Clinical Trials Unit, Royal Adelaide Hospital, Adelaide, Australia*

Correspondence should be addressed to Eva Bezak; eva.bezak@health.sa.gov.au

Received 25 July 2014; Accepted 14 October 2014

Academic Editor: Loredana G. Marcu

There is a lack of data related to activity uptake and particle track distribution in targeted alpha therapy. These data are required to estimate the absorbed dose on a cellular level as alpha particles have a limited range and traverse only a few cells. Tracking of individual alpha particles is possible using the Timepix semiconductor radiation detector. We investigated the feasibility of imaging alpha particle emissions in tumour sections from mice treated with Thorium-227 (using APOMAB), with and without prior chemotherapy and Timepix detector. Additionally, the sensitivity of the Timepix detector to monitor variations in tumour uptake based on the necrotic tissue volume was also studied. Compartmental analysis model was used, based on the obtained imaging data, to assess the Th-227 uptake. Results show that alpha particle, photon, electron, and muon tracks were detected and resolved by Timepix detector. The current study demonstrated that individual alpha particle emissions, resulting from targeted alpha therapy, can be visualised and quantified using Timepix detector. Furthermore, the variations in the uptake based on the tumour necrotic volume have been observed with four times higher uptake for tumours pretreated with chemotherapy than for those without chemotherapy.

1. Introduction

The relationship between the characteristics of a particular radiation type and its impact on irradiated biological tissues and cells plays an important role in estimating the efficacy and applicability of targeted radiotherapies [1]. In a specific case of targeted alpha therapy (TAT), a tumour-specific antibody or protein is radiolabelled with an alpha-emitting radionuclide, termed a radioimmunoconjugate [2, 3]. This radioimmunoconjugate attaches preferentially to tumour-specific antigens that can be expressed on a tumour cell membrane and release high-linear energy transfer (LET) alpha particles with kinetic energy of a few MeV. The traversal of these short-ranged alpha particles through target and neighbouring tumour cells results in localised radiation damage and ultimately cell death [2, 4]. TAT can, however, also result in so-called cross fire irradiation in which antigen-negative nontumour cells in close vicinity of the radioimmunoconjugate are also irradiated and damaged. The magnitude of this radiation damage (to tumour or healthy cells) strongly depends on the tumour-specific uptake of the particular radioimmunoconjugate.

To date, there is a lack of methods that can quantify alpha particle emissions in biological systems. One of the few devices presently available (known as the "α-camera") combines autoradiography with a scintillation detector and optical registration using a charge-coupled device. In the study of Bäck and Jacobsson, the distribution of At-211 labelled antibody and antibody fragments in human tumour, mouse kidney, and whole-body sections were examined [6]. The α-camera had a resolution of $35 \pm 11\,\mu$m, and

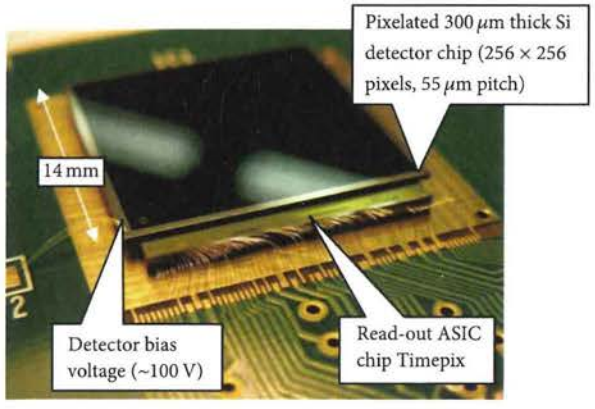

FIGURE 1: Timepix detector structure, courtesy of [5].

the quantitative analysis proved that the pixel intensity has a linear relationship with the activity of the imaged tissue. The results demonstrated the ability of the α-camera to be employed in small-scale dosimetry for TAT as it was able to provide quantitative data on a microscopic scale [6]. Furthermore, the α-camera was also used to examine the accumulation of an At-211 radioimmunoconjugate administered to mice with ovarian cancer micrometastases. The activity level and the number of tumour cell clusters were determined by imaging one section with the α-camera and by staining a consecutive section with hematoxylin and eosin [7]. The study demonstrated that the radioimmunoconjugate had high uptake and retention at the tumour surface and that dose estimates to micrometastases could be calculated using the α-camera.

Timepix is a new prototype radiation detector which takes advantage of recent developments of the complementary metal-oxide-semiconductor (CMOS) technology for constructing integrated circuits. Timepix consists of a silicon semiconductor layer, divided into an array of pixels, which is bumped-bonded to an electronics integrated layer (Figure 1). Each pixel is connected to an individual charge-sensitive preamplifier, a discriminator and a counter [8, 9], and a 4-bit digital-to-analogue converter (DAC) to adjust the voltage threshold (4-bit DAC for threshold adjustment) [10].

Timepix is a sophisticated microdosimeter that can be used for a wide range of experiments with photons, electrons, and other charged particles and has applications in fields such as space physics, nuclear physics, radiotherapy physics, imaging, and radiation protection. One of its main advantages is that it can measure energy deposition directly and in real time [11]. For example, in the work of Esposito et al., Timepix was used to trace β-particles froma C-14 sample [12, 13]. C-14 was deposited on a low-density paper foil, evaporated before packing in 10 μm thick Mylar, and being read by the detector [12]. The image was analysed in terms of clusters of hit pixels, which gave an indication of the interaction position of the β particle with the detector. The result showed that Timepix was highly sensitive with a minimum detectable activity of 0.0077 Bq and with a spatial resolution of 76.9 μm at full width at half maximum (FWHM) [13].

In this paper, we present the first results for using Timepix to visualise TAT *ex vivo* in mouse tumour sections. As mentioned above, the α-emitting radioimmunoconjugate binds to its cancer-specific antigen. The emitted α particles deposit their kinetic energy inside a target cell, as well as in surrounding cells, potentially resulting in cell death. In the current work, the DAB4 murine monoclonal antibody (trademarked as APOMAB), which binds to necrotic tumour cells [14, 15], was used and was radiolabelled with Thorium-227 as described in [4]. Since there is a spatial correlation inside a tumour between the necrotic and the hypoxic regions [4], we hypothesised that targeting or binding of DAB4 to necrotic tumour regions would result in nearby hypoxic tumour cells receiving cross dose and hence undergoing radiation-induced death. Hypoxic tumour cells are generally resistant to low LET radiation like that of X-rays, which is typically employed in clinical radiation therapy. Furthermore, by increasing the number of dead tumour cell targets, for example, after chemotherapy, the tumour uptake of the radioimmunoconjugate would be increased, consequently increasing the tumour dose [16]. In order to confirm this hypothesis, qualitative and quantitative detection and analysis of the radioimmunoconjugate uptake and its distribution within the tumour volume are required, using suitable microdosimetric detection techniques. In this study, we used the Timepix microdosimeter to detect radiation emissions from tumour sections of mice treated with Thorium-227 APOMAB to image and quantify alpha particle emissions at a micrometre level.

2. Materials and Methods

2.1. Th-227. The radionuclide Thorium-227 is an alpha emitter produced from actinium-227 with a half-life of 18.7 days, making it, attractive for use in therapeutic applications [17, 18]. Alpha particles have a short range of only a few cell diameters in tissue (<100 μm [18]). The higher LET of alpha particles results in greater biological effectiveness compared to other radiation types such as X-rays or electrons [19]. Along with alpha particle emissions, the Th-227 decay chain also results in the release of β-particles and a low percentage of X- and gamma rays prior to reaching a stable isotope (Lead-207). The Th-227 decay chain and the mean energies of major particles produced in this decay chain are presented in Figure 2. Th-227 used in the current work was purchased through the National Isotope Development Centre, Department of Energy, USA.

2.2. Preparation of Autoradiography Sample

2.2.1. Monoclonal Antibody Production, Conjugation, and Radiolabelling with ^{227}Th. The La-specific murine monoclonal antibody DAB4 (APOMAB) [20] in conjugation buffer (0.1 M sodium bicarbonate, 0.1 M monosodium phosphate, and pH 8.5) was mixed with 50-fold molar excess of the bifunctional chelator p-SCN-Bn-DOTA (Macrocyclics, USA) and incubated at room temperature for four hours with rotation. After buffer-transfer to 0.5 M sodium acetate buffer

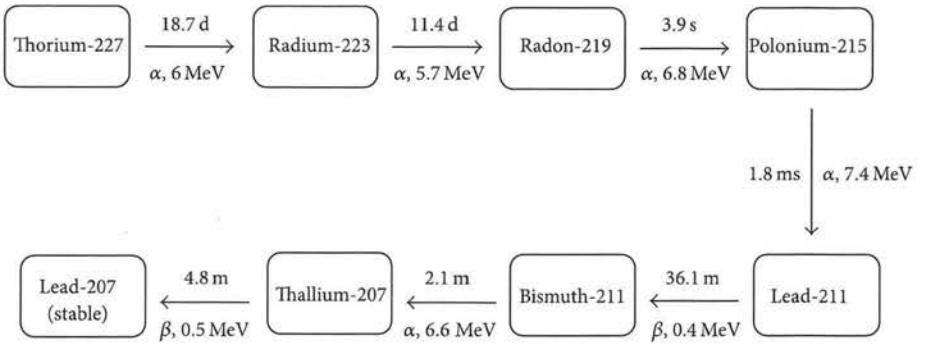

FIGURE 2: The decay chain of Th-227, half-lives, and mean energies of emitted particles.

(pH 5), the ratio of DOTA : mAb was determined as previously described [21] and was approximately 4 : 1.

^{227}Th was purified as previously described [18] immediately prior to radiolabelling. DAB4-p-SCN-DOTA was incubated overnight with purified Th-227 using an Eppendorf Thermomixer (37°C, 550 rpm constant). Samples were washed three times and buffer-transferred to phosphate-buffered saline (pH 7.4). The activity of the radioimmunoconjugate was determined using a Germanium detector and MCDWIN version 3.08 software (FAST ComTec, Germany), with the main gamma peaks of 236 and 256 keV (17.6% and 9.5% abundance, resp.) used to quantify Th-227 activity and of 269 and 154 keV peaks (13.9% and 5.7% abundance, resp.) used to quantify Radium-223. The specific activity of radioimmunoconjugates was 400 kBq/mg, with <1% Ra-223 and <1% unbound Th-227 present, as determined by instant thin-layer chromatography.

2.2.2. LL2 Tumour Model and Treatment of Tumour-Bearing Mice. All animal experiments were approved by the SA Pathology Animal Ethics Committee, Adelaide, and conducted following institutional ethical guidelines. Six- to eight-week-old female C57Bl/6 mice were injected subcutaneously in the right flank with 10^6 LL2 cells (this cell line is derived from transplantable murine Lewis lung carcinoma). Tumour size was measured using electronic callipers, and tumour volume was determined using the following calculation: tumour volume = $(a^2 \times b)/2$, where a is the shortest diameter and b is the longest diameter of the tumour. Treatment commenced when tumours reached 45–60 mm^3. To generate more necrotic tumour cells for Th-227-DAB4 binding, some mice also received chemotherapy prior to injection with Th-227-DAB4. These were treated intravenously with 50 mg/kg gemcitabine (Hospira, Australia) on days 1 and 2 and 2.5 mg/kg cisplatin (Hospira) on day 1. 18 kBq of ^{227}Th-DAB4 was administered on day 3. Mice were euthanised 2 days after administration of Th-227 labelled antibody via cervical dislocation, and tumours were collected and fixed in 10% neutral-buffered formalin. Tumours were paraffin embedded, and 5 μm sections were cut for imaging.

2.3. Timepix Radiation Detector. The Timepix radiation detector, used in the current work, was purchased from Amsterdam Scientific Instruments (ASI), the Netherlands. The device consists of a silicon chip, 1.408×1.408 cm^2 in size containing 256×256 pixels, with each pixel having an area of 55×55 μm^2 and 300 μm depth.

The chip can collect positive or negative charges [9], and the range of particle energies to be detected can be selected for a uniform performance using adjustable thresholds. The device can be operated in one of three main modes to either count single particles (Medipix mode), measure the arrival time of events/particles (Timepix mode), or measure the energy deposited in each pixel for events between the thresholds (time over threshold (TOT) mode) [10]. This offers the possibility of using the detector for a wide range of applications for photon and particle detection and energy spectrometry in addition to imaging and tomography.

The ASI Timepix detector is combined with the beam data acquisition software, SoPhy (Software for Physics), developed by the provider. The SoPhy software allows one to control Timepix acquisition modes such as selection of the operation mode, adjustment of suitable energy thresholds, cluster sizes, and other acquisition settings using multiwindows. The recorded data and frames/images can be exported to and processed using other programs such as Matlab or ImageJ.

In the current work, before any measurements and following manufacturer recommended procedure, pixel equalisation was performed to ensure a uniform response of all pixels. Subsequently, tumour sections mounted on glass microscope slides were placed 2 cm away from the detector with the front face of the detector uncovered to allow the emitted alpha particles to penetrate the Timepix silicon chip (Figure 3). A simple steel collimator with 1 cm radius and 2 cm in length was manufactured in-house and positioned around the tumour section using epoxy glue. Bias voltage of 5 V was applied to Timepix. The TOT mode was selected along with alpha particle filter. This acquisition filter allows identification of individual alpha particles detected (amongst other detected particles) as well as determination of the centre pixel in a charge cluster produced in the Timepix silicon chip by a traversing alpha particle. The total acquisition time was approximately 14 hours with 0.01 seconds per frame. Individual frames as well as the total integrated image can be evaluated. In the current work, the detected number of alpha particle hits from individual samples was evaluated and

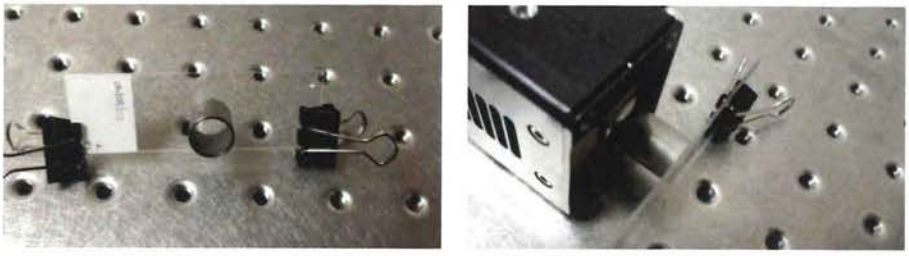

(a) (b)

FIGURE 3: Image of the experimental setup. (a) Tumour section with a 2 cm diameter collimator mounted on top of a tumour section. (b) A tumour section in front of the uncovered Timepix detector.

compared after correction for decay and normalisation for tumour section size and acquisition time.

2.4. Compartmental Analysis. The compartmental model [22] was used in the current work to calculate and compare the radioimmunoconjugate uptake in TAT-treated tumours. It is assumed that there are three main compartment volumes: the blood volume (B), tumour volume (T), and a free volume (E), where the radioactive source will escape from the blood. It is assumed that, after injection, the Th-227-DAB4 will distribute throughout all volumes. The blood and the escape volumes are open volumes where the radiolabelled immunoconjugate can escape from. The tumour volume, however, is a closed volume where the taken-up Th-227-DAB4 concentration will remain steady as shown in Figure 4.

For simplicity, it is assumed in the current work that, at time zero, the initial activity concentration of the isotope in blood, C_{B_o}, is equal to the administered activity, A_o; that is, all of the injected activity has been taken up by blood. Subsequent changes of the Th-227-DAB4 concentration in the blood volume, dC_B/dt, are due to isotope uptake by the tumour and due to excretion/depletion through escape volume. This can be expressed as [2, 22]

$$\frac{dC_B}{dt} = -k_T C_{B_o} - k_E C_{B_o},$$
$$C_B(t) = A_o e^{-(k_T+k_E)t}, \tag{1}$$

where k_T and k_E are the so-called transfer (uptake) coefficients for tumour and for the escape volumes.

Variations in Th-227-DAB4 concentration in tumour volume, dC_T/dt, are due to Th-227 uptake from the blood volume and due to its depletion through radioactive decay of Th-227. This can be then written as

$$\frac{dC_T}{dt} = k_T C_{B_o}(t) - \lambda C_T,$$
$$\frac{dC_T}{dt} = k_T A_o e^{-(k_T+k_E)t} - \lambda C_T, \tag{2}$$

where λ is the decay probability constant for Th-227.

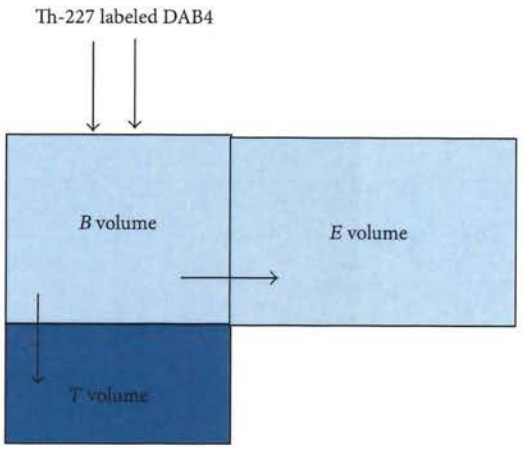

FIGURE 4: Compartmental model for the autoradiography using Th-227 labelled DAB4.

Assuming, for simplicity, that the tumour volume transfer coefficient, k_T, is much higher than escape volume transfer coefficient, k_E, the previous equation becomes

$$\frac{dC_T}{dt} = k_T A_o e^{-k_T t} - \lambda C_T,$$
$$C_T(t) = \frac{k_T}{\lambda - k_T} A_o \left(e^{-k_T t} - e^{-\lambda t}\right). \tag{3}$$

In our case, for tumour sections treated with only Th-227-DAB4, the concentration of the radioactive material at time t can be expressed as

$$C_{T,\text{nochemo}}(t) = \frac{k_{T,\text{nochemo}}}{\lambda - k_{T,\text{nochemo}}} A_o \left(e^{-k_{T,\text{nochemo}} t} - e^{-\lambda t}\right). \tag{4}$$

Similarly, for tumour sections treated with chemotherapy prior to Th-227-DAB4 administration, the concentration of Th-227 at time t can be expressed as

$$C_{T,\text{chemo}}(t) = \frac{k_{T,\text{chemo}}}{\lambda - k_{T,\text{chemo}}} A_o \left(e^{-K_{T,\text{chemo}} t} - e^{-\lambda t}\right). \tag{5}$$

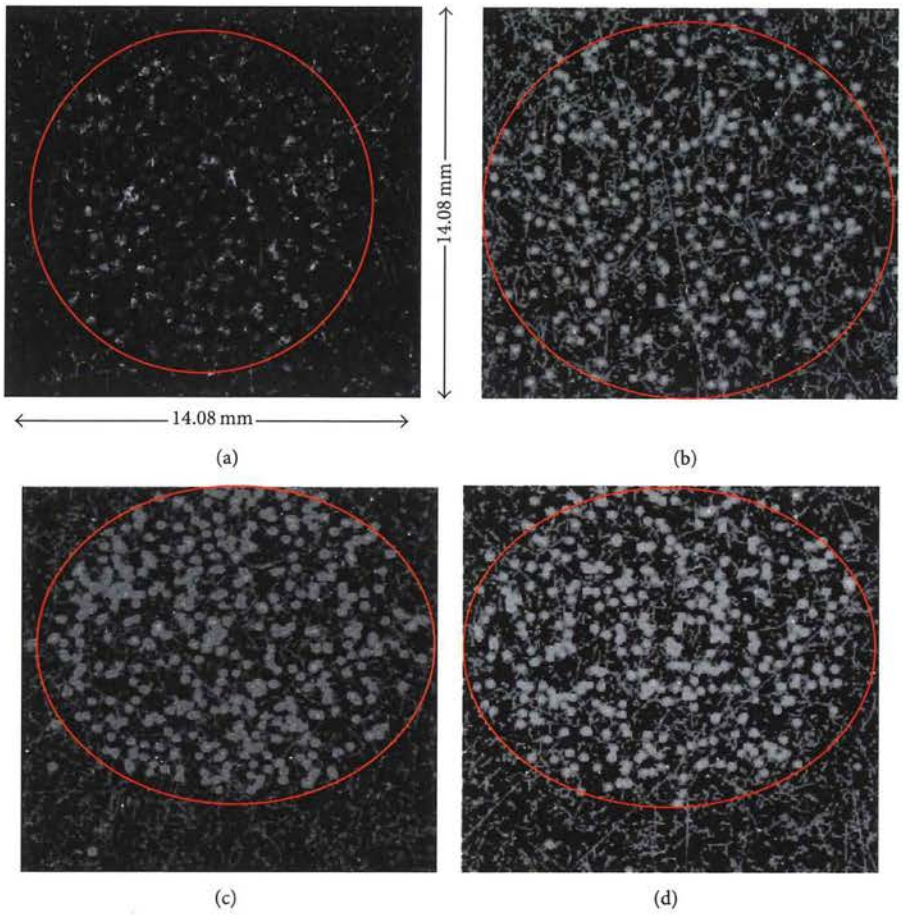

FIGURE 5: (a) and (b): images of tumour sections from mice treated with ^{227}Th-DAB4 alone. (c) and (d): images of two tumour sections from mice treated with chemotherapy followed by ^{227}Th-DAB4. The red circle indicates the approximate tumour section boundaries.

The ratio of radioisotope concentrations between the radiolabelled tumour samples with and without chemotherapy is

$$\frac{C_{T,\text{chemo}}(t)}{C_{T,\text{nochemo}}(t)} = \frac{e^{-k_{T,\text{chemo}}t} - e^{-\lambda t}}{e^{-k_{T,\text{nochemo}}t} - e^{-\lambda t}} = \frac{e^{-k_{T,\text{chemo}}t}\left(1 - e^{-(\lambda - k_{T,\text{chemo}})}\right)}{e^{-k_{T,\text{nochemo}}t}\left(1 - e^{-(\lambda - k_{T,\text{nochemo}})}\right)}. \quad (6)$$

Considering that the decay probability coefficient λ is much smaller compared to the transfer coefficient k_T, the above ratio can be reduced to

$$\frac{C_{T,\text{chemo}}(t)}{C_{T,\text{nochemo}}(t)} = \frac{e^{-k_{T,\text{chemo}}t} - 1}{e^{-k_{T,\text{nochemo}}t} - 1}. \quad (7)$$

Once the mouse has been euthanised and/or all of the initial activity has been taken up by the tumour and escape volumes (e.g., at time $t_{\max}$), the amount of radioisotope in the tumour volume, C_T, will only vary as a result of radioactive decay:

$$\frac{dC_T}{dt} = -\lambda C_T(t_{\max}). \quad (8)$$

As both tumour sample types (treated and not treated with chemotherapy) will decay with the same decay probability, the number of recorded alpha emissions will be directly proportional to the amount of radioisotope taken up by the tumour prior to a mouse being euthanatised. As a result, from the measurement point of view, the number of alpha hits detected by Timepix detector is proportional to isotope concentrations, $C_{T,\text{chemo}}$ and $C_{T,\text{nochemo}}$, during measurements. As a result, from the number of recorded alpha hits measured at different time intervals, the transfer coefficients for the two scenarios could be determined.

3. Results and Discussion

Figure 5 shows acquired integrated images of sections from four tumours: two tumours from mice treated with ^{227}Th-DAB4 alone ((a), (b)) and two tumours from mice treated with chemotherapy followed by ^{227}Th-DAB4 ((c), (d)). Even though the collimator was positioned around the tumour section, the collimator was not touching the detector, leaving a small (~2 mm) air gap. As a result, particles emitted at smaller angles, compared to a trajectory perpendicular to the

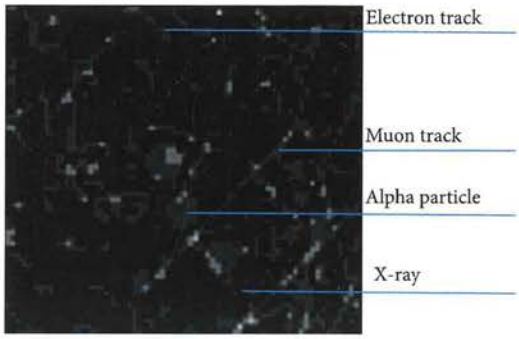

FIGURE 6: Timepix responses to electron, Muon, X-/gamma ray, and alpha particle.

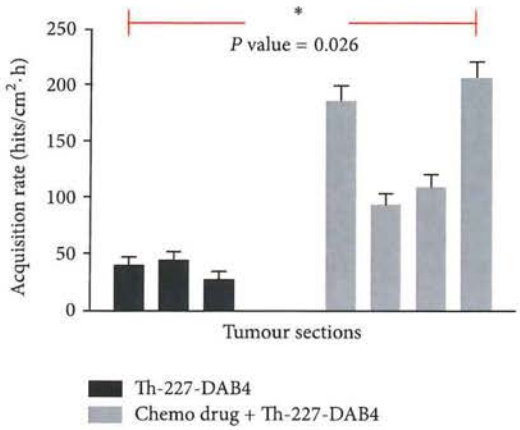

FIGURE 7: Measured alpha particle hits per unit tumour area per 1 hour for two groups of tumour sections: 4 sections with and 3 sections without application of chemotherapy prior to administration of Th-227 radioimmunoconjugate.

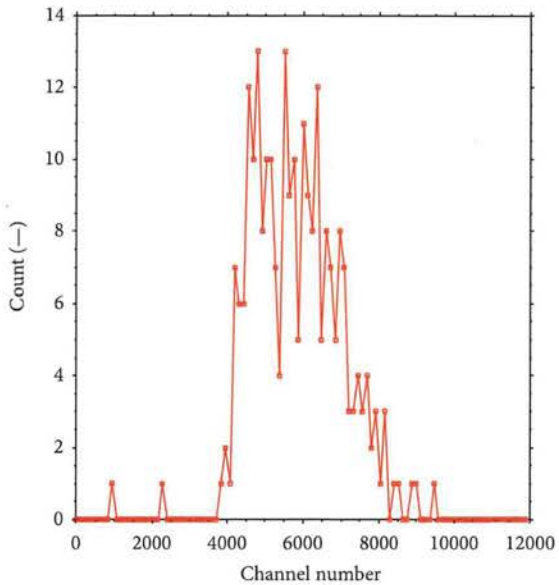

FIGURE 8: The detected alpha particle spectrum as emitted from Th-227-DAB4 from a single tumour section.

detector, can still reach the detector. These are observed as hits outside the red circle in Figure 5.

High LET alpha particles release their kinetic energy in more than one pixel as they pass in the semiconductor detector, forming a charge cluster. The small dots recorded in the image represent X- and gamma rays. An electron passage will result in a wavy and short track, and a muon track will be detected as a straight, long line (Figure 6).

An automated method using ImageJ was used to determine the number of alpha particle hits. These were also counted manually for comparison. The differences between the two methods varied between 4 and 20 hits. Using the automated method, the number of hits varied between 93 and 251, for the sections that did not receive chemotherapy, and between 445 and 582, for the sections that were treated with chemotherapy before administering Th-227-DAB4.

As shown in Figure 7, the recorded alpha particle hits for each sample were corrected for radioactive decay (based on the time elapsed between the Th-227 administration and Timepix measurement), the area of each sample, and total acquisition time, resulting in the alpha particle acquisition rate between 27.6 and 44.8 hits/cm^2·hour for tumour sections of mice not previously given chemotherapy and between 94.0 and 206.8 hits/cm^2·hour for sections that were treated with chemotherapy followed by ^{227}Th-DAB4.

Corrected alpha particle acquisition rates were statistically analysed using one-way ANOVA for their significance, using GraphPad Prism software, yielding P value of 0.026 (<0.05, two-tailed), confirming that the observed differences between the two sample groups are significant.

Energy spectra of alpha particles detected from decay of Th-227 and its daughters were also acquired and an example is presented in Figure 8 where the lowest and the highest energies can be determined. The energy varies between 4 and 7.4 MeV, corresponding to the expected energy range of alpha particles produced by Th-227 decay chain.

Using the compartmental analysis, corresponding transfer coefficients for the two samples can be determined when repeating the measurements for at least one sample type at different times. The data can be plotted using (4) or (5) and the transfer coefficient can be estimated. The ratio in detected alpha particles between the two sample types was found to be approximately 4. If one of the transfer coefficients is known from repeated measurements, the second one can be determined from (7).

4. Conclusion

Tumour sections were imaged in the current work to characterise the pattern of uptake and distribution of Th-227-DAB4. High resolution autoradiographs of radiolabelled tumour sections were acquired, showing alpha particles, β particles, electrons, and X-ray tracks. The Timepix measurements also showed an increased uptake of Th-227–DAB4 following chemotherapy due to an increase in necrotic tissue volume.

The experiment showed that the Timepix detector can be used effectively for autoradiography in TAT to provide high-resolution images. Development of a fine collimator can improve the definition of the tumour boundaries and identify the geometrical origin of detected alpha particles within the sample. It was also shown that, in principle, the data acquired by Timepix can be used for compartmental analysis to quantify the uptake of radioimmunoconjugate in targeted alpha therapy.

Conflict of Interests

The authors declare that there is no conflict of interests regarding the publication of this paper.

References

[1] P. Mayles, A. Nahum, and J. C. Rosenwald, *Handbook of Radiotherapy Physics: Theory and Practice*, Taylor & Francis, New York, NY, USA, 2007.

[2] L. Marcu, E. Bezak, and B. J. Allen, *Biomedical Physics in Radiotherapy for Cancer*, CSIRO, Collingwood, Australia, 2012.

[3] C.-Y. Huang, S. Guatelli, B. M. Oborn, and B. J. Allen, "Microdosimetry for targeted alpha therapy of cancer," *Computational and Mathematical Methods in Medicine*, vol. 2012, Article ID 153212, 6 pages, 2012.

[4] A. H. Staudacher, E. Bezak, A. Borysenko, and M. P. Brown, "Targeted α-therapy using 227Th-APOMAB and cross-fire antitumour effects: preliminary in-vivo evaluation," *Nuclear Medicine Communications*, vol. 35, no. 12, pp. 1284–1290, 2014.

[5] V. Kraus, M. Holik, J. Jakubek, M. Kroupa, P. Soukup, and Z. Vykydal, "FITPix—fast interface for Timepix pixel detectors," *Journal of Instrumentation*, vol. 6, no. 1, Article ID C01079, 2011.

[6] T. Bäck and L. Jacobsson, "The α-camera: a quantitative digital autoradiography technique using a charge-coupled device for ex vivo high-resolution bioimaging of α-particles," *The Journal of Nuclear Medicine*, vol. 51, no. 10, pp. 1616–1623, 2010.

[7] N. Chouin, S. Lindegren, S. H. L. Frost et al., "Ex vivo activity quantification in micrometastases at the cellular scale using the α-camera technique," *Journal of Nuclear Medicine*, vol. 54, no. 8, pp. 1347–1353, 2013.

[8] T. K. Rügheimer, U. Gebert, T. Michel, G. Anton, J. Séguinot, and C. Joram, "Experimental demonstration of a hybrid photon detector concept based on the Timepix detector," *Nuclear Instruments and Methods in Physics Research, Section A: Accelerators, Spectrometers, Detectors and Associated Equipment*, vol. 595, no. 2, pp. 353–358, 2008.

[9] CERN, Medipix, 2011, http://medipix.web.cern.ch/medipix/.

[10] X. Llopart, R. Ballabriga, M. Campbell, L. Tlustos, and W. Wong, "Timepix, a 65k programmable pixel readout chip for arrival time, energy and/or photon counting measurements," *Nuclear Instruments and Methods in Physics Research Section A: Accelerators, Spectrometers, Detectors and Associated Equipment*, vol. 581, no. 1-2, pp. 485–494, 2007.

[11] M. Campbell, V. Havranek, E. Heijne et al., "Charge collection from proton and alpha particle tracks in silicon pixel detector devices," in *Proceedings of the IEEE Nuclear Science Symposium Conference Record (NSS '07)*, vol. 2, pp. 1047–1050, Honolulu, Hawaii, USA, October-November 2007.

[12] M. Esposito, J. Jakubek, G. Mettivier, S. Pospisil, P. Russo, and J. Solc, "Energy sensitive Timepix silicon detector for electron imaging," *Nuclear Instruments and Methods in Physics Research Section A: Accelerators, Spectrometers, Detectors and Associated Equipment*, vol. 652, no. 1, pp. 458–461, 2011.

[13] M. Esposito, G. Mettivier, and P. Russo, "^{14}C autoradiography with an energy-sensitive silicon pixel detector," *Physics in Medicine and Biology*, vol. 56, no. 7, pp. 1947–1965, 2011.

[14] F. Al-Ejeh, J. M. Darby, C. Tsopelas, D. Smyth, J. Manavis, and M. P. Brown, "APOMAB, a La-specific monoclonal antibody, detects the apoptotic tumor response to life-prolonging and DNA-damaging chemotherapy," *PLoS ONE*, vol. 4, no. 2, Article ID e4558, 2009.

[15] F. Al-Ejeh, J. M. Darby, and M. P. Brown, "Chemotherapy synergizes with radioimmunotherapy targeting La autoantigen in tumors," *PLoS ONE*, vol. 4, no. 2, Article ID e4630, 2009.

[16] A. H. Staudacher, F. Al-Ejeh, C. K. Fraser et al., "The La antigen is over-expressed in lung cancer and is a selective dead cancer cell target for radioimmunotherapy using the la-specific antibody APOMAB," *EJNMMI Research*, vol. 4, no. 1, pp. 1–13, 2014.

[17] IAEA, "Alpha emitting radionuclides and radiopharmaceuticals for therapy," Tech. Rep. TM-44815, IAEA, Wien, Austria, 2013.

[18] R. H. Larsen, J. Borrebaek, J. Dahle et al., "Preparation of TH227-labeled radioimmunoconjugates, assessment of serum stability and antigen binding ability," *Cancer Biotherapy and Radiopharmaceuticals*, vol. 22, no. 3, pp. 431–437, 2007.

[19] *Advancing Nuclear Medicine Through Innovation*, National Academies Press, Washington, DC, USA, 2007.

[20] F. Al-Ejeh, J. M. Darby, and M. P. Brown, "The La autoantigen is a malignancy-associated cell death target that is induced by DNA-damaging drugs," *Clinical Cancer Research*, vol. 13, no. 18, part 2, pp. 5509s–5518s, 2007.

[21] F. Al-Ejeh, J. M. Darby, B. Thierry, and M. P. Brown, "A simplified suite of methods to evaluate chelator conjugation of antibodies: effects on hydrodynamic radius and biodistribution," *Nuclear Medicine and Biology*, vol. 36, no. 4, pp. 395–402, 2009.

[22] S. Cherry, J. Sorenson, and M. Phelps, *Physics in Nuclear Medicine*, Elsevier Health Sciences, London, UK, 2012.

6.3 Investigation of Cr-51 Uptake by A549 Cells using Timepix

6.3.1 Chromium (Cr-51)

Chromium-51 with a half-life of 27.7 days decays by electron capture (Figure 6.1) to reach the stable state of Vanadium-51 (Lederer, Hollander et al. 1967). The main radiation emissions are 0.320 MeV γ-rays (9.9%), 0.005 MeV X-rays (22%) and Auger Electrons (energies between 10 eV and 0.004 MeV; 68%) (Kassis, Sastry et al. 1985). Since Cr-51 can penetrate into cells and bind to cellular proteins, it has been used in cell biology for precise and accurate quantification of tumour response to chemotherapy and immunotherapy (i.e. to assess cytotoxicity of a treatment) (Pearson, Hodes et al. 1969; Kassis, Sastry et al. 1985; Micheau, Solary et al. 1997; Santin, Hermonat et al. 2000; Yang and Haluska 2004; Fehniger, Cai et al. 2007). The amount of radioactivity in the supernatant (i.e. the liquid lying above the cells) indicates the cytotoxicity of therapy, as Cr-51 will only be released as a result of cell lysis following the treatment (Biomedicals 2016). This is usually monitored using a gamma counter such as Geiger–Muller (GM) counter and well-type scintillation counter (Pearson, Hodes et al. 1969; Karimi, Lee et al. 2014).

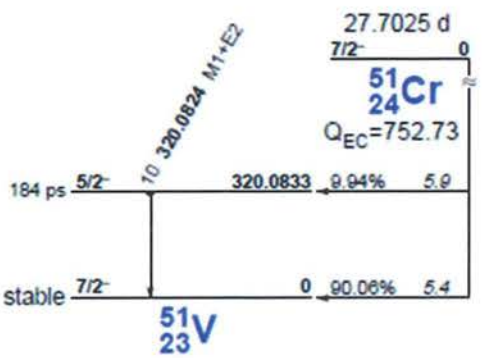

Figure 6.1. Cr-51 decay scheme, courtesy of (Lederer, Hollander et al. 1967).

In this experiment, uptake of Cr-51 (purchased through PerkinElmer, Inc., USA) by A549 cells was investigated. The effects of different factors such as the number of seeded cells and changes in pH level of the medium on the uptake were evaluated using the Timepix detector.

6.3.2 Preparation of Autoradiography Sample of A549 Cells with Cr-51

For the *in vitro* radiolabelling, 5 x 10^5 of A549 cells were seeded in a 96-well plate (Corning, USA) (the diameter is 6.4 mm). Cells were labelled with 1.1 Bq/cell liquid ^{51}Cr (sodium chromate) which was added to 100 µl media. Cells were incubated at 37° C for an hour to allow Cr-51 uptake. The cells were then washed three times with PBS to remove any unincorporated Cr-51 and a varying number of labelled cells (10^5, 2 x 10^5, 4 x 10^5, 6 x 10^5, 8 x 10^5, 10^6 cells) was spotted onto a microscopic slide and dried. The slides were placed in front the Timepix detector and the emitted photons were counted (see details below) to evaluate the relationship between the cell number and Cr-51 uptake.

As Cr-51 uptake is affected by the pH level, the second part of this study investigated the effects of changes in the pH level on Cr-51 uptake. The pH of media used for Cr-51 labelling is 7.5. Hydrochloric acid was added to the media to create a more acidic solution (pH 6.5) and sodium hydroxide was added to the media to create a more neutral solution (pH 8.4). In triplicate, 500,000 cells in 100 µl of media at pH of 6.5, 7.5 or 8.4 were incubated with 1.1 MBq Cr-51. After washing, cells were spotted onto glass slides, dried and photon emissions were detected using Timepix.

6.3.3 Timepix Preparation

In order to investigate the uptake of Cr-51 by A549 cells, the slide containing the radiolabelled A549 cells was placed directly in front of Timepix (covered face) to monitor photons emitted from the slide. TOT mode was chosen in SoPhy software along with a photon filter (i.e. the acquisition filter type) to detect photons emitted from the samples. Bias voltage of 5 V was applied to Timepix. Acquisition time was approximately 2 hours with 0.1 s for each frame. The resultant image was analysed using Matlab to identify the total number of recorded counts which is proportional to the Cr-51 uptake.

6.3.4 Results

Figure 6.2 shows two images for 1000 and 1000,000 Cr-51 labelled cells, respectively. The photon counts are higher for 1000,000 cells which means a higher uptake of Cr-51 as expected for a larger number of cells. The images also show uniform uptakes of Cr-51 by cells in all samples with different cells number for a uniform spread of cells across the slide.

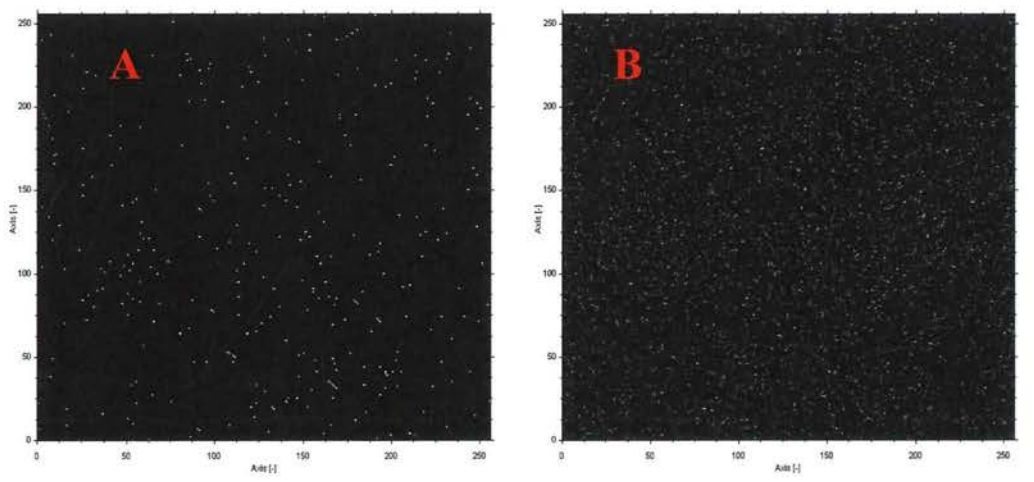

Figure 6.2. A and B: Cr-51 uptake of 1000 and 1000,000 A459 cells, respectively.

For A549 cell numbers between 100,000 and 1,000,000, the photons counts as a function of the cell number with pH of 7.5 is presented in Figure 6.3 (Acquired counts per frame corrected for the activity and normalized to 100,0000 cells). The figure shows a linear relationship between the number of cells and Cr-51 uptake confirming that Timepix response is linear and has a good sensitivity to detect differences in the uptake.

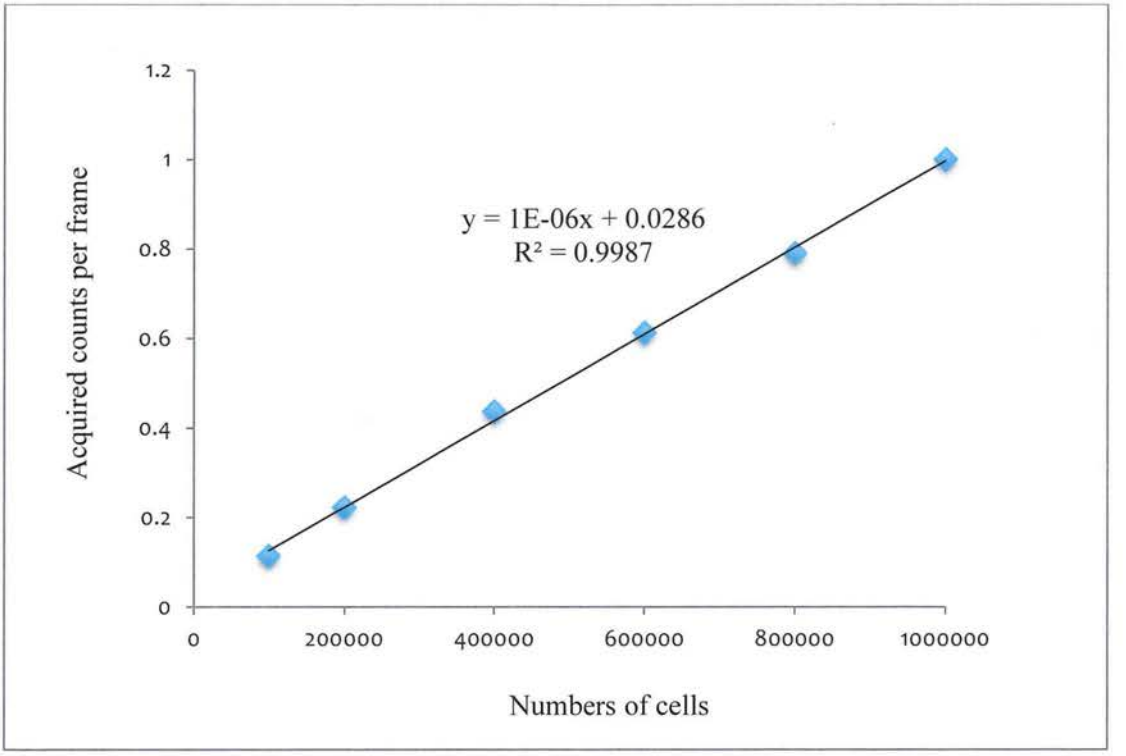

Figure 6.3. Cr-51 photon counts per frame as a function of the cell number where the count is corrected for the activity and normalized to 1,000,000 cells. The error bars per frame (calculated for 256 * 256 pixels) were ~ 2%.

Changing the pH of the medium can affect the total uptake of Cr-51. Three levels of pH: 6.5, 7.5 and 8.4 were used and the acquired images show a uniform uptake of Cr-51 but also show differences in the photon counts for these three pH levels (Figure 6.4).

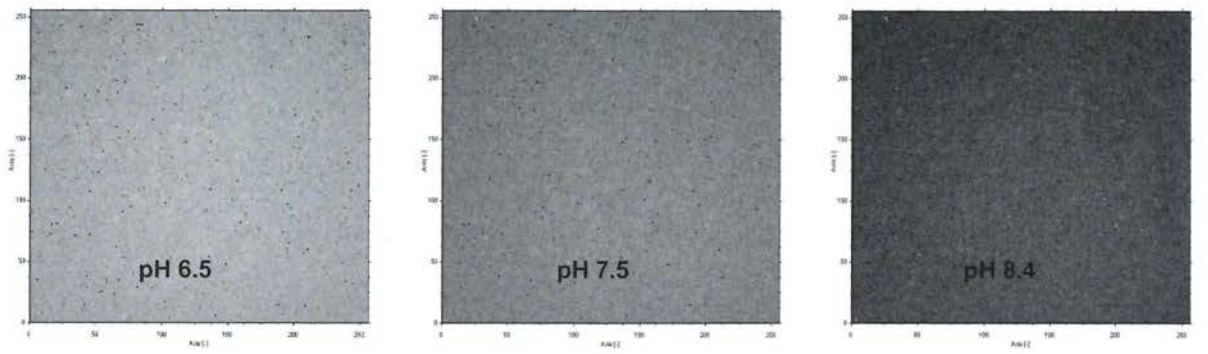

Figure 6.4. Photon emission from Cr-51 labelled A549 cells seeded in media with different pH levels.

The relationship between the number of counts and the pH level is presented in Figure 6.5. pH of 6.5 resulted in the highest uptake of Cr-51, followed by 7.5 and 8.4 with the slope of (-0.26).

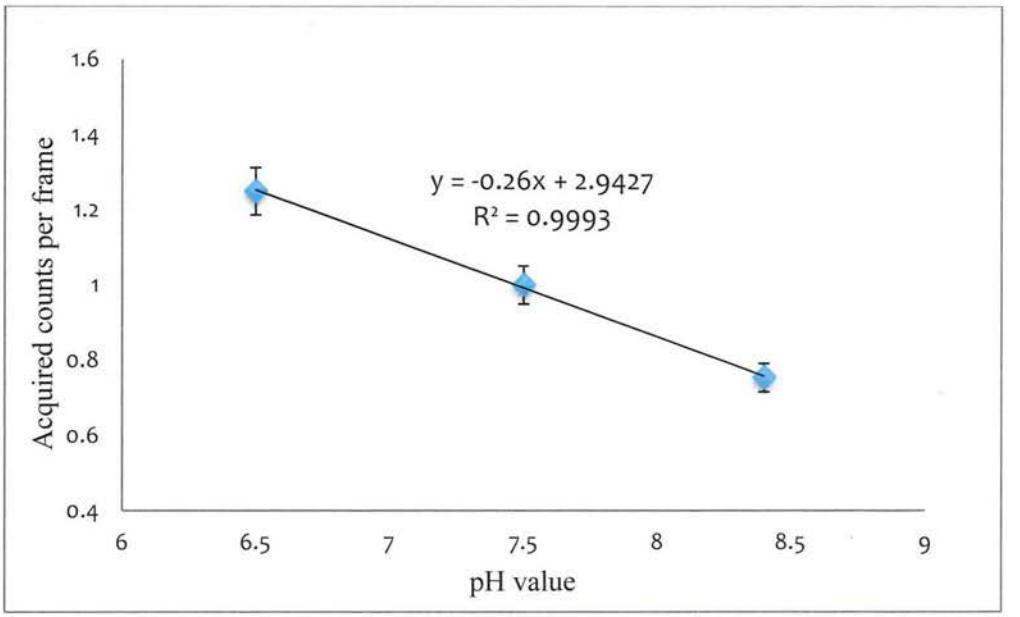

Figure 6.5. Relationship between the photon counts and the media pH level. The acquired counts are corrected for the activity and normalized to the media pH level of 7.5. The error bars per frame (calculated for 256 * 256 pixels) were ~ 0.023.

6.4 Conclusion

The investigations showed that Timepix radiation detector is a good device to quantitatively and assess cellular labelling by Th-227 and Cr-51 and is suitable for use in autoradiography and for estimation of uptake of Cr-51 by cells. This means that Timepix is a suitable detector to estimate radioisotope uptake. The results showed good linearity between the number of labelled cells and the photons detected by Timepix.

The acquired images (autoradiography using both Th-227 and labelling using Cr-51) were of high resolution and showed differences in the uptake when changing measurement conditions (such as using chemotherapy prior to Th-227 for autoradiography and changing the number of cells or pH level of the media in labelling with Cr-51), demonstrating thus Timepix sensitivity to detect changes in the experimental parameters.

Timepix provides an easy monitoring tool of the uptake and gives 2D images that can be used not only to quantify the uptake but also to examine the uniformity of the uptake across the sample.

Chapter 7

Transmitted Alpha Particle Microdosimetry Design for TAT

This chapter is based on the submitted manuscript number 5:

Ruqaya AL Darwish, Alex Hugo Staudacher, Yanrui Li, Michael Paul Brown and Eva Bezak, Development of a Transmission Alpha Particle Microdosimetry Technique using A549 cells and a Ra-223 source for Targeted Alpha Therapy.

7.1 Motivation

Microdosimetry of alpha particles for targeted alpha therapy is believed to be complex due to a number of factors such as alpha particle energy and range in tissue. This chapter describes a design for transmitted alpha particle microdosimetry for TAT using A549 cells and a Ra-223 source.

Prior to microdosimetry experiment, radiation sensitivity of A549 cell line was determined using clonogenic assay.

7.2 Clonogenic Assay

The human lung carcinoma A549 cell line was cultured in RPMI-1640 (Sigma-Aldrich, St. Louis, MO, USA) medium with 5% foetal bovine serum (Bovogen Biologicals, Keilor East, Victoria, Australia).

Clonogenic assay is an in vitro tool to study the radiation effects by studying the ability of a cell to grow into a colony of at least 50 cells (Munshi, Hobbs et al. 2005; Franken, Rodermond et al. 2006).

For clonogenic assay study, A549 cells were seeded at 1.5×10^6 cells/flask in 25 cm^2 tissue culture flasks (T-75 flask (Corning, USA)). To irradiate cells, the flasks were placed in a wax mould to generate full scatter conditions and then irradiated at room temperature using a Varian 21EX Linear Accelerator (Varian, Palo Alto, CA, USA) at the Radiation Oncology Department, Royal Adelaide Hospital, South Australia, using a 6 MV photon beam, 20×20 cm^2 field size, with the clinical nominal dose rate of 3 Gy/min at 100 cm from the beam focal spot. The flasks were positioned at the depth of maximum dose (i.e. on top of 1.5 cm solid water) and were irradiated from below (i.e. gantry at 180°) so as to not irradiate through the air gap in the flask. Cells were irradiated with 2, 4, 6, 8 and 10 Gy radiation doses. An unirradiated (sham) flask with cells was used as a control. Accelerator radiation output, calibrated using IAEA TRS 398 protocol (Agency 2000) was checked with Daily QA 3™ device (Sun Nuclear, USA) prior to irradiation.

After irradiation, the cells were collected, counted, diluted to the desired seeding concentration; 250, 500, 500, 750, 1000, 2000 cells (for each irradiation dose 0, 2, 4, 6, 8 and 10, respectively) and replated (in triplicate) in 6 well plates. Dishes were placed in an incubator until cells in the control dishes (unirradiated dishes) grow adequate number of colonies taking 12 - 14 days. Cells were then washed with phosphate-buffered saline (PBS), fixed and stained using crystal violet solution (6.0% glutaraldehyde, 0.5% crystal violet, PBS) for 30 minutes, followed by washing with water. Colonies were then counted manually and the plating efficiency of the control (from sham) and surviving fraction were determined using equations (7.1) and (7.2), respectively (Munshi, Hobbs et al. 2005; Franken, Rodermond et al. 2006).

$$\text{Plating Efficiency (PE)} = \frac{\text{number of colonies fromed}}{\text{number of cell seeded}} \times 100\% \qquad (7.1)$$

$$\text{Surviving Fraction} = \frac{\text{number of colonies fromed after treatment}}{\text{number of cell seeded} \times \text{PE}} \qquad (7.2)$$

An example of colonies formed for sham-unirradiated (control) cells and for cells irradiated with 4 Gy photon dose is shown in Figure 7.1.

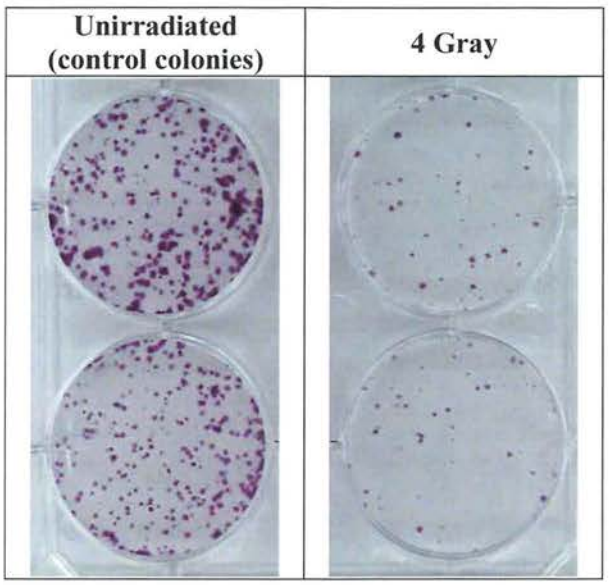

Figure 7.1. A549 cell colonies from unirradiated (control colonies) and 4 Gy irradiated cells.

7.3 Statement of Contribution

7.3.1 Conception

The first concept of investigation of targeted alpha therapy dosimetry was suggested by Eva Bezak. The use of Timepix for this application was suggested by Ruqaya Al Darwish. The use of A549 cells is suggested by Alex Staudacher. The final design of the transmission alpha particle microdosimetry has evolved through a number of development stages that have been tested by Ruqaya Al Darwish, Alex Staudacher and Eva Bezak.

7.3.2 Realisation

The experimental works were done by Ruqaya Al Darwish with the help of Alex Staudacher and Yanrui Li in practical biological parts. Data collection and the analysis was performed by Ruqaya AL Darwish.

7.3.3 Documentation

This paper was primarily written by Ruqaya Al Darwish. Editing was conducted by Eva Bezak and Alex Staudacher. Michael Brown provided advice on biological content.

Statement of Authorship

Title of Paper	Development of a Transmission Alpha Particle Dosimetry Technique using A549 cells and a Ra-223 source for Targeted Alpha Therapy
Publication Status	■ Published ☑ Accepted for Publication ☐ Submitted for Publication ☐ Unpublished and Unsubmitted work written in manuscript style
Publication Details	Ruqaya AL Darwish, Alex Hugo Staudacher, Yanrui Li, Michael Paul Brown and Eva Bezak, Development of a Transmission Alpha Particle Microdosimetry Technique using A549 cells and a Ra-223 source for Targeted Alpha Therapy.

Principal Author

Name of Principal Author (Candidate)	Ruqaya AL Darwish
Contribution to the Paper	Suggested Timepix radiation detector for this application and contributed to the final design of the transmission alpha particle microdosimetry. Performed majority of experimental works and data collection and the analysis. This paper was primarily written by Ruqaya Al Darwish who also acted as a corresponding author.
Overall percentage (%)	80%
Certification:	This paper reports on original research I conducted during the period of my Higher Degree by Research candidature and is not subject to any obligations or contractual agreements with a third party that would constrain its inclusion in this thesis. I am the primary author of this paper.
Signature	Date 30/8/16

Co-Author Contributions

By signing the Statement of Authorship, each author certifies that:

i. the candidate's stated contribution to the publication is accurate (as detailed above);

ii. permission is granted for the candidate in include the publication in the thesis; and

iii. the sum of all co-author contributions is equal to 100% less the candidate's stated contribution.

Name of Co-Author	Alex Hugo Staudacher
Contribution to the Paper	The use of A549 cells was suggested by Alex Staudacher. He assisted to improve the final design of the transmission alpha particle microdosimetry system and with biological practical works. He also assissted with editing this manuscript.
Signature	Date 30/8/16

Name of Co-Author	Yanrui Li		
Contribution to the Paper	Assissted with MTT assay measurements.		
Signature		Date	30/8/2016

Name of Co-Author	Michael Paul Brown		
Contribution to the Paper	Michael Paul Brown provided advice on biological content of the manuscript.		
Signature		Date	

Name of Co-Author	Eva Bezak		
Contribution to the Paper	The first concept of investigation of targeted alpha therapy dosimetry was suggested by Eva Bezak who also contributed to the final design of the system. All irradiation was done under Eva Bezak's supervision. She also assessed with manuscript editing.		
Signature		Date	30/8/2016.

Name of Co-Author	Yanrui Li		
Contribution to the Paper	Assissted with MTT assay measurements.		
Signature		Date	

Name of Co-Author	Michael Paul Brown		
Contribution to the Paper	Michael Paul Brown provided advice on biological content of the manuscript.		
Signature		Date	30-AUG-2016

Name of Co-Author	Eva Bezak		
Contribution to the Paper	The first concept of investigation of targeted alpha therapy dosimetry was suggested by Eva Bezak who also contributed to the final design of the system. All irradiation was done under Eva Bezak's supervision. She also assessed with manuscript editing.		
Signature		Date	

Development of a transmission alpha particle dosimetry technique using A549 cells and a Ra-223 source for targeted alpha therapy

R. AL Darwish
Department of Medical Physics, Royal Adelaide Hospital, Adelaide 5000, Australia and School of Physical Sciences, University of Adelaide, Adelaide 5005, Australia

A. H. Staudacher
Translational Oncology Laboratory, Centre for Cancer Biology, SA Pathology and University of South Australia, Adelaide 5001, Australia and School of Medicine, University of Adelaide, Adelaide 5005, Australia

Y. Li
International Centre for Allied Health Evidence, Sansom Institute, University of South Australia, Adelaide 5001, Australia and Sansom Institute for Health Research, University of South Australia, Adelaide 5001, Australia

M. P. Brown
Translational Oncology Laboratory, Centre for Cancer Biology, SA Pathology and University of South Australia, Adelaide 5001, Australia; School of Medicine, University of Adelaide, Adelaide 5005, Australia; and Cancer Clinical Trials Unit, Royal Adelaide Hospital, Adelaide 5000, Australia

E. Bezak[a)]
School of Physical Sciences, University of Adelaide, Adelaide 5005, Australia; International Centre for Allied Health Evidence, Sansom Institute, University of South Australia, Adelaide 5001, Australia; and Sansom Institute for Health Research, University of South Australia, Adelaide 5001, Australia

(Received 10 May 2016; revised 16 August 2016; accepted for publication 6 October 2016; published 27 October 2016)

Purpose: In targeted radionuclide therapy, regional tumors are targeted with radionuclides delivering therapeutic radiation doses. Targeted alpha therapy (TAT) is of particular interest due to its ability to deliver alpha particles of high linear energy transfer within the confines of the tumor. However, there is a lack of data related to alpha particle distribution in TAT. These data are required to more accurately estimate the absorbed dose on a cellular level. As a result, there is a need for a dosimeter that can estimate, or better yet determine the absorbed dose deposited by alpha particles in cells. In this study, as an initial step, the authors present a transmission dosimetry design for alpha particles using A549 lung carcinoma cells, an external alpha particle emitting source (radium 223; Ra-223) and a Timepix pixelated semiconductor detector.

Methods: The dose delivery to the A549 lung carcinoma cell line from a Ra-223 source, considered to be an attractive radionuclide for alpha therapy, was investigated in the current work. A549 cells were either unirradiated (control) or irradiated for 1/2, 1, 2, or 3 h with alpha particles emitted from a Ra-223 source positioned below a monolayer of A549 cells. The Timepix detector was used to determine the number of transmitted alpha particles passing through the A549 cells and DNA double strand breaks (DSBs) in the form of γ-H2AX foci were examined by fluorescence microscopy. The number of transmitted alpha particles was correlated with the observed DNA DSBs and the delivered radiation dose was estimated. Additionally, the dose deposited was calculated using Monte Carlo code SRIM.

Results: Approximately 20% of alpha particles were transmitted and detected by Timepix. The frequency and number of γ-H2AX foci increased significantly following alpha particle irradiation as compared to unirradiated controls. The equivalent dose delivered to A549 cells was estimated to be approximately 0.66, 1.32, 2.53, and 3.96 Gy after 1/2, 1, 2, and 3 h irradiation, respectively, considering a relative biological effectiveness of alpha particles of 5.5.

Conclusions: The study confirmed that the Timepix detector can be used for transmission alpha particle dosimetry. If cross-calibrated using biological dosimetry, this method will give a good indication of the biological effects of alpha particles without the need for repeated biological dosimetry which is costly, time consuming, and not readily available. © *2016 American Association of Physicists in Medicine.* [http://dx.doi.org/10.1118/1.4965805]

Key words: targeted alpha therapy, Timepix, dosimetry, A549 cells, γ-H2AX

1. INTRODUCTION

Alpha particles, compared to x-rays and electrons, are considered to have 100–1000 times higher linear energy transfer (LET) and have a much shorter range (50–100 μm in tissue).[1,2] High LET radiation is much more damaging biologically compared to low LET radiation, resulting in higher relative biological effectiveness (RBE) of alpha particles relative to x-rays for the same absorbed dose. The RBE of alpha particles is generally considered to be between 10 and 20 for radiation protection purposes,[3–5] compared to 1 for x-rays. This is, however, likely to vary depending on the cell type, radiation dose, and biological endpoint; for example, the RBE for targeted therapies with alpha particles has been reported to be between 2 and 10.[1,6–9]

Evidence from a number of preclinical and clinical studies suggests that alpha particle emitting radionuclides can be used in cancer radiation therapy as they cause multiple irreparable DNA double-strand breaks, resulting in cell death.[1,2,10] In targeted alpha therapy (TAT), tumor cells are targeted with alpha particle emitting radionuclides, and only several alpha particle traversals are required to kill a tumor cell compared to several hundred or thousands required for low LET electrons or x-rays.[8,11] The short path length of emitted alpha particles means that the radiation dose is confined to a small volume, potentially limiting off-target effects, and the absence of oxygen-dependence for tumor cytotoxicity with high LET radiation means that the treatment will not encounter tumor radioresistance associated with hypoxia as observed with conventional radiotherapy.[1,2,12–14] For alpha particles to deliver dose to a tumor, an alpha emitting radionuclide is chelated to a specific carrier molecule (typically a protein or antibody) that specifically targets the tumor cells, resulting in the tumor being traversed by alpha particles and receiving a radiation dose.[13] Although the use of TAT is gradually advancing, to our knowledge there are currently only two methods to detect alpha emissions and to determine biodistribution: the α-camera (which is an autoradiography system using scintillating technique and optical registration by a charge-coupled device)[15–17] and iQID camera (which combines a scintillator and an image intensifier).[17,18] However, limited measurements, using these techniques for cellular uptake, have been applied to dosimetry to date. As a result, there is an ongoing need for real-time dosimetry of alpha particles to determine the radiation dose delivered to the tumor from TAT.[2] Radionuclide dosimetry is difficult and complex to accurately determine due to a number of factors including the physical properties of the radionuclide including radiation type and half-life, and biological transit time (uptake and clearance). Additionally on a cellular level, the dose can be quite heterogeneous depending on the spatial distribution of the radioisotope in the tumor.[19]

The Timepix radiation detector[20] has the ability to identify individual radiation particles including photons (x-rays or gamma rays), electrons, and alpha particles.[21–26] Our previous study confirmed that Timepix could be used to detect and quantify spatial distribution of alpha particles, electrons, and x-rays resulting from thorium-227 (Th-227) decay in tumor sections from mice treated with a Th-227-labeled antibody.[26] These features along with the ability of Timepix to measure deposited energy suggest that Timepix could be used to estimate absorbed dose in targeted alpha therapy.

In this paper, as an initial step, we present a transmission dosimetry design for alpha particles using A549 lung carcinoma cells, an external Ra-223 source, and a Timepix detector. Using this setup, several issues mentioned above related to the radioisotope kinetics and uneven distribution can be avoided and the practicality of Timepix for alpha particle dosimetry can be evaluated.

In this work, the number of transmitted alpha particles, detected by Timepix for several irradiation times, was correlated with the observed DNA DSBs, in the form of γ-H2AX foci, which is typically used for biological dosimetry.

2. MATERIALS AND METHODS

2.A. Timepix

Timepix is a semiconductor radiation detector developed by the European Organization for Nuclear Research (CERN). Taking advantage of the complementary metal-oxide-semiconductor (CMOS) technology, the detector consists of a semiconductor layer, divided into an array of pixels, which is bump-bonded to an integrated electronics layer (Fig. 1). Timepix used in the current work was purchased from Amsterdam Scientific Instruments, Netherlands and consists of a silicon detector with 256×256 pixels (approximately 1.41 cm^2), with a 55×55 μm^2 pixel size, making it suitable for dosimetry measurements. Each pixel is connected to its own charge-sensitive preamplifier, a discriminator, and a counter.[20,27] This sophisticated microdosimeter can be used in different research fields such as space physics, nuclear physics, radiotherapy physics, imaging, and radiation protection.

In our system, a fine brass collimator (50 μm thick) was positioned in front of Timepix with <50 μm diameter holes drilled with a laser system as shown in Fig. 2. The collimator was manufactured by OptoFab (Macquarie University, NSW) and is required essentially for autoradiography purposes. As the collimator was carefully aligned with Timepix, it is fixed in place permanently (3 mm away from the sensitive detector layer). A correction factor for collimator alpha particle absorption was measured previously in order to use this detector assembly for dosimetry purposes as well.

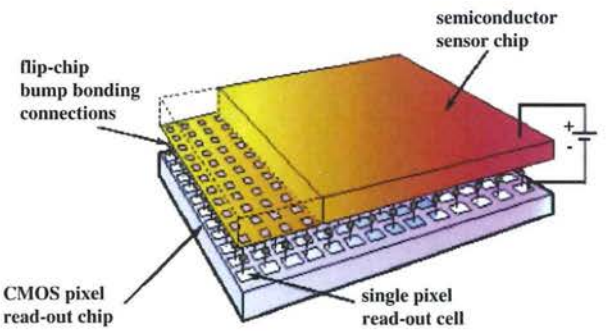

FIG. 1. Timepix structure, courtesy of (Ref. 28).

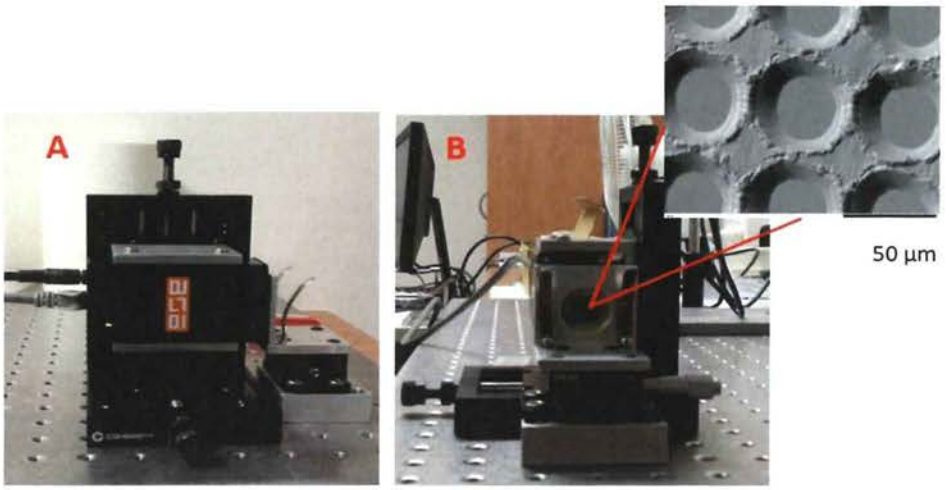

FIG. 2. Side (A) and front (B) view of Timepix with the brass collimator. The top right image shows the laser-drilled microcollimator structure details.

2.B. Ra-223

Ra-223 is an alpha emitter produced from actinium-227 decay

$$^{227}\mathrm{Ac}(T_{1/2}=21.7y) \rightarrow \beta^- + {}^{227}\mathrm{Th}(T_{1/2}=18.7d) \rightarrow \alpha + {}^{223}\mathrm{Ra}(T_{1/2}=11.43d). \quad (1)$$

Ra-223 has a half-life of 11.43 days, and its decay chain results in the emission of additional alpha particles, beta particles, and γ-rays until reaching a stable isotope of lead-207.[29,30] The mean energies of alpha particles produced in this decay chain are presented in Fig. 3. Ra-223 used in the current work was a product of thorium-227 decay, which was purchased through the National Isotope Development Centre, Department of Energy (USA).

Ra-223 is an attractive isotope to deliver high LET radiation to a tumor because it has a suitable half-life, and delivers multiple alpha particles from the first three nuclides in the decay chain which are emitted almost instantaneously, and contribute to the radiation dose.[29,30] Indeed, Ra-223 is being used to effectively treat castration-resistant prostate cancer patients with bone metastases.[31]

2.C. A549 cell line

The human lung carcinoma A549 cells have a diameter of approximately 12.5 μm. A549 was cultured in RPMI-1640 (Sigma-Aldrich, USA) with 5% foetal bovine serum (Bovogen Biologicals, Australia). The relative biological effectiveness of alpha particles for this cell line has been estimated to be 5.5 for 10% survival using clonogenic assays, nuclei staining, and gene expression.[7]

2.C.1. Irradiation and cell survival assay

Initially, to evaluate the radiation sensitivity of the cell line, the cell survival after irradiation with x-rays and alpha particles was obtained in the current work using the MTT assay.[33–35] For photon irradiation, A549 cells in 75 cm^2 flasks were placed in a wax mould to generate full scatter conditions and then irradiated at room temperature using a Varian 21EX Linear Accelerator (Varian, Palo Alto, CA, USA) at the Radiation Oncology Department, Royal Adelaide Hospital, South Australia, using a 6 MV photon beam, 20×20 cm^2 field size, with the clinical nominal dose rate of 3 Gy/min at 100 cm from the beam focal spot. The flasks were positioned at the depth of maximum dose (i.e., on top of 1.5 cm solid water) and were irradiated from below (i.e., gantry at 180°) so as to not irradiate through the air gap in the flask. Cells were irradiated with 2, 4, 6, 8, and 10 Gy radiation doses. An unirradiated (sham) flask with cells was used as a control. Accelerator radiation output, calibrated using IAEA TRS 398 protocol,[36] was checked with Daily QA 3™ device (Sun Nuclear, USA) prior to radiation treatments.

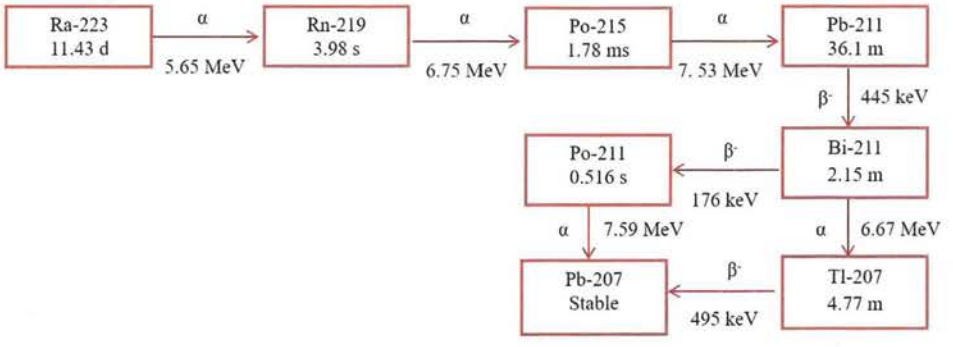

FIG. 3. ^{223}Ra decay scheme (Refs. 2, 8, 30, and 32).

For testing cell viability after irradiation with alpha particles, approximately 3×10^4 cells were seeded in a single well of 96-well transwell in 30 μl of media. The cells were then irradiated from above with an evaporated Ra-223 source (18.2 kBq) for times varying between 5 and 60 min. An unirradiated well with cells was used as a control.

After irradiation, the cells were collected, seeded at 10^4 cells/well in a 96-well plate and kept at 37 °C with 5% CO_2. Three days later, the media were removed, and replaced with fresh media containing 0.4 mg/ml thiazolyl blue tetrazolium bromide (Sigma-Aldrich) and incubated for 2 h. The supernatant was removed and the resulting purple crystals dissolved in isopropanol. The absorbance was read at 570 nm using a FLUOstar Omega microplate reader (BMG Labtech, Germany). The absorbance is directly proportional to the number of viable cells,[34] and the absorbance value was normalized to percentage of viable cells remaining.

2.D. Experimental setup for transmission alpha particle dosimetry

In transmission alpha dosimetry, alpha particles that have passed through a layer of interest, cells for example, are measured. However, due to the short range of alpha particles (50–100 μm in tissue), they can be absorbed by the source itself, the cells, the cell medium, and/or the support material on which the cells grow, making the transmission dosimetry quite challenging. The approaches used in the current study were aimed at minimising the noncellular sources of absorption to ensure that some alpha particles traversed the measuring setup and reached the Timepix detector.

The HTS Transwell® 96 well system (Corning, USA), consisting of two compartments, was used to develop a method for tracking alpha particles through a cell monolayer. This system comprises of two compartments (Fig. 4), with liquid Ra-223 evaporated in the lower compartment [the activity was measured with a germanium detector (GR2519; Canberra Industries, Meriden, CT, USA)], to avoid alpha particle selfabsorption inside the liquid. The measured activity of 5 kBq was uniformly distributed, as confirmed by the Timepix detector. The second compartment consists of a flat bottom polycarbonate membrane (10 μm thick) where cells are plated. The membrane surface area is 0.143 cm^2 and contains pores of 3 μm diameter. The distance between the first and the inserted compartment was 1 mm. It is sufficiently thin to allow alpha particles to penetrate through and hit the cells. Fifteen thousand A549 cells were seeded in the upper compartment and allowed to adhere overnight before exposure to alpha particles. The following day, the medium was removed and only a minimal amount of fresh medium was added to the cells to minimize absorption of alpha particles in the medium. The upper transwell compartment was then inserted into the lower compartment containing the evaporated Ra-223. The transwell system was positioned under the Timepix detector, with the plastic cover removed and the brass collimator in place. Transmitted alpha particles were detected for 1/2, 1, 2, or 3 h irradiation times. These times were used as the experiments were limited by the time that the cells could be left at ambient temperature and CO_2 levels. Three transwell systems were sham irradiated and used as controls.

Timepix was operated using Software for Physics (SoPhy) software, developed by the device manufacturer. Reading was done in time-over-threshold (TOT) mode which allows Timepix to measure the energy deposited in each pixel for the events between the set thresholds. An alpha particle filter was applied to detect and accept alpha particles only if the detected signals met the acquisition requirements for shape (round cluster) and size (7×7 pixels or more).[37] Reading using this setup was done without cells (i.e., the upper compartment) first to measure the entrance activity and then with the cell

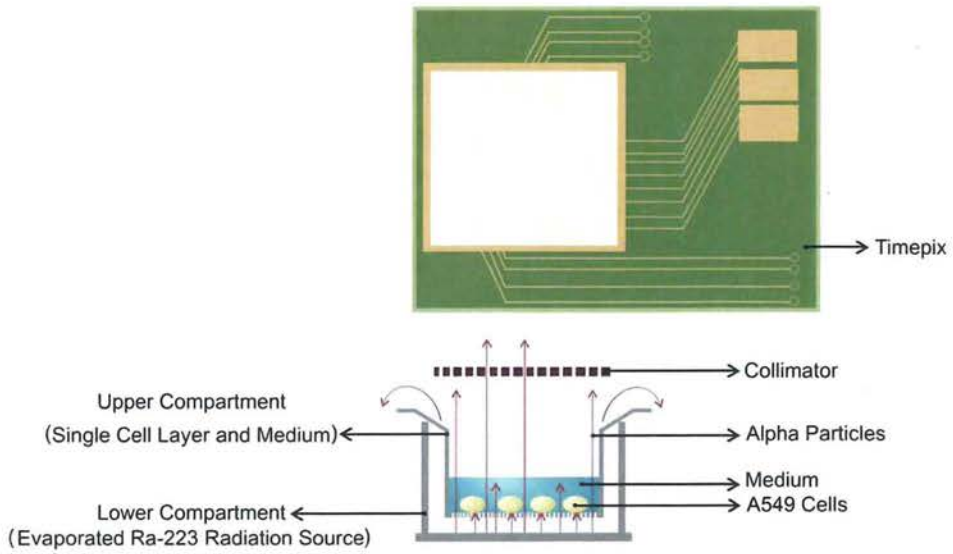

FIG. 4. Schematic diagram of the experimental setup showing the transwell system with two compartments: the lower compartment with the evaporated Ra-223 source and the upper compartment with seeded cells (cell diameter: 12.5 μm) and a thin layer of medium (approximately 45 μm height). Transmitted alpha particles are detected by Timepix.

compartment in place to measure the exit/transmitted activity. The frame acquisition time of 0.1 s was selected during the total acquisition times of 1/2, 1, 2, and 3 h.

Due to the brass collimator, a correction factor for alpha particle absorption in the collimator was added to the collected data. The collimator correction factor, CF, had been determined previously, using a Ra-223 source and defined as the ratio of the total number of hits (i.e., detected alpha particles) with, $N_c(t)$, and without, $N_0(t)$, the collimator in place for the same irradiation time,

$$\mathrm{CF} = \frac{N_C(t)}{N_0(t)}.$$

The collimator correction factor, for the Ra-223 source, was determined to be 0.96. To correct for the collimator absorption, the detected hits were multiplied by $1/\mathrm{CF} = 1.04$.

2.E. Dose assessment

Theoretically, considering the mean energy of Ra-223 and its daughters to be 6.735 MeV, the energy absorbed, E_{ab}, in the cell layer and the medium can be crudely estimated for 1/2, 1, 2, and 3 h irradiation times using the following equation:

$$E_{ab}(\mathrm{MeV}) = (A_{en} - A_{ex})\bar{E}t, \quad (2)$$

where A_{en} is the measured entrance activity (Bq) of the Ra-223 source and A_{ex} is the measured exit activity (Bq). $\bar{E}$ is the mean energy (MeV) of all alpha particles emitted in the decay chain and t is the exposure time. As the mass of the cell and media layers, m, can be calculated from the known volume and density, the absorbed dose, D_{ab}, can be calculated as well as

$$D_{ab}(\mathrm{Gy}) = \frac{E_{ab}}{m}. \quad (3)$$

Additionally, simulation of alpha particle energy loss while penetrating the cells and the media was also performed using Monte Carlo code SRIM (Stopping and Range of Ions in Matter), version 2008.[38–40] SRIM can simulate a semi-infinite target (i.e., an infinite layer of a given thickness) made of compound materials and up to eight layers.[38] In the simulation, a thickness of 57.3 μm for the cell and media layers (considered as water with density of 1 g/cm^3) and a 1 mm air gap (0.001 25 g/cm^3 density) was included between the source of alpha particles (10^6 particles) with energy of 6.735 MeV (i.e., only a monoenergetic point source was considered). The air gap represents the distance between the lower and upper compartments of the transwell system. Five runs of one million alpha particles were performed. The simulation setup with transmitted alpha particles is shown in Fig. 5.

Absorbed dose to cells and media, and cells alone can be estimated using Eq. (3) and from SRIM simulations. When the RBE value for alpha particles is applied, the equivalent dose to A549 cells can be estimated and correlated with biological damage as described above.

2.F. Biological dosimetry with γ-H2AX assay

To verify the design and to correlate the number of particles absorbed in the cell layer (based on the number of transmitted alpha particles), a biological dosimetry[41,42] (γ-H2AX) was also used. γ-H2AX is a biomarker for DNA DSBs as any DNA DSB is followed by the phosphorylation of the histone H2AX at the break site.[43,44]

For γ-H2AX staining, the transwell membrane was cut from the transwell using a scalpel, and cells were fixed with 10% neutral-buffered formalin for 10 min at room temperature. After washing with PBS, cells were blocked and permeabilized using 5% bovine serum albumin (BSA)/0.2% Triton-X in PBS for 30 min at room temperature. Cells were washed three times with PBS and incubated overnight at 4 °C with 1 μg/ml mouse antihuman anti-phospho-histone H2AX (ser139) (clone JBW301, Millipore). Cells were washed again three times in

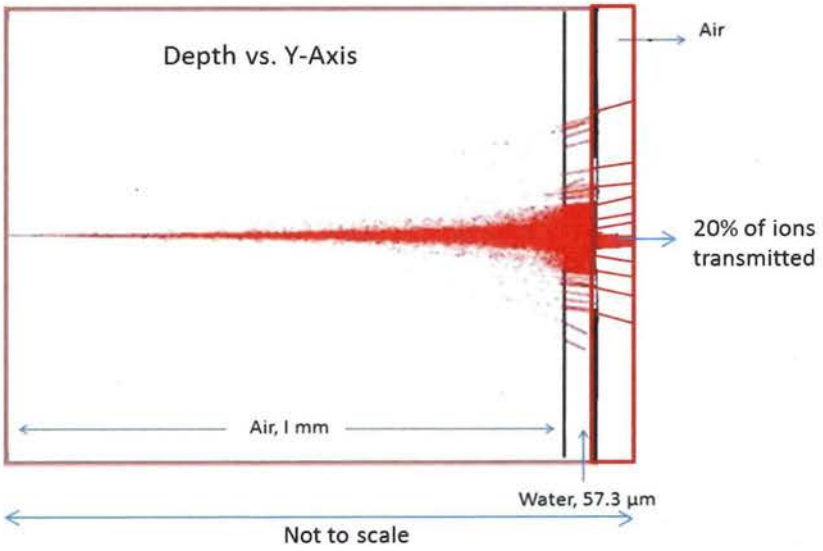

FIG. 5. SRIM simulation of transmitted alpha particles with 1 mm air gap between the source and cells and media (represented as water with a mass of 0.816 mg). Mass was calculated using the irradiated volume dimensions of 0.816 mm^3).

PBS and incubated with 4 μg/ml goat anti-mouse Alexa488 for 1 h at 37 °C. After washing with PBS, cell nuclei were counterstained with 1 μg/ml DAPI, cover-slipped, and examined using an Olympus IX71 microscope with CellSens Standard software (version 1.6; Olympus, USA). After irradiation and cell staining, ten randomly selected microscope images per well (at 40× magnification) were taken. Two images were taken for each field: one of DAPI stained cells (blue) and one of the γ-H2AX foci (green). The two images were combined in ImageJ (version 1.48V)[45] and the number of cells as well as the number of γ-H2AX foci per cell were counted manually. Cells that had seven or more foci were assigned to one group.

3. RESULTS AND DISCUSSION

3.A. MTT assay result

From the absorbance value, which is proportional to the number of cells with metabolic activity, the relationship between the dose and the percentage of viable A549 cells following irradiation with 6 MV photons and Ra-223 alpha particles was determined (Fig. 6). Previously published studies have shown similar relative cell viability trends after cellular irradiation to gamma rays and alpha particles.[35] The data show that the percentage of viable cells is lower for the same dose of alpha particle irradiation as compared to the x-ray irradiation.

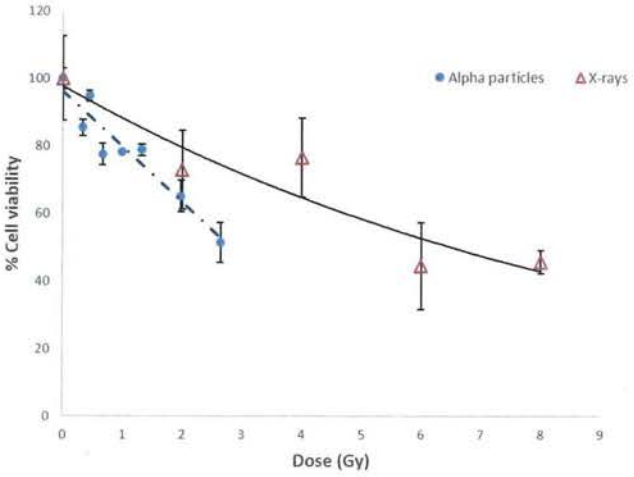

FIG. 6. The percentage of viable A549 cells following irradiation with 6 MV photons and Ra-223 alpha particles, using an MTT assay. The relative errors were calculated from standard deviations of the mean obtained from triplicate samples.

3.B. Timepix results

About 80% of alpha particles emitted from Ra-223 decay were stopped in the cell and medium layer. The particles transmitted through (~20%) hit the pixelated silicon surface of Timepix and deposited energy (i.e., caused production of charge) in an area larger than the size of one pixel; i.e., more than one pixel was involved in the energy deposition. This is known as charge sharing effect.[25] The resulting image of a single alpha particle hit is a charge cluster covering around 7×7 pixels. The total number of transmitted alpha particles acquired with Timepix during irradiation of A549 cells with Ra-223 for 1 and 3 h is shown in Fig. 7(a). The corresponding particle energy spectrum (in channel numbers) is shown in

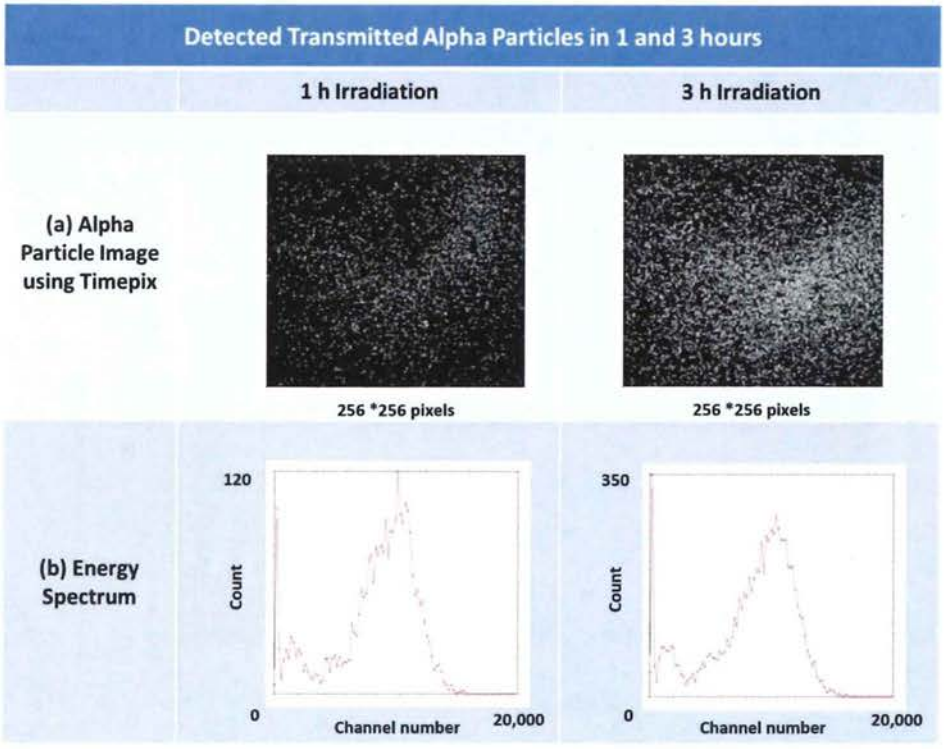

FIG. 7. (a) The total number of transmitted alpha particles acquired with Timepix during irradiation of A549 cells with Ra-223 for 1 and 3 h, (b) the energy spectrum of these particles.

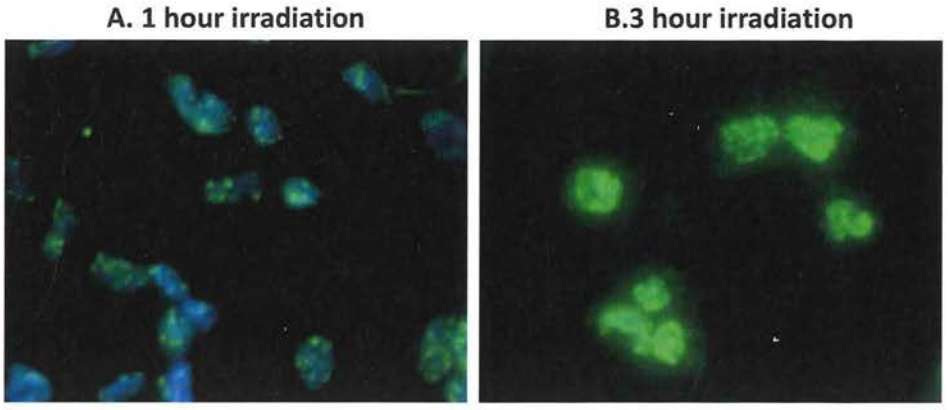

FIG. 8. Microscopic/fluorescence image of part of cell samples after 1 h (A) and 3 h (B) irradiation. γ-H2AX foci appearing as green dots (40× magnification).

Fig. 7(b). The total number of alpha particles hitting the detector ranged from 1433, 3077, 4903, and 8520 (corresponding to 1/2, 1, 2, and 3 h irradiation times). The readings were then corrected for absorption in the collimator, using a 1/CF value of 1.04.

3.C. γ-H2AX assay results

Figure 8 shows an example of observed γ-H2AX foci following irradiation, confirming the presence of DNA damage. The distribution of foci numbers observed in irradiated cells compared to control cells is shown in Fig. 9. For example, the 1 h untreated control cells had only a small number of cells with DSB breaks (i.e., 90% of these cells had no foci present). The 3 h untreated control cells have more DSBs present compared to 1 h control, and is most likely due to the extended period of time that the untreated cells were outside the incubator at room temperature without CO_2-buffering. Nevertheless, the cells irradiated for 3 h contained significantly more cells with DSBs than the corresponding control, with almost all cells having six or more γ-H2AX foci (p-value of 0.019 for 1/2 h irradiation, 0.009 for 1 h irradiation, 0.049 for 2 h irradiation and p-value of 0.0008 for 3 h irradiation compared to their respective controls). Comparisons were done using unpaired t-test in GraphPad Prism 6 software (GraphPad Software, Inc., CA, USA).

3.D. Dose assessment and SRIM calculation

Based on the SRIM simulation, the energy deposited in the cell layer only and in the cell and media layer was ~812 000 and ~5 960 000 MeV, respectively (for 10^6 particles). The corresponding absorbed doses for 1/2, 1, 2, and 3 h irradiation times were determined using both the SRIM results as well as Eq. (3) and are shown in Table I.

The standard errors for the simulations were ~5% and were determined from the multiple simulation runs. The standard error in dose using the detected activity was ~10%. There is a good agreement between the simulation and the calculation using the measured activities.

The equivalent dose to the A549 cells resulting from alpha particle irradiation is a combination of the estimated absorbed

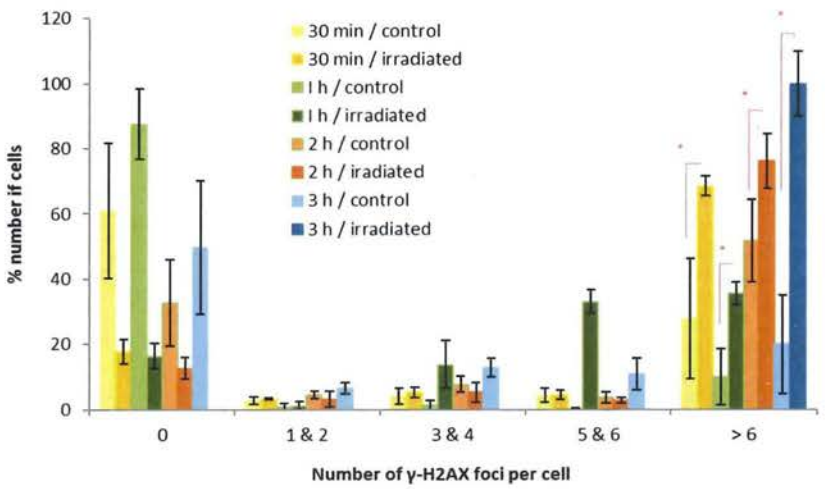

FIG. 9. The number of observed γ-H2AX foci per 100 cells after 1/2, 1, 2, and 3 h irradiation times compared to γ-H2AX foci in control cells (the asterisks indicate a significant difference with p-value of 0.019 for 1/2 h irradiation, 0.009 for 1 h irradiation, 0.049 for 2 h irradiation and p-value of 0.0008 for 3 h irradiation compared to their respective controls).

TABLE I. Estimated absorbed dose, D_{ab} to the cell layer only and to the cell and media layer using SRIM simulation and Eq. (3).

	Analytical calculation Eq. (3)	SRIM calculation	
Irradiation time (h)	D_{ab} cells and media (Gy)	D_{ab} cells and media (Gy)	D_{ab} cell layer (Gy)
1/2	1.00 ± 0.10	0.89 ± 0.09	0.12 ± 0.01
1	1.96 ± 0.20	1.73 ± 0.09	0.24 ± 0.012
2	3.85 ± 0.39	3.41 ± 0.34	0.46 ± 0.05
3	5.98 ± 0.60	5.29 ± 0.26	0.72 ± 0.035

(physical) dose and the radiation weighting factor which reflects the RBE of alpha particles. Depending on the RBE, the effective doses delivered to the cell layer were estimated to be 0.66, 1.32, 2.53, and 3.96 Gy after 1/2, 1, 2, and 3 h irradiation, respectively using an RBE of 5.5.

3.E. Cell damage and alpha particle absorbed dose

The relationship between the percentage of cells containing γ-H2AX foci due to alpha particle irradiation and environmental conditions (expressed as the percentage of cells containing one or more γ-H2AX foci) and the absorbed dose is shown in Fig. 10, using SRIM calculations of absorbed dose.

Two microscopic images of a small part of the membranes with the seeded cells after 1 and 3 h irradiation times are shown in Fig. 8. Cells with multiple γ-H2AX foci are more dominant after 3 h irradiation. Additionally, the foci are larger and more intense following the 3 h irradiation compared to 1 h irradiation and both control samples. Figure 11 presents the pan-nuclear stained cells for irradiated samples compared to their controls for the same time.

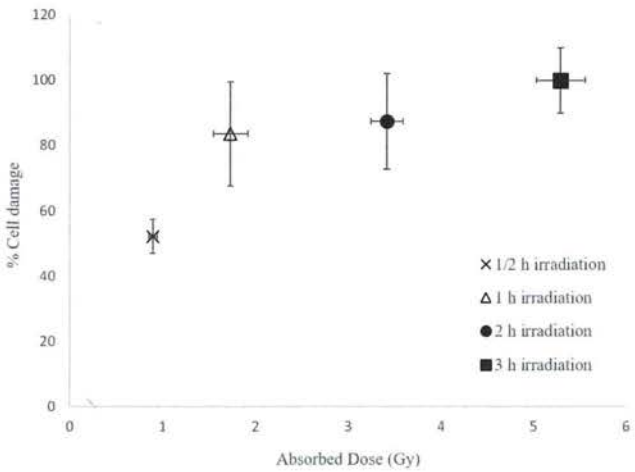

FIG. 10. Relationship between the absorbed dose to the cell layer and the media and the % of cell damage ascertained from biological dosimetry (induced by radiation and the environmental factors) after 1/2, 1, 2, and 3 h irradiation times.

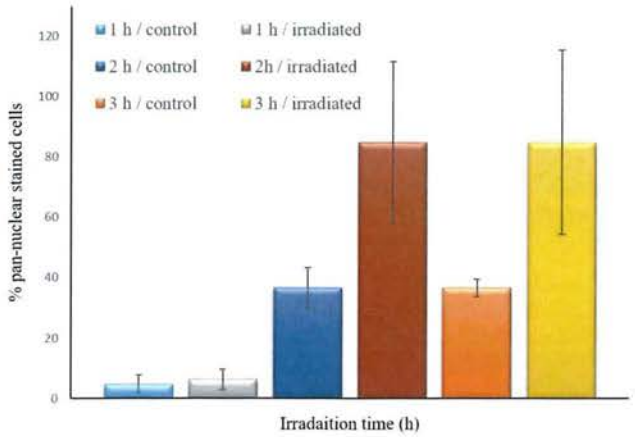

FIG. 11. Percentage pan-nuclear stained cells for different irradiation times with their corresponding controls "unirradiated" for the same time.

4. CONCLUSION

The Timepix detector can be used for transmission alpha particle dosimetry. If cross-calibrated using biological dosimetry, this method will give a good indication of the biological effects without the need for repeated biological dosimetry that is costly, time consuming, and not readily available. However, we expect that different cell lines will have different radiation responses resulting in differences in the number and intensity of γ-H2AX foci; thus having some estimate of these differences, as we have provided here, is essential. In future studies, we will extend this concept to measuring alpha particles emitted from radio-labeled tumor sections using Timepix as a real time targeted alpha therapy dosimeter.

CONFLICT OF INTEREST DISCLOSURE

The authors have no COI to report.

[a]Author to whom correspondence should be addressed. Electronic mail: Eva.Bezak@unisa.edu.au

[1]G. Sgouros, "Alpha-particles for targeted therapy," Adv. Drug Delivery Rev. **60**, 1402–1406 (2008).
[2]Y.-S. Kim and M. W. Brechbiel, "An overview of targeted alpha therapy," Tumor Biol. **33**, 573–590 (2012).
[3]A. B. Cognetta and W. M. Mendenhall, *Radiation Therapy for Skin Cancer* (Springer, Dordrecht, 2013).
[4]ICRP, "The 2007 recommendations of the international commission on radiological protection," in *Annals of the ICRP*, edited by J. Valentin (Elsevier, New York, NY, 2007), Vol. 37, p. 1.
[5]J. Elgqvist, S. Frost, J.-P. Pouget, and P. Albertsson, "The potential and hurdles of targeted alpha therapy—Clinical trials and beyond," Front. Oncol. **3**, 1–9 (2014).
[6]P. Thomas, B. Tracy, T. Ping, A. Baweja, M. Wickstrom, N. Sidhu, and L. Hiebert, "Relative biological effectiveness (RBE) of alpha radiation in cultured porcine aortic endothelial cells," Int. J. Radiat. Biol. **83**, 171–179 (2007).
[7]H. Riquier, A.-C. Wera, A.-C. Heuskin, O. Feron, S. Lucas, and C. Michiels, "Comparison of X-ray and alpha particle effects on a human cancer and endothelial cells: Survival curves and gene expression profiles," Radiother. Oncol. **106**, 397–403 (2013).
[8]G. Sgouros, J. C. Roeske, M. R. McDevitt, S. Palm, B. J. Allen, D. R. Fisher, A. B. Brill, H. Song, R. W. Howell, G. Akabani, A. B. B. In collaboration

with the SNM MIRD Committee, W. E. Bolch, D. R. Fisher, R. W. Howell, R. F. Meredith, G. Sgouros, B. W. Wessels, and P. B. Zanzonico, "Mird pamphlet no. 22 (Abridged): Radiobiology and dosimetry of α-particle emitters for targeted radionuclide therapy," J. Nucl. Med. **51**, 311–328 (2010).

[9]J. Dahle, N. Abbas, O. S. Bruland, and R. H. Larsen, "Toxicity and relative biological effectiveness of alpha emitting radioimmunoconjugates," Curr. Radiopharmaceuticals **4**, 321–328 (2011).

[10]D. A. Mulford, D. A. Scheinberg, and J. G. Jurcic, "The promise of targeted α-particle therapy," J. Nucl. Med. **46**, 199S–204S (2005); available at http://jnm.snmjournals.org/content/46/1_suppl/199S.abstract.

[11]A. I. Kassis, C. R. Harris, S. J. Adelstein, T. J. Ruth, R. Lambrecht, and A. P. Wolf, "The *in vitro* radiobiology of astatine-211 decay," Radiat. Res. **105**, 27–36 (1986).

[12]L. Marcu, E. Bezak, and B. J. Allen, *Biomedical Physics in Radiotherapy for Cancer* (CSIRO Publishing Australia, Collingwood, Victoria, 2012).

[13]Committee on State of the Science of Nuclear Medicine; Nuclear and Radiation Studies Board; Board on Health Sciences Policy; Division on Earth and Life Studies; Institute of Medicine; National Research Council, *Advancing Nuclear Medicine Through Innovation* (National Academies, Washington, DC, 2007).

[14]A. H. Staudacher, E. Bezak, A. Borysenko, and M. P. Brown, "Targeted α-therapy using 227Th-APOMAB and cross-fire antitumour effects: Preliminary *in-vivo* evaluation," Nucl. Med. Commun. **35**, 1284–1290 (2014).

[15]T. Bäck and L. Jacobsson, "The α-camera: A quantitative digital autoradiography technique using a charge-coupled device for *ex vivo* high-resolution bioimaging of α-particles," J. Nucl. Med. **51**, 1616–1623 (2010).

[16]N. Chouin, S. Lindegren, S. H. L. Frost, H. Jensen, P. Albertsson, R. Hultborn, S. Palm, L. Jacobsson, and T. Bäck, "*Ex vivo* activity quantification in micrometastases at the cellular scale using the α-camera technique," J. Nucl. Med. **54**, 1347–1353 (2013); available at http://jnm.snmjournals.org/content/early/2013/06/12/jnumed.112.113001.full.pdf+html.

[17]S. H. L. Frost, B. W. Miller, T. A. Bäck, E. B. Santos, D. K. Hamlin, S. E. Knoblaugh, S. L. Frayo, A. L. Kenoyer, R. Storb, O. W. Press, D. S. Wilbur, J. M. Pagel, and B. M. Sandmaier, "α-imaging confirmed efficient targeting of CD45-positive cells after 211At-radioimmunotherapy for hematopoietic cell transplantation," J. Nucl. Med. **56**, 1766–1773 (2015).

[18]B. W. Miller, S. J. Gregory, E. S. Fuller, H. H. Barrett, H. B. Barber, and L. R. Furenlid, "The iQID camera: An ionizing-radiation quantum imaging detector," Nucl. Instrum. Methods Phys. Res., Sect. A **767**, 146–152 (2014).

[19]D. Brady, J. M. O'Sullivan, and K. M. Prise, "What is the role of the bystander response in radionuclide therapies?," Front. Oncol. **3**, 215 (2013).

[20]CERN, Medipix, Vol. 2011, 2011.

[21]T. Michel, M. Bohnel, J. Durst, P. Sievers, and G. Anton, "Low energy dosimetry with photon counting pixel detectors such as Medipix," IEEE Trans. Nucl. Sci. **56**, 417–423 (2009).

[22]M. Campbell, V. Havranek, E. Heijne, T. Holy, J. Idarraga, J. Jakubek, C. Lebel, C. Leroy, X. Llopart, J. Novotny, S. Pospisil, L. Tlustos, and Z. Vykydal, *Presented at the Nuclear Science Symposium Conference Record, NSS '07* (IEEE, New York, NY, 2007).

[23]J. Jakubek, M. Platkevic, P. Schmidt-Wellenburg, P. Geltenbort, C. Plonka-Spehr, and M. Daum, "Position-sensitive spectroscopy of ultra-cold neutrons with Timepix pixel detector," Nucl. Instrum. Methods Phys. Res., Sect. A **607**, 45–47 (2009).

[24]J. Žemlička, J. Jakůbek, M. Kroupa, and V. Tichý, "Energy- and position-sensitive pixel detector Timepix for X-ray fluorescence imaging," Nucl. Instrum. Methods Phys. Res., Sect. A **607**, 202–204 (2009).

[25]J. Jakubek, "Energy-sensitive X-ray radiography and charge sharing effect in pixelated detector," Nucl. Instrum. Methods Phys. Res., Sect. A **607**, 192–195 (2009).

[26]R. AL Darwish, A. H. Staudacher, E. Bezak, and M. P. Brown, "Autoradiography imaging in targeted alpha therapy with Timepix detector," Comput. Math. Methods Med. **2015**, 1–7; available at https://www.hindawi.com/journals/cmmm/2015/612580/.

[27]T. K. Rügheimer, U. Gebert, T. Michel, G. Anton, J. Séguinot, and C. Joram, "Experimental demonstration of a hybrid photon detector concept based on the Timepix detector," Nucl. Instrum. Methods Phys. Res., Sect. A **595**, 353–358 (2008).

[28]G. Anton, U. Gebert, T. Michel, and T. K. Rügheimer, "A hybrid photodetector using the Timepix semiconductor assembly for photoelectron detection," Nucl. Instrum. Methods Phys. Res., Sect. A **602**, 205–208 (2009).

[29]S. Nilsson, R. H. Larsen, S. D. Fosså, L. Balteskard, K. W. Borch, J.-E. Westlin, G. Salberg, and Ø. S. Bruland, "First clinical experience with α-emitting Radium-223 in the treatment of skeletal metastases," Clin. Cancer Res. **11**, 4451–4459 (2005).

[30]Ø. S. Bruland, S. Nilsson, D. R. Fisher, and R. H. Larsen, "High-linear energy transfer irradiation targeted to skeletal metastases by the α-emitter 223Ra: Adjuvant or alternative to conventional modalities?," Clin. Cancer Res. **12**, 6250s–6257s (2006).

[31]C. Parker, S. Nilsson, D. Heinrich, S. I. Helle, J. M. O'Sullivan, S. D. Fosså, A. Chodacki, P. Wiechno, J. Logue, M. Seke, A. Widmark, D. C. Johannessen, P. Hoskin, D. Bottomley, N. D. James, A. Solberg, I. Syndikus, J. Kliment, S. Wedel, S. Boehmer, M. Dall'Oglio, L. Franzén, R. Coleman, N. J. Vogelzang, C. G. O'Bryan-Tear, K. Staudacher, J. Garcia-Vargas, M. Shan, Ø. S. Bruland, and O. Sartor, "Alpha emitter Radium-223 and survival in metastatic prostate cancer," N. Engl. J. Med. **369**, 213–223 (2013).

[32]Laboratorie National Henri Becquerel (LNHB), *Table of Radionuclides* (Laboratorie National Henri Becquerel (LNHB), France); available at http://www.nucleide.org/.

[33]A. T. C. Collection Report: American Type Culture Collection, MTT Cell Proliferation Assay. Document number: 306/59 01, (6pp.); available at https://www.atcc.org/~/media/DA5285A1F52C414E864C966FD78C9A79.ashx.

[34]T. L. Riss, R. A. Moravec, A. L. Niles, H. A. Benink, T. J. Worzella, and L. Minor, "Cell viability assays," in *Assay Guidance Manual*, edited by G. S. sittampalam, N. P. Coussens, H. Nelson, M. Arkin, D. Auld, C. Austin, B. Bejcek, M. Glicksman, J. Inglese, P. W. Iversen, Z. Li, J. McGee, O. McManus, L. Minor, A. Napper, J. M. Peltier, T. Riss, O. J. Trask, Jr., and J. Weidner (Bethesda MD, 2004); available at https://www.ncbi.nlm.nih.gov/books/NBK53196/.

[35]S. Supiot, A. Faivre-Chauvet, O. Couturier, M. F. Heymann, N. Robillard, F. Kraeber-Bodere, L. Morandeau, M. A. Mahe, and M. Cherel, "Comparison of the biologic effects of MA5 and B-B4 monoclonal antibody labeled with iodine-131 and bismuth-213 on multiple myeloma," Cancer **94**, 1202–1209 (2002).

[36]I. A. E. Agency, *Absorbed Dose Determination in External Beam Radiotherapy: An International Code of Practice for Dosimetry Based on Standards of Absorbed Dose to Water* (IAEA, Vienna, Austria, 2000).

[37]J. Bouchami, A. Gutiérrez, T. Holy, A. Houdayer, J. Jakůbek, C. Lebel, C. Leroy, J. Macana, J. P. Martin, S. Pospíšil, S. Prak, P. Sabella, and C. Teyssier, "Measurement of pattern recognition efficiency of tracks generated by ionizing radiation in a Medipix2 device," Nucl. Instrum. Methods Phys. Res., Sect. A **633**(Suppl.1), S187–S189 (2011).

[38]J. F. Ziegler, "Interactions of ions with matter" (2015); available at http://www.srim.org/.

[39]H. Hofsäss, K. Zhang, and A. Mutzke, "Simulation of ion beam sputtering with SDTrimSP, TRIDYN and SRIM," Appl. Surf. Sci. **310**, 134–141 (2014).

[40]R. E. Stoller, M. B. Toloczko, G. S. Was, A. G. Certain, S. Dwaraknath, and F. A. Garner, "On the use of SRIM for computing radiation damage exposure," Nucl. Instrum. Methods Phys. Res., Sect. B **310**, 75–80 (2013).

[41]IAEA, "Cytogenetic dosimetry: Applications in preparedness for and response to radiation emergencies," in *EPR-BioDosimetry* (IAEA, Vienna, 2011).

[42]IAEA, "Cytogenetic analysis for radiation dose assessment a manual," Technical Reports Series No. 405 (IAEA, Vienna, 2001).

[43]S. H. Macphail, J. P. BanÁth, T. Y. Yu, E. H. M. Chu, H. Lambur, and P. L. Olive, "Expression of phosphorylated histone H2AX in cultured cell lines following exposure to X-rays," Int. J. Radiat. Biol. **79**, 351–359 (2003).

[44]L. J. Kuo and L. X. Yang, "Gamma-H2AX - A novel biomarker for DNA double-strand breaks," In vivo (Athens, Greece) **22**, 305–309 (2008); available at https://www.ncbi.nlm.nih.gov/pubmed/18610740.

[45]W. S. Rasband, *ImageJ* (U.S. National Institutes of Health, 1997-2014); available at https://imagej.nih.gov/ij/.

7.4 Clonogenic Assay Result

From the number of viable colonies grown, the survival curve for the A549 cell line following irradiation with 6 MV photons was determined (Figure 7.2). The LD_{50} (radiation dose at which 50% of the cells survived) was found to be close to 2 Gy, which is similar to previously published studies (Wéra, Borlon et al. 2012; Riquier, Wera et al. 2013). This result confirmed the cell line is radiation sensitive. It has been conducted that A549 cell line is a suitable candidate for experiments with α-particles presented in this chapter.

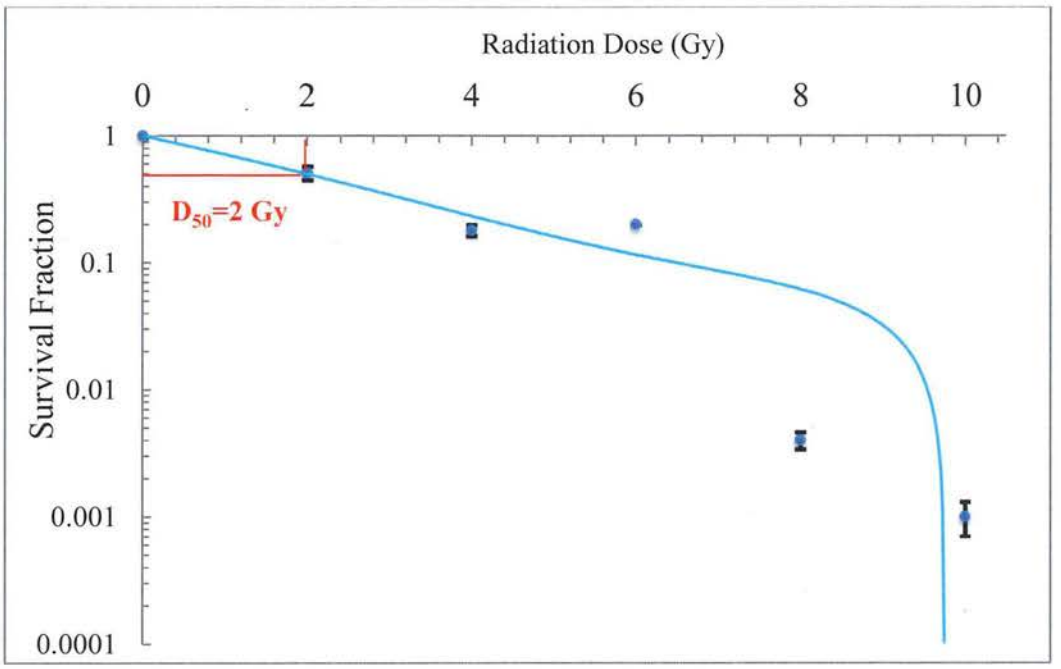

Figure 7.2. A549 cell survival curve following irradiation with 6 MV photons. The relative errors were calculated from standard deviations of the mean obtained from triplicate samples.

7.5 Conclusion

The results confirmed the potential of this transmission alpha particle microdosimetry design using Timepix. Furthermore, using both the transmission microdosimetry system, calculated

using the biological dosimetry, can be used to estimate the biological effects in TAT without the need for repeated biological dosimetry that is costly, time consuming and not readily available.

Chapter 8

Conclusions and Future Work

8.1 Conclusion

Targeted alpha therapy is a type of radionuclide therapy where a suitable alpha emitter is attached to a cancer cell-targeting vehicle. Once at the cancer site, α-particles are emitted causing localized damage to cancer cells. Several factors should be considered when dealing with TAT, such as the short range of α-particles in tissue, the nature of α-particle distribution and selective uptake in the organs and also the physical and the biological half-life of the alpha emitter.

Due to limited dosimetric data available, related to this type of radiation treatment, the objective of this project was to develop a semiconductor microdosimetry system to use in targeted alpha therapy. The main goals of this study were to develop techniques for estimation of the absorbed dose deposited by α-particles at a cellular level and determination of biodistribution of a radioisotope in the tumour.

In this work, a unique and novel semiconductor microdosimetry system was successfully designed, tested and verified, taking advantage of a novel pixelated semiconductor detector developed at CERN, known as Timepix. This groundbreaking microdosimetry system is expected to be used in development of new targeted alpha therapy radiopharmaceuticals, for both in vitro and in vivo studies.

This development was preceded by thorough characterization of Timepix at low radiation doses (chapter 4). Basic performance characteristics, including linearity, reproducibility, energy dependence and sensitivity were determined in the absorbed dose range from μGy to mGy. The study confirmed superb sensitivity of Timepix to low radiation dose levels down to 0.1 μGy. It was demonstrated that Timepix pixel value increased linearly with delivered dose, as required for a dosimetric device. It was, however, based on the results of studying different kV/HVL X-ray beams, found to be energy dependent. This means that Timepix must be carefully calibrated for a given radiation type and its energy spectrum before it can be used for dosimetric measurements. A good medium term reproducibility of Timepix was observed.

The work conducted in chapter 5 identified that while Timepix, if energy calibrated for a given bias voltage and a given radiation type, can be used for spectrometry of low energy γ-rays, X-rays and alpha particles in the MeV range, its energy resolution is not excellent and is inferior to, for example, germanium detectors. This is possibly a consequence of the pixel sharing effect as well as of the very thin detector layer (300 μm). Deconvolution of γ-ray and alpha particle energy spectra has also been also studied using Mylar foils positioned on top of the radiation source. The energy resolution was found to be 17% and 26% for Am-241 α-particles with a bias voltage of 5 and 100 V, respectively. For Ra-223 α-particles, the energy resolution found to be 32%, using a bias voltage of 100 V.

Moreover, imaging applications of Timepix were briefly evaluated using several objects with internal submillimeter design (e.g. optical fibres). The image resolution was investigated using the edge response function (ERF) and I-125 seed and a Pu-238 source. The measured ERF based spatial resolution for imaging applications was determined to be 0.79 mm and 1.28 mm, respectively for γ-rays and alpha particles respectively. These values result from the fact that the sources used were not point sources. Far superior resolution can be achieved with Timepix if a point source, for example a nano-focus X-ray tube with a focal spot size of less than 1 μm (Dammer, Frallicciardi et al. 2009), is used.

First ever application of Timepix to measure radioisotope biodistribution (i.e. autoradiography) was developed in Chapter 6, allowing semi-quantitative assessments of doses in tumour samples and visualization of α-activity spatial distribution in tumour samples. In this part of the project, tumor sections were taken from mice with Lewis lung (LL2) tumours that were treated with about 18 kBq of ^{227}Th-labelled DAB4 murine monoclonal antibody, where DAB4 binds to necrotic tumour cells. Some of the mice were also treated with chemotherapy prior to radiotherapy treatment in order to increase necrotic tissue volume and to increase tumour uptake of DAB4. Sections of tumours were then mounted 2 cm away from the Timepix detector. During the 14 h image acquisition, particles emitted from the tumour sections were collected. α-particles, X-rays and electron tracks were identified in the tumour autoradiography images. The results showed that the administration of chemotherapy prior to TAT radiation therapy increased Th-227–DAB4 uptake approximately 4 times compared to using TAT only.

Finally, the carefully constructed experimental studies, conducted in this thesis, culminated in a design and development of a novel transmitted α-particle microdosimetry technique with potentially widespread in vitro and in vivo applications in dosimetry of targeted alpha particle therapy. The work has met with international interest and was presented in an invited

presentation on novel technologies in radiation oncology at the Medical Physics World Congress 2015, Toronto, Canada.

In this work, this cell line was found to be sensitive to radiation and D_{50} found to be ~ 2 Gy for X-ray irradiation. The cell line was seeded in a HTS Transwell® and irradiated with α-particles emitted from below using an evaporated Ra-223 source for ½, 1, 2 and 3 hours. Unirradiated cells were used as a control. The Transwell system was placed under Timepix to detect transmitted α-particles. In addition, after irradiation, the cells were processed and DNA double strand breaks (DSBs) in the form of γ-H2AX foci, were examined by fluorescence microscopy. The number of transmitted α-particles after ½, 1, 2 or 3 hour irradiation times were measured and were correlated with the observed DNA DSBs. Moreover, the dose deposited at a cellular level was calculated using Monte Carlo code SRIM. The experiment found that 20% of α-particles were transmitted and detected by Timepix and the number of γ-H2AX foci increased significantly following α-particle irradiation compared to unirradiated controls and was proportional to dose. The absorbed dose deposited by α-particles in the cells was estimated to be 0.12, 0.24, 0.46 and 0.72 Gy after ½, 1, 2 and 3 h irradiation time, respectively,

In conclusion, this thesis investigated the performance of Timepix as a detector, an imager and a spectrometer. The sensitivity of Timepix to low doses, its linearity, reproducibility and energy dependence were also examined. Due to energy dependence observed, Timepix energy calibration is required for each radiation modality and energy range prior to use for dosimetric purposes. Timepix can also be used effectively for autoradiography in TAT to monitor the uptake and biodistribution of a radioisotope. Furthermore, this thesis presented a novel transmitted α-particle microdosimetry system. It has been suggested that both transmitted α-particle microdosimetry detector and a biological dosimetry can give a quantitative information on the biological effects of α-particles at a cellular level.

8.2 Future Work

Future work, which could be done to further enhance the performance of Timepix microdosimetry system include:

Firstly, further investigation of more parameters that could affect Timepix radiation performance as a detector and a spectrometer should be conducted. These include temperature dependence, parameters from the global DACs in the device (e.g. IKrum, baseline (FBK) and THL) and a bias voltage.

Other applications of Timepix in medical physics could also be studied and developed; for example measurement of neutron doses received by a patient during high megavoltage (above 10 MV) radiotherapy.

Another area for further study relates to the transmission of α-particle microdosimetry system. Further investigation on the same cell line and other cell lines can be performed using different radioactive sources. Furthermore, correlation between the events detected by Timepix and the γ-H2AX foci on a cell by cell basis could be studied. Ideally, it would be useful to image the cell layer with Timepix and a nano-focus X-ray tube, then irradiate the sample with an alpha-emitter. The X-ray image of individual cells and the alpha-particle hits image could then be correlated to identify the number of alpha particle traversals through individual cells.

Finally, future applications of this system may include modelling of the system using Geant4 to predict and assist with interpretation of experimental results.

Appendix

SRIM Calculation

SRIM is a Monte Carlo code, with its name abbreviated fromStopping and Ranges of Ions in Matter. In this work, version 2008 was used (Ziegler ; Stoller, Toloczko et al. 2013; Hofsäss, Zhang et al. 2014) SRIM can simulate a target as a semi-infinite layer of a given thickness. Up to eight layers can be simulated (Ziegler). Each layer can be made of compound materials, using SRIM libraries.

SRIM simulation in this work was performed to simulate α-particle energy loss while penetrating cells and media. The cells and the media were considered as water (density of 1 g/cm^3) with a thickness of 57.3 μm and simulated as a single layer. The thickness was adjusted via repeated simulations to get ~ 20% α-particles transmission, that was measured using the Timepix radiation detector with and without the cells and the media. In the simulation, 1 mm air gap (0.00125 g/cm^3) density was placed between the α-particle source and the cells and media as shown in Figure A.1. The α-particle source was simulated as a monoenergetic point

source with the energy of 6.735 MeV (1.e. the mean energy of α-particles emitted from Ra-223) as shown in Figure A.2. The simulation was run five times using 10^6 α-particles.

The results of α-particle energy loss in each layer can be found in the output file, called IONZ.txt file. Using the data in this file, the energy deposition in the cells can be calculated. The energy list for one run is attached as a table and the cells and media layer thickness is highlighted.

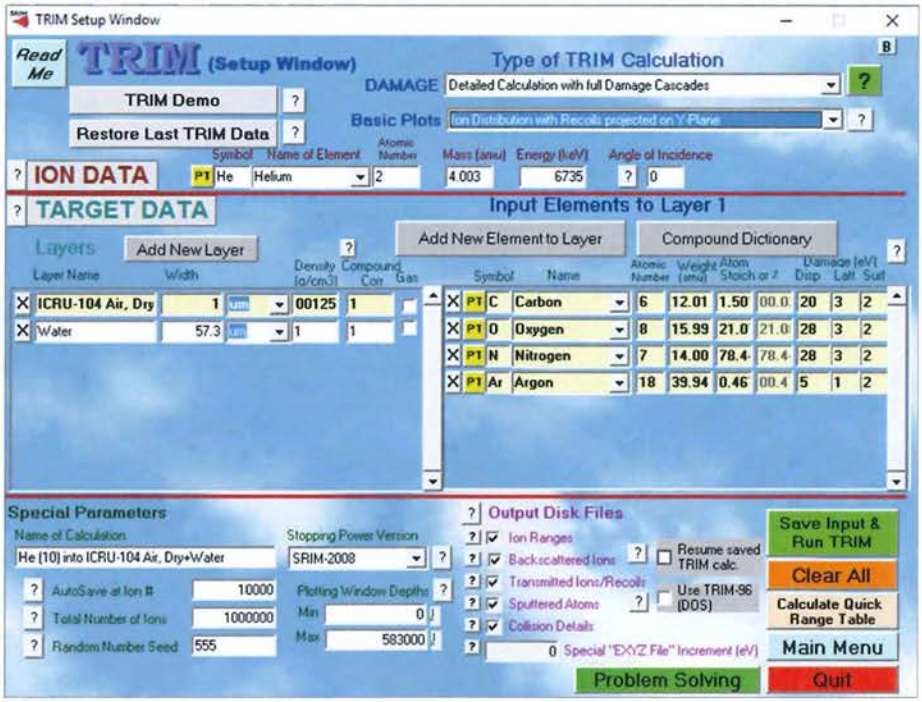

Figure A.1. SRIM simulation set up.

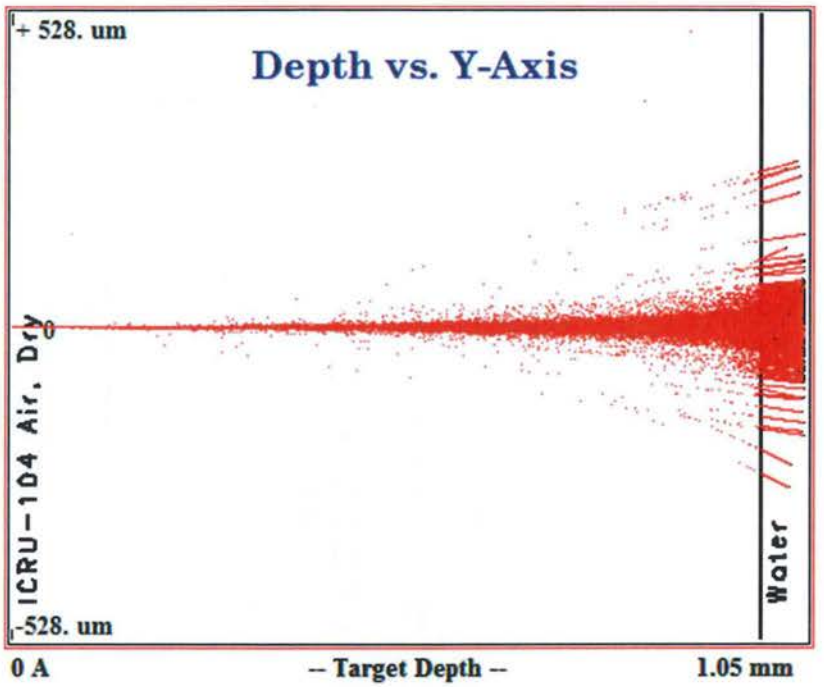

Figure A.2. SRIM simulation of transmitted alpha particles with 1 mm air gap between the source and cells and media (represented as water).

TARGET depth (Ang)	TARGET depth (mm)	IONIZ. By ions (eV/(angstrom-Ion)	IONIZ. By recoils (eV/(Angstrom-Ion)
1.06E+05	1.06E-02	7.71E-03	1.05E-08
2.11E+05	2.11E-02	7.71E-03	8.31E-08
3.17E+05	3.17E-02	7.71E-03	5.88E-08
4.23E+05	4.23E-02	7.71E-03	4.85E-07
5.29E+05	5.29E-02	7.71E-03	1.93E-07
6.34E+05	6.34E-02	7.71E-03	6.77E-08
7.40E+05	7.40E-02	7.72E-03	9.68E-08
8.46E+05	8.46E-02	7.72E-03	3.79E-07
9.52E+05	9.52E-02	7.72E-03	1.73E-07
1.06E+06	1.06E-01	7.72E-03	1.05E-07
1.16E+06	1.16E-01	7.72E-03	2.08E-07
1.27E+06	1.27E-01	7.72E-03	4.09E-07
1.37E+06	1.37E-01	7.72E-03	5.82E-07
1.48E+06	1.48E-01	7.72E-03	2.97E-07
1.59E+06	1.59E-01	7.72E-03	2.33E-07
1.69E+06	1.69E-01	7.72E-03	9.15E-07
1.80E+06	1.80E-01	7.72E-03	4.19E-07
1.90E+06	1.90E-01	7.72E-03	3.55E-07
2.01E+06	2.01E-01	7.72E-03	2.83E-07
2.11E+06	2.11E-01	7.72E-03	9.95E-07
2.22E+06	2.22E-01	7.72E-03	3.88E-07
2.33E+06	2.33E-01	7.72E-03	3.11E-07
2.43E+06	2.43E-01	7.72E-03	2.95E-06
2.54E+06	2.54E-01	7.72E-03	3.30E-06
2.64E+06	2.64E-01	7.72E-03	1.97E-06
2.75E+06	2.75E-01	7.72E-03	8.30E-07
2.85E+06	2.85E-01	7.72E-03	4.56E-07
2.96E+06	2.96E-01	7.72E-03	3.43E-07
3.07E+06	3.07E-01	7.72E-03	8.06E-06
3.17E+06	3.17E-01	7.72E-03	4.51E-07
3.28E+06	3.28E-01	7.72E-03	6.38E-07
3.38E+06	3.38E-01	7.72E-03	4.41E-07
3.49E+06	3.49E-01	7.72E-03	8.97E-07
3.59E+06	3.59E-01	7.72E-03	6.74E-07
3.70E+06	3.70E-01	7.72E-03	1.68E-06
3.81E+06	3.81E-01	7.72E-03	8.05E-07
3.91E+06	3.91E-01	7.73E-03	4.77E-07
4.02E+06	4.02E-01	7.73E-03	2.74E-06

4.12E+06	4.12E-01	7.73E-03	6.88E-07
4.23E+06	4.23E-01	7.73E-03	1.77E-06
4.33E+06	4.33E-01	7.73E-03	2.64E-06
4.44E+06	4.44E-01	7.73E-03	8.84E-07
4.55E+06	4.55E-01	7.73E-03	6.09E-07
4.65E+06	4.65E-01	7.73E-03	9.66E-07
4.76E+06	4.76E-01	7.73E-03	7.35E-07
4.86E+06	4.86E-01	7.73E-03	1.13E-06
4.97E+06	4.97E-01	7.73E-03	5.67E-07
5.08E+06	5.08E-01	7.73E-03	1.70E-06
5.18E+06	5.18E-01	7.74E-03	7.76E-07
5.29E+06	5.29E-01	7.74E-03	1.05E-06
5.39E+06	5.39E-01	7.73E-03	8.66E-07
5.50E+06	5.50E-01	7.73E-03	1.51E-06
5.60E+06	5.60E-01	7.74E-03	1.04E-06
5.71E+06	5.71E-01	7.74E-03	1.04E-06
5.82E+06	5.82E-01	7.74E-03	2.76E-06
5.92E+06	5.92E-01	7.74E-03	5.73E-07
6.03E+06	6.03E-01	7.74E-03	1.05E-06
6.13E+06	6.13E-01	7.74E-03	7.45E-06
6.24E+06	6.24E-01	7.74E-03	5.81E-07
6.34E+06	6.34E-01	7.74E-03	2.17E-06
6.45E+06	6.45E-01	7.74E-03	9.64E-07
6.56E+06	6.56E-01	7.74E-03	2.31E-05
6.66E+06	6.66E-01	7.74E-03	1.12E-06
6.77E+06	6.77E-01	7.75E-03	3.17E-06
6.87E+06	6.87E-01	7.75E-03	1.13E-06
6.98E+06	6.98E-01	7.75E-03	1.75E-06
7.08E+06	7.08E-01	7.75E-03	8.89E-07
7.19E+06	7.19E-01	7.75E-03	1.30E-06
7.30E+06	7.30E-01	7.75E-03	1.14E-06
7.40E+06	7.40E-01	7.75E-03	3.09E-06
7.51E+06	7.51E-01	7.75E-03	1.12E-06
7.61E+06	7.61E-01	7.75E-03	1.11E-06
7.72E+06	7.72E-01	7.76E-03	1.02E-06
7.82E+06	7.82E-01	7.76E-03	2.14E-06
7.93E+06	7.93E-01	7.76E-03	1.33E-06
8.04E+06	8.04E-01	7.76E-03	2.02E-06
8.14E+06	8.14E-01	7.76E-03	1.36E-06
8.25E+06	8.25E-01	7.76E-03	9.10E-06
8.35E+06	8.35E-01	7.76E-03	1.26E-06

8.46E+06	8.46E-01	7.77E-03	1.25E-06
8.56E+06	8.56E-01	7.77E-03	1.42E-06
8.67E+06	8.67E-01	7.76E-03	4.74E-06
8.78E+06	8.78E-01	7.76E-03	3.51E-06
8.88E+06	8.88E-01	7.77E-03	2.44E-06
8.99E+06	8.99E-01	7.77E-03	1.01E-06
9.09E+06	9.09E-01	7.77E-03	1.25E-05
9.20E+06	9.20E-01	7.77E-03	2.64E-06
9.30E+06	9.30E-01	7.77E-03	1.57E-06
9.41E+06	9.41E-01	7.77E-03	1.55E-06
9.52E+06	9.52E-01	7.77E-03	3.17E-06
9.62E+06	9.62E-01	7.77E-03	2.61E-06
9.73E+06	9.73E-01	7.77E-03	2.28E-06
9.83E+06	9.83E-01	7.78E-03	1.09E-06
9.94E+06	9.94E-01	7.79E-03	1.54E-06
1.00E+07	1.00E+00	3.18E+00	9.11E-04
1.02E+07	1.02E+00	8.11E+00	2.53E-03
1.03E+07	1.03E+00	9.13E+00	2.96E-03
1.04E+07	1.04E+00	1.07E+01	3.70E-03
1.05E+07	1.05E+00	1.39E+01	5.27E-03
1.06E+07	1.06E+00	1.77E+01	3.41E-02
sum=		5.96E+01	4.86E-02

Bibliography

Table of Radionuclides [Online]. FRANCE: Laboratorie National Henri Becquerel (LNHB).

1996. The IPEMB code of practice for the determination of absorbed dose for x-rays below 300 kV generating potential (0.035 mm Al-4 mm Cu HVL; 10-300 kV generating potential). Institution of Physics and Engineering in Medicine and Biology. *Phys Med Biol,* 41, 2605-25.

2007. *Advancing Nuclear Medicine Through Innovation,* Washington, DC, USA, National Academies Press.

(NIST), T. N. I. O. S. A. T. *X-Ray Mass Attenuation Coefficients* [Online]. Available: http://physics.nist.gov/PhysRefData/XrayMassCoef/tab3.html.

ABATE, L., BERTOLUCCI, E., CONTI, M., DI COSMO, A., DI CRISTO, C., METTIVIER, G., MONTESI, M. C. & RUSSO, P. 2000. Quantitative dynamic imaging of biological processes with solid state radiation detector. *Nuclear Science, IEEE Transactions on,* 47, 1907-1910.

ABBAS, N., BRULAND, O. S., BREVIK, E. M. & DAHLE, J. 2012. Preclinical evaluation of 227Th-labeled and 177Lu-labeled trastuzumab in mice with HER-2-positive ovarian cancer xenografts. *Nucl Med Commun,* 33, 838-47.

ABBAS, N., HEYERDAHL, H., BRULAND, Ø. S., BORREBÆK, J., NESLAND, J. & DAHLE, J. 2011. Experimental α-particle radioimmunotherapy of breast cancer using 227Th-labeled p-benzyl-DOTA-trastuzumab. *EJNMMI Research,* 1, 1-12.

AGENCY, I. A. E. 2000. Absorbed Dose Determination in External Beam Radiotherapy An International Code of Practice for Dosimetry Based on Standards of Absorbed Dose to Water. Vienna, Austria IAEA.

AL-EJEH, F., DARBY, J. M. & BROWN, M. P. 2007. The La autoantigen is a malignancy-associated cell death target that is induced by DNA-damaging drugs. *Clin Cancer Res,* 13, 5509s-5518s.

AL-EJEH, F., DARBY, J. M. & BROWN, M. P. 2009a. Chemotherapy Synergizes with Radioimmunotherapy Targeting La Autoantigen in Tumors. *PLoS ONE,* 4, e4630.

AL-EJEH, F., DARBY, J. M., THIERRY, B. & BROWN, M. P. 2009b. A simplified suite of methods to evaluate chelator conjugation of antibodies: effects on hydrodynamic radius and biodistribution. *Nucl Med Biol.,* 36, 395-402.

AL-EJEH, F., DARBY, J. M., TSOPELAS, C., SMYTH, D., MANAVIS, J. & BROWN, M. P. 2009c. APOMAB®, a La-Specific Monoclonal Antibody, Detects the Apoptotic Tumor Response to Life-Prolonging and DNA-Damaging Chemotherapy. *PLoS ONE,* 4, e4558.

AL DARWISH, R., STAUDACHER, A. H., BEZAK, E. & BROWN, M. P. 2015. Autoradiography Imaging in Targeted Alpha Therapy with Timepix Detector. *Computational and Mathematical Methods in Medicine,* 2015, 7.

ALLEN, B. J. 2006. Internal high linear energy transfer (LET) targeted radiotherapy for cancer. *Phys Med Biol,* 51, R327-41.

ALLEN, B. J. 2013. Systemic Targeted Alpha Radiotherapy for Cancer. *Journal of Biomedical Physics & Engineering,* 3, 67-80.

ALLEN, B. J., HUANG, C.-Y. & CLARKE, R. A. 2014. Targeted alpha anticancer therapies: update and future prospects. *Biologics : Targets & Therapy,* 8, 255-267.

ALLEN, B. J., RAJA, C., RIZVI, S., LI, Y., TSUI, W., ZHANG, D., SONG, E., QU, C. F., KEARSLEY, J., GRAHAM, P. & THOMPSON, J. 2004. Targeted alpha therapy for cancer. *Phys Med Biol,* 49, 3703-12.

AMENDOLIA, S. R., BERTOLUCCI, E., BISOGNI, M. G., BOTTIGLI, U., CECCOPIERI, A., CIOCCI, M. A., CONTI, M., DELOGU, P., FANTACCI, M. E., MAESTRO, P., MARZULLI, V., PERNIGOTTI, E., ROMEO, N., ROSSO, V., ROSSO, P., STEFANINI, A. & STUMBO, S. 1999. MEDIPIX: a VLSI chip for a GaAs pixel detector for digital radiology. *Nuclear Instruments and Methods in Physics Research Section A: Accelerators, Spectrometers, Detectors and Associated Equipment,* 422, 201-205.

AMENDOLIA, S. R., BISOGNI, M. G., BOTTIGLI, U., CIOCCI, M. A., DELOGU, P., DIPASQUALE, G., FANTACCI, M. E., GIANNELLI, M., MAESTRO, P., MARZULLI, V. M., PERNIGOTTI, E., ROSSO, V.,

STEFANINI, A. & STUMBO, S. 2000. Low contrast imaging with a GaAs pixel digital detector. *Nuclear Science, IEEE Transactions on,* 47**,** 1478-1482.

ANTON, G., GEBERT, U., MICHEL, T. & RÜGHEIMER, T. K. 2009. A hybrid photodetector using the Timepix semiconductor assembly for photoelectron detection. *Nuclear Instruments and Methods in Physics Research Section A: Accelerators, Spectrometers, Detectors and Associated Equipment,* 602**,** 205-208.

ATTIX, F. H. 1986. *Introduction to radiological physics and radiation dosimetry* New York Wiley.

BACK, T. & JACOBSSON, L. 2010. The alpha-camera: a quantitative digital autoradiography technique using a charge-coupled device for ex vivo high-resolution bioimaging of alpha-particles. *J Nucl Med,* 51**,** 1616-23.

BÄCK, T. & JACOBSSON, L. 2010. The α-Camera: A Quantitative Digital Autoradiography Technique Using a Charge-Coupled Device for Ex Vivo High-Resolution Bioimaging of α-Particles. *Journal of Nuclear Medicine,* 51**,** 1616-1623.

BAEK, S. H. & UHER, J. Simulated dental cone beam computed tomography using Timepix. Nuclear Science Symposium and Medical Imaging Conference (NSS/MIC), 2013 IEEE, Oct. 27 2013-Nov. 2 2013 2013. 1-3.

BALLABRIGA, R., CAMPBELL, M., HEIJNE, E., LLOPART, X., TLUSTOS, L. & WONG, W. 2011. Medipix3: A 64 k pixel detector readout chip working in single photon counting mode with improved spectrometric performance. *Nuclear Instruments and Methods in Physics Research Section A: Accelerators, Spectrometers, Detectors and Associated Equipment,* 633, Supplement 1**,** S15-S18.

BALLABRIGA, R., CAMPBELL, M., HEIJNE, E. H. M., LLOPART, X. & TLUSTOS, L. 2007. The Medipix3 Prototype, a Pixel Readout Chip Working in Single Photon Counting Mode With Improved Spectrometric Performance. *Nuclear Science, IEEE Transactions on,* 54**,** 1824-1829.

BAMBERGER, A., DESCH, K., RENZ, U., TITOV, M., VLASOV, N., WIENEMANN, P. & ZWERGER, A. 2007. Resolution studies on 5 GeV electron tracks observed with triple-GEM and MediPix2/TimePix-readout. *Nuclear Instruments and Methods in Physics Research Section A: Accelerators, Spectrometers, Detectors and Associated Equipment,* 581**,** 274-278.

BARDELLONI, G., BERTOLUCCI, E., BOERKAMP, A. L. J., CALVET, D., CONTI, M., MAIORINO, M., RUSSO, P. & VISSCHERS, J. L. A new read-out system for an imaging pixel detector. Nuclear Science Symposium Conference Record, 2000 IEEE, 2000 2000. 12/57-12/60 vol.2.

BARDIES, M. & PIHET, P. 2000. Dosimetry and Microdosimetry of Targeted Radiotherapy. *Current Pharmaceutical Design,* 6**,** 1469.

BELLO, D. S. S., NAUTA, B. & VISSCHERS, J. 2001. Design of analog-to-digital converters for energy-sensitive hybrid pixel detectors. *Nuclear Instruments and Methods in Physics Research Section A: Accelerators, Spectrometers, Detectors and Associated Equipment,* 466**,** 218-225.

BENSALEH, S. & BEZAK, E. 2011. *The impact of uncertainties associated with MammoSite brachytherapy on the dose distribution in the breast.*

BERT, C., NIEDERLÖHNER, D., GIERSCH, J., PFEIFFER, K. F. & ANTON, G. 2003. Computed tomography using the Medipix1 chip. *Nuclear Instruments and Methods in Physics Research Section A: Accelerators, Spectrometers, Detectors and Associated Equipment,* 509**,** 240-250.

BERTOLUCCI, E., CONTI, M., METTIVIER, G., RUSSO, P., AMENDOLIA, S. R., BISOGNI, M. G., BOTTIGLI, U., CECCOPIERI, A., CIOCCI, M. A., DELOGU, P., FANTACCI, M. E., MAESTRO, P., MARZULLI, V. M., PERNIGOTTI, E., ROMEO, N., ROSSO, V., STEFANINI, A. & STUMBO, S. 1999. GaAs pixel radiation detector as an autoradiography tool for genetic studies. *Nuclear Instruments and Methods in Physics Research Section A: Accelerators, Spectrometers, Detectors and Associated Equipment,* 422**,** 242-246.

BIOMEDICALS, M. 2016. *Cell Culture -- Chromium Release Assay* [Online]. Available: http://www4.mpbio.com/ecom/docs/proddata.nsf/5f64ffd4f38c2fda8525645d00769d68/53d2a75653615bab852568cb00572ff3?OpenDocument [Accessed 25 June 2016.

BIRD, J. 2007. *Electrical and Electronic Principles and Technology,* Oxford, Elsevier Ltd.

BISOGNI, M. G., CAMPBELL, M., CONTI, M. D., P ; FANTACCI, M. E., HEIJNE, E. H. M., MAESTRO, P., MAGISTRATI, G., MARZULLI, V. M., MEDDELER, G., MIKULEC, B., PERNIGOTTI, E., ROSSO, V., SCHWARZ, C., SNOEYS, W., STUMBO, S. & WATT, J. 1998. Performance of 4096 pixel photon counting chip. *43rd SPIE International Symposium on Optical Science, Engineering and Instrumentation : Hard X-ray and Gamma-Ray Detector Physics and Applications.* San Diego, CA, USA.

BISOGNI, M. G., DELOGU, P., FANTACCI, M. E., METTIVIER, G., MONTESI, M. C., NOVELLI, M., QUATTROCCHI, M., ROSSO, V., RUSSO, P. & STEFANINI, A. A Medipix2-based imaging system for digital mammography with silicon pixel detectors. Nuclear Science Symposium Conference Record, 2003 IEEE, 19-25 Oct. 2003 2003. 1509-1512 Vol.3.

BOUCHAMI, J., GUTIÉRREZ, A., HOLY, T., HOUDAYER, A., JAKŮBEK, J., LEBEL, C., LEROY, C., MACANA, J., MARTIN, J. P., POSPÍŠIL, S., PRAK, S., SABELLA, P. & TEYSSIER, C. 2011. Measurement of pattern recognition efficiency of tracks generated by ionizing radiation in a Medipix2 device. *Nuclear Instruments and Methods in Physics Research Section A: Accelerators, Spectrometers, Detectors and Associated Equipment,* 633, Supplement 1**,** S187-S189.

BRADY, D., O'SULLIVAN, J. M. & PRISE, K. M. 2013. What is the Role of the Bystander Response in Radionuclide Therapies? *Frontiers in Oncology,* 3**,** 215.

BRULAND, Ø. S., NILSSON, S., FISHER, D. R. & LARSEN, R. H. 2006. High-Linear Energy Transfer Irradiation Targeted to Skeletal Metastases by the α-Emitter 223Ra: Adjuvant or Alternative to Conventional Modalities? *Clinical Cancer Research,* 12**,** 6250s-6257s.

BULANEK, B., EKENDAHL, D. & PROUZA, Z. 2013. Fast Neutron Dosemeter using Pixelated Deetctor Timepix. *Radiat Prot Dosimetry.*

BUSHBERG, J. T., SEIBERT, J. A., LEIDHOLDT, E. M. & BOONE, J. M. 2002. *The Essential Physics of Medical Imaging,* Philadelphia, Philadelphia : Lippincott Williams & Wilkins.

CAMPBELL, M. 2011. 10 years of the Medipix2 Collaboration. *Nuclear Instruments and Methods in Physics Research Section A: Accelerators, Spectrometers, Detectors and Associated Equipment,* 633, Supplement 1**,** S1-S10.

CAMPBELL, M., HAVRANEK, V., HEIJNE, E., HOLY, T., IDARRAGA, J., JAKUBEK, J., LEBEL, C., LEROY, C., LLOPART, X., NOVOTNY, J., POSPISIL, S., TLUSTOS, L. & VYKYDAL, Z. Charge collection from proton and alpha particle tracks in silicon pixel detector devices. Nuclear Science Symposium Conference Record, 2007. NSS '07. IEEE, Oct. 26 2007-Nov. 3 2007 2007. 1047-1050.

CAMPBELL, M., HEIJNE, E. H. M., MEDDELER, G., PERNIGOTTI, E. & SNOEYS, W. 1998. Readout for a 64 x 64 pixel matrix with 15-bit single photon counting. *Nuclear Science, IEEE Transactions on,* 45**,** 751-753.

CERN. 2011. *Medipix* [Online]. Available: http://medipix.web.cern.ch/medipix/ [Accessed 29/10/2011 2011].

CHAO, K. S. C., PEREZ, C. A. & BRADY, L. W. 2011. *Radiation Oncology: Management Decisions,* Philadelphia, Lippincott Williams & Wilkins.

CHMEISSANI, M. & MIKULEC, B. 2001. Performance limits of a single photon counting pixel system. *Nuclear Instruments and Methods in Physics Research Section A: Accelerators, Spectrometers, Detectors and Associated Equipment,* 460**,** 81-90.

CHOUIN, N., LINDEGREN, S., FROST, S. H. L., JENSEN, H., ALBERTSSON, P., HULTBORN, R., PALM, S., JACOBSSON, L. & BÄCK, T. 2013. Ex Vivo Activity Quantification in Micrometastases at the Cellular Scale Using the α-Camera Technique. *Journal of Nuclear Medicine.*

CLINICALTRIALS.GOV. 2015. *Targeted Atomic Nano-Generators (Actinium-225-Labeled Humanized Anti-CD33 Monoclonal Antibody HuM195) in Patients With Advanced Myeloid Malignancies* [Online]. Available: https://clinicaltrials.gov/show/NCT00672165.

COGNETTA, A. B. & MENDENHALL, W. M. 2013. *Radiation Therapy for Skin Cancer,* Dordrecht : Springer

COLEMAN, R., AKSNES, A. K., NAUME, B., GARCIA, C., JERUSALEM, G., PICCART, M., VOBECKY, N., THURESSON, M. & FLAMEN, P. 2014. A phase IIa, nonrandomized study of radium-223

dichloride in advanced breast cancer patients with bone-dominant disease. *Breast Cancer Res Treat,* 145**,** 411-8.

COLLECTION, A. T. C. MTT Cell Proliferation Assay. USA.

CROKE, J., LEUNG, E., SEGAL, R. & MALONE, S. 2012. Clinical benefits of alpharadin in castrate-chemotherapy-resistant prostate cancer: case report and literature review. *BMJ Case Rep,* 2012.

CUDIE, X. L. 2007. *Design and characterization of 64K pixels chips working in single photon processing mode* Doctor of Technology, Mid Sweden University.

DAHLE, J., ABBAS, N., BRULAND, O. S. & LARSEN, R. H. 2011. Toxicity and relative biological effectiveness of alpha emitting radioimmunoconjugates. *Curr Radiopharm,* 4**,** 321-8.

DAHLE, J., BORREBAEK, J., JONASDOTTIR, T. J., HJELMERUD, A. K., MELHUS, K. B., BRULAND, O. S., PRESS, O. W. & LARSEN, R. H. 2007. Targeted cancer therapy with a novel low-dose rate alpha-emitting radioimmunoconjugate. *Blood,* 110**,** 2049-56.

DAHLE, J., JONASDOTTIR, T. J., HEYERDAHL, H., NESLAND, J. M., BORREBAEK, J., HJELMERUD, A. K. & LARSEN, R. H. 2010. Assessment of long-term radiotoxicity after treatment with the low-dose-rate alpha-particle-emitting radioimmunoconjugate (227)Th-rituximab. *Eur J Nucl Med Mol Imaging,* 37**,** 93-102.

DAMMER, J., FRALLICCIARDI, P. M., JAKUBEK, J., JAKUBEK, M., POSPISIL, S., PRENEROVA, E., VAVRIK, D., VOLTER, L., WEYDA, F. & ZEMEK, R. 2009. Real-time in-vivo μ-imaging with Medipix2. *Nuclear Instruments and Methods in Physics Research Section A: Accelerators, Spectrometers, Detectors and Associated Equipment,* 607**,** 205-207.

DAMMER, J., WEYDA, F., BENES, J., SOPKO, V., JAKUBEK, J. & VONDRACEK, V. 2011. Microradiography of biological samples with Timepix. *Journal of Instrumentation,* 6**,** C11005.

DAVID, J. R. 1990. *Bipolar semiconductor devices* NewYork, McGraw-Hill.

DAVIDSON, D. W., WATT, J., TLUSTOS, L., MIKULEC, B., CAMPBELL, M., MATHIESON, K., O'SHEA, V., SMITH, K. M. & RAHMAN, M. 2003. Detective quantum efficiency of the Medipix pixel detector. *Nuclear Science, IEEE Transactions on,* 50**,** 1659-1663.

DUDAK, J., ZEMLICKA, J., KREJCI, F., POLANSKY, S., JAKUBEK, J., MRZILKOVA, J., PATZELT, M. & TRNKA, J. 2015. X-ray micro-CT scanner for small animal imaging based on Timepix detector technology. *Nuclear Instruments and Methods in Physics Research Section A: Accelerators, Spectrometers, Detectors and Associated Equipment,* 773**,** 81-86.

ELGQVIST, J., FROST, S., POUGET, J.-P. & ALBERTSSON, P. 2014. The potential and hurdles of targeted alpha therapy - clinical trials and beyond. *Frontiers in Oncology,* 3**,** 1-9.

ESPOSITO, M., JAKUBEK, J., METTIVIER, G., POSPISIL, S., RUSSO, P. & SOLC, J. 2011a. Energy sensitive Timepix silicon detector for electron imaging. *Nuclear Instruments and Methods in Physics Research Section A: Accelerators, Spectrometers, Detectors and Associated Equipment,* 652**,** 458-461.

ESPOSITO, M., METTIVIER, G. & RUSSO, P. 2011b. 14 C autoradiography with an energy-sensitive silicon pixel detector. *Physics in Medicine and Biology,* 56**,** 1947.

FARUQI, A. R. & CATTERMOLE, D. M. 2002. Digital detectors for electron microscopy. *Nuclear Instruments and Methods in Physics Research Section A: Accelerators, Spectrometers, Detectors and Associated Equipment,* 478**,** 88-94.

FEHNIGER, T. A., CAI, S. F., CAO, X., BREDEMEYER, A. J., PRESTI, R. M., FRENCH, ANTHONY R. & LEY, T. J. 2007. Acquisition of Murine NK Cell Cytotoxicity Requires the Translation of a Pre-existing Pool of Granzyme B and Perforin mRNAs. *Immunity,* 26**,** 798-811.

FICHOU, N., GOUARD, S., MAUREL, C., BARBET, J., FERRER, L., MORGENSTERN, A., BRUCHERTSEIFER, F., FAIVRE-CHAUVET, A., BIGOT-CORBEL, E., DAVODEAU, F., GASCHET, J. & CHÉREL, M. 2015. Single-Dose Anti-CD138 Radioimmunotherapy: Bismuth-213 is More Efficient than Lutetium-177 for Treatment of Multiple Myeloma in a Preclinical Model. *Frontiers in Medicine,* 2**,** 76.

FRANKEN, N. A., RODERMOND, H. M., STAP, J., HAVEMAN, J. & VAN BREE, C. 2006. Clonogenic assay of cells in vitro. *Nat Protoc,* 1**,** 2315-9.

FROST, S. H. L., MILLER, B. W., BÄCK, T. A., SANTOS, E. B., HAMLIN, D. K., KNOBLAUGH, S. E., FRAYO, S. L., KENOYER, A. L., STORB, R., PRESS, O. W., WILBUR, D. S., PAGEL, J. M. & SANDMAIER, B. M. 2015. α-Imaging Confirmed Efficient Targeting of CD45-Positive Cells After 211At-Radioimmunotherapy for Hematopoietic Cell Transplantation. *Journal of Nuclear Medicine,* 56**,** 1766-1773.

GEBERT, U., RÜGHEIMER, T. K., MICHEL, T., ANTON, G., SÉGUINOT, J. & JORAM, C. 2010. Detection of optical photons with the Timepix in an HPD set-up. *Nuclear Instruments and Methods in Physics Research Section A: Accelerators, Spectrometers, Detectors and Associated Equipment,* 623**,** 288-290.

GIMENEZ, E. N., BALLABRIGA, R., CAMPBELL, M., HORSWELL, I., LLOPART, X., MARCHAL, J., SAWHNEY, K. J. S., TARTONI, N. & TURECEK, D. 2011. Characterization of Medipix3 With Synchrotron Radiation. *Nuclear Science, IEEE Transactions on,* 58**,** 323-332.

GRANJA, C., JAKUBEK, J., KOPATCH, Y., POSPISIL, S., TELEZHNIKOV, S. & VYKYDAL, Z. Position-, spectral- and time-sensitive spectroscopy of fission fragments with TimePix pixel detectors. Nuclear Science Symposium Conference Record, 2008. NSS '08. IEEE, 19-25 Oct. 2008 2008. 1659-1660.

GRANJA, C., JAKUBEK, J., KÖSTER, U., PLATKEVIC, M. & POSPISIL, S. 2011. Response of the pixel detector Timepix to heavy ions. *Nuclear Instruments and Methods in Physics Research Section A: Accelerators, Spectrometers, Detectors and Associated Equipment,* 633, Supplement 1**,** S198-S202.

GRANJA, C., JAKUBEK, J., PLATKEVIC, M., POSPISIL, S. & VYKYDAL, Z. 2010. Detection and Real Time Spectroscopy of Charged Particles with the TimePix Pixel Detector. *AIP Conference Proceedings,* 1204**,** 75-79.

GRANJA, C. & POSPISIL, S. 2014. Quantum dosimetry and online visualization of X-ray and charged particle radiation in commercial aircraft at operational flight altitudes with the pixel detector Timepix. *Advances in Space Research,* 54**,** 241-251.

HALL, E. J. & GIACCIA, A. J. 2006. *Radiobiology for the radiologist* Philadelphia Lippincott Williams & Wilkins.

HASSFJELL, S. & BRECHBIEL, M. W. 2001. The Development of the α-Particle Emitting Radionuclides 212Bi and 213Bi, and Their Decay Chain Related Radionuclides, for Therapeutic Applications. *Chemical Reviews,* 101**,** 2019-2036.

HEYERDAHL, H., ABBAS, N., BREVIK, E. M., MOLLATT, C. & DAHLE, J. 2012. Fractionated Therapy of HER2-Expressing Breast and Ovarian Cancer Xenografts in Mice with Targeted Alpha Emitting ²²⁷Th-DOTA-p-benzyl-trastuzumab. *PLoS ONE,* 7**,** e42345.

HOFSÄSS, H., ZHANG, K. & MUTZKE, A. 2014. Simulation of ion beam sputtering with SDTrimSP, TRIDYN and SRIM. *Applied Surface Science,* 310**,** 134-141.

HUANG, C.-Y., GUATELLI, S., OBORN, B. M. & ALLEN, B. J. 2012. Microdosimetry for Targeted Alpha Therapy of Cancer. *Computational and Mathematical Methods in Medicine,* 2012**,** 6.

IAEA 2001. Cytogenetic analysis for radiation dose assessment a manual. *Technical reports series no. 405.* Vienna: IAEA.

IAEA 2011. Cytogenetic Dosimetry: Applications in Preparedness for and Response to Radiation Emergencies *EPR-BioDosimetry.* VIENNA: IAEA.

IAEA 2013. Alpha Emitting Radionuclides and Radiopharmaceuticals for Therapy. Austria: IAEA.

ICRP 2007. The 2007 Recommendations of the International Commission on Radiological Protection. *In:* VALENTIN, J. (ed.) *Annals of the ICRP.* Elsevier.

ICRU 1983. Microdosimetry. *ICRU Report 36.* Maryland: International Commission on Radiation Units and Meaurments.

ICRU 2007. 4DOSIMETRY. *Journal of the ICRU,* 7**,** 49-81.

INSTRUMENTS, A. S. 2013. Timepix QTPX-262k and STPX-65k Quick start manual The Netherlands. .

ISHIKURA, T., AOYAMA, K., FUJIMOTO, T., TOMOTAKA, M. & NAKAMURA, T. 2008. Development of a small semiconductor detector using a printed circuit silicon-board for a personal dosemeter. *Radiation Measurements,* 43, 546-549.

JAKUBEK, J. 2009. Energy-sensitive X-ray radiography and charge sharing effect in pixelated detector. *Nuclear Instruments and Methods in Physics Research Section A: Accelerators, Spectrometers, Detectors and Associated Equipment,* 607, 192-195.

JAKUBEK, J. 2011. Precise energy calibration of pixel detector working in time-over-threshold mode. *Nuclear Instruments and Methods in Physics Research Section A: Accelerators, Spectrometers, Detectors and Associated Equipment,* 633, Supplement 1, S262-S266.

JAKUBEK, J., CEJNAROVA, A., HOLY, T., POSPISIL, S., UHER, J. & VYKYDAL, Z. 2008a. Pixel detectors for imaging with heavy charged particles. *Nuclear Instruments and Methods in Physics Research Section A: Accelerators, Spectrometers, Detectors and Associated Equipment,* 591, 155-158.

JAKUBEK, J., CEJNAROVA, A., PLATKEVIC, M., SOLC, J. & VYKYDAL, Z. Event by event energy sensitive imaging with TimePix pixel detector and its application for gamma photon tracking. Nuclear Science Symposium Conference Record, 2008. NSS '08. IEEE, 19-25 Oct. 2008 2008b. 3451-3458.

JAKUBEK, J., PLATKEVIC, M., SCHMIDT-WELLENBURG, P., GELTENBORT, P., PLONKA-SPEHR, C. & DAUM, M. 2009a. Position-sensitive spectroscopy of ultra-cold neutrons with Timepix pixel detector. *Nuclear Instruments and Methods in Physics Research Section A: Accelerators, Spectrometers, Detectors and Associated Equipment,* 607, 45-47.

JAKUBEK, J., SCHMIDT-WELLENBURG, P., GELTENBORT, P., PLATKEVIC, M., PLONKA-SPEHR, C., SOLC, J. & SOLDNER, T. 2009b. A coated pixel device TimePix with micron spatial resolution for UCN detection. *Nuclear Instruments and Methods in Physics Research Section A: Accelerators, Spectrometers, Detectors and Associated Equipment,* 600, 651-656.

JANIK, M., PLOC, O., FIEDERLE, M., PROCZ, S. & KAVASI, N. 2016. Optimization of the Timepix chip to measurement of radon, thoron and their progenies. *Appl Radiat Isot,* 107, 220-4.

JOSE, J. M., ČERMÁK, P., ŠTEKL, I., ČERMÁK, J., FIEDERLE, M., FAULER, A., SHITOV, Y. A., RUKHADZE, E. N., RUKHADZE, N. I., BRUDANIN, V. B., ZUBER, K. & LOAIZA, P. 2011. Timepix background studies for double beta decay experiments. *Journal of Instrumentation,* 6, C11030.

JOUNG, J. Y., HA, Y. S. & KIM, I. Y. 2013. Radium Ra 223 dichloride in castration-resistant prostate cancer. *Drugs Today (Barc),* 49, 483-90.

JURCIC, J. G., LARSON, S. M., SGOUROS, G., MCDEVITT, M. R., FINN, R. D., DIVGI, C. R., BALLANGRUD, Å. M., HAMACHER, K. A., MA, D., HUMM, J. L., BRECHBIEL, M. W., MOLINET, R. & SCHEINBERG, D. A. 2002. Targeted α particle immunotherapy for myeloid leukemia. *Blood,* 100, 1233-1239.

KARIMI, M. A., LEE, E., BACHMANN, M. H., SALICIONI, A. M., BEHRENS, E. M., KAMBAYASHI, T. & BALDWIN, C. L. 2014. Measuring Cytotoxicity by Bioluminescence Imaging Outperforms the Standard Chromium-51 Release Assay. *PLoS ONE,* 9, e89357.

KASSIS, A. I., HARRIS, C. R., ADELSTEIN, S. J., RUTH, T. J., LAMBRECHT, R. & WOLF, A. P. 1986. The in vitro radiobiology of astatine-211 decay. *Radiation Research,* 105, 27-36.

KASSIS, A. I., SASTRY, K. S. & ADELSTEIN, S. J. 1985. Intracellular distribution and radiotoxicity of chromium-51 in mammalian cells: Auger-electron dosimetry. *J Nucl Med,* 26, 59-67.

KEEFFE, S. O., LEWIS, E., SANTHANAM, A., WINNINGHAM, A. & ROLLAND, J. P. Low dose plastic optical fibre radiation dosimeter for clinical dosimetry applications. Sensors, 2009 IEEE, 25-28 Oct. 2009 2009. 1689-1692.

KHAN, F. M. 1994. *The physics of radiation therapy* Baltimore Williams & Wilkins.

KHAN, F. M. & POTISH, R. A. 1998. *Treatment planning in radiation oncology,* Williams & Wilkins.

KIM, Y.-S. & BRECHBIEL, M. W. 2012. An overview of targeted alpha therapy. *Tumor Biology,* 33, 573-590.

KOPANS, D. B. 2002. *Breast Imaging,* Philadelphia, lippincott Williams & Wikins.

KRAUS, V., HOLIK, M., JAKUBEK, J., KROUPA, M., SOUKUP, P. & VYKYDAL, Z. 2011. FITPix — fast interface for Timepix pixel detectors. *JINST,* 6, C01079.

KRISHNAMURTHY, G. T., SWAILEM, F. M., SRIVASTAVA, S. C., ATKINS, H. L., SIMPSON, L. J., WALSH, T. K., AHMANN, F. R., MEINKEN, G. E. & SHAH, J. H. 1997. Tin-117m(4+)DTPA: Pharmacokinetics and Imaging Characteristics in Patients with Metastatic Bone Pain. *Journal of Nuclear Medicine,* 38, 230-237.

KUO, L. J. & YANG, L. X. 2008. Gamma-H2AX - a novel biomarker for DNA double-strand breaks. *In Vivo,* 22, 305-9.

LARSEN, R. H., BORREBAEK, J., DAHLE, J., MELHUS, K. B., KROGH, C., VALAN, M. H. & BRULAND, O. S. 2007. Preparation of TH227-labeled radioimmunoconjugates, assessment of serum stability and antigen binding ability. *Cancer Biother Radiopharm,* 22, 431-7.

LEDERER, C. M., HOLLANDER, J. M. & PERLMAN, I. 1967. *Table of isotopes,* New York John Wiley & Sons.

LEE, B.-S. 2001. Measurement of Spatial Resolution in Fiber-optic Image Guides. *Journal of the Optical Society of Korea,* 5, 33-36.

LEMAIRE, H., AMGAROU, K., KHALIL, R. A., ANGELIQUE, J. C., BONNET, F., DE TORO, D., CARREL, F., GIARMANA, O., GMAR, M., MENAA, N., MENESGUEN, Y., NORMAND, S., PATOZ, A., SCHOEPFF, V., TALENT, P. & TIMI, T. 2013. Implementation of an imaging spectrometer for localization and identification of radioactive sources. *2013 3rd International Conference on Advancements in Nuclear Instrumentation, Measurement Methods and their Applications (ANIMMA),* 5 pp.-5 pp.

LIEN, L. M., TVEDT, B. & HEINRICH, D. 2015. Treatment of castration-resistant prostate cancer and bone metastases with radium-223 dichloride. *Int J Urol Nurs,* 9, 3-13.

LLOPART, X., BALLABRIGA, R., CAMPBELL, M., TLUSTOS, L. & WONG, W. 2007. Timepix, a 65k programmable pixel readout chip for arrival time, energy and/or photon counting measurements. *Nuclear Instruments and Methods in Physics Research Section A: Accelerators, Spectrometers, Detectors and Associated Equipment,* 581, 485-494.

LLOPART, X., CAMPBELL, M., DINAPOLI, R., SAN SEGUNDO, D. & PERNIGOTTI, E. 2002. Medipix2: A 64-k pixel readout chip with 55-μm square elements working in single photon counting mode. *Nuclear Science, IEEE Transactions on,* 49, 2279-2283.

LOO, K. J., JAKUBEK, J., ZEMLICKA, J., PETASECCA, M., SAFAVI-NAEINI, M., BUCCI, J., ZAIDER, M. & ROSENFELD, A. B. 2014. BrachyView: Feasibility study into the application of Timepix detectors for soft tissue thickness imaging in prostate brachytherapy treatment. *Radiation Measurements,* 71, 329-332.

LOO, K. J., PETASECCA, M., SAFAVI-NAENI, M., HAN, Z., LERCH, M., BUCCI, J., JAKUBEK, J., ZEMLICKA, J., MEIKLE, S., ZAIDER, M. & ROSENFELD, A. BrachyView: Tomographic reconstruction using Timepix detectors in post-implant dosimetry checks for permanent prostate brachytherapy implants. Nuclear Science Symposium and Medical Imaging Conference (NSS/MIC), 2013 IEEE, Oct. 27 2013-Nov. 2 2013 2013. 1-3.

LUTZ, G. 2007. *Semiconductor Radiation Detectors Device Physics,* New York, Springer-Verlag Berlin Heidelberg.

MACPHAIL, S. H., BANÁTH, J. P., YU, T. Y., CHU, E. H. M., LAMBUR, H. & OLIVE, P. L. 2003. Expression of phosphorylated histone H2AX in cultured cell lines following exposure to X-rays. *International Journal of Radiation Biology,* 79, 351-359.

MANACH, E. & GAL, O. 2002. Simulation of single-event energy-deposition spreading in a hybrid pixellated detector for γ imaging. *Nuclear Instruments and Methods in Physics Research Section A: Accelerators, Spectrometers, Detectors and Associated Equipment,* 487, 142-150.

MARCU, L., BEZAK, E. & ALLEN, B. J. 2012. *Biomedical physics in radiotherapy for cancer* Australia, Collingwood, Vic. : CSIRO Publishing

MARTIŠÍKOVÁ, M., GRANJA, C., JAKŮBEK, J., HARTMANN, B., TELSEMEYER, J., HUBER, L., BRONS, S., POSPÍŠIL, S. & JÄKEL, O. 2012. Two-dimensional silicon-based detectors for ion beam therapy. *AIP Conference Proceedings,* 1423, 327-334.

MARTISIKOVA, M., HARTMANN, B., GWOSCH, K., JAKUBEK, J., GRANJA, C. & JAKEL, O. 2012a. Study of the Capabilities of the Timepix Detector for Ion Beam Radiotherapy Applications. *2012 IEEE Nuclear Science Symposium and Medical Imaging Conference Record (NSS/MIC 2012) & Workshop on Room-Temperature Semiconductor X-Ray and Gamma-Ray Detectors*, 4324-4328.

MARTISIKOVA, M., JAKUBEK, J., GRANJA, C., HARTMANN, B., OPALKA, L., POSPISILB, S. & JAKELA, O. 2011. Measurement of secondary radiation during ion beam therapy with the pixel detector Timepix. *Journal of Instrumentation,* 6, C11014.

MARTISIKOVA, M., JAKUBEK, J., GWOSCH, K., HARTMANN, B., TELSEMEYER, J., POSPISIL, S. & JAKEL, O. 2012b. Monitoring of ion beam energy by tracking of secondary ions: First measurements in a patient-like phantom. *2012 IEEE Nuclear Science Symposium and Medical Imaging Conference Record (NSS/MIC 2012) & Workshop on Room-Temperature Semiconductor X-Ray and Gamma-Ray Detectors*, 1914-1917.

MASSILLON-JL, G., MINNITI, R., MITCH, M. G., MARYANSKI, M. J. & SOARES, C. G. 2009. The use of gel dosimetry to measure the 3D dose distribution of a 90 Sr/ 90 Y intravascular brachytherapy seed. *Physics in Medicine and Biology,* 54, 1661.

MATHER, S. J. & BRITTON, K. E. 2004. Radioimmunotherapy. Progress, potential and problems. *Q J Nucl Med Mol Imaging,* 48, 248-50.

MAYLES, P., NAHUM, A. & ROSENWALD, J. C. 2007. *Handbook of Radiotherapy Physics: Theory and Practice,* New York, ayler & Francis Group.

MCDEVITT, M. R., MA, D., LAI, L. T., SIMON, J., BORCHARDT, P., FRANK, R. K., WU, K., PELLEGRINI, V., CURCIO, M. J., MIEDERER, M., BANDER, N. H. & SCHEINBERG, D. A. 2001. Tumor Therapy with Targeted Atomic Nanogenerators. *Science,* 294, 1537-1540.

MCDEVITT, M. R., SGOUROS, G., FINN, R. D., HUMM, J. L., JURCIC, J. G., LARSON, S. M. & SCHEINBERG, D. A. 1998. Radioimmunotherapy with alpha-emitting nuclides. *European Journal of Nuclear Medicine,* 25, 1341-1351.

METTIVIER, G., MONTESI, M. C. & RUSSO, P. 2003. First images of a digital autoradiography system based on a Medipix2 hybrid silicon pixel detector. *Phys Med Biol,* 48, N173-81.

MICHEAU, O., SOLARY, E., HAMMANN, A., MARTIN, F. & DIMANCHE-BOITREL, M.-T. 1997. Sensitization of Cancer Cells Treated With Cytotoxic Drugs to Fas-Mediated Cytotoxicity. *Journal of the National Cancer Institute,* 89, 783-789.

MICHEL, T., BOHNEL, M., DURST, J., SIEVERS, P. & ANTON, G. 2009a. Low Energy Dosimetry With Photon Counting Pixel Detectors Such as Medipix. *Nuclear Science, IEEE Transactions on,* 56, 417-423.

MICHEL, T., DURST, J. & JAKUBEK, J. 2009b. X-ray polarimetry by means of Compton scattering in the sensor of a hybrid photon counting pixel detector. *Nuclear Instruments and Methods in Physics Research Section A: Accelerators, Spectrometers, Detectors and Associated Equipment,* 603, 384-392.

MIKULEC, B. 2000. *Single Photon Detection with Semiconductor Pixel Arrays for Medical Imaging Applications*. Vienna U. patent application.

MIKULEC, B., CAMPBELL, M., DIPASQUALE, G., SCHWARZ, C. & WATT, J. 2001. Characterisation of a single photon counting pixel system for imaging of low-contrast objects. *Nuclear Instruments and Methods in Physics Research Section A: Accelerators, Spectrometers, Detectors and Associated Equipment,* 458, 352-359.

MILLER, B. W., GREGORY, S. J., FULLER, E. S., BARRETT, H. H., BARBER, H. B. & FURENLID, L. R. 2014. The iQID camera: An ionizing-radiation quantum imaging detector. *Nuclear instruments & methods in physics research. Section A, Accelerators, spectrometers, detectors and associated equipment,* 767, 146-152.

MITSCHKE, M., GIERSCH, J. & ANTON, G. 2004. Simulation of signal generation processes in semiconductor sensor layers for Medipix1 and 2. *Nuclear Instruments and Methods in Physics*

Research Section A: Accelerators, Spectrometers, Detectors and Associated Equipment, 531, 62-67.

MOATS, R. A., YANG, T., HUGG, J. W., MEIER, D., KOOS, D., HARTSOUGH, N. E., PATT, B. E. & WAGENAAR, D. J. 2011. Basic design and simulation of a SPECT microscope for in vivo stem cell imaging. *Proceedings of the SPIE - The International Society for Optical Engineering,* 7961, 79614B (8 pp.)-79614B (8 pp.).

MULFORD, D. A., SCHEINBERG, D. A. & JURCIC, J. G. 2005. The Promise of Targeted α-Particle Therapy. *Journal of Nuclear Medicine,* 46, 199S-204S.

MUNSHI, A., HOBBS, M. & MEYN, R. E. 2005. Clonogenic cell survival assay. *Methods Mol Med,* 110, 21-8.

NEUDECK, G. W. 1989. *The PN junction diode* California, Addison-Wesley Publishing

NIEDERLÖHNER, D., BERT, C., GIERSCH, J., PFEIFFER, K. F. & ANTON, G. 2003. Threshold characterisation of the Medipix1 chip. *Nuclear Instruments and Methods in Physics Research Section A: Accelerators, Spectrometers, Detectors and Associated Equipment,* 509, 138-145.

NILSSON, S. 2014. Alpha-emitter radium-223 in the management of solid tumors: current status and future directions. *Am Soc Clin Oncol Educ Book,* e132-9.

NILSSON, S., FRANZEN, L., PARKER, C., TYRRELL, C., BLOM, R., TENNVALL, J., LENNERNAS, B., PETERSSON, U., JOHANNESSEN, D. C., SOKAL, M., PIGOTT, K., YACHNIN, J., GARKAVIJ, M., STRANG, P., HARMENBERG, J., BOLSTAD, B. & BRULAND, O. S. 2007. Bone-targeted radium-223 in symptomatic, hormone-refractory prostate cancer: a randomised, multicentre, placebo-controlled phase II study. *Lancet Oncol,* 8, 587-94.

NILSSON, S., LARSEN, R. H., FOSSÅ, S. D., BALTESKARD, L., BORCH, K. W., WESTLIN, J.-E., SALBERG, G. & BRULAND, Ø. S. 2005. First Clinical Experience with α-Emitting Radium-223 in the Treatment of Skeletal Metastases. *Clinical Cancer Research,* 11, 4451-4459.

O'DONOGHUE, J. A. & WHELDON, T. E. 1996. Targeted radiotherapy using Auger electron emitters. *Phys Med Biol,* 41, 1973-92.

O'KEEFFE, S., FITZPATRICK, C., LEWIS, E. & AL-SHAMMA'A, A. I. 2008. A review of optical fibre radiation dosimeters. *Sensor Review,* 28, 136-142.

OPALKA, L., GRANJA, C., HARTMANN, B., JAKUBEK, J., JAEKEL, O., MARTISIKOVA, M., POSPISIL, S. & SOLC, J. 2012. 3D measurement of the radiation distribution in a water phantom in a hadron therapy beam. *Journal of Instrumentation,* 7, C01085.

OPALKA, L., GRANJA, C., HARTMANN, B., JAKUBEK, J., JAEKEL, O., MARTISIKOVA, M., POSPISIL, S. & SOLC, J. 2013. Linear energy transfer and track pattern recognition of secondary radiation generated in hadron therapy beam in a PMMA target. *Journal of Instrumentation,* 8, C02047.

PARKER, C., NILSSON, S., HEINRICH, D., HELLE, S. I., O'SULLIVAN, J. M., FOSSÅ, S. D., CHODACKI, A., WIECHNO, P., LOGUE, J., SEKE, M., WIDMARK, A., JOHANNESSEN, D. C., HOSKIN, P., BOTTOMLEY, D., JAMES, N. D., SOLBERG, A., SYNDIKUS, I., KLIMENT, J., WEDEL, S., BOEHMER, S., DALL'OGLIO, M., FRANZÉN, L., COLEMAN, R., VOGELZANG, N. J., O'BRYAN-TEAR, C. G., STAUDACHER, K., GARCIA-VARGAS, J., SHAN, M., BRULAND, Ø. S. & SARTOR, O. 2013. Alpha Emitter Radium-223 and Survival in Metastatic Prostate Cancer. *New England Journal of Medicine,* 369, 213-223.

PEARSON, G. R., HODES, R. J. & FRIBERG, S. 1969. Cytotoxic potential of different lymphoid cell populations against chromium-51 labelled tumour cells. *Clinical and Experimental Immunology,* 5, 273-284.

PELGROM, M. J. M. 1991. Matching properties of MOS transistors. *Nuclear Instruments and Methods in Physics Research Section A: Accelerators, Spectrometers, Detectors and Associated Equipment,* 305, 624-626.

PFEIFFER, K. F. G., GIERSCH, J. & ANTON, G. 2004. How good is better? A comparison between the Medipix1 and the Medipix2 chip using mammographic phantoms. *Nuclear Instruments and Methods in Physics Research Section A: Accelerators, Spectrometers, Detectors and Associated Equipment,* 531, 246-250.

PFEIFFER, K. F. G., GIERSCH, J., ANTON, G., BÄTZ, L. & HOHEISEL, M. 2003. Large-scale images taken with the Medipix1 chip. *Nuclear Instruments and Methods in Physics Research Section A: Accelerators, Spectrometers, Detectors and Associated Equipment,* 509, 340-345.

PINSKY, L., CHANCELLOR, J. & MINTHAKA, D. Evolving the Medipix2 Technology For Use As An Active Space Radiation Dosimeter. Aerospace Conference, 2008 IEEE, 1-8 March 2008 2008. 1-8.

PINSKY, L., STOFFLE, N., EMPL, A., JAKUBEK, J., POSPISIL, S., LEROY, C., KITAMURA, H., YASUDA, N. & UCHIHORI, Y. 2011a. Application of the Medipix2 technology to space radiation dosimetry and hadron therapy beam monitoring. *Radiation Measurements,* 46, 1610-1614.

PINSKY, L. S., EMPL, A., GUTIERREZ, A., JAKUBEK, J., KITAMURA, H., MILLER, J., LEROY, C., STOFFLE, N., POSPISIL, S., UCHIHORI, Y., YASUDA, N. & ZEITLIN, C. 2011b. Penetrating heavy ion charge and velocity discrimination with a TimePix-based Si detector (for space radiation applications). *Nuclear Instruments and Methods in Physics Research Section A: Accelerators, Spectrometers, Detectors and Associated Equipment,* 633, Supplement 1, S190-S193.

PINSKY, L. S., EMPL, A., GUTIERREZ, A., JAKUBEK, J., KITAMURA, H., MILLER, J., LEROY, C., STOFFLE, N., POSPISIL, S., UCHIHORI, Y., YASUDA, N. & ZEITLIN, C. 2011c. Penetrating heavy ion charge and velocity discrimination with a TimePix-based Si detector (for space radiation applications). *Nuclear Instruments and Methods in Physics Research Section A: Accelerators, Spectrometers, Detectors and Associated Equipment,* 633, Supplement 1, S190-S193.

PINSKY, L. S., EMPL, A., STOFFLE, N., LEROY, C., GUTIERREZ, A., JAKUBEK, J., POSPISIL, S., KITAMURA, H., UCHIHORI, Y., NAKAHIRO, Y., MILLER, J. & ZEITLIN, C. Heavy ion charge and velocity resolution with a Medipix-based active Space Radiation Dosimeter. Aerospace Conference, 2010 IEEE, 6-13 March 2010 2010. 1-6.

PLATKEVIC, M., JAKUBEK, J., HAVRANEK, V., JAKUBEK, M., POSPISIL, S., SEMIAN, V. & ZEMLICKA, J. 2013. Evaluation of local radiation damage in silicon sensor via charge collection mapping with the Timepix read-out chip. *Journal of Instrumentation,* 8, C04001.

PODGORSAK, E. B. 2005. *Radiation Oncology Physics : a Handbook for Teachers and Students,* Vienna, IAEA.

PUGATCH, V., CAMPBELL, M., CHAUS, A., EREMENKO, V., HOMENKO, S., KOVALCHUK, O., LLOPART, X., OKHRIMENKO, O., POSPISIL, S., SHELEKHOV, A., STORIZHKO, V. & TLUSTOS, L. 2011. Metal and hybrid TimePix detectors imaging beams of particles. *Nuclear Instruments and Methods in Physics Research Section A: Accelerators, Spectrometers, Detectors and Associated Equipment,* 650, 194-197.

RAJA, C., GRAHAM, P., ABBAS RIZVI, S. M., SONG, E., GOLDSMITH, H., THOMPSON, J., BOSSERHOFF, A., MORGENSTERN, A., APOSTOLIDIS, C., KEARSLEY, J., REISFELD, R. & ALLEN, B. J. 2007. Interim analysis of toxicity and response in phase 1 trial of systemic targeted alpha therapy for metastatic melanoma. *Cancer Biol Ther,* 6, 846-52.

RASBAND, W. S. 1997-2014. ImageJ 1.48V ed. USA: U. S. National Institutes of Health.

REILLY, R. M. 2010. *Monoclonal Antibody and Peptide-Targeted Radiotherapy of Cancer,* Hoboken, NJ, USA, John Wiley & Sons, Incorporated.

RIQUIER, H., WERA, A.-C., HEUSKIN, A.-C., FERON, O., LUCAS, S. & MICHIELS, C. 2013. Comparison of X-ray and alpha particle effects on a human cancer and endothelial cells: Survival curves and gene expression profiles. *Radiotherapy and Oncology,* 106, 397-403.

RISS, T. L., MORAVEC, R. A., NILES, A. L., BENINK, H. A., WORZELLA, T. J. & MINOR, L. 2004. Cell Viability Assays. *In:* SITTAMPALAM, G. S., COUSSENS, N. P., NELSON, H., ARKIN, M., AULD, D., AUSTIN, C., BEJCEK, B., GLICKSMAN, M., INGLESE, J., IVERSEN, P. W., LI, Z., MCGEE, J., MCMANUS, O., MINOR, L., NAPPER, A., PELTIER, J. M., RISS, T., TRASK, O. J., JR. & WEIDNER, J. (eds.) *Assay Guidance Manual.* Bethesda MD.

ROESKE, J. C. & STINHCOMB, T. G. 1997. Dosimetric Framework for Therapeutic Alpha-Particle Emitters. *Journal of Nuclear Medicine,* 38, 1923-1929.

ROSENFELD, A. B. & BRADLEY, P. D. 1999. Semiconductor Microdosimetry in Mixed Radiation and Photon Fields: Present and Future. *Radiation Protection Dosimetry,* 85, 385-388.

ROSENFELD, A. B., BRADLEY, P. D., CORNELIUS, I., KAPLAN, G. I., ALLEN, B. J., FLANZ, J. B., GOITEIN, M., MEERBEECK, A. V., SCHUBERT, J., BAILEY, J., TAKADA, Y., MARUHASHI, A. & HAYAKAWA, Y. 2000. A new silicon detector for microdosimetry applications in proton therapy. *IEEE Transactions on Nuclear Science,* 47, 1386-1394.

ROSENFELD, A. B., CUTAJAR, D., LERCH, M. L. F., TAKACS, G., CORNELIUS, I. M., YUDELEV, M. & ZAIDER, M. 2006. Miniature semiconductor detectors for in vivo dosimetry. *Radiation Protection Dosimetry,* 120, 48-55.

ROSSI, L., FISCHER, P., ROHE, T. & WERMES, N. 2006. *Pixel Detectors: From Fundamentals to Applications,* The Netherlands, Springer Berlin Heidelberg.

RUDDON, R. W. 1995. *Cancer Biology,* Oxford Oxford University Press.

RÜGHEIMER, T. K., GEBERT, U., MICHEL, T., ANTON, G., SÉGUINOT, J. & JORAM, C. 2008. Experimental demonstration of a hybrid photon detector concept based on the Timepix detector. *Nuclear Instruments and Methods in Physics Research Section A: Accelerators, Spectrometers, Detectors and Associated Equipment,* 595, 353-358.

SABOL, J. & WENG, P.-S. 1995. *Introduction to Radiation Protection Dosimetry,* Singapore, World Scientific Publishing.

SANTIN, A. D., HERMONAT, P. L., RAVAGGI, A., BELLONE, S., PECORELLI, S., CANNON, M. J. & PARHAM, G. P. 2000. In vitro induction of tumor-specific human lymphocyte antigen class I–restricted CD8+ cytotoxic T lymphocytes by ovarian tumor antigen–pulsed autologous dendritic cells from patients with advanced ovarian cancer. *American Journal of Obstetrics and Gynecology,* 183, 601-609.

SCHWARZ, C., CAMPBELL, M., GOEPPERT, R., HEIJNE, E. H. M., LUDWIG, J., MEDDELER, G., MIKULEC, B., PERNIGOTTI, E., ROGALLA, M., RUNGE, K., SÖLDNER-REMBOLD, A., SMITH, K. M., SNOEYS, W. & WATT, J. 1999. X-ray imaging using a hybrid photon counting GaAs pixel detector. *Nuclear Physics B - Proceedings Supplements,* 78, 491-496.

SEIDL, C. 2014. Radioimmunotherapy with alpha-particle-emitting radionuclides. *Immunotherapy,* 6, 431-58.

SEVERINO, C. T. 2014. *Real-time measurement of radon activity and mixed radiation fields characterization with silicon pixel detector.* the University of Bern.

SGOUROS, G. 2008. Alpha-particles for targeted therapy. *Advanced Drug Delivery Reviews,* 60, 1402-1406.

SGOUROS, G., BALLANGRUD, A. M., JURCIC, J. G., MCDEVITT, M. R., HUMM, J. L., ERDI, Y. E., MEHTA, B. M., FINN, R. D., LARSON, S. M. & SCHEINBERG, D. A. 1999. Pharmacokinetics and dosimetry of an alpha-particle emitter labeled antibody: 213Bi-HuM195 (anti-CD33) in patients with leukemia. *J Nucl Med,* 40, 1935-46.

SGOUROS, G., ROESKE, J. C., MCDEVITT, M. R., PALM, S., ALLEN, B. J., FISHER, D. R., BRILL, A. B., SONG, H., HOWELL, R. W., AKABANI, G., IN COLLABORATION WITH THE SNM MIRD COMMITTEE: WESLEY E. BOLCH, A. B. B., DARRELL R. FISHER, ROGER W. HOWELL, RUBY F. MEREDITH, GEORGE SGOUROS , BARRY W. WESSELS, & ZANZONICO, P. B. 2010. MIRD Pamphlet No. 22 (Abridged): Radiobiology and Dosimetry of α-Particle Emitters for Targeted Radionuclide Therapy. *Journal of Nuclear Medicine,* 51, 311-328.

SHIRLEY, M. & MCCORMACK, P. L. 2014. Radium-223 dichloride: a review of its use in patients with castration-resistant prostate cancer with symptomatic bone metastases. *Drugs,* 74, 579-86.

SHORE, N. D. 2015. Radium-223 Dichloride for Metastatic Castration-resistant Prostate Cancer: The Urologist's Perspective. *Urology,* 85, 717-724.

SINOR, M., JAKUBEK, J., LINHART, V., MIKULEC, B., POSPISIL, S. & SOPKO, B. 2003. Charge sharing studies with a Medipix1 pixel device. *Nuclear Instruments and Methods in Physics Research Section A: Accelerators, Spectrometers, Detectors and Associated Equipment,* 509, 346-354.

SMITH, S. W. 1997-1998. *The Scientist and Engineer's Guide to Digital Signal Processing,* San Diego, California Technical Publishing.

STAUDACHER, A. H., AL-EJEH, F., FRASER, C. K., DARBY, J. M., RODER, D. M., RUSZKIEWICZ, A., MANAVIS, J. & BROWN, M. P. 2014a. The La antigen is over-expressed in lung cancer and is a selective dead cancer cell target for radioimmunotherapy using the La-specific antibody APOMAB®. *EJNMMI Research,* 4, 1-13.

STAUDACHER, A. H., BEZAK, E., BORYSENKO, A. & BROWN, M. P. 2014b. Targeted alpha-therapy using 227Th-APOMAB and cross-fire antitumour effects: preliminary in-vivo evaluation. *Nucl Med Commun.*

STAUDACHER, A. H., BEZAK, E., BORYSENKO, A. & BROWN, M. P. 2014c. Targeted α-therapy using 227Th-APOMAB and cross-fire antitumour effects: preliminary in-vivo evaluation. *Nuclear Medicine Communications,* 35, 1284-1290.

STIGBRAND, T., CARLSSON, J. & ADAMS, G. P. 2008. *Targeted Radionuclide Tumor Therapy: Biological Aspects*, Springer Science & Business Media.

STOFFLE, N., PINSKY, L., KROUPA, M., HOANG, S., IDARRAGA, J., AMBERBOY, C., RIOS, R., HAUSS, J., KELLER, J., BAHADORI, A., SEMONES, E., TURECEK, D., JAKUBEK, J., VYKYDAL, Z. & POSPISIL, S. 2015. Timepix-based radiation environment monitor measurements aboard the International Space Station. *Nuclear Instruments and Methods in Physics Research Section A: Accelerators, Spectrometers, Detectors and Associated Equipment,* 782, 143-148.

STOLLER, R. E., TOLOCZKO, M. B., WAS, G. S., CERTAIN, A. G., DWARAKNATH, S. & GARNER, F. A. 2013. On the use of SRIM for computing radiation damage exposure. *Nuclear Instruments and Methods in Physics Research Section B: Beam Interactions with Materials and Atoms,* 310, 75-80.

SUOMINEN, M. I., RISSANEN, J. P., KAKONEN, R., FAGERLUND, K. M., ALHONIEMI, E., MUMBERG, D., ZIEGELBAUER, K., HALLEEN, J. M., KAKONEN, S. M. & SCHOLZ, A. 2013. Survival benefit with radium-223 dichloride in a mouse model of breast cancer bone metastasis. *J Natl Cancer Inst,* 105, 908-16.

SUPIOT, S., FAIVRE-CHAUVET, A., COUTURIER, O., HEYMANN, M. F., ROBILLARD, N., KRAEBER-BODERE, F., MORANDEAU, L., MAHE, M. A. & CHEREL, M. 2002. Comparison of the biologic effects of MA5 and B-B4 monoclonal antibody labeled with iodine-131 and bismuth-213 on multiple myeloma. *Cancer,* 94, 1202-9.

THOMAS, P., TRACY, B., PING, T., BAWEJA, A., WICKSTROM, M., SIDHU, N. & HIEBERT, L. 2007. Relative biological effectiveness (RBE) of alpha radiation in cultured porcine aortic endothelial cells. *Int J Radiat Biol,* 83, 171-9.

THWAITES, D. I. & WILLIAMS, J. R. 2000. *Radiotherapy Physics in Practice,* Oxford Oxford University Press.

TURECEK, D., HOLY, T., JAKUBEK, J., POSPISIL, S. & VYKYDAL, Z. 2011a. Pixelman: a multi-platform data acquisition and processing software package for Medipix2, Timepix and Medipix3 detectors. *Journal of Instrumentation,* 6, C01046.

TUREČEK, D., HOLÝ, T. & VYKYDAL, Z. *Pixelman - Manual* [Online]. Available: http://aladdin.utef.cvut.cz/ofat/others/Pixelman/Pixelman_manual.html [Accessed 26 April 2016].

TURECEK, D., PINSKY, L., JAKUBEK, J., VYKYDAL, Z., STOFFLE, N. & POSPISIL, S. 2011b. Small Dosimeter based on Timepix device for International Space Station. *Journal of Instrumentation,* 6, C12037.

UHER, J. & JAKUBEK, J. 2011. Detection of fast neutrons with particle tracking detector Timepix combined with plastic scintillator. *Radiation Measurements,* 46, 1624-1627.

VAJDA, N., MARTIN, P. & KIM, C.-K. 2012. Chapter 6 - Alpha Spectrometry A2 - L'Annunziata, Michael F. *Handbook of Radioactivity Analysis (Third Edition).* Amsterdam: Academic Press.

VALLERGA, J., MCPHATE, J., TREMSIN, A. & SIEGMUND, O. 2008. High-resolution UV, alpha and neutron imaging with the Timepix CMOS readout. *Nuclear Instruments and Methods in Physics Research Section A: Accelerators, Spectrometers, Detectors and Associated Equipment,* 591, 151-154.

WAKER, A. J. 1995. Principals of Experimental Microdosimetry. *Radiation Protection Dosimetry,* 61, 297-308.

WAMBERSIE, A., PIHET, P. & MENZEL , H. G. 1990. The Role of Microdosimetry in Radiotherapy. *Radiation Protection Dosimetry,* 31, 421-432.

WELFARE, A. I. O. H. A. 2010. Cancer in Australia an overview 2010. *In:* WELFARE, A. I. O. H. A. (ed.). Canberra: Australian Institute of Health and Welfare.

WÉRA, A.-C., BORLON, C., NUTTENS, V. E., RIQUIER, H., FERON, O., MICHIELS, C. & LUCAS, S. 2012. Comparison of the clonogenic survival of A549 non-small cell lung adenocarcinoma cells after irradiation with low-dose-rate beta particles and high-dose-rate X-rays. *International Journal of Radiation Biology,* 88, 253-257.

WHELDON, T. E. & O'DONOGHUE, J. A. 1990. The Radiobiology of Targeted Radiotherapy. *International Journal of Radiation Biology,* 58, 1-21.

WHO 2008. World Cancer Report 2008. *In:* BOYLE;, P. & LEVIN, B. (eds.). Albany, NY, USA: World Health Organization.

WHO 2014. World Cancer Report 2014. *In:* STWART;, B. W. & WILD, C. P. (eds.). Albany, NY, USA: World Health Organization.

YANG, S. & HALUSKA, F. G. 2004. Treatment of Melanoma with 5-Fluorouracil or Dacarbazine In Vitro Sensitizes Cells to Antigen-Specific CTL Lysis through Perforin/Granzyme- and Fas-Mediated Pathways. *The Journal of Immunology,* 172, 4599-4608.

ŽEMLIČKA, J., JAKŮBEK, J., KROUPA, M. & TICHÝ, V. 2009. Energy- and position-sensitive pixel detector Timepix for X-ray fluorescence imaging. *Nuclear Instruments and Methods in Physics Research Section A: Accelerators, Spectrometers, Detectors and Associated Equipment,* 607, 202-204.

ZIEGLER, J. F. *Interactions of ions with matter* [Online]. Available: http://www.srim.org/ 2 July 2015].